

Electronic Thesis and Dissertation Repository

12-12-2016 12:00 AM

Creating Functional Materials with Phosphorus

Tyler John Cuthbert, *The University of Western Ontario*


Supervisor: Elizabeth R. Gillies, *The University of Western Ontario*

Joint Supervisor: Paul J. Ragogna, *The University of Western Ontario*

A thesis submitted in partial fulfillment of the requirements for the Doctor of Philosophy degree in Chemistry

© Tyler John Cuthbert 2016

Follow this and additional works at: <https://ir.lib.uwo.ca/etd>

 Part of the [Inorganic Chemistry Commons](#), [Materials Chemistry Commons](#), and the [Polymer Chemistry Commons](#)

Recommended Citation

Cuthbert, Tyler John, "Creating Functional Materials with Phosphorus" (2016). *Electronic Thesis and Dissertation Repository*. 4305.

<https://ir.lib.uwo.ca/etd/4305>

This Dissertation/Thesis is brought to you for free and open access by Scholarship@Western. It has been accepted for inclusion in Electronic Thesis and Dissertation Repository by an authorized administrator of Scholarship@Western. For more information, please contact wlsadmin@uwo.ca.

Abstract

Understanding the relationship between small molecules or polymers and how they affect the properties of materials they compose is the basis of materials science. Using unique and versatile components can impart useful and interesting properties to materials. Here, we aimed to extend this understanding to phosphorus, and the known properties it possesses. This included the production of photopolymerizable coatings containing phosphonium molecules and polymers for antifouling and antibacterial applications. The synthesis and characterization of these phosphonium components was completed and materials were produced utilizing UV curing technology. Addition of these components produced coatings that could resist bacteria attachment and efficiently kill bacteria that come in contact with the surface. Typical polyphosphonium antibacterials all possess similar alkyl functional groups. An alternative approach explored the use of different phosphonium substituents, including sugars and hydroxyl functional groups. The synthesis of these interesting phosphoniums from $\text{PH}_{3(\text{g})}$ is described, along with their polymerization and antibacterial activity against both Gram-positive and Gram-negative bacteria. They were efficient at killing both strains of bacteria at low concentrations with corresponding low hemolytic activity. These results present a new direction for the design of antibacterial polymers in this field. Utilizing hydrophilic phosphonium polymers, self-healing ionic networks with poly(acrylic acid) were produced. The rheological and mechanical properties of the networks were studied to understand the effect of the polyphosphonium content within the networks. These properties were found to directly affected the materials ability to heal. Healing could be completed at low salt concentrations ($<0.1 \text{ M NaCl}$) where *in vivo* applications could be realized. Finally, phosphane-ene chemistry was utilized to create polymer networks directly from $\text{PH}_{3(\text{g})}$ containing Lewis basic tertiary phosphine. The materials were characterized and their metal scavenging of popular Wilkinson's and Grubbs catalysts are reported. Regeneration of the polymer networks for repeat use was attempted with promising results. The efficiency of the metal scavenging was $>99\%$ for optimized polymer networks. This works presents a new direction and an alternative, simple method for homogeneous catalyst removal.

Co-Authorship Statement

The work described in chapter two was coauthored by Cuthbert, T.J.; Guterman, R.; Ragogna, P.J.; Gillies, E.R. *J. Mater. Chem. B* **2015**, *3*, 1474-1478. Tyler Cuthbert was the primary experimentalist with Ryan Guterman contributing to the initial synthesis of **2.1** and charge density experiments, and Aneta Borecki completed the MTT assay. Tyler Cuthbert wrote the manuscript, but all authors contributed to the editing process.

The work described in chapter three was coauthored by Cuthbert, T.J.; Harrison, T.D.; Ragogna, P.J.; Gillies, E.R. *J. Mater. Chem. B* **2016**, *4*, 4872-4883. Tyler Cuthbert was the primary experimentalist with Tristan Harrison contributing to the synthesis of **3.1**, **3.3**, **3.1-P**, and **3.3-P**. Tyler Cuthbert wrote the manuscript, but all authors contributed to the editing process.

The work described in chapter four was coauthored by Cuthbert, T.J.; Ragogna, P.J.; Gillies, E.R. and is in the pre-submission stage for publication. Tyler Cuthbert was the primary experimentalist.

The work described in chapter five was coauthored by Cuthbert, T.J.; Jadischke, J.J.; de Bruyn, J.R.; Ragogna, P.J.; Gillies, E.R. and is pre submission. Tyler Cuthbert was the primary experimentalist with Josh Jadischke contributing to the synthesis of the polymers and some initial healing experiments. Tyler Cuthbert wrote the manuscript, but all authors contributed to the editing process.

The work described in chapter six was coauthored by Cuthbert, T.J.; Bow, J.P.; Evoy, E.; Guterman, R.; Gillies, E.R.; Ragogna, P.L.; Blacquiere, J.M. and is pre submission. Tyler Cuthbert, J.P. Bow, and Erin Evoy were the main experimentalists. J.P. Bow and Erin Evoy contributed the Rh and Ru metal scavenging experiments and Tyler Cuthbert contributed the synthesis of **6.1**, **6.2**, **6.7**, **6.8**, polymer regeneration and Ru scavenging experiments. Tyler Cuthbert wrote the PH₃ polymer section containing **6.7** and **6.8**, and Johanna Blacquiere wrote the metal scavenging section for **6.2**.

Acknowledgements

I would like to start by thanking my supervisors Paul J. Ragona and Elizabeth R. Gillies. Your guidance, support, knowledge, and patience has been an invaluable component of my degree. Thank you for everything that you've done over the past four years to lead to this thesis.

I would like to thank everyone that has been a part of both the Ragona and Gillies group over the years. There is more to a research group than just the science. We lean on each other every day and you are an indispensable part of a graduate degree. I would also like to thank the support staff: John and Jon in the machine shop, Dr. Mat Willans for all the NMR spectroscopy help, Aneta for the cell work, and the folks in the ChemBioStores.

My family and friends, parents John and Wendy, sister Lauren, niece and nephew Sophie and Connor, my greyhound Tox, Brad and family, I thank you for always being there and your unconditional support.

Lastly, I would like to thank my committee members Dr. Brian Pagenkopf and Dr. Mark Workentin for their feedback on my yearly reports, and my examiners Dr. Michael Brook and Dr. Carole Creuzenet for reading my thesis.

Table of Contents

Abstract.....	i
Co-Authorship Statement	ii
Acknowledgements.....	iii
Table of Contents.....	iv
List of Tables	viii
List of Figures.....	ix
List of Schemes	xii
List of Appendices	xiii
List of Abbreviations	xiv
Chapter 1	1
1 Introduction	1
1.1 Materials chemistry introduction and background	1
1.1.1 Functional Materials – Advancing current societal demands	1
1.2 Polymerization	2
1.2.1 Basics of polymerization	2
1.2.2 Radical polymerization	3
1.2.3 RAFT agent Z and R substituent effects ^{12,13}	6
1.2.4 Step-growth radical polymerization	8
1.2.5 Photopolymerization	8
1.2.6 Photopolymer (UV cured) networks.....	10
1.3 Phosphorus-based materials and selected applications of these materials.....	11
1.3.1 Functional materials containing phosphorus	11
1.3.2 Phosphonium polymers as antibacterial agents and their application in antibacterial materials	14
1.3.3 Antibacterial phosphonium-containing materials.....	15
1.3.4 Ionic networks	15
1.3.5 Metal scavenging materials.....	16
1.4 Scope of Thesis	17
1.5 References.....	19

Chapter 2	25
2 Contact active antibacterial phosphonium coatings cured with UV light.	25
2.1 Introduction	25
2.2 Results and Discussion	26
2.3 Conclusions.....	32
2.4 Experimental.....	33
2.5 References.....	38
Chapter 3	41
3 Synthesis, properties, and antibacterial activity of polyphosphonium semi-interpenetrating networks.....	41
3.1 Introduction	41
3.2 Results and discussion.....	43
3.2.1 Synthesis of polyphosphonium	43
3.2.2 Preparation and characterization of polyphosphonium SIPNs.....	47
3.2.3 Antibacterial testing of the SIPNs.....	52
3.3 Conclusions.....	55
3.4 Experimental.....	56
3.4.1 Preparation and characterization of polyphosphonium SIPNs.....	61
3.5 References.....	65
Chapter 4	70
4 Increasing the hydrophilicity of phosphonium polymers to increase antibacterial activity and decrease hemolytic activity.....	70
4.1 Introduction	70
4.2 Results and Discussion	73
4.2.1 Synthesis of phosphonium mannoside and glucoside monomers 4.3 and 4.4	73
4.2.2 Polymerization of 4.3 and 4.4.....	79
4.2.3 Antibacterial testing.....	83
4.3 Conclusions.....	91
4.4 Experimental.....	92
4.5 References.....	100
Chapter 5	103
5 Self-healing polyphosphonium ionic networks.	103

5.1	Introduction	103
5.2	Results and Discussion	105
5.2.1	Synthesis and characterization of the polyphosphonium.....	105
5.2.2	Preparation and characterization of ionic networks	106
5.2.3	Rheological and mechanical properties.....	113
5.2.4	Self-healing.....	116
5.3	Conclusions.....	118
5.4	Experimental.....	119
5.5	References.....	123
Chapter 6		125
6	A Phosphorus-rich polymer as a homogeneous catalyst scavenger	125
6.1	Introduction	125
6.2	Results and Discussion	126
6.2.1	Metal scavenging with polymers from primary di-phosphine 6.1.....	126
6.2.2	Polymer Network Metal scavengers from PH_3	131
6.3	Conclusions.....	134
6.4	Experimental.....	134
6.5	References.....	139
Chapter 7		141
7	Conclusions and Future work	141
7.1	Conclusions.....	141
7.2	Future work.....	143
7.2.1	Antibacterial surfaces with accessible zwitterions	143
7.2.2	Solution based antibacterial agents.....	143
7.2.3	Smart Materials	144
7.2.4	Phosphane-ene metal scavengers	146
7.3	References.....	146
Appendix		147
8	Appendix	147
8.1	American Chemical Society's Policy on Theses and Dissertations	147
8.2	Supplementary Information for Chapter 2	148
8.2.1	References	151
8.3	Supplementary Information for Chapter 3	153

8.3.1	References	166
8.4	Supplementary Information for Chapter 4	167
8.5	Supplementary Information for Chapter 5	177
8.6	Supplementary Information for Chapter 6	188
8.6.1	References	192
Curriculum Vitae		193

List of Tables

Table 2-1: Effect of film formulation on accessible surface charge, as measured by fluorescein exchange.....	27
Table 2-2: Properties of coatings prepared from 47.5 wt% of (2.1), 47.5 wt% (2.2), and 5 wt% (2.3) under air or N ₂ atmospheres.....	29
Table 3-1: Summary of the polyphosphonium prepared for this study as well as their molar mass characteristics and thermal properties.....	46
Table 3-2: Summary of the composition and properties of polyphosphonium SIPNs.	48
Table 4-1: MIC and MBC values for polyphosphonium and their corresponding monomers. All concentrations correspond to the concentration of phosphonium ion.	84
Table 4-2: Selected MIC and HC ₅₀ values for previously reported amphiphilic antibacterial polymers. Concentrations correspond to the concentrations of cations.....	91
Table 5-1: Summary of the tensile properties of PAA/5.1-P networks.	116
Table 6-1: Sequestration of GI from RCM of 6.5. ^a	130
Table 6-2: Regeneration of metal free 6.2 from 6.2-Ru.	131
Table 6-3: Sequestration of GI from RCM of 6.5.....	133

List of Figures

Figure 1-1: Representation of the chain-growth and step-growth polymerization mechanisms.....	3
Figure 1-2: Free radical polymerization processes: initiation, propagation, and termination. .	3
Figure 1-3: RAFT, ATRP, and NMP reagents and radical adducts.....	4
Figure 1-4: Mechanism of RAFT polymerization.	6
Figure 1-5: The components of a RAFT agent and common Z and R substituents.....	7
Figure 1-6: Commercially available photoinitiators.	9
Figure 1-7: Jablonski diagram depicting common photochemical processes with HDMAP. 10	
Figure 1-8: Schematic diagram of main-chain and side-chain functional groups.	11
Figure 1-9: Examples of side-chain (1.8-1.10) and main-chain (1.11) phosphonium polymers.....	12
Figure 1-10: Copolymer, di-block copolymer, ABA tri-block copolymer, and metallo-phosphonium block copolymers used as precursors for functional materials.	13
Figure 1-11: Phosphonium polymer derivatives and their relative antibacterial activities against <i>S. aureus</i>	14
Figure 1-12: Antibacterial phosphonium-functionalized materials.	15
Figure 1-13: Phosphonium-based ionically cross-linked networks from polyphosphonium and small molecule anionic cross-linkers	16
Figure 1-14: Examples of previously reported and commercially available functionalized silica and polystyrene beads.....	17
Figure 2-1: Schematic showing the coating preparation process.....	26
Figure 2-2: AFM images following application of a diamond tip surface profiler with a 0.5 mN force to: a) a film cured in air and b) a film cured under N ₂	29
Figure 2-3: Antibacterial testing results for a surface containing 47.5 wt% of 2.1 and cured under N ₂	31
Figure 3-1: Schematic illustrating the incorporation of polyphosphonium into an SIPN.	43

Figure 3-2: ^1H NMR spectra (400 MHz, D_2O) of a) The 3.1 polymerization mixture prior to polymerization; b) Unpurified 3.1-P-40k polymerization mixture at 81% conversion; c) Purified 3.1-P-40k.....	46
Figure 3-3: DSC curves for 3.2-P-10k, an SIPN prepared using 10 wt% of 3.2-P-10k, and an SIPN prepared from TEGDA without polyphosphonium.. ..	50
Figure 3-4: SIPN activity versus a) <i>S. aureus</i> and b) <i>E. coli</i> in the dynamic contact antibacterial test.	53
Figure 3-5: Control and SIPN surfaces following Live/Dead® analysis after incubation of the surfaces in a suspension of 10^7 CFUs/mL of <i>S.aureus</i> for 24 hours.....	55
Figure 4-1: Example of hydrophilic-hydrophobic balance by charge-hydrophobic combination vs. separation.....	71
Figure 4-2: Examples of antibacterial polymers from β -lactams (left), heightened potency of antibiotics when used in conjunction with metabolites such as mannitol (middle), and antibacterial mannoside-derived glycosides (right).	72
Figure 4-3: Structure of proposed targeted phosphonium monomer.	73
Figure 4-4: $^{31}\text{P}\{^1\text{H}\}$ (top) and ^1H coupled ^{31}P (bottom) NMR spectra of an attempt at creating a tertiary phosphine from an allylether sugar resulting in a mixture of primary, secondary, tertiary, and oxidized products.	75
Figure 4-5: $^{31}\text{P}\{^1\text{H}\}$ NMR Spectra of the reaction mixtures for the resulting sugar functionalized primary phosphines 4.1.P and 4.2.P from α -allylether mannose (4.1) and α -allylether glucose (4.2).....	76
Figure 4-6: $^{31}\text{P}\{^1\text{H}\}$ NMR spectra of tertiary phosphines 4.1.T and 4.2.T from the reaction of 1-hexene with primary phosphines 4.1.P and 4.2.P, respectively.....	77
Figure 4-7: $^{31}\text{P}\{^1\text{H}\}$ NMR spectra of 4.3 and 4.4 from the quaternization of 4.1.T and 4.2.T with 4-vinylbenzyl chloride.	78
Figure 4-8: ^1H NMR spectrum of the polymerization of 4.3.....	79
Figure 4-9: ^1H NMR spectrum of the polymerization of 4.4.....	80
Figure 4-10: ^1H NMR spectra of the deprotection of 4.5 to 4.5-d.....	81
Figure 4-11: ^1H NMR spectra of the deprotection of 4.6 to 4.6-d.....	82
Figure 4-12: Synthesis of a control polymer 4.8 with hydroxypropyl substituents on the phosphonium.....	83

Figure 4-13: Growth of <i>E. coli</i> at different concentrations of phosphonium polymers.....	85
Figure 4-14: Growth of <i>S. aureus</i> at different concentrations of A) polymers 4.5-d and 4.6-d; B) polymer 4.8.	86
Figure 4-15: A. log(concentration) plotted against its % hemolysis to determine approximate HC ₅₀ values by the intersection with the black line.....	89
Figure 5-1: SEM-EDX analyses of ionic networks: A.	108
Figure 5-2: Swelling in weight % of polymer networks at different NaCl concentrations. .	113
Figure 5-3: Comparison of the rheology frequency sweep data of PAA/5.1-P networks. ...	114
Figure 5-4: Tensile properties of PAA/5.1-P networks and a sample showing the dog bone structure used in accordance with ASTM D638 14.	116
Figure 5-5: Digital images of a PAA>5.1-P network damaged by a 0.5 mm diameter hole self-healing over 24 hours in 0.1 M NaCl.....	117
Figure 5-6: Tensile properties of PAA/5.1-P networks prior to and after healing in 0.1 M NaCl following complete severing of the sample.....	118
Figure 6-1: Consumption of styrene (1) by hydrogenation with WI without additive (x) and with 6.2 (16 g/mmol Rh) added at the outset of reaction (■).	128
Figure 6-3: ³¹ P{ ¹ H} NMR spectroscopy of 6.7 and 6.8 composing of primarily tertiary phosphines.....	133
Figure 7-1: Left: Switchable antibacterial-antifouling surface based on acid catalyzed ring opening to produce carboxy betaine; Right: Accessible antibacterial-antifouling phosphonium using a phosphonium-thiolate zwitterion.	143
Figure 7-2: Proposed sugar containing phosphonium monomers containing different sugars including β-D-mannose and α/β-D-galactose, and β-D-glucose to determine the effect of the anomeric conformation; 7.2 represents a tri-sugar-substituted phosphonium monomer.	144
Figure 7-3: Ionically cross-linked networks for small molecule release.	145
Figure 7-4: Proposed UV curable polymer network possessing ionic cross-linking for self- healing.....	146

List of Schemes

Scheme 1-1: Examples of RAFT agent modification to afford terminal functional groups on the polymer ⁷	7
Scheme 1-2: Step-growth radical thiol-ene polymerization.	8
Scheme 3-1: Synthesis of phosphonium monomers and polymers.	44
Scheme 4-1: Overall synthetic approach for producing 4.3 and 4.4 from α -allylether sugars 4.1 and 4.2, respectively.	73
Scheme 4-2: Deprotection of the polymers 4.5 and 4.6 with sodium methoxide to yield 4.5-d and 4.6-d.	81
Scheme 4-3: Deprotection procedure for monomers 4.3 and 4.4 to yield 4.3-d and 4.4-d.	82
Scheme 5-1: Synthesis of the polyphosphonium and their combination with PAA to form ion pairs.	105
Scheme 6-1: Loading the Soft Polymer Network (6.2) with Wilkinson's catalyst (W1) to give 6.2-Rh.	127
Scheme 6-2: Hydrogenation of styrene (6.3) with Wilkinson's catalyst (W1) and with scavenger 6.2 added at the outset of reaction.	128
Scheme 6-3: RCM of 6.5 with GI followed by sequestration of the catalyst with 6.2, 6.7, and 6.8.	128
Scheme 6-4: Synthesis of PH ₃ containing networks with TTT (6.8) and TEGDAE (6.7). ...	132

List of Appendices

8	Appendix	147
8.1	American Chemical Society's Policy on Theses and Dissertations	147
8.2	Supplementary Information for Chapter 2	148
8.2.1	References	151
8.3	Supplementary Information for Chapter 3	153
8.3.1	References	166
8.4	Supplementary Information for Chapter 4	167
8.5	Supplementary Information for Chapter 5	177
8.6	Supplementary Information for Chapter 6	188
8.6.1	References	192

List of Abbreviations

ω_c	frequency
$^\circ$	degree
$^\circ\text{C}$	degrees celsius
Φ_r	quantum yield
ϵ	extinction coefficient
μg	microgram
μL	microliter
μM	micromolar
λ_{max}	maximum absorbance wavelength
3D	three dimensional
ATCC	American type culture collection
ASTM	American society for testing materials
ATRP	atom transfer radical polymerization
AFM	atomic force microscopy
AIBN	azobisisobutyronitrile
BAPO	phenylbis(2,4,6-trimethylbenzoyl)phosphine oxide
cm	centimeter
CFU	colony forming unit
CTA	chain transfer agent
\bar{D}	dispersity
DEPA	diethyl phosphoramidate
DMPA	2,2-dimethoxy-2-phenylacetophenone
DMF	N,N-dimethylformamide
DSC	differential scanning calorimetry
DMSO	dimethylsulfoxide
<i>E.coli</i>	Escherichia coli
FBS	fetal bovine serum
g	gram
G''	viscous modulus
G'	elastic modulus
GC-FID	gas chromatograph free induction decay
Hz	Hertz
HDMAP	2-hydroxy-2,2-dimethyl-acetophenone
HCPK	1-hydroxycyclohexylphenyl ketone
IC	internal conversion
ISC	intersystem crossing
ICP-MS	inductively coupled plasma mass spectrometry
kPa	kiloPascals
kHz	kiloHertz
kg	kilogram
L	litre
MTT	3-(4,5-dimethylthiazol-2-yl)-2,5-diphenyltetrazolium bromide

MHz	megaHertz
mg	milligram
mL	milliLiter
mm	millimeter
M_w	weight average molecular weight
M_n	number average molecular weight
M_i	mass of the <i>i</i> th fraction
M	molar
MeOH	methanol
mM	millimolar
NMR	nuclear magnetic resonance
N_i	number of the <i>i</i> th fraction
nm	nanometer
NMP	nitroxyl mediated polymerization
Oz/in	ounce per inch
PAA	poly(acrylic acid)
PAH	poly(allylamine hydrochloride)
PEO	poly(ethylene oxide)
PET	poly(ethylene terephthalate)
PBS	phosphate buffered saline
Pa	Pascals
PS	polystyrene
rad/s	radians per second
RAFT	reversible addition fragmentation chain transfer
RCM	ring closing metathesis
SEC	size exclusion chromatography
SEM-EDX	scanning electron microscope energy dispersive x-ray
<i>S.aureus</i>	staphylococcus aureus
SYTO 9	green fluorescent nucleic acid stain
SDS	sodium dodecyl sulfate
SIPN	semi interpenetrating network
T1	triplet state
TEGDA	tetraethyleneglycol diacrylate
TEGDAE	tetraethyleneglycol diallylether
TGA	thermogravimetric analysis
T_g	glass transition
T_o	onset decomposition temperature
TON	turnover number
TMEDA	tetramethylenediamine
THF	tetrahydrofuran
TTT	1,3,5-triallyl-1,3,5-triazine-2,4,6(1 <i>H</i> ,3 <i>H</i> ,5 <i>H</i>)-trione
UV	ultraviolet
UATR	universal attenuated total reflectance mode
VR	vibrational relaxation
Wt%	weight percent
WCA	water contact angle

Chapter 1

1 Introduction

1.1 Materials chemistry introduction and background

Materials chemistry can be defined as understanding the relationship of the atoms, molecules, or polymers that a material is composed of, and how they affect the resulting bulk properties.¹ A material is defined as a solid-state component or device that was used, currently used, or could be used to address a societal need.¹ Historically, materials used to create devices were naturally occurring, such as bone, wood, and solid mineral aggregates. As science advanced so did the manipulation of the components to create materials that either performed a task more efficiently or solved a specific problem. Polymers were discovered in the late 19th century and progressed slowly until the 1930s, at which point there was a shortage of natural rubber. This was also when the concept of polymers was introduced by Staudinger. Poly(vinyl chloride) and polyphosphazene were among the first polymers produced as replacements for natural rubber.² This brought about the first uses of synthetic materials composed of polymers.¹

Synthetic materials progressed with the discovery of polyamides (e.g., Nylon), poly(ethylene terephthalate) (PET), and polyurethanes, all of which are still used today. These discoveries resulted in synthetic materials such as fibers, protective coatings, plastics and elastomers. Materials produced from polymers can be divided into two categories: thermoplastics and thermosets.¹ Thermoplastics are composed of linear or branched polymers and can be melted, extruded, and annealed into desired shapes, whereas thermosets are composed of cross-linked linear polymers that do not possess melt temperatures, and therefore cannot be processed after production.

1.1.1 Functional Materials – Advancing current societal demands

The functionalization and derivatization of molecules and materials forms the basis for materials science, and has evolved into a discipline of its own. Utilization of chemistry to add desirable chemical or physical characteristics to tailor materials for a specific function is the basis of material progression. Fundamental knowledge of molecules and their chemical

and physical properties can be utilized to manipulate macromolecules (i.e., polymers) including their chemical and physical characteristics such as elasticity, viscosity, melting temperature, glass transition, and crystallization. These polymer characteristics directly affect the material that it comprises.¹ An alternative way to functionalize materials is the use of additives to impart desired properties such as increased hardness, flame-retardancy, pigmentation, or adhesion, and is a popular method for tuning photopolymer network properties.³⁻⁶

1.2 Polymerization

1.2.1 Basics of polymerization

Polymers are macromolecules composed of smaller repeating units.⁷ Initially, polymers were composed of organic components with carbon backbones but have progressed to include a wide array of elements of the periodic table. Examples containing main group compounds such as boron, silicon, phosphorus, sulfur; and metals have been known for some time but their potential for many different applications has only been realized since the late part of the 20th century.^{8,9}

1.2.1.1 Chain-growth vs step-growth

Polymers are created in one of two ways: by chain-growth or step-growth mechanisms.^{7,10} In a chain-growth mechanism, monomers are added sequentially to a propagating chain. Chain-growth results in high molecular weight molecules early in the reaction mixture, with monomeric species still present. Typical polymerization techniques that utilize chain-growth are ionic, ring opening, and free radical. A step-growth mechanism requires a di-functional monomer and initially result in a large concentration of dimers. These dimers then combine to become tetramers, and this process repeats until the final stages of conversion where high molecular weight species are formed (Figure 1-1).

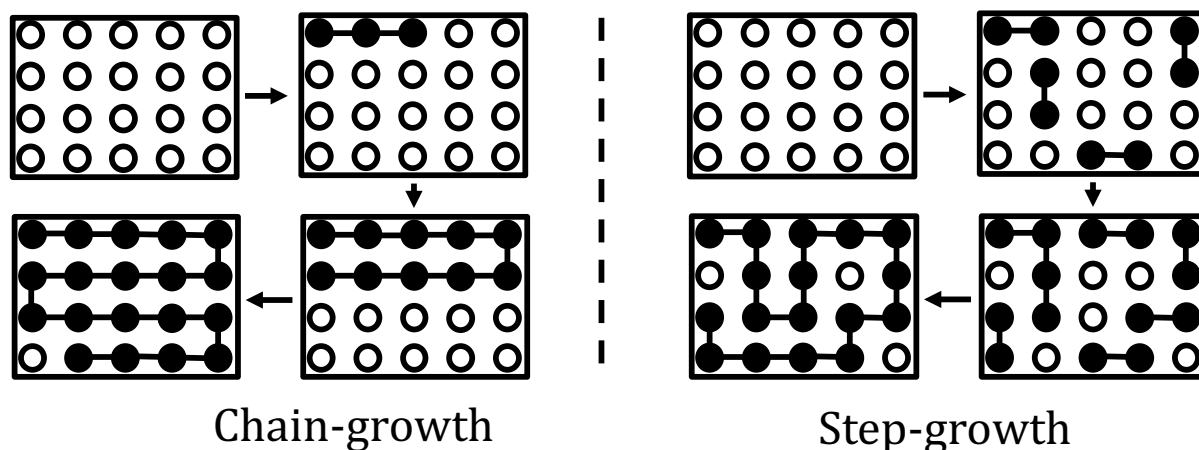


Figure 1-1: Representation of the chain-growth and step-growth polymerization mechanisms. Chain-growth involves the attachment of monomers to a growing polymer chain. Step-growth creates dimers, which combine to create tetramers, and this process is repeated until high molecular weight species are formed.

1.2.2 Radical polymerization

1.2.2.1 Chain-growth radical polymerizations

Radical chain-growth polymerizations have typically been used in polymerizing olefins such as acrylates, styrenes, and acrylamides, that can be transformed into stable radical intermediates (Figure 1-2).¹¹ C-C bond forming radical polymerizations typically create stable backbones and are the most popular type of chain-growth polymerization.

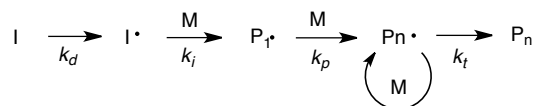


Figure 1-2: Free radical polymerization processes: initiation, propagation, and termination.

The disadvantage of chain-growth free radical polymerization is the lack of control of molecular weight distribution (or the polymers dispersity), due to unwanted termination processes such as radical combination, and disproportionation. Molecular weight distribution is important because it can affect the resulting properties of the polymer, such as antibacterial activity, which will be discussed later in this chapter. Molecular weight distributions are reported as Dispersities (\mathfrak{D}), and are calculated by M_w/M_n where M_n is the

number average molecular weight, and M_w is the weight average molecular weight. M_n and M_w are the two most commonly used molecular weight values to calculate the average molar mass. The equations defining M_n and M_w are as follows:

$$M_w = \frac{\sum M_i^2 N_i}{\sum M_i N_i} \quad M_n = \frac{\sum M_i N_i}{\sum N_i} \quad \mathfrak{D} = \frac{M_w}{M_n} \quad (\text{Eq. 1.1})$$

Where N_i is the number of moles of a polymer molecule (i) and M_i is its molar mass. M_n is therefore the total mass of all the polymer molecules divided by the number of molecules. M_w puts more emphasis on the larger molecular weights, weighting the distribution in terms of their molecular weight instead of just the number of polymers. M_w is always greater than M_n and therefore \mathfrak{D} will always be ≥ 1 , with low dispersity typically defined as ≤ 1.1 . To avoid large molecular weight dispersities, reagents that reversibly combine with propagating radicals to allow control over the polymerization have been developed. The most commonly used types of controlled radical polymerizations include reversible addition fragmentation chain transfer (RAFT),^{12,13} atom transfer radical polymerization (ATRP),¹⁴ and nitroxyl mediated polymerization (NMP)¹⁵ (Figure 1-3).

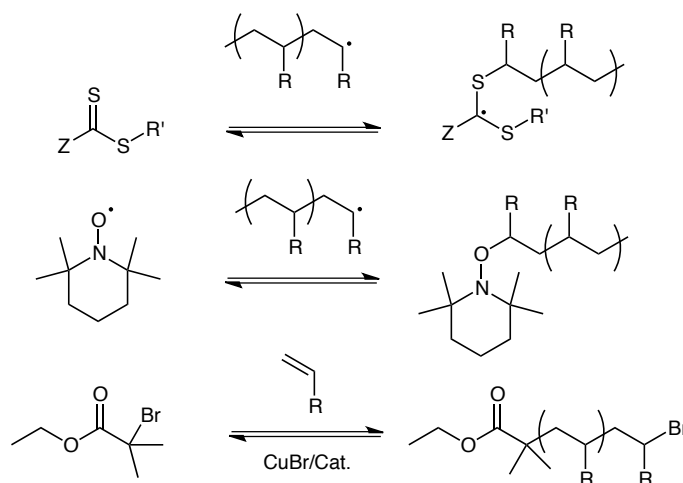


Figure 1-3: RAFT, ATRP, and NMP reagents and radical adducts.

ATRP requires a specific reagent containing a bromine-carbon bond, copper and a catalyst, whereas NMP requires a nitroxyl based molecule. RAFT polymerization utilizes chain-transfer reactions to induce control. All of these controlled polymerization approaches utilize the concept of reversibly forming a dormant species from the propagating radical, thereby

minimizing the free radical concentration and consequently the termination reactions. Each controlled living polymerization has its benefits, but RAFT polymerization will be the focus for the remainder of this thesis.

1.2.2.2 RAFT controlled living polymerizations

RAFT polymerizations utilize either dithioesters or thiocarbonylthio functionality and have the ability to combine with propagating radical species using a chain-transfer mechanism with resulting control over polymer molecular weight and dispersity. The RAFT controlled polymerization mechanism is as follows (Figure 1-4): Typical thermal radical polymerization initiators such as azobisisobutyronitrile (AIBN) provide a flux of radicals and propagation ensues; propagating radical species then undergo reversible chain-transfer with the RAFT reagent (**1.1**) to produce an intermediate **1.2**; Release of the R substituent produces a macroRAFT agent **1.3** and a radical species able to undergo initiation and polymerization to produce a propagating polymer chain (P_m^\bullet); **1.2** can then undergo further chain-transfer with P_m^\bullet to produce **1.4**, a chain equilibrium stage that contains both polymer chains, and both have the ability to undergo release and propagation.¹³ Termination sequences are reduced with RAFT due to a low concentration of propagating polymers in solution, due to **1.4** being the dominant species. This reduces large increases in molecular weight that otherwise result from combination of propagating polymers.

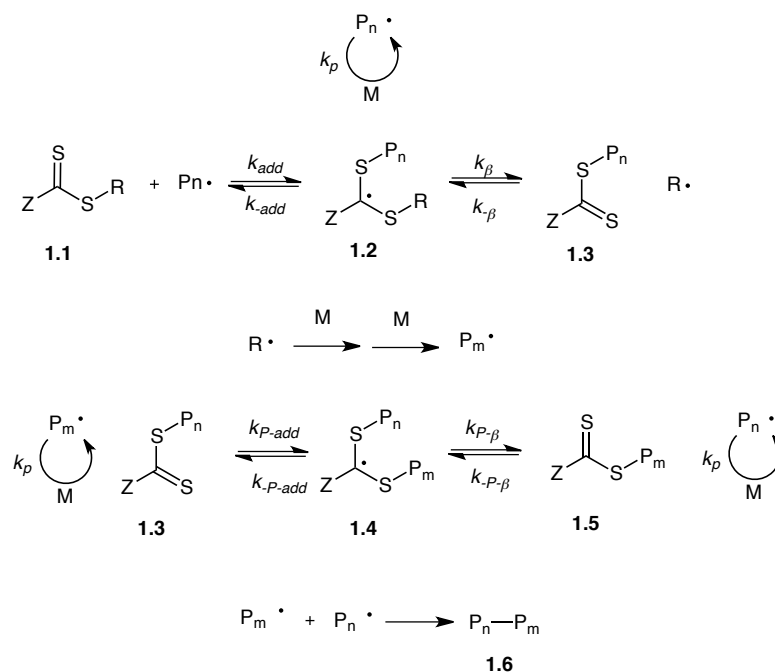


Figure 1-4: Mechanism of RAFT polymerization.

1.2.3 RAFT agent Z and R substituent effects^{12,13}

The reactivity of the RAFT agent can be tuned by changing the R and Z substituents (Figure 1-5).^{12,13} This is advantageous for tuning the RAFT agent's chain equilibrium, and is important when utilizing different types of polymerizable monomers. The rate of addition (k_{add}) to produce chain equilibrium species (Figure 1-4, **1.2**) must be slower than the rate of homolytic cleavage of the R group ($k_{\beta} > k_{add}$), otherwise polymeric chains may be irreversibly trapped, preventing further polymerization. The intermediate (Figure 1-4, **1.4**) should have a partition coefficient similar to R ($k_{P-\beta} \geq k_{P-add}$), to ensure release of polymer chains for propagation will happen. The choice of Z group is also important for adjusting the rate of addition to the C=S bond (k_{add} and k_{P-add}) and rate of fragmentation (k_{β} and $k_{P-\beta}$). Incorporation of aryl, alkyl, or *S*-alkyl Z groups increases the rate of addition to the C=S bond, while incorporation of *O*-alkyl and *N-N*-dialkyl Z groups decreases the rate of addition, which allows the RAFT agent to be tuned for different polymerizable monomers (Figure 1-5).

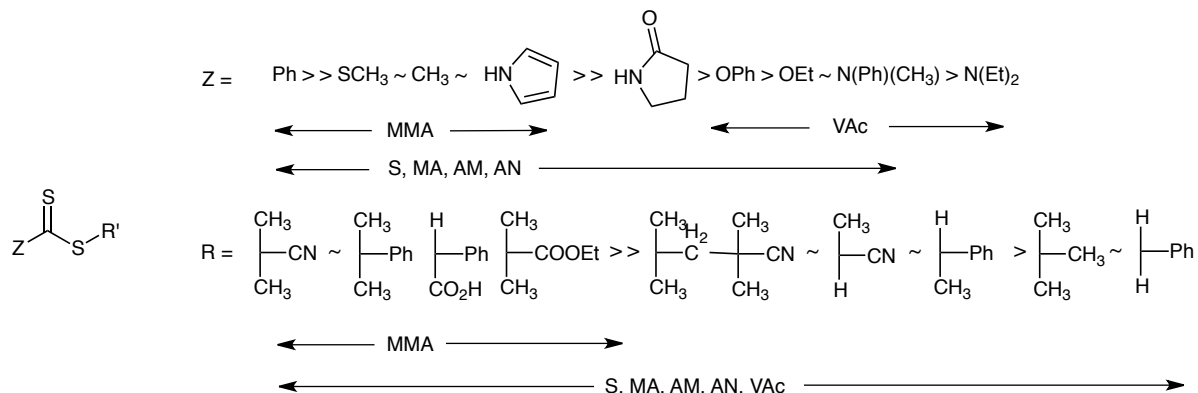
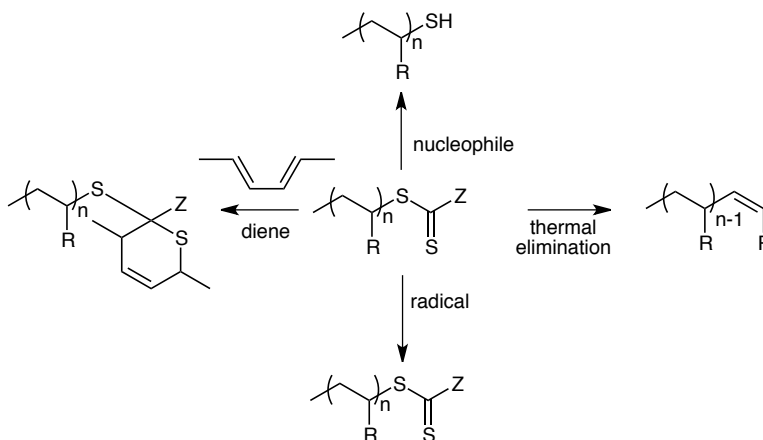


Figure 1-5: The components of a RAFT agent and common Z and R substituents guidelines that can be used with different polymerizations. MMA = methyl methacrylate, S = styrene, MA = methyl acrylate, AM = acrylamide, AN = acrylonitrile, VAc = vinyl acetate.¹³

RAFT polymerization also results in polymer chains being capped with the RAFT agent. These end capped polymers can be used as macroRAFT agents to create di-block or tri-block copolymers, or cleaved to result in thiol or vinyl functionalities (Scheme 1-1).^{16,17} This functionality on the product can be useful for further reactivity with small molecules, other polymers, or conjugation to solid substrates or surfaces.



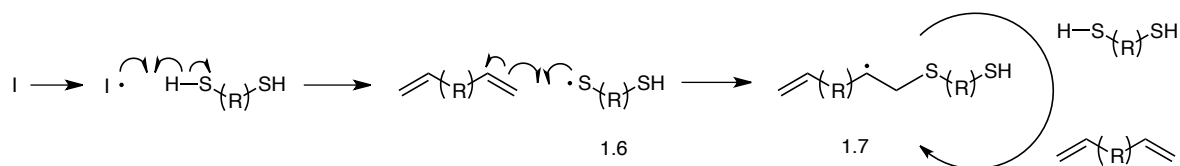
Scheme 1-1: Examples of RAFT agent modification to afford terminal functional groups on the polymer.¹⁷

The versatility of RAFT in many different solvents and conditions has been reported. Polymerization conditions can affect the RAFT agent performance, although even high

pressure (>5 kbar), and high temperature (140 °C) have been reported to provide polymerization control.¹³

1.2.4 Step-growth radical polymerization

Step-growth polymerizations can be performed with a wide range of functional groups including esters, alcohols, isocyanates, amines, and acid chlorides, but in the area of main group chemistry a particularly noteworthy example is the use of di-thiol monomers and di-allyl monomers (Scheme 1-2).¹⁸⁻²⁰ This is commonly referred to as “thiol-ene” chemistry.



Scheme 1-2: Step-growth radical thiol-ene polymerization.

This polymerization process results from initiation of a radical source, abstraction of a hydrogen from the thiol, producing a thiyl radical that can then add to the allyl monomer, resulting in a secondary carbon radical. This radical can then abstract a hydrogen from another thiol, repeating the process, and propagating S-H addition across the olefins. The analogous phosphorus chemistry, phosphane-ene photopolymerization, has also been used for creating functional phosphorus containing materials.^{21,22}

1.2.5 Photopolymerization

1.2.5.1 The basics photoinitiation

Photopolymerization involves the use of light to initiate polymerization.^{23,24} The advantage of photoinitiation is the spatial control, the speed, and the efficiency of the polymerization. The efficiency of photoinitiation to create radical species is defined by the quantum yield (Φ_r) of the photochemical process.²³ This is defined by the following equation:

$$\frac{\# \text{ of reactions}}{\# \text{ absorbed photons}} = \Phi_r \quad (\text{Eq. 1.2})$$

The maximum yield is 1, and would correspond to all absorbed photons resulting in the desired chemical process. In this case the chemical process is an α -cleavage reaction,

resulting in two radical species. Polymerizations typically use a photoinitiator to start polymerization, although some scenarios do not require them.²⁵ Most commercially available unimolecular photoinitiators possess an acetophenone functionality that absorbs in the UV range of the spectrum between 300-400 nm (Figure 1-6).²⁶⁻²⁸

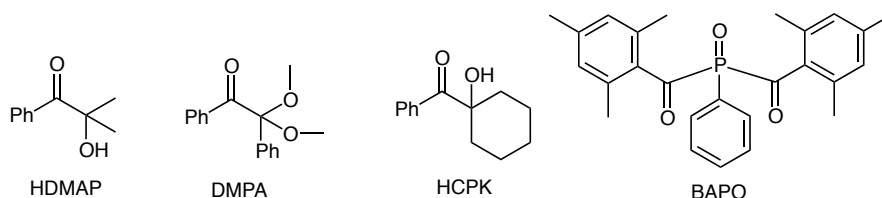


Figure 1-6: Commercially available photoinitiators: HDMAP = 2-hydroxy-2-dimethyl acetophenone, DMPA = 2-dimethoxy-2-phenyl-acetophenone, HCPK = 1-hydroxycyclohexylphenyl ketone, BAPO = phenylbis(2,4,6- trimethyl benzoyl)phosphine oxide.

Excitations from $n-\pi^*$ or $\pi-\pi^*$, shown in Figure 1-7, are the two relevant excitation processes that occur in acetophenone photoinitiators.²⁷ The initiation relies on the excited molecule undergoing the correct sequence of vibrational relaxation (VR), internal conversion (IC), and intersystem crossing (ISC) from the excited state to result in α -cleavage and is best described using a Jablonski Diagram, with the example of 2-hydroxy-dimethyl-acetophenone (HDMAP) (Figure 1-7). This is an example of a photoinitiator that undergoes α -cleavage from an excited triplet state (T1) to produce two radical species, the benzoyl radical being the dominant initiating species.²⁷

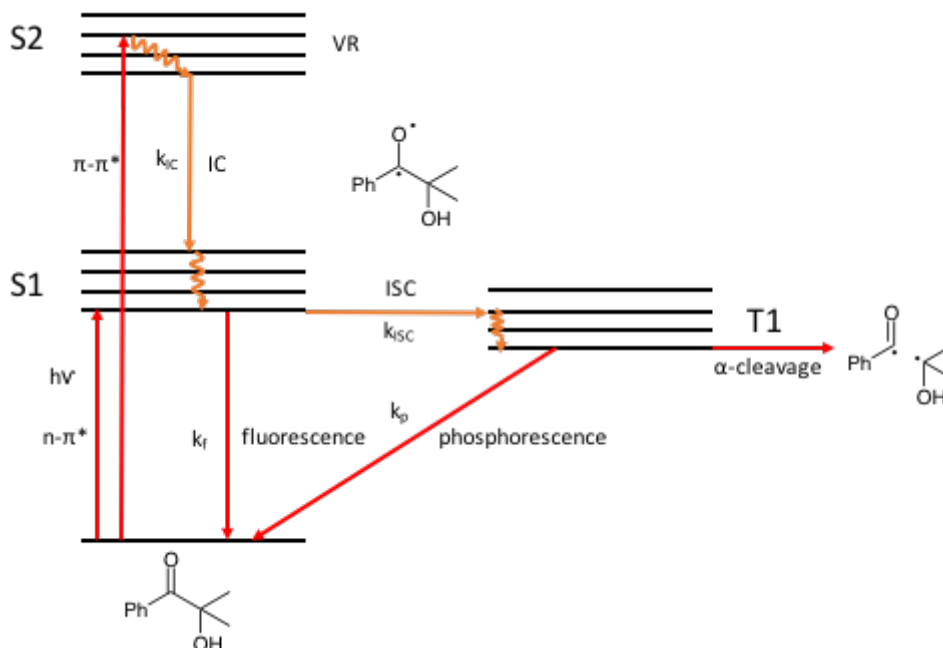


Figure 1-7: Jablonski diagram depicting common photochemical processes with HDMAP, resulting in α -cleavage and radical species.

1.2.6 Photopolymer (UV cured) networks

Polymer network formation can be completed using photoinitiation of liquid formulations to create solid thermoset materials.²⁹ The process is advantageous due to the speed of the reaction, the solvent free process, spatial control over polymerization, and a lower energy footprint compared to thermal methods. Photopolymerization is used in electronic integrated circuitry and wiring boards manufacturing, dental materials, 3D printing, coatings and surface modifications.³⁰ Commercially available additives for photopolymer networks are available for coating modification to provide pigments or impart properties such as scratch resistance, adhesion, or hardness.⁶ These coatings are primarily used for protection of the surface, and do not provide further function.

Photopolymerization of liquid formulations can utilize chain-growth or step-growth mechanisms using multifunctional monomers.³¹ Multifunctionality results in cross-linking of linear chains, effectively increasing the molecular weight to the point of insolubility. The light intensity and penetration, irradiation time, oxygen concentration, viscosity, and initiator concentration all affect the efficiency of the polymerization procedure.²⁹ Most radical

reactions in solvent require oxygen free environments, but often photopolymerization can proceed without the need for an inert atmosphere due to limited oxygen diffusion beyond the surface, resulting in bulk polymerization but incomplete surface curing. This can be overcome by utilizing an N₂ atmosphere or additives to reduce oxygen quenching. It is useful to note that photopolymerization using thiol-ene chemistry can be completed in the absence of a photoinitiator. It is not inhibited completely by oxygen, but rather proceeds at a slower rate in the presence of oxygen.²⁵

1.3 Phosphorus-based materials and selected applications of these materials

1.3.1 Functional materials containing phosphorus

Phosphorus has been incorporated into polymers as both a side-chain and main-chain functionality. Side-chain functionalities refer to pendant phosphonium atoms on an organic backbone, whereas main-chain functionalities incorporate phosphorus atoms in the backbone (Figure 1-8).

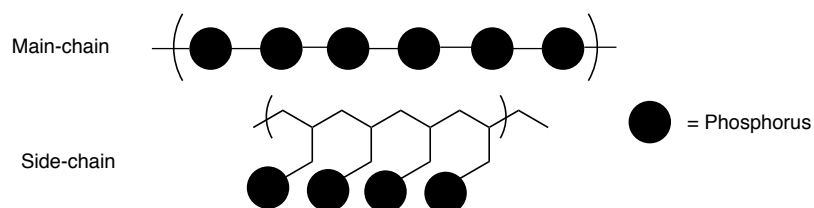


Figure 1-8: Schematic diagram of main-chain and side-chain functional groups.

Phosphorus in the following examples will be limited to phosphine or phosphonium ions in the +3 or +5 oxidation state, respectively. Main-chain phosphonium polymers have been prepared utilizing a step-growth mechanism (Figure 1-9, **1.11**),³² and side-chain examples of phosphonium polymers with P-N substituents have also been reported (Figure 1-9, **1.10**).³³ Many of the side side-chain phosphonium polymers incorporate trialkyl phosphoniums. Typically, phosphonium monomers are prepared by a simple quaternization reaction, with an alkyl halide or benzyl halide, producing polymerizable monomers, and resulting in polymers such as in Figure 1-9 compounds **1.8** and **1.9**.³⁴⁻³⁸

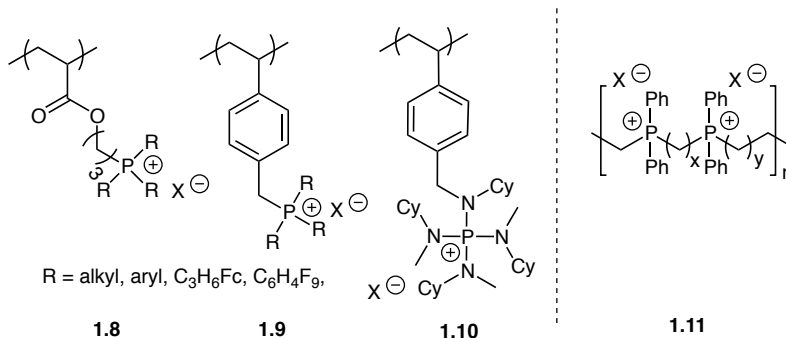


Figure 1-9: Examples of side-chain (1.8-1.10) and main-chain (1.11) phosphonium polymers.

Select examples of higher order phosphonium polymers involved in different applications are outlined in Figure 1-10, including co-polymers for non-viral gene delivery (**1.12**),³⁹ ABA-triblock copolymers for fuel cell membranes (**1.13**),⁴⁰ phosphonium/metallic block copolymers to produce inorganic metallic materials (**1.14**),⁴¹ and the production of gold nanoparticles in polymer networks (**1.15**).⁴² Phosphonium containing materials have also been used in applications as part of functional membranes for CO_2 capture, desalination, anion exchange,⁴³⁻⁴⁷ carbon nanotube dispersants,⁴⁸ supramolecular assemblies and ionic cross-linked networks,⁴⁹⁻⁵² and for antibacterial activity.⁵³⁻⁵⁸ Phosphonium polymers are often compared to ammonium analogues for many applications, with the ammonium analogues dominating the literature. This is most likely due to the air sensitive properties of the phosphorus starting materials compared to those of analogous amines. This is especially apparent for antibacterial applications, where most work has focused on polyammonium.⁵⁹⁻⁶⁶

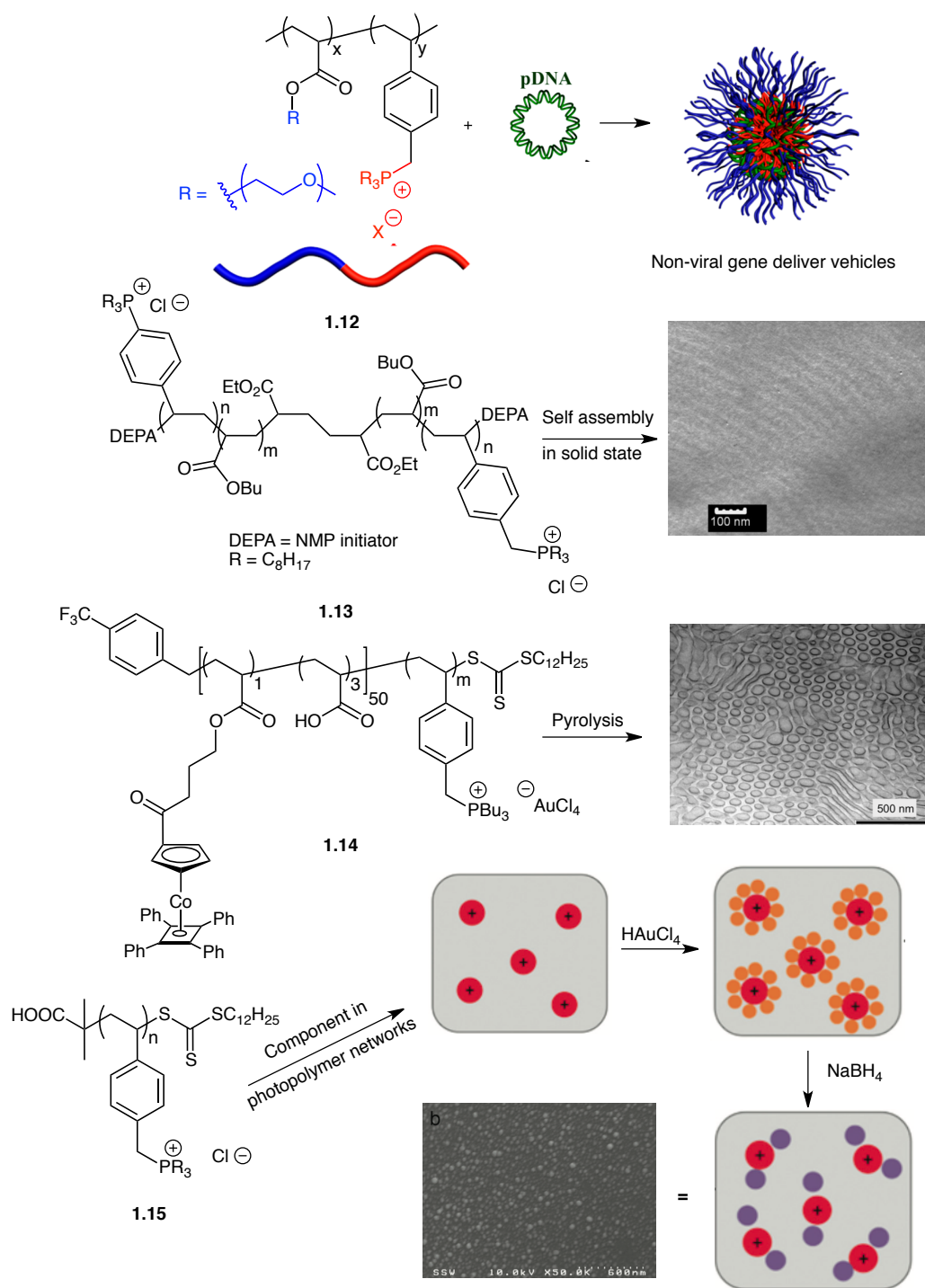


Figure 1-10: Copolymer, di-block copolymer, ABA tri-block copolymer, and metallo-phosphonium block copolymers used as precursors for functional materials.

1.3.2 Phosphonium polymers as antibacterial agents and their application in antibacterial materials

Antibacterial polymers were discovered in 1965 with the discovery of polymers composed of 2-methacryloyloxypropionates,⁶⁷ while ammonium antibacterial polymers were first reported in the 1970's and early 1980's.^{68,69} In the early 1990's, Kanazawa and coworkers showed that phosphonium polymers were also active against bacteria, and performed better than the ammonium analogues.³⁶ Extensive studies were performed examining the activity of phosphonium monomers and polymers, as well as the effects of altering alkyl phosphonium substituent length,^{36,70} backbone to phosphonium spacer length,⁷¹ polymer molecular weight, phosphonium counter anion,⁷² phosphonium in the main-chain instead of side-chain,⁷³ copolymers with ammoniums,⁷⁴ and the functionalization of fibers and filters.^{53,54,75,76} The results from the antibacterial tests by Kanazawa and coworkers suggested that increasing the length of the alkyl substituent on the phosphonium increased the bactericidal activity. This has complications of increased hemolytic activity against non-bacterial cells, which was not initially reported, but was later reported.⁷⁷⁻⁸⁰ Increasing the length of one alkyl chain decreased the activity of the phosphonium polymer with respect to Gram-positive bacteria, and little activity was observed against Gram-negative bacteria. Anion exchange for a hydrophobic anion decreased the activity, while increasing the polymer molecular weight increased the activity. Changing the alkyl substituents on the phosphonium to octyl chains increased the activity compared to shorter butyl alkyl chains, and was the best performing phosphonium antibacterial polymer they reported (Figure 1-11).

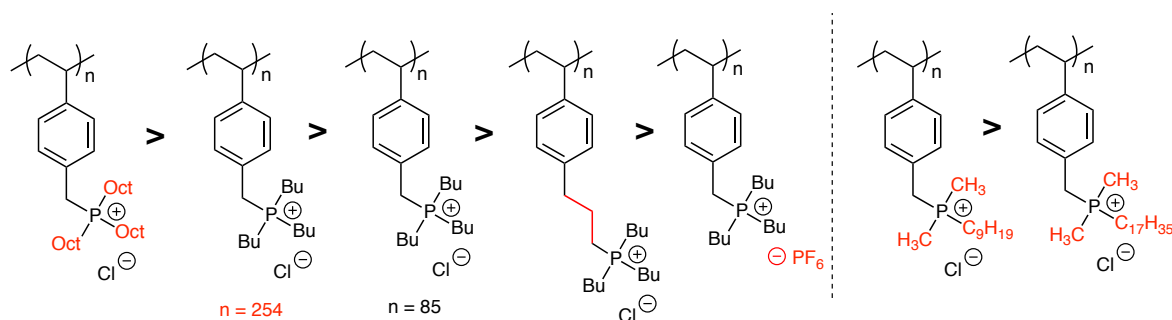


Figure 1-11: Phosphonium polymer derivatives and their relative antibacterial activities against *S. aureus*.

1.3.3 Antibacterial phosphonium-containing materials

With the knowledge that phosphonium polymers possess antibacterial activity, there have been attempts to use phosphoniums to introduce antibacterial activity into materials. Phosphonium additives have been used to impart antibacterial activity to filters (Figure 1-12, **1.16**),⁵⁴ fibers that release phosphonium biocides (**1.17**),⁷⁶ polystyrene beads (**1.18**),⁵⁷ rubber (**1.19**),⁵⁵ poly(butylene adipate) (**1.20**),⁸¹ and chitosan (**1.21**).⁵⁶

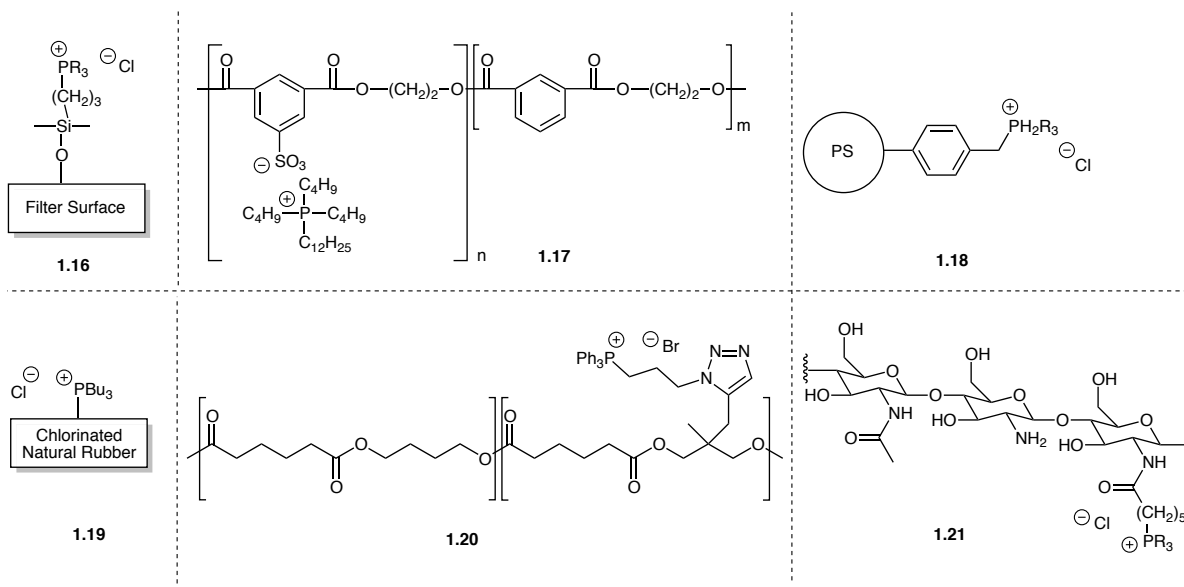


Figure 1-12: Antibacterial phosphonium-functionalized materials.

1.3.4 Ionic networks

A recent alternative to covalently cross-linked polymer networks is the creation of materials that have reversible cross-links that can undergo dynamic processes in response to an external stimulus, and that can repair damage or possess shape memory effects.^{82–86} Examples of these types of cross-links are hydrogen bonds,⁸⁷ disulfide bonds,⁸⁸ Diels-Alder adducts,⁸⁹ metal coordination,⁹⁰ and ionic bonds.⁹¹ These materials are typically made up of linear polymers that can undergo some chemical process to cross-link the materials and achieve thermoset properties. They are also able to revert back to thermoplastic materials by addition of some stimulus that breaks the cross-links and results in material that can be processed, undergo dynamic damage repair, or revert to a memorized shape. Ionic networks are of interest because phosphonium supramolecular networks with tunable viscoelastic

properties have previously been reported based on phosphonium monomers and dimers combined with mono-, di-, tri-, and tetra anionic molecule,⁵² as well as polyanions.⁵¹ The combination of phosphonium polymers with mono- and di- acetate cross-linkers has also been reported.⁵⁰ In these studies, increasing the cross-linker functionality decreased the fluid-like character in a dehydrated state (Figure 1-13). Polycationic-polyanionic cross-linked networks have been well established, but so far this combination has not yet been reported using phosphonium polymers.

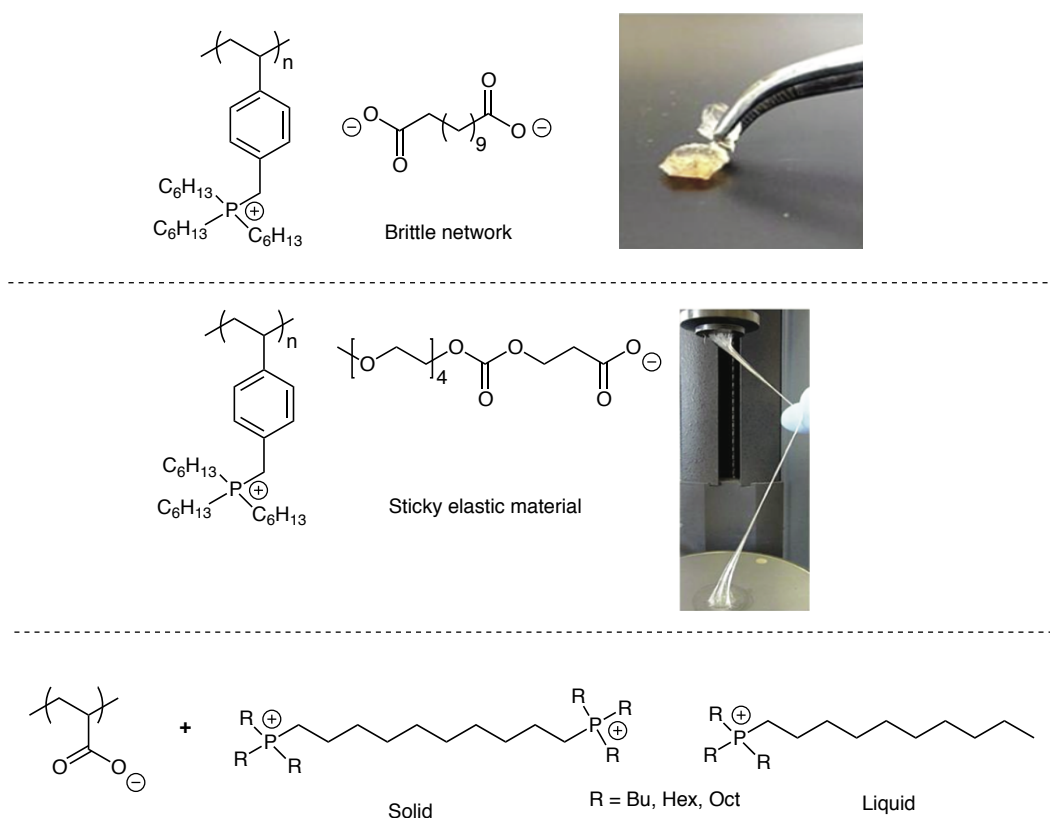


Figure 1-13: Phosphonium-based ionic cross-linked networks from polyphosphonium and small molecule anionic cross-linkers, as well as from polyacrylate and di- and mono- functional phosphoniums.

1.3.5 Metal scavenging materials

Metal removal from processes that utilize homogeneous catalysis can be problematic due to small remaining concentrations of metal that can be problematic in the production of

pharmaceuticals and electronics.⁹² Solid-supported metal scavengers have been reported and are currently available commercially for purification techniques that rely on insoluble materials that can be removed by filtration. Some examples of functionalized silica and polystyrene beads are outlined in Figure 1-14.

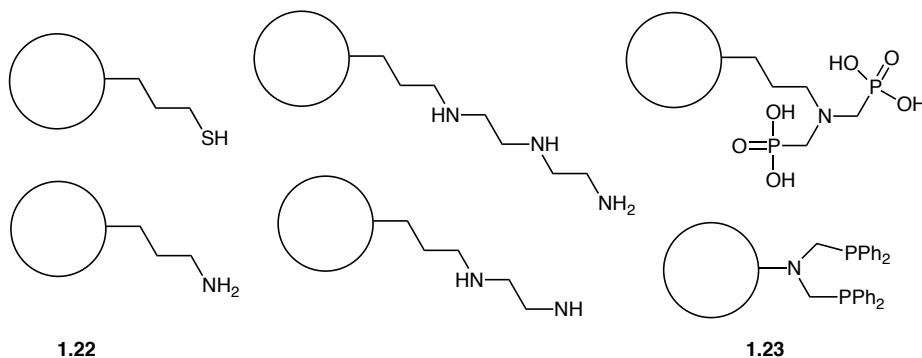


Figure 1-14: Examples of previously reported and commercially available functionalized silica and polystyrene beads.

The focus of metal scavenging applications will be on the removal of ruthenium-based catalysts. The performance of functionalized silica for metal scavenging has been reported for use on ring closing metathesis reactions of diethyl diallylmalonate using a Ruthenium catalyst (Grubbs 1), with a reported 88.88% reduction in metal concentration using amine functionalized silica (Figure 1-14, **1.22**).⁹² Metal scavengers based on insoluble phosphine-containing materials have been reported with similar functionalized polystyrene beads, with as high as 96% ruthenium removal (Figure 1-14, **1.23**).⁹³ Functionalized silica beads are also commercially available under the names Silicycle, Quadrapure™, and QuadraSil™, with reported > 99% ruthenium removal.⁹⁴⁻⁹⁶

1.4 Scope of Thesis

This dissertation focuses on the use of Phosphorus-containing molecules and polymers for use in material synthesis to impart specific functionality. Chapter 2 focuses on realizing the potential of phosphonium additives for UV cured materials to impart their known antibacterial properties into photopolymerized networks. Inclusion of phosphoniums into these networks was hypothesized to create surfaces with accessible phosphonium biocides that could interact with and kill bacteria. Synthesis, characterization, and bacterial

attachment was explored on these surfaces at different loadings of the phosphonium additive. The attachment of both *E. coli* and *S. aureus* to the surfaces was determined, and it was found that the resulting surfaces could resist the attachment of bacteria.

Chapter 3 focuses on creating UV cured surfaces with improved killing of bacteria in solution relative to those described in Chapter 2. We aimed to decrease the amount of additive by using trialkylphosphonium polymers with varied substituent alkyl chain lengths. These polyphosphonium were synthesized by RAFT polymerization. The effects of polymer molecular weight and phosphonium substituent alkyl chain length on the performance and surface characteristics of the photopolymer networks were studied.

Chapter 4 explores the idea of utilizing bacterial attachment, something that is generally undesirable for most antibacterial surfaces and materials, to increase bacterial killing in solution. It focuses on the synthesis and performance of phosphonium polymers with pendant sugars, specifically mannose, a molecule known to bind to *E. coli*, for increased interaction with the bacteria. The antibacterial activity against *E. coli* and *S. aureus*, as well the hemolytic activity against red blood cells were determined.

Chapter 5 describes the use of phosphonium polymers to create self-healing ionically cross-linked materials. Synthesis of high molecular weight polymers and their complexation with poly(acrylic acid) was performed to provide networks with different ratios of components. The rheology and tensile properties of the networks were determined and self-healing at low salt concentrations was demonstrated.

Chapter 6 focuses on the synthesis, characterization, and metal scavenging abilities of phosphine-based polymers that were prepared by a step-growth radical polymerization (phosphane-ene chemistry). Three different networks, two directly from PH_3 , and one from a previously reported air stable di-phosphines were prepared and studied.²¹ The synthesis, characterization, and ruthenium scavenging abilities were analyzed and compared to previously reported polymer networks and commercially available scavengers.

1.5 References

- 1) Fahlman, B. D. *Materials Chemistry*; Springer: New York, 2007.
- 2) Maiti, S.; Banerjee, S.; Palit, S. K. *Prog. Polym. Sci.* **1993**, *18*, 227–261.
- 3) Grigale-Sorocina, Z.; Kalnins, M.; Simanovska, J.; Vindedze, E.; Birks, I.; Brazdauska, E. *Proc. Est. Acad. Sci.* **2015**, *64*, 88–92.
- 4) Funke, W. *Additives for Coatings*; Bieleman, J.; WILEY-VCH Verlag GmbH & Co. KGaA: Weinheim, Germany, 2001; Vol. 41.
- 5) Chen, L.; Wang, Y. Z. *Materials* **2010**, *3*, 4746–4760.
- 6) Allnex. Industrial Coatings RADCURE. <http://allnex.com/industrial>.
- 7) Hiemenz, P. C. *Polymer Chemistry The Basic Concepts*; Marcel Dekker, Inc.: New York, New York, 1984.
- 8) Priegert, A. M.; Rawe, B. W.; Serin, S. C.; Gates, D. P. *Chem. Soc. Rev.* **2016**, *45*, 922–953.
- 9) Manners, I. *Synthetic Metal-Containing Polymers*; WILEY-VCH Verlag GmbH & Co. KGaA: Weinheim, Germany, 2003.
- 10) Odian, G. *Principles of Polymerization*; 4th ed.; John Wiley & Sons, Inc: Staten Island, NY, 2004.
- 11) Moad, G.; Solomon, D. H. *The Chemistry of Free Radical Polymerization*; Pergamon: Tarrytown, New York, 1995.
- 12) Keddie, D. J.; Moad, G.; Rizzardo, E.; Thang, S. H. *Macromolecules* **2012**, *45*, 5321–5342.
- 13) Moad, G.; Rizzardo, E.; Thang, S. H. *Aust. J. Chem.* **2005**, *58*, 379–410.
- 14) Matyjaszewski, K.; Xia, J. *Chem. Rev.* **2001**, *101*, 2921–2990.
- 15) Hawker, C. J.; Bosman, A. W.; Harth, E. *Chem. Rev.* **2001**, *101*, 3661–3688.
- 16) Keddie, D. J. *Chem. Soc. Rev.* **2014**, *43*, 496–505.
- 17) Willcock, H.; O'Reilly, R. K. *Polym. Chem.* **2010**, *1*, 149–157.
- 18) Hoyle, C. E.; Lee, T. Y.; Roper, T. J. *J. Polym. Sci. Part A Polym. Chem.* **2004**, *42*, 5301–5338.
- 19) Hoyle, C. E.; Bowman, C. N. *Angew. Chem. Int. Ed.* **2010**, *49*, 1540–1573.
- 20) Lowe, A. B. *Polym. Chem.* **2010**, *1*, 17–36.
- 21) Guterman, R.; Rabiee Kenaree, A.; Gilroy, J. B.; Gillies, E. R.; Ragogna, P. J. *Chem.*

- Mater.* **2015**, *27*, 1412–1419.
- 22) Guterman, R.; Gillies, E. R.; Ragona, P. J. *Dalton Trans.* **2015**, 15664–15670.
 - 23) Wardle, B. *Principles and Applications of Photochemistry*; John Wiley & Sons, Ltd: West Sussex, 2009.
 - 24) Wayne, R. P. *Principles and Applications of Photochemistry*; Oxford: New York, 1988.
 - 25) Cramer, N. B.; Scott, J. P.; Bowman, C.N. *Macromolecules* **2002**, *35*, 5361–5365.
 - 26) Hageman, H. J. *Prog. Org. Coatings* **1985**, *13*, 123–150.
 - 27) Fouassier, J. P.; Lalevée, J. In *Photoinitiators for polymer synthesis: scope, reactivity, and efficiency.*; WILEY-VCH Verlag GmbH & Co. KGaA: Weinheim, Germany, 2012; pp. 127–197.
 - 28) Sigma Aldrich. Applications: Free Radical Initiators. http://www.sigmaldrich.com/content/dam/sigmaaldrich/docs/Aldrich/General_Information/thermal_initiators.pdf.
 - 29) Bowman, C. N.; Kloxin, C. J. *AIChE J.* **2008**, *54*, 2775–2795.
 - 30) Peiffer, R. W. *Photopolymerization Fundamentals and Applications*; Scranton, A. B.; Bowman, C. N.; Peiffer, R. W., Eds; American Chemical Society: Washington, DC, 1996.
 - 31) Faulkner, R. A.; Carstens, R. M.; Omiwade, O.; Cavitt, T. B. *Basic Principles and Applications of Photopolymerization Reactions, in Photoinitiators for Polymer Synthesis: Scope, Reactivity and Efficiency*; Fouassier, J. P.; Allonas, X., Eds.; Third Edit.; WILEY-VCH Verlags GmbH & Co. KGaA: Weinheim, Germany, 2012.
 - 32) Hemp, S. T.; Zhang, M.; Tamami, M.; Long, T. E. *Polym. Chem.* **2013**, *4*, 3582.
 - 33) Womble, C. T.; Coates, G. W.; Matyjaszewski, K.; Noonan, K. J. T. *ACS Macro Lett.* **2016**, *5*, 253–257.
 - 34) Rabiee Kenaree, A.; Berven, B. M.; Ragona, P. J.; Gilroy, J. B. *Chem. Commun.* **2014**, *50*, 10714–10717.
 - 35) Rabiee Kenaree, A.; Gilroy, J. B. *Dalton Trans.* **2016**.
 - 36) Kanazawa, A.; Ikeda, T.; Endo, T. *J. Polym. Sci. Part A Polym. Chem.* **1993**, *31*, 335–343.
 - 37) Guterman, R.; Hesari, M.; Ragona, P.; Workentin, M. *Langmuir* **2013**, *29*, 6460–

- 6466.
- 38) Guterman, R.; Berven, B. M.; Chris Corkery, T.; Nie, H. Y.; Idacavage, M.; Gillies, E. R.; Ragogna, P. J.; Corkery, C. T.; Nie, H. Y.; Idacavage, M.; Gillies, E. R.; Ragogna, P. J. *J. Polym. Sci. Part A Polym. Chem.* **2013**, *51*, 2782–2792.
 - 39) Hemp, S. T.; Smith, A. E.; Bryson, J. M.; Allen, M. H.; Long, T. E. *Biomacromolecules* **2012**, *13*, 2439–2445.
 - 40) Cheng, S.; Beyer, F. L.; Mather, B. D.; Moore, R. B.; Long, T. E. *Macromolecules* **2011**, *44*, 6509–6517.
 - 41) Hadadpour, M.; Gwyther, J.; Manners, I.; Ragogna, P. J. *Chem. Mater.* **2015**, *27*, 3430–3440.
 - 42) Guterman, R.; Gillies, E. R.; Ragogna, P. J. *Can. J. Chem.* **2015**, *481*, 1–24.
 - 43) Wang, J.; Wei Yang, J. G.; Yi, G.; Zhang, Y. *Chem. Commun.* **2015**, *51*, 15708–15711.
 - 44) Wang, K.; Zeng, Y.; He, L.; Yao, J.; Suresh, A. K.; Bellare, J.; Sridhar, T.; Wang, H. *Desalination* **2012**, *292*, 119–123.
 - 45) Noonan, K. J. T.; Hugar, K. M.; Kostalik, H. A.; Lobkovsky, E. B.; Abruña, H. D.; Coates, G. W. *J. Am. Chem. Soc.* **2012**, *134*, 18161–18164.
 - 46) Guterman, R.; Gillies, E. R.; Ragogna, P. J. *Langmuir* **2015**, *31*, 5181–5189.
 - 47) Ye, Y.; Stokes, K. K.; Beyer, F. L.; Elabd, Y. A. *J. Memb. Sci.* **2013**, *443*, 93–99.
 - 48) Biswas, Y.; Maji, T.; Dule, M.; Mandal, T. K. *Polym. Chem.* **2016**, *7*, 867–877.
 - 49) Lin, X.; Navailles, L.; Nallet, F.; Grinstaff, M. W. *Macromolecules* **2012**, *45*, 9500–9506.
 - 50) Godeau, G.; Navailles, L.; Nallet, F.; Lin, X.; McIntosh, T. J.; Grinstaff, M. W. *Macromolecules* **2012**, *45*, 2509–2513.
 - 51) Wathier, M.; Grinstaff, M. W. *Macromolecules* **2010**, *43*, 9529–9533.
 - 52) Wathier, M.; Grinstaff, M. W. *J. Am. Chem. Soc.* **2008**, *130*, 9648–9649.
 - 53) Kanazawa, A.; Ikeda, T.; Endo, T. *J. Polym. Sci. Part A Polym. Chem.* **1993**, *31*, 1467–1472.
 - 54) Kanazawa, A.; Ikeda, T.; Endo, T. *J. Polym. Sci. Part A Polym. Chem.* **1994**, *54*, 1305–1310.
 - 55) Qiu, T.; Zeng, Q.; Ao, N. *Mater. Lett.* **2014**, *122*, 13–16.

- 56) Guo, A.; Wang, F.; Lin, W.; Xu, X.; Tang, T.; Shen, Y.; Guo, S. *Int. J. Biol. Macromol.* **2014**, *67*, 163–171.
- 57) Popa, A.; Davidescu, C. M.; Trif, R.; Illia, G.; Iliescu, S.; Dehelean, G. *React. Funct. Polym.* **2003**, 151–158.
- 58) Choi, S. Y.; Rodríguez, H.; Gunaratne, H. Q. N.; Puga, A. V.; Gilpin, D.; McGrath, S.; Vyle, J. S.; Tunney, M. M.; Rogers, R. D.; McNally, T. *RSC Adv.* **2014**, *4*, 8567–8581.
- 59) Hasan, J.; Crawford, R. J.; Ivanova, E. P. *Trends Biotechnol.* **2013**, *31*, 295–304.
- 60) Cloutier, M.; Mantovani, D.; Rosei, F. *Trends Biotechnol.* **2015**, *33*, 637–652.
- 61) Murata, H.; Koepsel, R. R.; Matyjaszewski, K.; Russell, I. J. *Biomaterials* **2007**, *28*, 4870–4879.
- 62) Muñoz-Bonilla, A.; Fernández-García, M. *Prog. Polym. Sci.* **2012**, *37*, 281–339.
- 63) Campoccia, D.; Montanaro, L.; Arciola, C. R. *Biomaterials* **2013**, *34*, 8533–8554.
- 64) Siedenbiedel, F.; Tiller, J. C. *Polymers* **2012**, *4*, 46–71.
- 65) Timofeeva, L.; Kleshcheva, N. *Appl. Microbiol. Biotechnol.* **2011**, *89*, 475–492.
- 66) Nigmatullin, R.; Gao, F. *Macromol. Mater. Eng.* **2012**, *297*, 1038–1074.
- 67) Cornell, R. J.; Donaruma, L. G. *J. Med. Chem* **1965**, *8*, 388–390.
- 68) Panarin, E. F.; Solovski, M.; Ekzemply, O. *Khim.-Farm. Zh.* **1971**, *5*, 24–28.
- 69) Ikeda, T.; Ledwith, A.; Bamford, C. H.; Hann, R. A. *Biochim. Biophys. Acta* **1984**, *769*, 57–66.
- 70) Kanazawa, A.; Ikeda, T.; Endo, T. *J. Appl. Polym. Sci.* **1994**, *53*, 1237–1244.
- 71) Kanazawa, A.; Ikeda, T.; Endo, T. *J. Polym. Sci. Part A Polym. Chem.* **1994**, *32*, 1997–2001.
- 72) Kanazawa, A.; Ikeda, T.; Endo, T. *J. Polym. Sci. Part A Polym. Chem.* **1993**, *31*, 1441–1447.
- 73) Kanazawa, A.; Ikeda, T.; Endo, T. *J. Polym. Sci. Part A Polym. Chem.* **1993**, *31*, 3031–3083.
- 74) Kanazawa, A.; Ikeda, T.; Endo, T. *J. Polym. Sci. Part A Polym. Chem.* **1994**, *53*, 1245–1249.
- 75) Kanazawa, A.; Ikeda, T.; Endo, T. *J. Polym. Sci. Part A Polym. Chem.* **1994**, *52*, 641–647.

- 76) Kanazawa, A.; Ikeda, T.; Endo, T. *J. Polym. Sci. Part A Polym. Chem.* **1993**, *31*, 3003–3011.
- 77) Fischer, D.; Li, Y.; Ahlemeyer, B.; Krieglstein, J.; Kissel, T. *Biomaterials* **2003**, *24*, 1121–1131.
- 78) Ilker, M. F.; Nüsslein, K.; Tew, G. N.; Coughlin, E. B. *J. Am. Chem. Soc.* **2004**, *126*, 15870–15875.
- 79) Sambhy, V.; Peterson, B. R.; Sen, A. *Angew. Chem. Int. Ed.* **2008**, *47*, 1250–1254.
- 80) Punia, A.; Lee, K.; He, E.; Mukherjee, S.; Mancuso, A.; Banerjee, P.; Yang, N. L. *Int. J. Mol. Sci.* **2015**, *16*, 23867–23880.
- 81) Anthierens, T.; Billiet, L.; Devlieghere, F.; Du Prez, F. *Innov. Food Sci. Emerg. Technol.* **2012**, *15*, 81–85.
- 82) Bekas, D. G.; Tsirka, K.; Baltzis, D.; Paipetis, A. S. *Compos. Part B Eng.* **2016**, *87*, 92–119.
- 83) Hu, J.; Zhu, Y.; Huang, H.; Lu, J. *Prog. Polym. Sci.* **2012**, *37*, 1720–1763.
- 84) Ghosh, S. K. *Self-healing Materials: Fundamentals, Design Strategies, and Applications*; Ghosh, S. K., Eds.; WILEY-VCH Verlag GmbH & Co. KGaA: Weinheim, Germany, 2009.
- 85) Mauldin, T. C.; Kessler, M. R. *Int. Mater. Rev.* **2010**, *55*, 317–346.
- 86) Yang, Y.; Urban, M. W. *Chem. Soc. Rev.* **2013**, *42*, 7446–7467.
- 87) Chirila, T. V.; Lee, H. H.; Odon, M.; Nieuwenhuizen, M. M. L.; Blakey, I.; Nicholson, T. M. *J. Appl. Polym. Sci.* **2014**, *131*, 1–12.
- 88) Yoon, J. A.; Kamada, J.; Koynov, K.; Mohin, J.; Nicola, R.; Zhang, Y.; Balazs, A. C.; Kowalewski, T.; Matyjaszewski, K. *Macromolecules* **2012**, *45*, 142–149.
- 89) Yoshie, N.; Saito, S.; Oya, N. *Polymer* **2011**, *52*, 6074–6079.
- 90) Rao, Y.-L.; Chortos, A.; Pfattner, R.; Lissel, F.; Chiu, Y.-C.; Feig, V.; Xu, J.; Kurosawa, T.; Gu, X.; Wang, C.; He, M.; Chung, J. W.; Bao, Z. *J. Am. Chem. Soc.* **2016**, *138*, 6020–6027.
- 91) Reisch, A.; Roger, E.; Phoeung, T.; Antheaume, C.; Orthlieb, C.; Boulmedais, F.; Lavalle, P.; Schlenoff, J. B.; Frisch, B.; Schaaf, P. *Adv. Mater.* **2014**, 2547–2551.
- 92) McEleney, K.; Allen, D. P.; Holliday, A. E.; Crudden, C. M. *Org. Lett.* **2006**, *8*, 2663–2666.

- 93) Westhus, M.; Gonthier, E.; Brohm, D.; Breinbauer, R. *Tetrahedron Lett.* **2004**, *45*, 3141–3142.
- 94) Siliacycle. SiliaMetS Selection Guide.
<http://www.silicycle.com/ca/media/images/SiliaMetS-Selection-Guide.pdf>.
- 95) Sigma-Aldrich. QuadraPure and QuadraSil.
<http://www.sigmaaldrich.com/chemistry/chemical-synthesis/technology-spotlights/reaxa/quadrapures.html>.
- 96) Hinchcliffe, A.; Hughes, C.; Pears, D. A.; Pitts, M. R. *Org. Process Res. Dev.* **2007**, *11*, 477–481.

Chapter 2

2 Contact active antibacterial phosphonium coatings cured with UV light.

2.1 Introduction

Infections caused by bacteria such as *Escherichia coli* (*E. coli*) and *Staphylococcus aureus* (*S. aureus*) are widespread and increasingly problematic on a global scale. These bacteria have the ability to survive, proliferate, and form biofilms on surfaces, and can be easily spread through direct contact.¹ Therefore, the development of robust and effective antibacterial coatings to reduce bacterial attachment, proliferation, and biofilm formation is of significant interest in order to decrease transfer through common surfaces such as doorknobs, elevator buttons, hospital beds and food packaging. Coatings for medical devices such catheters and implants also have great potential to reduce the bacterial infections that result from these objects.² A commonly employed approach to antibacterial surfaces involves the physical encapsulation of biocides such as antibiotics,³⁻⁵ quaternary ammonium/phosphonium species,⁶ or active metals on the surface or in the bulk material.⁷⁻⁹ While this approach can be effective, some limitations include the release of toxic species into the environment, and the gradual exhaustion of the biocide, resulting in inactivity as well as subinhibitory concentrations of biocide near the surface and in the environment that will facilitate the development of bacterial resistance.¹⁰ Therefore, the covalent immobilization of antibacterial agents is a particularly attractive approach for the development of long-lasting antibacterial surfaces.

In recent years there has been significant interest in the preparation of antibacterial surfaces based on immobilized poly(quaternary amine)s. These have been prepared by various processes including the covalent grafting of polymers onto the surface,^{11,12} controlled polymerization,^{13,14} photopolymerization,¹⁵ or plasma polymerization from the substrate,¹⁶ layer by layer assembly,^{17,18} or simple painting on the surface.^{19,20} While phosphonium-based small molecules and polymers have been established to exhibit antibacterial properties,²¹⁻²³ there are very few reports detailing phosphonium-based antibacterial surfaces.²⁴⁻²⁶

Phosphonium salts are particularly attractive for surface applications because of their high thermal and chemical stability relative to ammonium salts.²⁷

In this context, we describe the development of a new simple and versatile approach towards antibacterial surfaces using polymerizable phosphonium salts and UV curing. The physical and chemical properties of phosphonium cations allow them to be readily coated onto various surfaces in a solvent-free process and cured with UV light to create cross-linked polymer thin films (Figure 2-1). It is demonstrated that the properties of the films can be tuned based on the phosphonium content and the curing conditions. The resultant coatings prevent both the growth and adhesion of bacteria on surfaces.

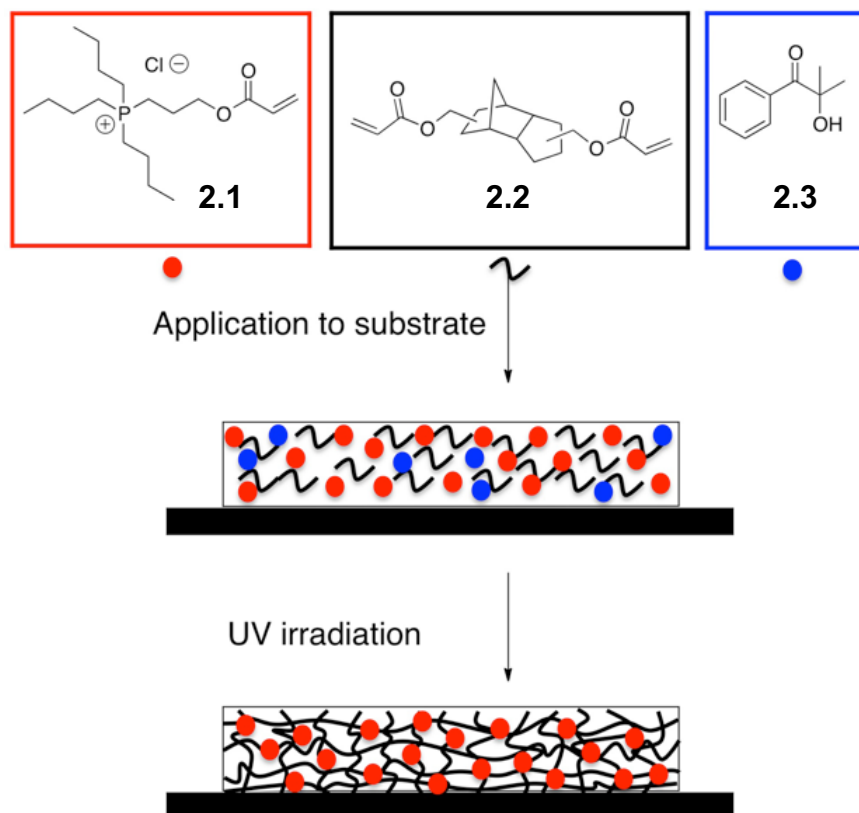


Figure 2-1: Schematic showing the coating preparation process.

2.2 Results and Discussion

((3-Acryloyloxypropyl)tributyl)phosphonium chloride (**2.1**) was prepared as previously reported²⁸ and was selected as the phosphonium monomer for this study because the butyl chains were anticipated to provide an appropriate balance of hydrophobicity and

hydrophilicity required for interactions with bacteria, and the acrylate functionality is known to exhibit high reactivity in UV curing processes.²⁹ The chloride counter ion results from the quaternization and acetylation steps used to prepare this molecule. Monomer **2.1** is a liquid at room temperature, allowing it to be cast on surfaces under solvent-free conditions. Tricyclodecanedimethanol diacrylate (**2.2**) and 2-hydroxy-2-methyl-1-phenylpropanone (**2.3**) were selected as the cross-linker and photoinitiator respectively, as they are both liquids, are widely used in UV curing and were found to effectively provide cross-linked thin films with **2.1**. Fixing the photoinitiator **2.3** concentration at 5 wt%, various weight ratios of **2.1** and **2.2** were formulated (Table 2-1), cast on substrates including poly(ethylene terephthalate) (PET) and glass using a Meyer rod, and irradiated with a mercury light source. This process resulted in smooth films with surface roughnesses less than 2 nm, as measured by atomic force microscopy (AFM) (Figure 8-1). The film thickness was ~25 μm . Adhesion testing using the Tape Test (ASTM D3359 – 09e2) indicated that the films generally exhibited strong adhesion to PET and lower adhesion to glass (Table 8-1). Beyond 47.5 wt% of **2.1**, the coatings did not adhere well to either substrate and delaminated upon washing, suggesting insufficient cross-linking.

Table 2-1: Effect of film formulation on accessible surface charge, as measured by fluorescein exchange. ^aFormulation contains 5 wt% of photoinitiator 2.3 and the remainder is cross-linker 2.2 to make up to 100%.

wt% of phosphonium monomer 2.1 ^a	Accessible surface charge density (cations/nm ²)
< 20	None detected
20	5.6
25	34
30	91
37.5	120
47.5	250

The accessible surface charges on the coatings prepared from each formulation were quantified using the fluorescein exchange experiment.¹⁴ It was found that when the content

of phosphonium monomer **2.1** was less than 20%, the charge density was below the detection limit of the assay (approximately 0.01 cations per nm²). However, as detailed in Table 2-1, from 20 – 47.5 wt% of **2.1**, the charge density steadily increased, reaching a value of 250 cations per nm² at 47.5 wt%. As several studies have suggested that cationic charge density is an important factor in achieving high antibacterial activity, further studies focused on the formulation containing 47.5 wt% of **2.1**.^{14,30}

A major advantage of UV curing is the speed with which it can be performed, which is on the order of seconds, in comparison with hours for thermal polymerizations. However, a potential disadvantage of UV curing is the inability to achieve 100% polymerization of the alkene moieties, because of radical termination reactions and limited cure depth.^{31,32} In particular, UV curing in air is subject to varying degrees of radical termination by oxygen and depends on the radical initiator and the growing polymer chain. To probe the efficiency of UV curing for the 47.5 wt% **2.1** formulation in air, the cure percentage was determined using attenuated total reflection Fourier transform infrared (ATR-FTIR) spectroscopy by comparing the intensity of the alkene peak at 810 cm⁻¹ which disappears upon curing, to that of the carbonyl peak at 1720 cm⁻¹ which does not change upon curing (Figure 8-2). As shown in Table 2-2, 80 ± 5% curing was obtained in air. The corresponding gel content was measured to be 84 ± 2%. While these values are quite typical for UV curing,³¹ and are acceptable for many applications, for antibacterial surfaces it is desirable to minimize the leaching of biocides from the surface as this can lead to ambiguity concerning the mechanism of action of bacterial killing and contribute to environmental contamination. Therefore, curing under an N₂ atmosphere was explored as a means of reducing radical termination by oxygen. This led to an increased cure percentage of 88 ± 4%, and an increased gel content of 88 ± 3%. The surfaces cured under N₂ were also noticeably harder and more durable. The application of a diamond tip surface profiler with a 0.5 mN force led to the etching of a 10 nm groove in the film cured in air, whereas the depth of the groove in the film cured under N₂ was indistinguishable from the surface roughness (Figure 2-2, Figure 8-1).

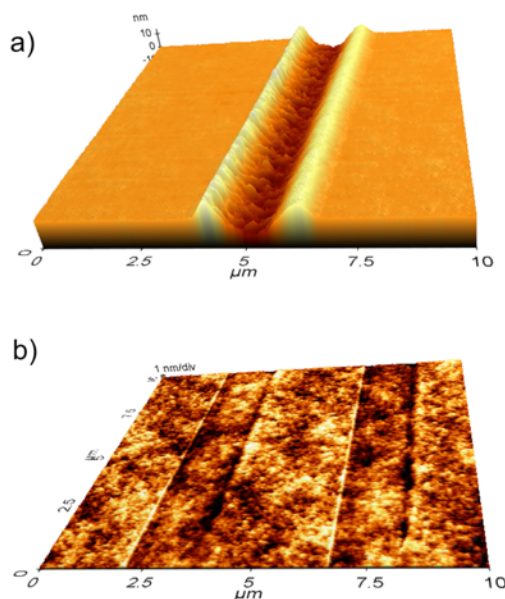


Figure 2-2: AFM images following application of a diamond tip surface profiler with a 0.5 mN force to: a) a film cured in air and b) a film cured under N₂.

After washing to remove any unbound molecules, the measured cure percentages were $87 \pm 1\%$ and $97 \pm 1\%$ for the air and N₂ cured surfaces respectively, with remaining double bond content that corresponded to molecules of cross-linker with only one of the acrylate groups reacted. Both coatings had water contact angles of $\sim 63^\circ$. This suggests that the surfaces were hydrophilic but not highly hydrophilic.³³

Table 2-2: Properties of coatings prepared from 47.5 wt% of (2.1), 47.5 wt% (2.2), and 5 wt% (2.3) under air or N₂ atmospheres.

Curing atmosphere	Cure % (ATR-IR) before washing	Cure % (ATR-IR) after washing	Gel Content	Water contact angle
Air	$80 \pm 5\%$	$87 \pm 1\%$	$84 \pm 2\%$	$63 \pm 1^\circ$
N ₂	$88 \pm 4\%$	$97 \pm 1\%$	$88 \pm 3\%$	$65 \pm 3^\circ$

Antibacterial testing focused on coatings cured under N₂ because of the increased curing efficiency and enhanced physical properties achieved under these conditions. N₂ cured surfaces containing 47.5% of **2.1** were thoroughly washed by incubation in water for 12 h,

with 3 changes of the water. This protocol was deemed sufficient to remove any unbound material as no further release of acrylate functionalities could be detected in the wash water by UV-visible spectroscopy (Figure 8-3). This ensured that it was the actual activity of the surfaces that were being measured, rather than that of leachable phosphonium monomers or oligomers. This is particularly important, as recent studies have suggested that some of the most active “immobilized” ammonium antibacterial surfaces may actually act through the release of unbound biocides.³⁴

A suitable antibacterial test for surfaces of intermediate or low hydrophilicity involves placing the surface in contact with agar that has been inoculated with bacteria, as this minimizes issues associated with surface tension in bacterial suspensions and maximizes contact with the bacteria. To achieve this, a procedure based on the Kirby-Bauer protocol was used.³⁵ *E. coli* (ATCC 29425) and *S. aureus* (ATCC 6538) were selected as representative strains of gram-negative and gram-positive bacteria, respectively. As shown in Figure 2-3 for *S. aureus* and Figure 8-4 for *E. coli*, after 24 h of contact between the phosphonium surface and the bacteria-inoculated agar, no bacteria grew in the region of the phosphonium surface. Possible mechanisms of antibacterial activity that have been proposed for cationic surfaces include the disruption of the bacterial cell membrane³⁶ and the mobilization of metal cations that are important for membrane structure.³⁰ The former mechanism was proposed to be dominant for soluble polyphosphonium²¹ and surfaces with phosphoniums attached by long flexible linkers.²⁴ The mechanism of action of the current cross-linked phosphonium films and others with short linkers²⁵ are still unclear, though by analogy with surfaces having short quaternary ammonium chains,³⁷ may involve the ion exchange mechanism.

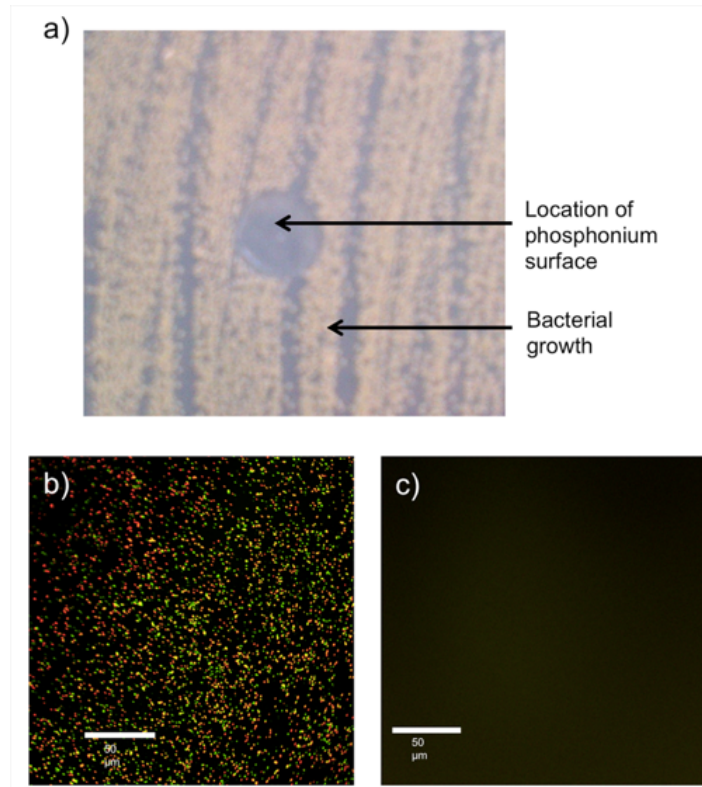


Figure 2-3: Antibacterial testing results for a surface containing 47.5 wt% of 2.1 and cured under N₂ : a) Image of an agar plate showing the absence of bacterial growth where the phosphonium surface was placed, following 24 h incubation with *S. aureus*; b) clean silicon wafer control and c) phosphonium surface following LIVE/DEAD[®] analysis after incubation of the surfaces with a suspension of *S. aureus* in PBS for 4 h. Live bacteria appear green in this assay, while dead bacteria appear red. No bacteria were detected on the phosphonium surface. Scale bar = 50 μm.

No zone of inhibition was detected for the surfaces in the above test, indicative that the observed activity was not the result of molecules leaching from the surface.³⁵ To probe this further, after the washing protocol described above was conducted, the surfaces were incubated in 0.3 mM phosphate buffer. The surfaces were then removed from this buffer and a suspension containing 10⁵ colony forming units (CFUs) of *S. aureus* was added. Following plating of this bacterial suspension on agar, no inhibition of bacterial growth was detected in this solution in comparison to a control buffer that was not in contact with the surfaces. This confirmed that the activity was not due to the leaching of biocides. An additional problem that can be encountered in antibacterial surfaces is the adhesion of either live or dead bacteria to surfaces, which renders them inactive and can promote the growth of biofilms. To ensure that our surfaces resisted the adhesion of bacteria, a LIVE/DEAD[®] BacLight bacterial

viability assay was performed using *S. aureus*. 100 uL of a PBS suspension containing 10^7 CFUs of bacteria per cm^2 was placed on the phosphonium surface. At time points of 4 and 24 h, the surface was gently rinsed with water and stained with SYTO 9 and propidium iodide. In this assay, live bacteria appear green due to the uptake of the dye SYTO 9, which permeates all bacterial membranes, while dead bacteria appear red due to the uptake of propidium iodide which permeates only damaged bacterial membranes and dominates over the fluorescence of SYTO 9. As shown in Figure 2-3b,c and Figure 8-5, no live or dead bacteria were detected on the phosphonium surfaces at either time point, suggesting that these surfaces can resist very high loadings of bacteria. In contrast both live and dead bacteria adhered to control silicon wafers under the same conditions. The ability of the phosphonium coatings to prevent bacterial attachment and colonization is very important as the colonization of bacteria on surfaces can lead to a faster development of resistance compared to that in solution, as resistance can be transferred by horizontal gene transfer.^{38,39}

Testing was also performed to evaluate the potential toxicity of biocide **2.1** using a 3-(4,5-dimethylthiazol-2-yl)-2,5-diphenyltetrazolium bromide (MTT) cell viability assay. C2C12 mouse myoblast cells, a model cell line, were found to exhibit > 80% viability at concentrations up to 0.2 mg/mL of **2.1** (Figure 8-6). In comparison, benzyldimethylhexadecyl ammonium chloride, a common commercial antibacterial agent, was highly toxic to cells even at the lowest studied concentration of 8 $\mu\text{g/mL}$. Therefore, while the surfaces do not leach biocide following the initial washing step as all materials are subsequently covalently attached to the coating, these results suggest that phosphonium **2.1** may exhibit advantages over widely used ammonium biocides in terms of its toxicity to mammalian cells.

2.3 Conclusions

In conclusion, a new method was developed for the incorporation of antibacterial phosphonium polymer networks into coatings via UV curing. Optimal performance in terms of coating integrity and cationic charge were obtained for surfaces containing 47.5 wt% of the phosphonium monomer, and it was found that performing the UV curing under N_2 led to increased curing efficiency, higher gel content, and more durable coatings. The

phosphonium-based coatings prevented the growth of *S. aureus* and *E. coli*, as demonstrated when they were placed in contact with bacteria-innoculated agar, and they also resisted the adhesion of both live and dead bacteria at very high loadings of 10^7 CFUs of *S. aureus* per cm^2 . Furthermore, the biocidal phosphonium monomer was found to be less toxic than a widely used ammonium biocide to mammalian cells. Overall, the results suggest that these new phosphonium coatings are highly promising for a wide range of applications ranging from medical devices to common objects such as keyboards and door handles. Further tuning of the coating formulation, casting process, and UV curing conditions to optimize the extent of curing and the coating properties, as well as further evaluation of the coating under a range of antibacterial testing conditions should enable their development for these applications.

2.4 Experimental

Coating preparation

Formulations containing 5 wt% of the photoinitiator 2-hydroxy-2-methyl-1-phenylpropanone (**2.3**) (Cytec Industries, Georgia, USA), and varying ratios of cross-linker tricyclodecanedimethanol diacrylate (**2.2**) (Cytec Industries, Georgia, USA) and ((3-acryloyloxypropyl)tributyl)phosphonium chloride (**2.1**)¹ were mixed by stirring for five minutes. The formulations were then deposited on either Melinex 725 Teijin PET films purchased from Tekra (Wisconsin, USA), glass slides, or silicon wafers and cast using a 25- μm Meyer Rod purchased from Gardco (Florida, USA). The glass slides and silicon wafers were first cleaned by immersion in 1:2 H_2SO_4 : H_2O_2 vol/vol (Piranha solution; attention – strong acid, strong oxidizer!) then they were rinsed with water, ethanol, and then dried under vacuum. If under an inert atmosphere, the film was inserted into an inert atmosphere cell and purged with N_2 for 30 seconds before irradiation. Free standing films were produced by drop casting the mixture on a clean glass slide and then adding spacers and another glass slide on top to create films in an air-free atmosphere, which were then removed from the glass using a razor blade. Photopolymerization was performed using a modified UV-curing system purchased from UV Process and Supply Inc. (Illinois, USA) equipped with a mercury bulb. Samples were irradiated with an energy density of $1878 \text{ mJ}/\text{cm}^2$ and an irradiance of $3325 \text{ mW}/\text{cm}^2$, as determined by a PP2-H-U Power Puck II purchased from EIT Instrument

Markets (Virginia, USA). Coatings cast on PET or glass were ~25 μm thick, while the free standing films were ~250 μm thick, as measured using a micrometer. Properties of the films on PET and glass were summarized in Table 2-2, while those of the free standing films are shown in Table 8-2. The coatings and free standing films had very similar properties.

Atomic force microscopy (AFM) and hardness testing

AFM was performed using a Park Systems XE-100 instrument (Suwon, Korea). The cantilever had a nominal spring constant of 40 N/m, resonant frequency of 300 kHz, and a tip apex radius of 10 nm. Hardness was evaluated using a KLA Tencor P-10 Surface Profiler equipped with a diamond tip and applied with a 0.5 mN force to scratch the surface. The resulting surface was imaged by AFM. The measured surfaces were prepared on a glass substrate as it is flat, allowing accurate assessment of film roughness.

Measurement of surface adhesion

Testing was performed in accordance with ASTM D3359 – 09e2. Briefly, the surfaces coated with the phosphonium thin films were cut through to the substrate with a scalpel, in a pattern of 6 parallel lines. Another set of 6 parallel lines perpendicular to the initial lines were then cut. The lines were approximately 0.25 cm apart. A line of tape was put across the lines and pressed down and left for 30 seconds. The tape (3M Scotch #2020; 35 oz/in adhesion strength to steel) was then removed from one end, and the number of removed squares compared to the number of starting squares was counted to provide the percentage of removed squares. The results are provided in Table 8-1: Results of surface adhesion testing by ASTM D3359 – 09e2. *The test was repeated 5 times on the same surface without any loss of adhesion.

Measurement of accessible surface charges using the fluorescein dye assay

This procedure was based on the previously reported protocol.² The surface (~ 1 cm^2) was immersed in a 1 w/v% solution of fluorescein sodium salt in deionized water for 10 minutes. The resulting surface was rinsed with deionized water, then immersed in 10 mL of a 0.1 v/v% solution of cetyltrimethylammonium chloride in deionized water and sonicated for 30 minutes. The surface was then removed and 10% v/v phosphate buffer added and the

absorbance of the solution at 501 nm was measured using a Varian Cary 300 UV-visible spectrometer. The concentration of accessible charges on the surface was then determined based on the extinction coefficient of fluorescein ($\epsilon = 77,000 \text{ M}^{-1}\text{cm}^{-1}$), assuming that each molecule of fluorescein binds to one accessible cation. The measured coatings were prepared on the PET substrate.

Measurement of cure percentage

Infrared spectra (IR) were recorded using a Bruker Tensor 27 spectrometer in attenuated total reflectance mode (ATR) using a ZnSe crystal. The peak corresponding to C=O (1720 cm^{-1}) was used as an internal standard as its intensity does not change upon curing. The intensity of the C=C peak (810 cm^{-1}) was compared to that of the internal standard before curing, after curing, and after incubation in water for a total of 12 h, with three water changes. The cure percentage was calculated as the percent decrease in the relative intensity of the C=C peak. Measurements were performed in triplicate. Samples for this experiment (Table 2-2) were cast on a PET substrate due to its flexibility, which allows ATR-IR to be easily performed. Free standing films were measured using the same procedure (Table 8-2).

Measurement of gel content

Surfaces with dimensions of 3 cm^2 cast on glass were used, due to the ease of creating a uniform coating over a large area on this highly flat substrate (Table 2-2). The large dimension was required for accurate measurement of coating mass for these films. Free standing films were also measured (Table 8-2). Cured but unwashed coatings were weighed then incubated in 10 mL of deionized water for 12 hours (water changed three times). The surfaces were then dried to constant mass in a vacuum oven overnight at $50 \text{ }^\circ\text{C}$. The gel content was calculated as the $(\text{initial dry weight}/\text{extracted dry weight}) \times 100\%$.

Measurement of water contact angle

Water contact angle measurements were performed using a Kruss DSA100 Drop Shape Analyzer and analyzed using drop shape analysis. Values were obtained two minutes after droplet application and the measurements were performed in triplicate. Coatings on PET

were used to obtain the values in Table 2-2, though the water contact angle has been observed to not depend on the underlying substrate.

Agar plate antibacterial procedure

This procedure was based on the Kirby-Bauer protocol.³ A loop of precultured *E. coli* (ATCC 29425) or *S. aureus* (ATCC 6538) was freshly cultured in LB broth (VWR International, Mississauga, Canada) for 18 - 24 hours at 37 °C in a shaker at 175 rpm. The resulting suspension was centrifuged for 10 minutes, decanted, and resuspended in phosphate buffered saline (PBS), vortexed, and centrifuged for 10 minutes. This was repeated twice. The resulting pellet was resuspended in PBS and diluted to a concentration of 10^8 colony forming units (CFU)/mL (calculated based on *E. coli* optical density of 0.2 at 600 nm and a *S. aureus* optical density of 0.3 at 600 nm). The suspension was further diluted to a concentration of 10^6 CFU/mL and 0.1 mL was plated onto an agar plate (Difco™ plate agar, BD, Sparks, MD, USA) and spread thoroughly and evenly on the plate. The plate was allowed to dry for 5 minutes. Free standing phosphonium polymer networks prepared with 47.5 wt% **1**, cured under nitrogen, pre-washed by 12 hour incubation in deionized water (with 3 water changes), and dried were placed on the agar and pressed into the agar to ensure contact. The agar plate was then incubated at 37 °C for 24 hours. The films were carefully removed with tweezers and the agar was imaged. The experiment was performed on at least 4 films for each strain of bacteria.

Evaluation of potential antibacterial properties of surface leachable molecules

A 1 cm² phosphonium surface (47.5 wt% **1**, cured under N₂) was prepared on a PET substrate and pre-washed for 12 hours with three water changes in the same manner as for the agar protocol above. It was then placed in an Erlenmeyer flask containing 5 mL of 0.3 mM pH 7.4 phosphate buffer. A control sample contained no surface. The samples were agitated using a wrist action shaker at 75 rpm for 1 hour then the surface was removed. A suspension of *S. aureus* in PBS at a concentration of 10^6 CFU/mL was prepared as described above. 100 μL of this suspension was added to the 5 mL of leachate described above, providing a final concentration of 10^5 CFU/5 mL. This solution was then agitated using a wrist action shaker at 75 rpm for 1 hour, diluted to 10^2 CFU/mL, pour plated into growth

agar in triplicate, and incubated at 37 °C for 24 hours. CFUs were then counted. No significant differences between the sample and control were observed, confirming the absence of leachable biocides in the coatings. The experiment was performed in triplicate.

LIVE/DEAD® BacLight bacterial viability assay

A suspension of *S. aureus* in PBS at a concentration of 10^8 CFU/mL was prepared as described above. 1 mL of this suspension was placed on each 4 cm² phosphonium coating (prepared on an activated silicon wafer and washed for 12 hours with three water changes). The control surface was an activated silicon wafer (washed with water and dried under vacuum). The surfaces were placed in a petri dish, the dish was sealed with paraffin, and the samples were incubated for either 4 or 24 hours at 37 °C at 40-50% humidity. The surfaces were then washed with 10 mL of PBS, then incubated with a mixture of the LIVE/DEAD® BacLight bacterial viability assay dyes (SYTO 9 and propidium iodide, Life Technologies, Burlington, Canada) for 30 minutes in the dark according to the manufacturer's directions. The surfaces were then gently washed with deionized water and dried in the dark overnight. The dry surfaces were then mounted on glass slides and imaged by laser confocal microscopy using an LSM 510 multichannel point scanning confocal microscope (Zeiss, Oberkochen, Germany) (Laser 488 nm for the SYTO 9 with a pass filter of 505-530 nm and a laser at 543 nm for the propidium iodide with a pass filter of 615 nm, magnification 40×). All the images were obtained and refined with the ZEN software. Each time point and surface was tested in triplicate.

Cell viability assay

C2C12 mouse myoblast cells were cultured in growth medium composed of Dulbecco's Modified Eagle Medium (DMEM) containing 10% fetal bovine serum (FBS) and supplemented with 1% Glutamax (100×) solution and antibiotics (Penicillin and Streptomycin, 100 units/mL each) (Life Technologies, Burlington, Canada). Cells were seeded onto a 96-well plate (flat bottom, Corning, USA) at a density of 10,000 cells per well with a final volume of 100 µL of culture medium. Cells were allowed to adhere for 24 hours at 37 °C in a humidified incubator with 5% CO₂. After 24 hours the growth medium was aspirated and replaced with either the positive control sodium dodecyl sulfate (SDS) in the

growth medium at concentrations of 0.2, 0.15, 0.10, 0.05 mg/ml, compound **2.1** at serial two-fold dilutions from 0.8 mg/mL to 0.007 mg/mL, or benzyldimethylhexadecylammonium chloride at serial two-fold dilutions starting from 1 mg/mL to 0.008 mg/mL. Control cells were grown in medium alone. The cells were then incubated for 24 hours under the conditions described above. All medium was aspirated, and then 100 μ L of fresh medium and 10 μ L of 3-(4,5-dimethylthiazol-2-yl)-2,5-diphenyltetrazolium bromide (MTT, Sigma-Aldrich, Mississauga, Canada) solution (5 mg/mL in growth medium) were added to each well. After incubation for 4 hours, the medium was aspirated and the formazan product was solubilized by addition of 50 μ L of DMSO to each well. The absorbance of each well was measured at 540 nm using a plate reader (M1000-Pro, Tecan, Mannedorf, Switzerland) and after subtraction of the blank, the absorbance was compared to that of the control cells that were not exposed to micelles in order to calculate the relative cell viability. Less than 2% cell viability was detected for the cells exposed to the highest concentrations of the positive control SDS, confirming the sensitivity of the assay.

2.5 References

- 1) Page, K.; Wilson, M.; Parkin, I. P. *J. Mater. Chem.* **2009**, *19*, 3819–3831.
- 2) Arciola, C. R.; Campoccia, D.; Speziale, P.; Montanaro, L.; Costerton, J. W. *Biomaterials* **2012**, *33*, 5967–5982.
- 3) Yang, M.; Santerre, J. P. *Biomacromolecules* **2001**, *2*, 134–141.
- 4) Woo, G. L. Y.; Yang, M. L.; Yin, H. Q.; Jaffer, F.; Mittelman, M. W.; Santerre, J. P. *J. Biomed. Mater. Res.* **2002**, *59*, 35–45.
- 5) Woo, G. L.; Mittelman, M. W.; Santerre, J. P. *Biomaterials* **2000**, *21*, 1235–1246.
- 6) Kenawy, E. R.; Abdel-Hay, F. I.; El-Shanshoury, A. E. R. R.; El-Newehy, M. H. *J. Polym. Sci. Part A Polym. Chem.* **2002**, *40*, 2384–2393.
- 7) López-Carballo, G.; Higuera, L.; Gavara, R.; Hernández-Muñoz, P. *J. Agric. Food Chem.* **2013**, *61*, 260–267.
- 8) Gladitz, M.; Reinemann, S.; Radusch, H.-J. *Macromol. Mater. Eng.* **2009**, *294*, 178–189.
- 9) Balogh, L.; Swanson, D. R.; Tomalia, D. a.; Hagnauer, G. L.; McManus, A. T. *Nano Lett.* **2001**, *1*, 18–21.

- 10) Russell, A. D. *J. Pharm. Pharmacol.* **2000**, *52*, 227–233.
- 11) Karamdoust, S.; Yu, B.; Bonduelle, C. V.; Liu, Y.; Davidson, G.; Stojcevic, G.; Yang, J.; Lau, W. M.; Gillies, E. R. *J. Mater. Chem.* **2012**, *22*, 4881–4889.
- 12) Klibanov, a M.; Lewis, K.; Liao, C. J.; Tiller, J. C.; Liao, C. J.; Lewis, K.; Klibanov, a M. *Proc. Natl. Acad. Sci. U. S. A.* **2001**, *98*, 5981–5985.
- 13) Allison, B. C.; Applegate, B. M.; Youngblood, J. P. *Biomacromolecules* **2007**, *8*, 2995–2999.
- 14) Murata, H.; Koepsel, R. R.; Matyjaszewski, K.; Russell, I. J. *Biomaterials* **2007**, *28*, 4870–4879.
- 15) Tang, R.; Muhammad, A.; Yang, J.; Nie, J. *Polym. Adv. Technol.* **2014**, *25*, 651–656.
- 16) Lotz, A.; Heller, M.; Dohm, N.; Cierniak, P.; Bender, K.; Jansenb, B.; Forch, R. *J. Mater. Chem.* **2011**, *22*, 19455–19461.
- 17) Pfaffenroth, C.; Winkel, A.; Dempwolf, W.; Gamble, L. J.; Castner, D. G.; Stiesch, M.; Menzel, H. *Macromol. Biosci.* **2011**, *11*, 1515–1525.
- 18) Wong, S. Y.; Moskowitz, J. S.; Veselinovic, J.; Rosario, R. A.; Timachova, K.; Blaisse, M. R.; Fuller, R. C.; Klibanov, A. M.; Hammond, P. T. *J. Am. Chem. Soc.* **2010**, *132*, 17840–17848.
- 19) Kocer, H. B.; Cerkez, I.; Worley, S. D.; Broughton, R. M.; Huang, T. S. **2011**, *3*, 3189–3194.
- 20) Haldar, J.; An, D.; Alvarez, L.; Cienfuegos, D.; Chen, J.; Klibanov, A. M. *Proc. Natl. Acad. Sci. U. S. A.* **2006**, *103*, 17667–17671.
- 21) Kanazawa, A.; Ikeda, T.; Endo, T. *J. Polym. Sci. Part A Polym. Chem.* **1993**, *31*, 335–343.
- 22) Kanazawa, A.; Ikeda, T.; Endo, T. *J. Polym. Sci. Part A Polym. Chem.* **1993**, *31*, 1441–1447.
- 23) Kanazawa, A.; Ikeda, T.; Endo, T. *J. Polym. Sci. Part A Polym. Chem.* **1993**, *31*, 3031–3083.
- 24) Kanazawa, A.; Ikeda, T.; Endo, T. *J. Polym. Sci. Part A Polym. Chem.* **1993**, *31*, 1467–1472.
- 25) Kanazawa, A.; Ikeda, T.; Endo, T. *J. Polym. Sci. Part A Polym. Chem.* **1994**, *54*, 1305–1310.

- 26) Kanazawa, A.; Ikeda, T.; Endo, T. *J. Polym. Sci. Part A Polym. Chem.* **1994**, *52*, 641–647.
- 27) Bradaric, C. J.; Downard, A.; Kennedy, C.; Robertson, A. J.; Zhou, Y. *Green Chem.* **2003**, *5*, 143–152.
- 28) Guterman, R.; Hesari, M.; Ragona, P.; Workentin, M. *Langmuir* **2013**, *29*, 6460–6466.
- 29) Shukla, V.; Bajpai, M.; Singh, D. K.; Singh, M.; Shukla, R. *Pigment Resin Technol.* **2004**, *33*, 272–279.
- 30) Kügler, R.; Bouloussa, O.; Rondelez, F. *Microbiology* **2005**, *151*, 1341–1348.
- 31) Wight, F. R. *J. Polym. Sci. Polym. Lett. Ed.* **1978**, *16*, 121–127.
- 32) Gatechair, L. R.; Tiefenthaler, A. M. In *Radiation Curing of Polymeric Materials*; American Chemical Society: New York, 1990; pp. 27–42.
- 33) Drelich, J.; Chibowski, E.; Desheng Meng, D.; Terpilowski, K.; Meng, D. D.; Terpilowski, K. *Soft Matter* **2011**, *1*, 9804.
- 34) Green, J. B. D.; Bickner, S.; Carter, P. W.; Fulghum, T.; Luebke, M.; Nordhaus, M. A.; Strathmann, S. *Biotechnol. Bioeng.* **2011**, *108*, 231–236.
- 35) Gaydos, J. M.; Harrington, B. J. *Antimicrob. Agents Chemother.* **1982**, *21*, 516–518.
- 36) Lewis, K.; Klibanov, A. M. *Trends Biotechnol.* **2005**, *23*, 343–348.
- 37) Huang, J.; Koepsel, R. R.; Murata, H.; Wu, W.; Lee, S. B.; Kowalewski, T.; Russell, A. J.; Matyjaszewski, K. **2008**, *24*, 6785–6795.
- 38) Roberts, P.; Pratten, J.; Wilson, M.; Mullany, P. *FEMS Microbiol. Lett.* **1999**, *177*, 63–66.
- 39) Hausner, M.; Wuertz, S. *Appl. Environ. Microbiol.* **1999**, *65*, 3710–3713.

Chapter 3

3 Synthesis, properties, and antibacterial activity of polyphosphonium semi-interpenetrating networks

3.1 Introduction

Polymer networks are 3-dimensional, insoluble high molar mass polymers comprising linear chains connected by covalent cross-links or non-covalent interactions between these chains.^{1,2} The ability to readily tune their properties by varying both molecular structure and the degree of cross-linking have enabled the use of polymer networks in a wide range of applications including industrial surface coatings,³ rubbers,⁴ 3D printed plastics,^{5,6} and hydrogels for drug delivery and regenerative medicine.^{7,8} The use of specific additives that do not constitute the backbone or primary component of the network but that enhance properties such as mechanical strength,^{9,10} coating adhesion,¹¹ thermal stability,¹² hydrophobicity,^{13,14} or introduce new functions such as self-healing,^{13,15,16} flame retardancy,¹⁷ or the ability to support cell growth¹⁸ is a commonly employed approach to further broaden the utility of polymer networks. Semi-interpenetrating polymer networks (SIPNs) are a special class of polymer network materials that are composed of one or more networks, and one or more linear or branched polymers that penetrate the network at the molecular scale, at least to some degree.¹⁹ In SIPNs, the linear polymer can impart functions such as conductivity,²⁰ swellability,²¹ shape memory effects,²² and antibacterial activity.²³ Polyelectrolyte networks and SIPNs contain charged polymers, where specific properties and functions are imparted to the network by the polyelectrolyte. For example, networks containing polysulfonates have been explored as proton exchange membranes in fuel cells.²⁴ The incorporation of polyammonium or polycarboxylates into hydrogels have been used to introduce pH-responsive properties.^{25,26} Our group has recently explored the preparation of phosphonium polymer networks by curing with ultra-violet (UV) light. In comparison to their widely-investigated nitrogen counterparts, phosphoniums are of particular interest because they exhibit differences in charge distribution and increased chemical and thermal stability relative to ammoniums that may translate into enhanced properties for various applications.²⁷ By tuning the chemical structure of the phosphonium monomer, counterion,

and cross-linker, it has been possible to readily tune properties such as coating hardness, hydrophobicity, swellability, and ion exchange rate.²⁸⁻³⁰ The deposition of gold nanoclusters through ion exchange was also explored.³¹ To the best of our knowledge, there are only two prior reports of SIPNs incorporating polyphosphonium. In one case, the SIPNs were used to template the synthesis of gold nanoparticles,³² and in another case for the 3-D printing of ion-conductive networks.³³

In addition to the aforementioned applications, the development of antibacterial coatings is currently of significant interest due to the increasing proliferation of antibiotic-resistant infections, and their spread through direct contact with surfaces in settings such as hospitals and food processing facilities.³⁴⁻³⁶ While many approaches involve the physical encapsulation and release of biocides such as conventional antibiotics,³⁷⁻³⁹ heavy metals,⁴⁰ and quaternary ammoniums,⁴¹ a more permanent immobilization approach can mitigate problems associated with the release of sub-inhibitory concentrations of biocide that can lead to resistance, environmental contamination, and the eventual depletion of the surface's bioactivity.⁴² Various approaches including covalent conjugation,⁴³ controlled polymerization,⁴⁴ photopolymerization,⁴⁵ plasma polymerization/immobilization,⁴⁶⁻⁴⁸ and layer-by-layer assembly³⁷ have been introduced for the grafting of antibacterial polymers on surfaces. However, many of these processes are relatively tedious or require a functionalized substrate onto which grafting is performed. In this context, UV curing of a polymer network coating is a rapid and simple method for preparing antibacterial surfaces.

Small molecule phosphonium and polyphosphonium antibacterial activity has been previously reported.^{35,49-51} Despite this, there are few examples of antibacterial phosphonium-based surfaces.^{52,53} We have recently reported antibacterial polymer network coatings prepared via the UV-initiated curing of ((3-acryloyloxypropyl)tributyl)phosphonium chloride in the presence of tricyclodecanedimethanol diacrylate and a photoinitiator.⁵² However, a high content (47.5 wt%) of the phosphonium monomer was required to obtain sufficient surface charge for bacterial killing. Herein we introduce a new and alternative approach to phosphonium-containing antibacterial surfaces involving the incorporation of relatively low loadings (0.1

to 10 wt%) of polyphosphonium into polymer networks formed from tetra(ethylene glycol) diacrylate (TEGDA) via UV-curing, thereby forming SIPNs (Figure 3-1). In addition, while the previous work involved tributylphosphoniums, the current work also explores triethylphosphonium and trioctylphosphonium groups in order to elucidate their effects on antibacterial efficacy, as well as other coating properties. Through comparisons of the properties of a library of SIPNs, as well as studies of their ability to kill *Escherichia coli* (*E. coli*) and *Staphylococcus aureus* (*S. aureus*), this work provides new insights into the preparation and properties of phosphonium SIPNs and into how the composition and architecture of phosphonium coatings can influence their antibacterial efficacy.

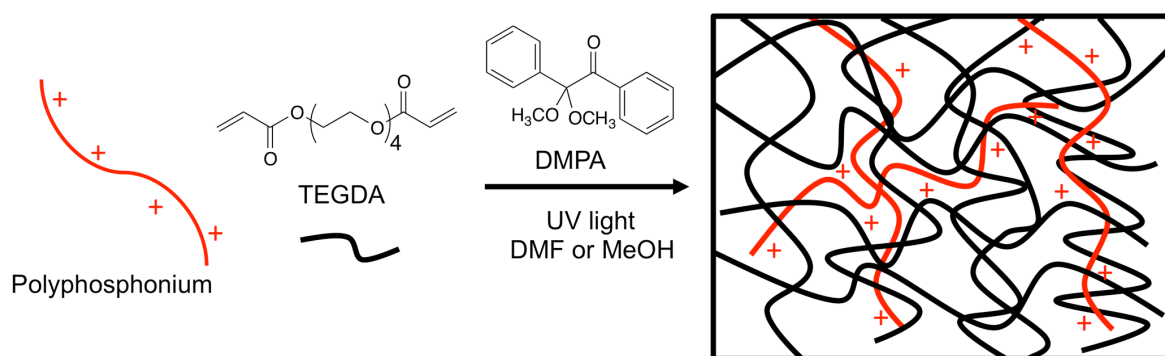


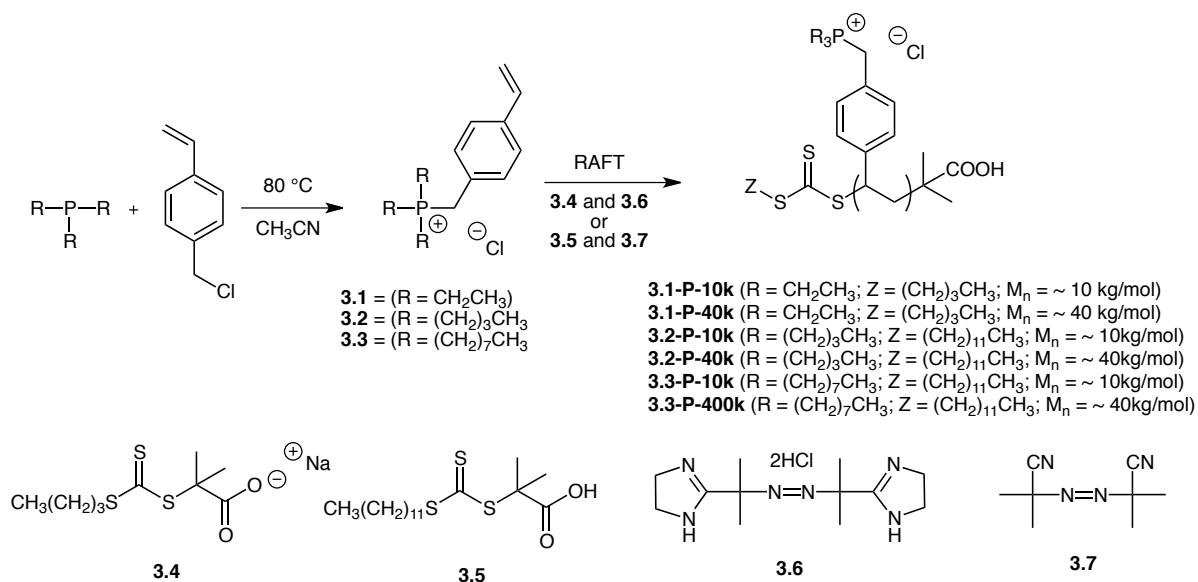
Figure 3-1: Schematic illustrating the incorporation of polyphosphonium into an SIPN.

3.2 Results and discussion

3.2.1 Synthesis of polyphosphonium

First the requisite phosphonium monomers were prepared. Triethyl, tributyl, and trioctylphosphine were selected as starting materials to investigate the effects of alkyl chain length and hydrophobicity on the properties of the materials. 4-Vinylbenzyl polymerizable groups were chosen because they are relatively stable during storage, yet readily undergo controlled free radical polymerization.^{58,59} The monomers **3.1**, **3.2**, and **3.3** were synthesized by the reaction of phosphine with 4-vinylbenzyl chloride at 80 °C in CH₃CN (Scheme 3-1). Reversible addition-fragmentation chain-transfer (RAFT) was selected as a controlled method for the polymerization, because it has been previously demonstrated by our group and others, to afford controlled polymerization of vinyl phosphonium monomers.^{60,61} The presence of the RAFT agent at the polymer terminus following polymerization also provides a possibility for covalent attachment of the polyphosphonium to the network during the UV-

initiated free radical curing process, which is desirable for preventing leaching of biocidal polymers from the resulting materials. **3.1** was polymerized in water using sodium 2-(((butylthio)carbonothioyl)thio)-2-methylpropanoate (**3.4**)⁵⁴ as the RAFT agent and 2,2'-azobis[2-(2-imidazolin-2-yl)propane]dihydrochloride (**3.6**) as the initiator to afford **3.1-P**. **3.2** and **3.3** were polymerized in CH₃CN using (((dodecylthio)carbonothioyl)thio)-2-methylpropionic acid (**3.5**)⁵⁵ as the RAFT agent and azobisisobutyronitrile (**3.7**) as the initiator to afford **3.2-P** and **3.3-P**. The monomer to RAFT agent stoichiometry was adjusted to target polymers with number average molar masses (M_n) of either 10 kg/mol or 40 kg/mol at 80% monomer conversion in order to study the effects of different polymer chain length incorporation into the networks and antibacterial activities of the resulting coatings. The concentrations of the polymerizations were chosen to ensure there was no visible increase in viscosity or phase separation during the reaction that would hinder the polymerization.



Scheme 3-1: Synthesis of phosphonium monomers and polymers.

The polymerization reactions were monitored by ¹H NMR spectroscopy based on the disappearance of peaks corresponding to the vinylic hydrogens relative to the peaks corresponding to the terminal methyl group on the alkyl chains of the phosphonium monomer and polymer, whose total integration remained constant in the monomer and polymer (Figure 3-2). The polymerizations were stopped at ~80% conversion as continued

radical generation after the monomer is fully converted can lead to side reactions and cleavage of the RAFT agent from the polymer terminus.⁶² Table 2-1 shows the M_n calculated for the polymers based on the monomer conversion measured by ^1H NMR spectroscopy. **3.1-P** and **3.2-P** were purified by precipitation in tetrahydrofuran (THF) from CH_2Cl_2 . **3.3-P** was purified by dialysis against acetone as it was not possible to selectively precipitate the polymer. The structures of the purified polymers were confirmed by ^1H and $^{31}\text{P}\{^1\text{H}\}$ NMR spectroscopy (Figure 8-10 to Figure 8-21). It was not possible to confirm the molar mass characteristics of the polymers by standard size exclusion chromatography due to interactions of these polyelectrolytes with the columns, as previously reported by our group and others.^{60,61} Therefore, to corroborate the expected molar masses, UV-visible spectroscopy was used to perform end group analysis based on the RAFT agent.⁶³ As shown in Table 1, these calculated values were in good agreement with those determined based on monomer conversion by NMR spectroscopy. The thermal properties of the polymers were measured by TGA and DSC. As shown in Table 3-1, all of the polymers were stable up to 345 °C or higher. The T_g s of the polymers were found to decrease with increasing alkyl chain length with **3.1-P-10k** and **3.1-P-40k** having T_g s of 219 and 215 °C respectively, **3.2-P-10k** and **3.2-P-40k** having T_g s of 143 and 158 °C respectively, and **3.3-P-10k** and **3.3-P-40k** having T_g s of 72 and 88 °C respectively (Figure 8-22, Figure 8-23). The decrease in T_g with increasing alkyl chain length can be explained by a trend toward increased segmental motion and free volume for the longer alkyl chains.⁶⁴

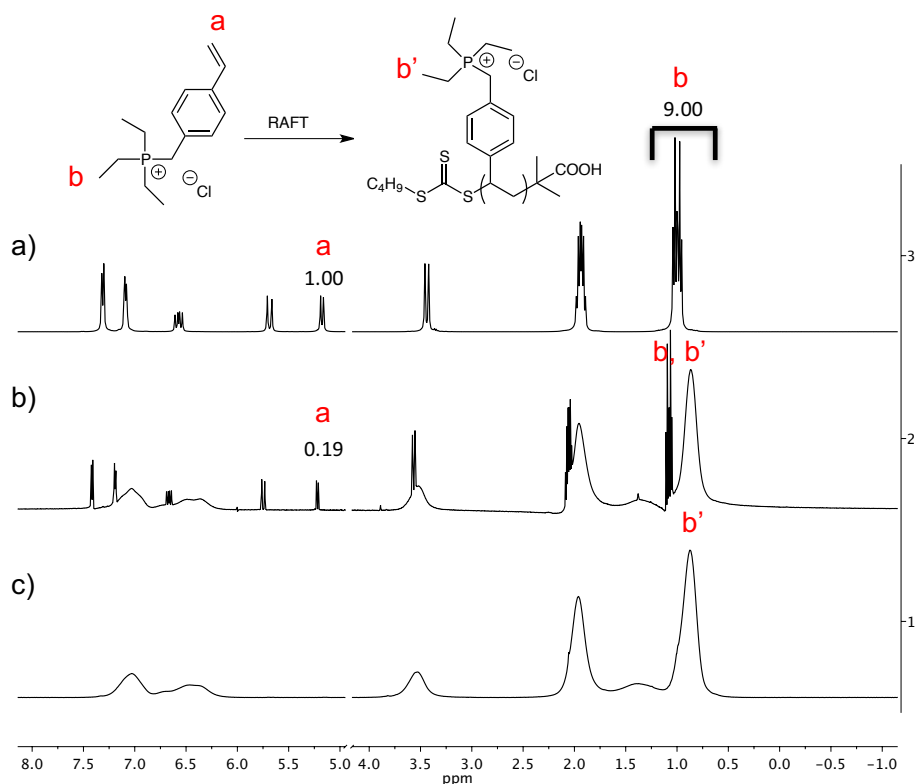


Figure 3-2: ^1H NMR spectra (400 MHz, D_2O) of a) The 3.1 polymerization mixture prior to polymerization; b) Unpurified 3.1-P-40k polymerization mixture at 81% conversion; c) Purified 3.1-P-40k. Monomer conversion was determined based on the relative integration of 9.0 throughout the polymerization.

Table 3-1: Summary of the polyphosphonium prepared for this study as well as their molar mass characteristics and thermal properties. ^aMeasured by ^1H NMR spectroscopy; ^bMeasured by UV-vis spectroscopy (error corresponds to the standard deviation on 3 measurements).

Polymer	M_n based on monomer conversion ^a (kg/mol)	M_n based on end-group analysis ^b (kg/mol)	Decomposition onset temperature (T_o , °C)	T_g (onset, °C)
3.1-P-10k	10.6	13.8 ± 0.4	386	219
3.1-P-40k	42.5	44 ± 1	389	215
3.2-P-10k	10.6	10 ± 3	368	143
3.2-P-40k	41.7	42 ± 1	363	158
3.3-P-10k	10.5	8.4 ± 1	345	72
3.3-P-40k	40.0	32 ± 1	356	88

3.2.2 Preparation and characterization of polyphosphonium SIPNs

For the preparation of SIPNs, tetra(ethylene glycol) diacrylate (TEGDA) was selected as the cross-linker because it provides robust, flexible networks with each of **3.1-P**, **3.2-P**, and **3.3-P**. The formulations were composed of TEGDA, a polyphosphonium, and 2,2-dimethoxy-2-phenylacetophenone (DMPA) as the photoinitiator ($\lambda_{\text{max}} = 325 \text{ nm}$). Each of the six polyphosphonium was incorporated at 0.1, 1, and 10 wt% (Table 2-2). The DMPA content was fixed at 5 wt% and the TEGDA was added to make up the remaining percentage to 100% in terms of the dry weight. All formulations were diluted 2-fold with solvent to obtain homogeneous solutions, using methanol for formulations containing **3.1-P** and N,N-dimethylformamide (DMF) for **3.2-P** and **3.3-P**. For curing, the formulations were cast on clean glass slides and spacers were used to define the thickness after another glass slide was placed on top (Figure 8-24). This reproducibly produced SIPNs approximately 250 μm thick, with a surface area of approximately 2.25 cm^2 , while simultaneously enabling the polymerization to occur in an environment relatively free of oxygen, thereby reducing the rate of radical termination. This thickness and film casting method were selected to afford sufficient material for the characterization experiments described below, but other techniques such as dip coating or spin coating can be used to achieve thinner films, depending on the application. Curing was performed using a conveyor UV-curing system equipped with a mercury bulb (Figure 8-24).

Table 3-2: Summary of the composition and properties of polyphosphonium SIPNs. Each formulation contained 5 wt% DMPA, 0.1, 1, or 10 wt% polyphosphonium, and TEGDA to make up the remaining percentage. Errors are reported as the standard deviation on at least 3 measurements.

Formulation composition	Cure %	Gel Content (%)	Water contact angle (°)	Charge density (charges/cm ²) × 10 ¹⁴
3.1-P-10k (10 wt%)	82 ± 4	90 ± 2	58 ± 1	1.1 ± 0.1
3.1-P-10k (1wt%)	86 ± 1	99 ± 1	45 ± 11	0.4 ± 0.1
3.1-P-10k (0.1 wt%)	85 ± 1	90 ± 3	47 ± 4	0.4 ± 0.1
3.1-P-40k (10 wt%)	85 ± 3	97 ± 1	59 ± 1	39 ± 1
3.1-P-40k (1 wt%)	87 ± 3	98 ± 1	48 ± 1	0.09 ± 0.03
3.1-P-40k (0.1 wt%)	88 ± 1	98 ± 1	48 ± 1	0.025 ± 0.002
3.2-P-10k (10 wt%)	94 ± 2	88 ± 1	64 ± 3	198.5 ± 1.3
3.2-P-10k (1 wt%)	94 ± 2	98 ± 1	59 ± 3	192.2 ± 1.2
3.2-P-10k (0.1 wt%)	98 ± 1	95 ± 1	63 ± 7	93.1 ± 34.6
3.2-P-40k (10 wt%)	96 ± 1	86 ± 5	61 ± 2	198.6 ± 1.3
3.2-P-40k (1 wt%)	95 ± 2	94 ± 2	65 ± 2	147.3 ± 0.2
3.2-P-40k (0.1 wt%)	95 ± 1	97 ± 1	59 ± 3	50.6 ± 3.7
3.3-P-10k (10 wt%)	97 ± 2	96 ± 1	73 ± 2	204.4 ± 4.0
3.3-P-10k (1 wt%)	98 ± 1	98 ± 1	65 ± 6	190.1 ± 13.2
3.3-P-10k (0.1 wt%)	88 ± 2	98 ± 1	66 ± 7	75.7 ± 12.8
3.3-P-40k (10 wt%)	91 ± 1	98 ± 1	58 ± 2	68.1 ± 17.4
3.3-P-40k (1 wt%)	98 ± 1	98 ± 1	62 ± 5	135.2 ± 13.7
3.3-P-40k (0.1 wt%)	97 ± 1	98 ± 1	52 ± 8	106.4 ± 24.0

The properties of the SIPNs are summarized in Table 3-2. The cure percentage indicates the percentage of reacted polymerizable functional groups and was determined by ATR-FTIR spectroscopy. This was estimated based on the decrease in the height of the peak corresponding to the acrylate C=C-H bend at 810 cm⁻¹ upon conversion from formulation to SIPN in comparison to the carbonyl C=O peak at 1720 cm⁻¹ as an internal standard (Figure

8-25). All cure percentages were above 80%, although this value is likely lower than the actual percentage because although the peak height was greater than zero, no observable peak was detected (Figure 8-25). While the cure percentage indicates the percentage of reacted polymerizable functional groups, the gel content is a measure of the mass percentage of material incorporated into the network. These two values may differ from one another, as TEGDA requires the reaction of only one of its functional groups in order for it to be incorporated covalently into the network. In addition, the polyphosphonium does not have any polymerizable group that could be detected by IR spectroscopy, but could be incorporated through physical entanglements and/or by fragmentation of the terminal RAFT agent and subsequent reaction of the resulting radical-terminated polymer with the network. To assess this, SIPNs were first dried under vacuum to remove residual solvent. The dry materials were weighed, and then swelled in excess methanol (for **3.1-P**) or CH₃CN (for **3.2-P** and **3.3-P**) to remove all monomers, oligomers, and polymers that were not incorporated into the network. They were dried and re-weighed, and the mass remaining was determined as the gel content. As shown in Table 3-2, all SIPNs had gel content greater than 86%, with most higher than 90%. There were no systematic reductions in gel content upon incorporation of increasing percentages of the polyphosphonium.

Differential Scanning Calorimetry (DSC) was also performed on the SIPNs in order to probe for the potential phase separation of the polyphosphonium from the TEGDA networks. As shown in Figure 3-3, a TEGDA network without polyphosphonium had a T_g of 25 °C. As summarized in Table 3-1 and Figure 8-22 and Figure 8-23, **3.1-P** and **3.2-P** had clear T_g s of 215-219 °C and 143-158 °C respectively, while **3.3-P** exhibited more subtle T_g s of 72 - 88°C. As shown in Figure 3-3 for **3.2-P-10k** (10 wt%) the SIPN exhibited a T_g similar to that of the TEGDA alone. Similarly, no polyphosphonium T_g was observed for any other **3.2-P** or **3.3-P** SIPN at 10 wt% (Figure 8-26). This suggests that there was no detectable phase separation of the polyphosphonium from the TEGDA network, and that the polyphosphoniums were reasonably well dispersed in the network. Unfortunately, the **3.1-P** SIPNs could not be analyzed by this method as their degradation temperature ($T_o \sim 220$ °C) is below that of the T_g of **3.1-P**. Clearly, the thermal stability of the network is limited by the

TEGDA component, rather than the polyphosphonium as the polyphosphonium were stable in TGA to $> 380\text{ }^{\circ}\text{C}$.

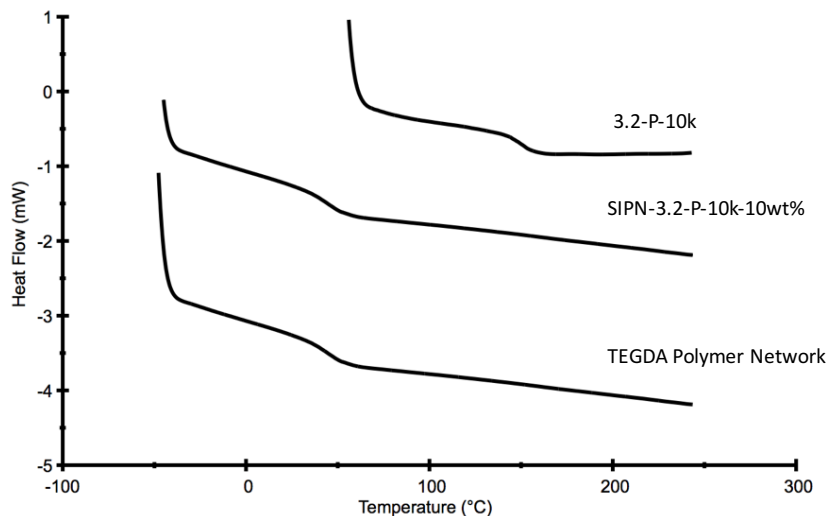


Figure 3-3: DSC curves for 3.2-P-10k, an SIPN prepared using 10 wt% of 3.2-P-10k, and an SIPN prepared from TEGDA without polyphosphonium. The results show that no polyphosphonium Tg was detected for the SIPN, suggesting the polyphosphonium is well-dispersed in the SIPN rather than phase-separated.

It has been previously reported that high surface charge is one of the most important parameters for polycationic surfaces to exhibit high antibacterial activity.⁶⁵ Specifically, a charge density of 10^{14} charges/cm² has been suggested as a minimum requirement for killing bacteria. The charge densities of the UV-cured SIPNs were evaluated by immersion of the SIPN in an aqueous solution of fluorescein dye, resulting in anion exchange with chloride anions associated with accessible phosphoniums.⁵⁶ After washing to remove excess unbound fluorescein, the surfaces were immersed in a solution of the anionic surfactant, hexadecyltrimethylammonium chloride, to exchange the fluorescein back into solution. This surfactant/fluorescein solution was measured by UV-visible spectroscopy for the quantitative analysis of fluorescein. As shown in Table 3-2, at 10 wt% loading, all phosphonium SIPNs had greater than 10^{14} cations/cm². In general, the accessible surface charge increased as the polyphosphonium content was increased from 0.1 to 10 wt%. However, there were no general trends relating the surface charge to the molar mass of the polyphosphonium. In comparison to our previously reported phosphonium networks prepared from an acrylate-functionalized phosphonium monomer via UV curing,⁵² the SIPNs prepared from **3.2-P**

displayed the same accessible surface charge at 1 – 10 wt% of polyphosphonium as the previous networks did at 40 – 50 wt% of phosphonium monomer. This may be attributed to the presence of long polyphosphonium chains at or near the surface, and the increased hydrophilicity and flexibility of the TEGDA relative to the previously used cross-linker tricyclodecanedimethanol diacrylate, which enables swelling and penetration of fluorescein into the networks.³⁰

While the SIPNs prepared from **3.2-P** and **3.3-P** had similar surface charge densities, the **3.1-P** surfaces had significantly lower surface charge densities. This initially appears counterintuitive as **3.1-P** is more hydrophilic, and has a higher charge density for a given molar mass or volume. However, hydrophilic surfaces have been reported to undergo hydrophobic recovery (surface reversion) to minimize their free energy.⁶⁶ The hydrophilicity of **3.1-P** may make it susceptible to becoming buried below the material surface, thereby reducing its accessibility. This is supported by analysis of the contact angles of the different SIPNs. SIPNs prepared at 10 wt% polyphosphonium, **3.1-P-10k** and **3.1-P-40k** had very similar contact angles ($\sim 60^\circ$) to those prepared from 10 wt% **3.2-P-10k** and **3.2-P-40k**. The contact angle of the TEGDA matrix is very similar to these values at $\sim 55^\circ$. For **3.1-P**, the contact angle decreased to less than 50° at lower loadings of 0.1 and 1 wt%, suggesting that these surfaces may be less susceptible to hydrophobic recovery, perhaps because their lower polyphosphonium content allows them to be more densely cross-linked. An SIPN prepared with **3.3-P-10k** at 10 wt% had the highest water contact angle of 73° , likely due to the long alkyl chains on the polyphosphonium. However, the SIPN prepared with **3.3-P-40k** at 10 wt% exhibited a much lower contact angle of 58° . During preparation of the SIPNs, it was noted that formulations containing **3.3-P-40k** were the most difficult to dissolve and it is likely that during UV curing some phase separation occurred, resulting in poor incorporation of the 10 wt% **3.3-P-40k** into the SIPN. This is corroborated by the relatively low surface charge for this SIPN in comparison with other **3.3-P** SIPNs.

The potential for the SIPNs to swell was probed by measuring the mass swelling ratios after incubation in water for 24 h. Upon incorporation of the polyphosphonium into the networks, the swelling increased from $4 \pm 2\%$ for a TEGDA network to 28 ± 2 , 52 ± 6 , and $35 \pm 2\%$

for **3.1-P-10k (10 wt%)**, **3.2-P-10k (10 wt%)**, and **3.3-P-10k (10 wt%)** respectively. The high swelling of the **3.2-P** SIPN may correlate with its high charge density and uniform incorporation into the network as suggested by the fluorescein assay and thermal analyses. To probe the potential for the surfaces of the SIPNs to reorganize over time, the phosphorus weight content was analyzed by SEM-EDX for freshly prepared and 8-month-old surfaces of **3.1-P-10k (10 wt%)**, **3.2-P-10k (10 wt%)**, and **3.3-P-10k (10 wt%)**. No significant changes in phosphorus content were observed, suggesting that network formation fixes the polyphosphonium in place, resulting in stable materials. Any organization of the **3.1-P-10k (10 wt%)** SIPN that serves to bury the phosphosphoniums occurred during or immediately following network formation and not over longer time periods.

3.2.3 Antibacterial testing of the SIPNs

Prior to antibacterial testing, the SIPNs were washed extensively (H₂O for **3.1-P** and CH₃CN for **3.3-P** and **3.2-P**) to ensure that any observed activity did not arise from leachable phosphoniums but rather from the SIPN itself (Figure 8-28). Washed and dried SIPNs were then freshly ground into dispersible powders for testing. Antibacterial testing was performed using the standard testing method ASTM E2149-13a,⁵⁷ involving the incubation of SIPNs with *S.aureus* (ATCC 6538) and *E.coli* (ATCC 29425) as representative strains of Gram-positive and Gram-negative bacteria respectively, for 1 hour at room temperature with agitation. The testing was performed at a concentration of 0.02 g/mL of SIPN and 10⁵ CFUs/mL in the case of *E.coli* and 10⁶ CFUs/mL for *S.aureus*. The experiments were performed in triplicate. Based on preliminary results suggesting that 10 wt% polyphosphonium was required for high bacterial killing, only the SIPNs prepared from 10 wt% polyphosphonium were tested.

The antibacterial activity against *S.aureus* was highest for **3.1-P** and **3.2-P** with a >99.9% reduction of bacterial CFUs, regardless of the molar mass of the polyphosphonium. The more hydrophobic **3.3-P-10k** SIPN provided a significantly ($P < 0.05$) lower, 50% reduction in *S.aureus* CFUs and the **3.3-P-40k** SIPN did not provide any reduction in *S.aureus* CFUs. This decrease in antibacterial activity with increasing alkyl chain length may be attributed to several factors. First, as noted above, the ~40 kg/mol **3.3-P** exhibited poor miscibility in the

SIPN formulation, leading to an unexpectedly low contact angle and low charge density, suggestive of poor incorporation into the SIPN. However, the SIPN prepared from the ~ 10 kg/mol **3.3-P** had a higher contact angle than the analogous SIPNs prepared from **3.1-P** and **3.2-P** and a similar surface charge density, suggesting the polyphosphonium was well-incorporated into the SIPN. Previously, a parabolic relationship between the hydrophobicity of polyphosphonium and their abilities to kill Gram-positive bacteria has been reported.⁴⁹ This arises from the complex mechanism by which phosphoniums are proposed to kill bacteria. The mechanism is proposed to involve 6 steps: (1) initial adsorption; (2) diffusion to the cytoplasmic membrane; (3) binding to the membrane; (4) disruption and disintegration of the membrane; (5) release of cytoplasmic components; and (6) death of the cell.⁶⁷ While increasing the hydrophobicity of the phosphonium may enhance binding to and disruption of the membrane, it may slow other steps such as the initial adsorption. This will be explored in more detail below.

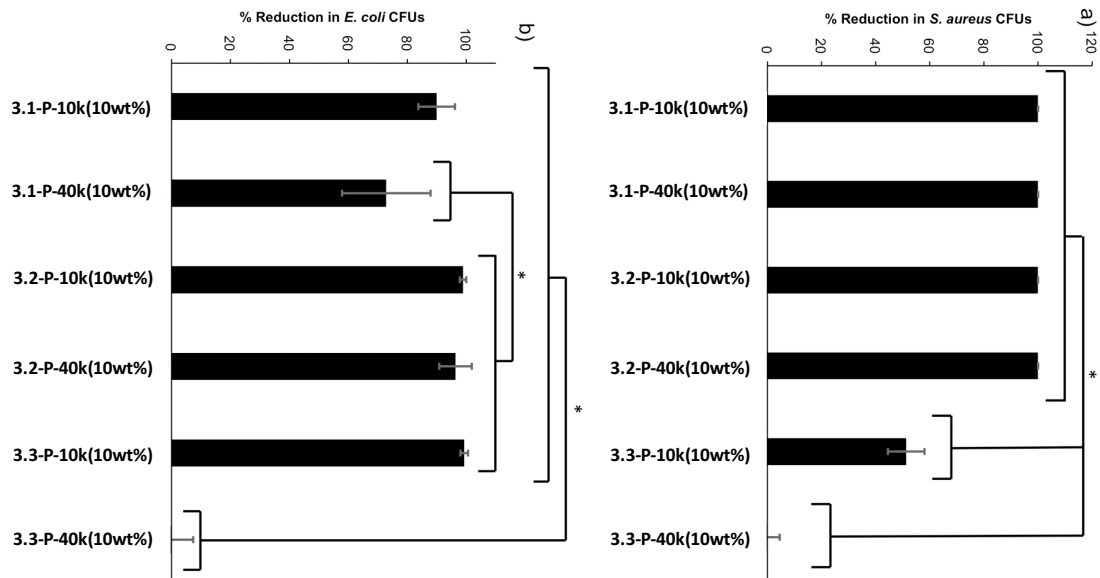


Figure 3-4: SIPN activity versus a) *S. aureus* and b) *E. coli* in the dynamic contact antibacterial test. SIPNs were tested at 0.02 g/mL against a bacterial concentration of 10^6 CFUs/mL of *S. aureus* and 10^5 CFUs/mL of *E. coli* for 1 hour. 0% reduction corresponds to the mean number of bacterial colonies counted when a control suspension of bacteria incubated in phosphate buffer without polymer was plated on agar, while 100% reduction corresponds to the observation of no bacterial colonies. Raw data can be found in

Table 8-3 and

Table 8-4. * Indicates statistical significance at the $P < 0.05$ level as determined by an ANOVA followed by a Tukey's test.

The ability to kill *E.coli* was lower than that of *S.aureus* for some of the SIPNs. This has also been observed for polyphosphonium and polyammonium previously.^{49,68} SIPNs prepared from **3.1-P-10k** and **3.1-P-40k** reduced *E.coli* CFUs by 90% and 73% respectively, though these results were not different statistically. SIPNs containing **3.2-P-10k** and **3.2-P-40k** both exhibited high killing of 99% and 97% of *E.coli* respectively, significantly greater than **3.1-P-40k**. Unlike for *S.aureus*, the **3.3-P-10k** SIPN also effectively killed *E.coli* at a level statistically greater than **3.1-P-40k**. This is consistent with previous results, where increasing the phosphonium alkyl substituent chain length also increased the antibacterial efficacy against *E.coli*⁶⁹ and can be explained by the different structures of the bacterial cell walls of Gram-negative and Gram-positive bacteria. Again, the SIPN prepared from **3.3-P-40k** did not exhibit any significant activity relative to the other SIPNs, likely due to poor incorporation of the polyphosphonium into the network.

To ensure that the decrease in measured viable bacteria was not due to bacterial attachment and colonization on the SIPNs, a Live/Dead® assay was performed. This assay focused on *S.aureus* as *E.coli* didn't exhibit any detectable colonization of the surfaces under the testing conditions. A suspension containing 10^7 CFUs/mL of *S. aureus* was deposited on the SIPNs or on a control glass slide and incubation for 24 hours. Non-adherent bacteria were rinsed off, and then the LIVE/DEAD™ cell viability assay was performed, resulting in the labeling of live bacteria on the SIPN surface in green and dead bacteria in red. As shown in Figure 3-5a, a high density of live bacteria was observed on the control surface. The SIPN **3.1-P-40k** had a very small number of live bacteria on the surface but a high density of dead bacteria. This suggests that the indications of the dynamic contact test that this surface was able to kill a high percentage of bacteria were valid. However, there was a tendency for dead bacteria to adhere to this surface, which may be undesirable in terms of the ability of the surface to kill bacteria over the longer term. SIPNs prepared from 10 wt% of **3.2-P-40k** and **3.3-P-40k** did

not have any detectable live bacteria on the surface and had much fewer dead bacteria. This suggests that increased hydrophobicity of the polyphosphonium may be beneficial for reducing fouling of the surface. It was also confirmed that the SIPNs were not leaching antibacterial phosphoniums as no zone of inhibition was observed for any of the materials in a standard zone of inhibition test (Figure 8-29).

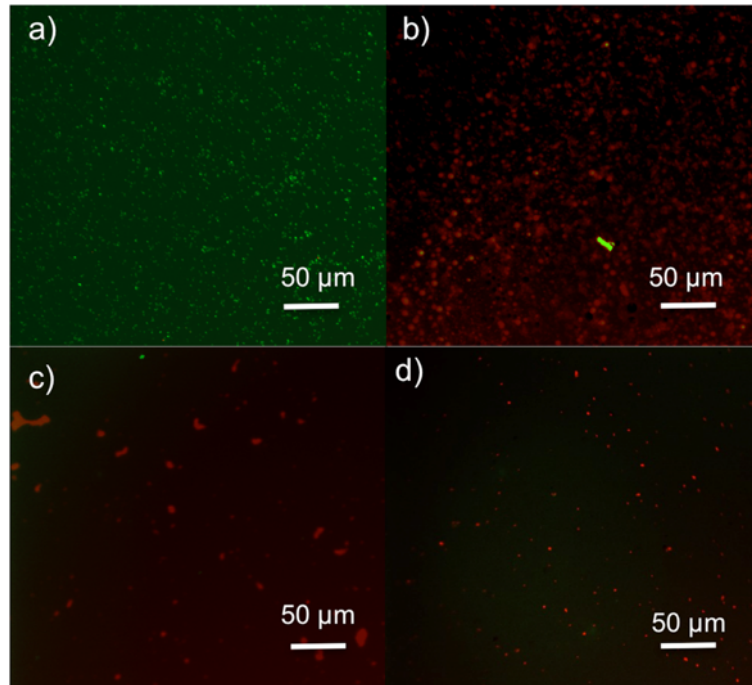


Figure 3-5: Control and SIPN surfaces following Live/Dead® analysis after incubation of the surfaces in a suspension of 10^7 CFUs/mL of *S.aureus* for 24 hours: a) control glass slide; b) SIPN 3.1-P-40k (10 wt%); c) SIPN 3.2-P-40k (10 wt%); d) SIPN 3.3-P-40k (10wt%). Live bacteria appear green in this assay due to staining with SYTO 9, while dead bacteria appear red due to staining with propidium iodide. While live bacteria are observed on the control surfaces, decreasing numbers of dead bacteria are observed on the SIPNs with increasing phosphonium alkyl chain length.

3.3 Conclusions

Six polyphosphonium with ethyl, butyl or octyl chains on the phosphonium and molar masses of either ~ 10 kg/mol or ~ 40 kg/mol were synthesized. Using UV curing, these polymers were incorporated into SIPNs based on TEGDA at loadings of either 0.1, 1 or 10 wt%. High curing and gel content were achieved. Thermal analyses suggested that the polyphosphonium that was incorporated into the network quite uniformly, without phase

separation. At 10 wt% of polyphosphonium in the formulation, all of the resulting SIPNs had greater than 10^{14} accessible surface charges per cm^2 , indicating that these SIPNs can present similar surface charge to previous polyphosphonium networks that contained much higher loadings of ~50 wt% phosphonium monomer. However, the SIPNs prepared from **3.1-P** generally had lower surface charge densities than would be expected, which was attributed to the tendency of these hydrophilic polyphosphonium to become buried below the surface to some extent due to the tendency of surface to minimize their free energy. The contact angles of the surfaces ranged from 45° for the **3.1-P-10k** at 1 wt% to 73° for **3.3-P-10k** at 10 wt%. On the other hand, the contact angle for **3.3-P-40k** was much lower, which was attributed to some miscibility issues that were encountered during the SIPN preparation. Other than this, no significant effects of polyphosphonium molar mass were observed. Antibacterial testing was performed on the SIPNs prepared from 10 wt% polyphosphonium with Gram-positive *S.aureus* and Gram-negative *E.coli*. All **3.1-P** and **3.2-P** SIPNs exhibited high activity against *S. aureus*, while the activity of the **3.3-P-10k** was somewhat lower and the **3.3-P-40k** SIPN did not kill *S. aureus*, likely due to the miscibility issue described above. On the other hand, the activities of the SIPNs against *E.coli* increased with the alkyl chain length on the phosphonium resulting in high activity for the **3.2-P** and the **3.3-P-10k** SIPNs. A Live/Dead® assay revealed that dead bacteria tended to adhere to the **3.1-P** SIPN surface, whereas it adhered to **3.2-P** and **3.3-P** SIPNs to a much lesser extent. These results suggest that **3.2-P** SIPNs provide the good balance of broad spectrum bacterial killing and anti-fouling properties. Overall, this study shows that polyphosphonium SIPNs can be prepared through a simple UV curing process and that their properties can be tuned according to the phosphonium content and phosphonium alkyl chain length. These SIPN coatings could be suitable for many different applications including high bacterial transfer objects in hospitals or public areas such as elevator buttons, door handles, railings, or beds.

3.4 Experimental

General materials and procedures

3.4⁵⁴ and **3.5**⁵⁵ were synthesized according to previously published procedures. **3.1**, **3.2**, and **3.3** were prepared by modifications of previously reported procedures. Solvents were purchased from Caledon Laboratory Chemicals (Georgetown, ON, Canada). Deuterated

solvents were purchased from Cambridge Isotopes Laboratories (Tewksbury, MA, USA). Phosphines were supplied by Cytec Solvay (Niagara Falls, ON, Canada). VA-044 was purchased from Toronto Research Chemicals (Toronto, ON, Canada). All other chemical reagents were purchased from Sigma Aldrich (St. Louis, MO, USA). All solvents and chemicals were used as received unless otherwise noted. Nuclear Magnetic Resonance (NMR) spectroscopy was conducted on a Varian Inova 400 MHz Spectrometer (Varian, Palo Alto, CA, USA) (^1H 400.09 MHz, $^{31}\text{P}\{^1\text{H}\}$ 161.82 MHz). All ^1H and $^{13}\text{C}\{^1\text{H}\}$ NMR spectra were referenced relative to the residual solvent peak (CHCl_3 : ^1H δ = 7.26, ^{13}C δ = 77; H_2O : ^1H δ = 4.79). All $^{31}\text{P}\{^1\text{H}\}$ NMR spectra were referenced using an external standard (85% H_3PO_4 : ^{31}P δ = 0). Coupling constants (J) are expressed in Hertz (Hz). Fourier transform infrared (FTIR) spectroscopy was conducted using a Bruker Tensor 27 spectrometer (Bruker, Billerica, MA, USA) in attenuated total reflectance mode (ATR) using a ZnSe crystal or a Perkin Elmer FT-IR Spectrum Two Spectrometer (Waltham, MA, USA) in the universal attenuated total reflectance mode (UATR), using a diamond crystal as well as the UATR sampling accessory (part number L1050231). Differential scanning calorimetry (DSC) was completed on a DSC Q20 TA Instruments (Waters, New Castle, DE, USA) at a heating rate of 10°/minute, under an N_2 atmosphere, in an aluminum Tzero™ pan with approximately 5 mg of sample. The glass transition temperature (T_g) was determined from the second heating cycle. Thermogravimetric analysis (TGA) was completed on a Q600 SDT TA Instruments and analyzed using TA Universal Analysis, under an N_2 atmosphere at a heating rate of 10 °C/min up to 600 °C using a ceramic pan with approximately 2 mg of sample. UV-Vis spectroscopy was conducted using a Varian Cary 300 Bio UV-Vis Spectrophotometer (Varian, Palo Alto, CA, USA) and quartz 1 cm path length cells.

General method for the polymerization of phosphonium monomers 3.1, 3.2 and 3.3

Monomer (**3.1**), initiator (**3.6**), and RAFT agent (**3.4**) were dissolved in H_2O in a round bottom flask, and the flask was sealed with a new Suba-Seal® septum (Sigma Aldrich, St. Louis, USA) and Teflon tape. Alternatively, monomers (**3.2**, and **3.3**), initiator (**3.7**), and RAFT agent (**3.5**) were dissolved in CH_3CN in a round bottom flask, and flask was sealed as above. The reaction mixture was degassed by bubbling N_2 through the solution with stirring at 0 °C for 30 minutes. The reaction flask was then put directly into an oil bath at the

appropriate temperature to initiate the polymerization. **3.1** was polymerized at 60 °C and **3.2** and **3.3** were polymerized at 80 °C. Aliquots were taken throughout the reaction to monitor the conversion by ^1H NMR spectroscopy, observing the decrease of the vinylic protons between 5 and 6 ppm in comparison to the protons at ~1 ppm corresponding to the methyl groups on the phosphonium alkyl substituents that were set to a constant integration of 9. When the reaction reached ~80% conversion, the reaction was removed from the oil bath, cooled to room temperature and exposed to air. The solvent was then removed *in vacuo*, the crude reaction mixture was redissolved (**3.1-P** in isopropanol, **3.2-P** in CH_2Cl_2) and then the polymer was precipitated in an anti-solvent (**3.1-P** and **3.2-P** in THF), collected by vacuum filtration, and dried *in vacuo*. **3.3-P** was purified by dialysis against $(\text{CH}_3)_2\text{CO}$ with a regenerated cellulose membrane (Spectra/Por® RC) with molecular weight cutoff (MWCO) of 35 kg/mol.

Synthesis of triethyl(4-vinylbenzyl)phosphonium chloride (3.1)

Triethylphosphine (5.46 g, 46.2 mmol) and 4-vinylbenzyl chloride (6.87 g, 45.0 mmol) were dissolved in CH_3CN (15 mL) under an N_2 atmosphere in a pressure tube and stirred at 80 °C for 16 hours. The solvent was then removed *in vacuo*. The resulting solid was dissolved in minimal CH_2Cl_2 (10 mL) and precipitated in Et_2O (500 mL). The precipitate was filtered, washed with Et_2O , and dried *in vacuo* yielding a white powder (13.2 g, 93%). Spectral data agreed with those previously reported.¹ A ^1H NMR spectrum is included for comparison with those of the polymers (Figure 8-7).

Synthesis of tributyl(4-vinylbenzyl)phosphonium chloride (3.2)

Tributylphosphine (12.1 g, 59.9 mmol) and 4-vinylbenzyl chloride (8.68 g, 56.9 mmol) were dissolved in CH_3CN (50 mL) under an N_2 atmosphere in a pressure tube and stirred at 80 °C for 16 hours. The solvent was then removed *in vacuo*. The resulting oil was dissolved in a minimal amount of CH_2Cl_2 (5 mL) and then precipitated in cold Et_2O (500 mL). The precipitate was filtered, washed with Et_2O , and dried *in vacuo* yielding a white powder (17.1 g, 85%). Spectral data agreed with those previously reported.¹ A ^1H NMR spectrum is included for comparison with those of the polymers (Figure 8-8).

Synthesis of trioctyl(4-vinylbenzyl)phosphonium chloride (3.3)

Trioctylphosphine (10.3 g, 19.7 mmol) and 4-vinylbenzyl chloride (4.07 g, 26.6 mmol) were dissolved in CH₃CN (30 mL) under an N₂ atmosphere in a pressure tube and stirred at 80 °C for 24 hours. The solvent was then removed in *vacuo*. The resulting solid was dissolved in minimal CH₂Cl₂ (3 mL) and precipitated in Et₂O (500 mL). The precipitate was filtered, washed with Et₂O, and dried in *vacuo*, yielding a white powder (9.61 g, 68 %). Spectral data agreed with those previously reported.¹ A ¹H NMR spectrum is included for comparison with those of the polymers (Figure 8-9).

3.1-P-10k

Monomer = **3.1** (1.50 g, 5.54 mmol); Initiator = **3.6** (0.010 g, 0.031 mmol); Solvent = H₂O (30 mL); RAFT agent = **3.4** (0.037 g, 0.14 mmol). The polymer was purified by precipitation from isopropanol into THF. Yield = 0.66 g, 55%; M_n based on ¹H NMR spectroscopy = 10.6 kg/mol; M_n based on UV-vis spectroscopy = 13.8 ± 0.4 kg/mol; ¹H NMR (D₂O): δ = 7.03 (broad, Ar-H, ortho to CH₂-P), 6.46 (broad, Ar-H, meta to CH₂-P), 3.52 (broad, Ar-CH₂-P), 1.96 (broad, P-CH₂-CH₃, backbone C-H), 1.37 (broad, backbone CH₂), 0.87 (broad, P-CH₂-CH₃); ³¹P{¹H} NMR (CDCl₃): δ = 37.6 (s); T_o = 386 °C; T_g = 224 °C.

3.1-P-40k

Monomer = **3.1** (1.51 g, 5.58 mmol); Initiator = **3.6** (3.0 mg, 9.3 μmol); Solvent = H₂O (30 mL); RAFT agent = **3.4** (8.0 mg, 0.032 mmol). The polymer was purified by precipitation from isopropanol into THF. Yield = 1.39 g, 92%. M_n based on ¹H NMR spectroscopy = 42.5 kg/mol; M_n based on UV-vis spectroscopy = 40.6 ± 1.1 kg/mol. ¹H NMR (D₂O): δ = 7.21 (broad, Ar-H, ortho to CH₂-P), 6.55 (broad, Ar-H, meta to CH₂-P), 3.55 (broad, Ar-CH₂-P), 2.14 (broad, P-CH₂-CH₃, backbone C-H), 1.57 (broad, backbone CH₂), 1.06 (broad, P-CH₂-CH₃); ³¹P{¹H} NMR (D₂O): 37.0; T_o = 389; T_g = 220 °C

3.2-P-10k

Monomer = **3.2** (0.913 g, 2.57 mmol); Initiator = **3.7** (3.0 mg, 0.018 mmol); Solvent = CH₃CN (3.6 mL); RAFT agent = **3.5** (0.021 g, 0.057 mmol). The polymer was purified by

precipitation from CH_2Cl_2 into THF. Yield = 0.528 g, 58%. M_n based on ^1H NMR spectroscopy = 10.6 kg/mol; M_n based on UV-vis spectroscopy = 9.9 ± 2.9 kg/mol. ^1H NMR (CDCl_3): δ = 7.49 (broad, Ar-H, ortho to $\text{CH}_2\text{-P}$), 6.51 (broad, Ar-H, meta to $\text{CH}_2\text{-P}$), 4.36 (broad, Ar- $\text{CH}_2\text{-P}$), 2.40 (broad, P- $\text{CH}_2\text{-(CH}_2\text{)}_2\text{-CH}_3$ and backbone CH), 1.40 (broad, P- $\text{CH}_2\text{-(CH}_2\text{)}_2\text{-CH}_3$ and backbone CH_2), 0.85 (broad, P- $\text{(CH}_2\text{)}_3\text{-CH}_3$); $^{31}\text{P}\{^1\text{H}\}$ NMR (161.82 MHz, CDCl_3): δ = 31.3; T_o = 363 °C; T_g = 147 °C

3.2-P-40k

Monomer = **3.2** (0.756 g, 2.13 mmol); Initiator = **3.7** (0.8 mg, 5 μmol); Solvent = CH_3CN (3.00 mL); RAFT agent = **3.5** (5.0 mg, 0.014 mmol). The polymer was purified by precipitation from CH_2Cl_2 into THF. Yield = 0.416 g, 55%. M_n based on ^1H NMR spectroscopy = 41.6 kg/mol. M_n based on UV-vis spectroscopy = 41.6 ± 1.1 kg/mol; ^1H NMR (CDCl_3): δ = 7.36 (broad, Ar-H, ortho to $\text{CH}_2\text{-P}$), 6.36 (broad, Ar-H, meta to $\text{CH}_2\text{-P}$), 4.36 (broad, Ar- $\text{CH}_2\text{-P}$), 2.54-2.38 (broad m, P- $\text{CH}_2\text{-(CH}_2\text{)}_2\text{-CH}_3$ and backbone CH), 1.40 (broad, P- $\text{CH}_2\text{-(CH}_2\text{)}_2\text{-CH}_3$ and backbone CH_2), 0.85 (broad, P- $\text{CH}_2\text{-(CH}_2\text{)}_2\text{-CH}_3$); $^{31}\text{P}\{^1\text{H}\}$ NMR (CDCl_3): δ = 31.3; T_o = 363 °C; T_g = 169 °C

3.3-P-10k

Monomer = **3.3** (0.821 g, 1.56 mmol); Initiator = **3.7** (4.0 mg, 0.024 mmol); Solvent = CH_3CN (3.28 mL); RAFT agent = **3.5** (2.3 mg, 0.063 mmol); The polymer was purified by dialysis. Yield = 0.295 g, 36%. M_n based on ^1H NMR spectroscopy = 10.5 kg/mol. M_n based on UV-vis spectroscopy = 8.4 ± 0.1 kg/mol; ^1H NMR (CDCl_3): δ = 7.50 (broad, Ar-H, ortho to $\text{CH}_2\text{-P}$), 6.51 (broad, Ar-H, meta to $\text{CH}_2\text{-P}$), 4.36 (broad s, Ar- $\text{CH}_2\text{-P}$), 2.40 (broad, P- $\text{CH}_2\text{-(CH}_2\text{)}_4\text{-CH}_3$ and backbone CH), 1.40 (broad, P- $\text{CH}_2\text{-(CH}_2\text{)}_6\text{-CH}_3$ and backbone CH_2), 0.85 (broad, P- $\text{(CH}_2\text{)}_7\text{-CH}_3$); $^{31}\text{P}\{^1\text{H}\}$ NMR (CDCl_3): δ = 31.8; T_o = 345 °C; T_g = 81 °C

3.3-P-40k

Monomer = **3.3** (1.003 g, 1.916 mmol); Initiator = **3.7** (1.0 mg, 6 μmol); Solvent = CH_3CN (4.00 mL); RAFT agent = **3.5** (7.0 mg, 0.019 mmol); Yield = 0.230 g, 23%; M_n based on ^1H NMR spectroscopy = 40 kg/mol; M_n based on UV-vis spectroscopy = 31.7 ± 1.3 kg/mol; ^1H NMR (CDCl_3): δ = 7.30 (broad, Ar-H, ortho to $\text{CH}_2\text{-P}$), 6.30 (broad, Ar-H, meta to $\text{CH}_2\text{-P}$),

4.37 (broad, Ar-CH₂-P), 2.36 (broad, P-CH₂-(CH₂)₆-CH₃ and backbone CH), 1.45-1.10 (broad m, P-CH₂-(CH₂)₆-CH₃ and backbone CH₂), 0.76 (broad s, P-(CH₂)₇-CH₃); ³¹P{¹H} NMR (CDCl₃): δ = 31.0; T_o = 353 °C; T_g = 94 °C

Determination of M_n by end-group analysis using UV-vis spectroscopy

Calibration curves were prepared using **3.4** (in H₂O) and **3.5** (in CH₃CN) over concentration ranges of 1 x 10⁻⁴ to 8 x 10⁻⁵ M and 1 x 10⁻³ to 1 x 10⁻⁴ M respectively to determine the extinction coefficients (ε) of the polymer end-groups. These were determined to be 12279 M⁻¹ cm⁻¹ and 1150 M⁻¹ cm⁻¹ for **3.4** and **3.5** respectively at 310 nm. Purified linear polymers were thoroughly dried in a vacuum oven at 50 °C overnight before testing. A mass (m) of polymer (~ 1 mg) was accurately weighed on an analytical balance, and then dissolved in solvent (**3.4** in H₂O; **3.5** in CH₃CN) in a volumetric flask to a volume (V) of 25 mL. The absorbance (A) of the solution at 310 nm was measured and the concentration (c) in mol/L was calculated using A = εbc where b is the path length in cm. After determining c, M_n was calculated as M_n = m/(cV). Each polymer was measured in triplicate and the results are reported as the mean ± standard deviation.

3.4.1 Preparation and characterization of polyphosphonium SIPNs

Polyphosphonium, TEGDA, and 2,2-dimethoxy-2-phenylacetophenone (DMPA) were combined in the ratios indicated in Table 2 and diluted to 50 wt% in either methanol (**3.1-P**) or N,N-dimethylformamide (DMF) (**3.2-P** and **3.3-P**). 80 μL of the resulting solution was deposited on a clean glass slide. Using ~170 μm thick electrical tape as a spacer to define the SIPN thickness, a second glass slide was then placed on top. The slides were passed 5 times at the slowest speed (~ 0.06 m/s) through a modified UV-curing system from UV Process Supply Inc. (Chicago, IL, USA) equipped with a Mercury Bulb with an energy and power density of UVA (1784 mJ/cm², 192 mW/cm²), UVB (1647 mJ/cm², 178 mW/cm²), and UVC (369 mJ/cm², 43 mW/cm²), and UVV (1869 mJ/cm², 199 mW/cm²) determined by a PP2-H-U Power Puck II purchased from EIT Instrument Markets (Sterling, VA, USA). Post irradiation, the glass slides were separated and the resulting material was dried overnight in a

vacuum oven at 50 °C. This process resulted in SIPNs with a thickness of ~ 150 μm as measured by a micrometer.

Measurement of cure percentage

ATR-FTIR spectra were obtained before curing and for freshly prepared SIPNs after drying overnight in a vacuum oven at 50 °C to remove solvent. The peak corresponding to C=O (1720 cm⁻¹) was used as an internal standard as its intensity does not change upon curing. The intensity of the C=C peak (810 cm⁻¹) was compared to that of the internal standard before curing and after curing and the cure percentage was calculated as the percent decrease in the relative intensity of the C=C peak, with 100% corresponding to zero C=C functionality remaining. Each SIPN was measured in triplicate and the results are reported as the mean ± standard deviation.

Measurement of gel content

SIPNs from the cure percentage analysis were used to calculate gel content. The SIPN was accurately weighed and then immersed in excess (~10 mL) of either methanol for **(3.1-P)**, or CH₃CN for **(3.2-P)** and **(3.3-P)** for 16 hours. The solvent was removed and the SIPN was dried in a vacuum oven at 50 °C overnight, then reweighed. The % mass remaining relative to the initial mass was determined to be the gel content. All samples were measured in triplicate and the results are reported as the mean ± standard deviation.

Measurement of the water contact angle

After incubation in solvent (as described above for the measurement of gel content) and drying, the SIPNs were placed on the stage of a Kruss DSA100 Drop Shape Analyzer (KRÜSS GmbH, Hamburg, Germany). Values were determined after one minute of droplet incubation on the surface. A static drop shape analyzer was used to determine the water contact angle on the surface. Each SIPN was measured in triplicate and the results are reported as the mean ± standard deviation.

Charge density determination

This procedure was based on the previously reported protocol.⁵⁶ After incubation in solvent (as described above for the measurement of gel content) and drying, the SIPNs (2.25 cm²)

were immersed in 10 mL of a 1% w/v aqueous sodium fluorescein solution overnight. The resulting films were washed with water, and then immersed in 10 mL of a 0.1% v/v aqueous cetyl trimethyl ammonium chloride solution overnight. The surface was then removed and 10 mM, pH 8 phosphate buffer was added and the absorbance of the solution at 501 nm was measured. The concentration of accessible charges on the surface was then determined based on the extinction coefficient of fluorescein ($\epsilon = 77,000 \text{ M}^{-1}\text{cm}^{-1}$), assuming that each molecule of fluorescein binds to one accessible cation. Each SIPN was measured in triplicate and the results are reported as the mean \pm standard deviation.

Measurement of mass swelling ratio in water

After incubation in solvent (as described above for the measurement of gel content) and drying, the SIPNs were weighed, and then swelled in deionized water for 24 hours. The SIPNs were then removed from the water, excess water was removed with a Kimwipe, and the SIPN was weighed. The mass swelling % was determined as (final mass-initial mass)/initial mass \times 100%. This experiment was performed in triplicate for SIPNs **3.1-P-10k (10wt%)**, **3.2-P-10k (10wt%)**, and **3.3-P-10k (10wt%)** and the error on the measurement was reported as the standard deviation.

Determination of surface phosphorus content over time

After incubation in solvent (as described above for the measurement of gel content) and drying, the SIPNs were either measured freshly prepared (within 24 h) or after 8 months under an air atmosphere at ambient temperature. Scanning electron microscopy with energy dispersive X-ray spectroscopy (SEM-EDX) was conducted using a Hitachi S-3400N microscope with an INCA EDX attachment and software, and all surfaces were sputter coated with 5 nm of osmium prior to analysis. This experiment was performed for **SIPNs 3.1-P-10k (10wt%)**, **3.2-P-10k (10wt%)**, and **3.3-P-10k (10wt%)**.

Dynamic contact antibacterial test

This procedure was based on ASTM E2149 13a.⁵⁷ SIPNs were prepared for testing by first ensuring the removal of any potentially leachable biocide. Each SIPN was immersed in solvent (**3.1-P** in H₂O, **3.2-P** in CH₃CN, **3.3-P** in CH₃CN) with three changes of solvent over

a period of 24 h. UV-vis spectroscopy of the washes indicated that no further components were released into solution after this protocol. The SIPNs were then dried in *vacuo* at 50 °C overnight. They were then ground using a mortar and pestle with 95% ethanol (5 drops) until solvent evaporated and a dry fine powder was obtained. The resulting solid was completely dried in a vacuum oven at 50 °C overnight and then used immediately for testing. A loop of precultured *E.coli* (ATCC 29425) or *S.aureus* (ATCC 6538) was freshly cultured in Lysogeny broth (LB) (VWR International, Mississauga, Canada) for 18 - 24 hours at 37 °C (75% humidity) in a shaker at 175 rpm. The resulting suspension was centrifuged for 10 minutes, decanted, and resuspended in 0.3 mM, pH 7, KH₂PO₄ buffer. This was repeated twice. The resulting pelletized bacteria was suspended in 0.3 mM KH₂PO₄ and diluted to concentrations of 10⁸ CFU/mL of *S.aureus* (optical density = 0.3 at 600 nm) and 10⁷ CFU/mL of *E. coli* (optical density = 0.2 at 600 nm) and as determined by optical density calibrations for each strain. The suspensions were each further diluted 100-fold (to 10⁶ CFU/mL for *S. aureus* and 10⁵ CFU/mL of *E. coli*) in 0.3 mM KH₂PO₄ and then 100 µL of this suspension was added to a sterilized centrifuge tube containing 2.0 mg of SIPN (prepared as described above). The resulting suspensions were then incubated at room temperature with shaking at 60 rpm on a wrist action shaker for 1 hour. Then, 900 µL of 0.3 mM KH₂PO₄ buffer was added to each suspension, diluting the suspension to 10⁵ CFU/mL for *S. aureus* and 10⁴ CFU/mL of *E. coli*. Each suspension was further diluted 10-fold, and 0.100 mL of this suspension (10³ CFU of *S. aureus* and 10² CFU of *E. coli*) were pour plated using tryptic soy agar, and incubated for 24 hours at 37 °C (75% humidity). CFUs were then counted and the results were compared with those of the control samples that were not exposed to any polymer. Each SIPN was measured in triplicate and the results are reported as the mean ± standard deviation. Statistical analyses (ANOVA followed by Tukey's test) were performed using the software Excel.

LIVE/DEAD™ BacLight bacterial viability assay

A suspension of *S.aureus* in 0.9% saline at a concentration of 10⁷ CFU/mL was prepared as described above. 1 mL of this suspension was placed on each 2.25 cm² SIPN coating (prepared on an a pristine glass slide and sterilized with ethanol). The control surface was a pristine glass slide, washed with ethanol and dried. The surfaces were placed in a petri dish,

the dish was sealed with parafilm, and the samples were incubated for 24 hours at 37 °C at 75% humidity. The surfaces were then gently washed with 10 mL of distilled water, then incubated with a mixture of the LIVE/DEAD™ BacLight bacterial viability assay dyes (SYTO 9 and propidium iodide, Life Technologies, Burlington, Canada) for 30 minutes in the dark according to the manufacturer's directions. The surfaces were then gently washed with deionized water and treated with Prolong Antifade mounting reagent (ThermoFisher Scientific, Massachusetts, USA) and covered with a slip cover. The prepared surfaces were then imaged by laser fluorescence microscopy using an Upright Zeiss Axioimager Z1 fluorescence microscope (Zeiss, Oberkochen, Germany) (Laser 488 nm for the SYTO 9 with a pass filter of 505-530 nm and a laser at 543 nm for the propidium iodide with a pass filter of 615 nm, magnification 40×). All the images were obtained and refined with the ZEN software. Each sample was tested in triplicate.

Zone of inhibition test for leaching

An even lawn of *S.aureus* was scratch plated onto an agar plate from a 10⁶ CFU/mL suspension of the bacteria. SIPNs were cut with a razor blade into squares of approximate dimensions of 1 cm x 1 cm. The SIPN was then placed face down on the agar and incubated for 24 hours at 37 °C and 75% humidity. Surfaces had no zone of inhibition (a ring or space from the edge of the SIPN surface where no bacteria are present) indicating a surface that does not leach an active amount of biocide.

3.5 References

- 1) Chen, Q.; Chen, H.; Zhu, L.; Zheng, J. *J. Mater. Chem. B*. **2015**, *3*, 3654–3676.
- 2) Kloxin, C. J.; Bowman, C. N. *Chem. Soc. Rev.* **2013**, *42*, 7161–7173.
- 3) Ligon, S.; Schwentenwein, M.; Gorsche, C.; Stampfl, J.; Liska, R. *Polym. Chem.* **2015**, *7*, 257–286.
- 4) Markovic, G.; Marinovic-Cincovic, M.; Jovanovic, V.; Samarzija-Jovanovic, S.; Budinski-Simendic, J. *Natural Rubber Materials*; Thomas, S.; Han Chan, C.; Pothen, L.; K. R., R.; Maria, H., Eds.; RSC Polymer Chemistry Series; The Royal Society of Chemistry, 2014.

- 5) Hart, L. R.; Li, S.; Sturgess, C.; Wildman, R.; Jones, J. R.; Hayes, W. *ACS Appl. Mater. Interfaces* **2016**, *8*, 3115–3122.
- 6) Yue, J.; Zhao, P.; Gerasimov, J. Y.; van de Lagemaat, M.; Grotenhuis, A.; Rustema-Abbing, M.; van der Mei, H. C.; Busscher, H. J.; Herrmann, A.; Ren, Y. *Adv. Funct. Mater.* **2015**, *25*, 6756–6767.
- 7) Ahadian, S.; Sadeghian, R. B.; Salehi, S.; Ostrovidov, S.; Bae, H.; Ramalingam, M.; Khademhosseini, A. *Bioconjug. Chem.* **2015**, *26*, 1984–2001.
- 8) Matricardi, P.; Di Meo, C.; Coviello, T.; Hennink, W. E.; Alhaique, F. *Adv. Drug Deliv. Rev.* **2013**, *65*, 1172–1187.
- 9) Gong, J. P.; Katsuyama, Y.; Kurokawa, T.; Osada, Y. *Adv. Mater.* **2003**, *15*, 1155–1158.
- 10) Pascal, T.; Mercier, R.; Sillion, B. *Polymer* **1990**, *31*, 78–83.
- 11) Do, H. S.; Park, Y. J.; Kim, H. J. *J. Adhes. Sci. Technol.* **2006**, *20*, 1529–1545.
- 12) Rumer, J. W.; Ashraf, R. S.; Eisenmenger, N. D.; Huang, Z.; Meager, I.; Nielsen, C. B.; Schroeder, B. C.; Chabinye, M. L.; McCulloch, I. *Adv. Energy Mater.* **2015**, *5*, 1401426.
- 13) Zhang, Y.; Rocco, C.; Karasu, F.; van der Ven, L. G. J.; van Benthem, R. A. T. M.; Allonas, X.; Croutxé-Barghorn, C.; Esteves, A. C. C.; de With, G. *Polymer* **2015**, *69*, 384–393.
- 14) Klibanov, A. M. *J. Mater. Chem.* **2007**, *17*, 2479–2482.
- 15) Yoshie, N.; Saito, S.; Oya, N. *Polymer* **2011**, *52*, 6074–6079.
- 16) Ahn, B. K.; Lee, D. W.; Israelachvili, J. N.; Waite, J. H. *Nat. Mater.* **2014**, *13*, 867–872.
- 17) Chen, S.; Li, J.; Zhu, Y.; Guo, Z.; Su, S. *J. Mater. Chem. A* **2013**, *1*, 15242–15246.
- 18) Plenderleith, R. A.; Pateman, C. J.; Rodenburg, C.; Haycock, J. W.; Claeysens, F.; Sammon, C.; Rimmer, S. *Soft Matter* **2015**, *11*, 7567–7578.
- 19) Sperling, L. H. In *Advances in Chemistry*; American Chemical Society: Washington, DC, 1994; pp. 3–38.
- 20) Shaplov, A. S.; Ponkratov, D. O.; Vlasov, P. S.; Lozinskaya, E. I.; Gumileva, L. V.; Surcin, C.; Morcrette, M.; Armand, M.; Aubert, P. H.; Vidal, F.; Vygodskii, Y. S. *J.*

- Mater. Chem. A* **2015**, *3*, 2188–2198.
- 21) Chen, S.; Liu, M.; Jin, S.; Chen, Y. *J. Appl. Polym. Sci.* **2005**, *98*, 1720–1726.
 - 22) Voit, W.; Ware, T.; Gall, K. *Polymer* **2010**, *51*, 3551–3559.
 - 23) Rao, K. M.; Rao, K. S. V. K.; Ramanjaneyulu, G.; Rao, K. C.; Subha, M. C. S.; Ha, C. *J. Biomed. Mater. Res. Part A* **2013**, *102*, 3196–3206.
 - 24) Chikh, L.; Delhorbe, V.; Fichet, O. *J. Memb. Sci.* **2011**, *368*, 1–17.
 - 25) Naficy, S.; Spinks, G. M.; Wallace, G. G. *ACS Appl. Mater. Interfaces* **2014**, *6*, 4109–4114.
 - 26) Sun, Y.; Liu, S.; Du, G.; Gao, G.; Fu, J. *Chem. Commun.* **2015**, *51*, 8512–8515.
 - 27) Bradaric, C. J.; Downard, A.; Kennedy, C.; Robertson, A. J.; Zhou, Y. *Green Chem.* **2003**, *5*, 143–152.
 - 28) Berven, B. M.; Oviasuyi, R. O.; Klassen, R. J.; Idacavage, M.; Gillies, E. R.; Ragogna, P. J. *J. Polym. Sci. Part A Polym. Chem.* **2013**, *51*, 499–508.
 - 29) Guterman, R.; Berven, B. M.; Chris Corkery, T.; Nie, H. Y.; Idacavage, M.; Gillies, E. R.; Ragogna, P. J.; Corkery, C. T.; Nie, H. Y.; Idacavage, M.; Gillies, E. R.; Ragogna, P. J. *J. Polym. Sci. Part A Polym. Chem.* **2013**, *51*, 2782–2792.
 - 30) Guterman, R.; Gillies, E. R.; Ragogna, P. J. *Langmuir* **2015**, *31*, 5181–5189.
 - 31) Guterman, R.; Hesari, M.; Ragogna, P.; Workentin, M. *Langmuir* **2013**, *29*, 6460–6466.
 - 32) Guterman, R.; Gillies, E. R.; Ragogna, P. J. *Can. J. Chem.* **2015**, *481*, 1–24.
 - 33) Schultz, A. R.; Lambert, P. M.; Chartrain, N. A.; Ruohoniemi, D. M.; Zhang, Z.; Jangu, C.; Zhang, M.; Williams, C. B.; Long, T. E. *ACS Macro Lett.* **2014**, *3*, 1205–1209.
 - 34) Cloutier, M.; Mantovani, D.; Rosei, F. *Trends Biotechnol.* **2015**, *33*, 637–652.
 - 35) Zhu, X.; Jun Loh, X. *Biomater. Sci.* **2015**, *3*, 1505–1518.
 - 36) Campoccia, D.; Montanaro, L.; Arciola, C. R. *Biomaterials* **2013**, *34*, 8533–8554.
 - 37) Wong, S. Y.; Moskowitz, J. S.; Veselinovic, J.; Rosario, R. A.; Timachova, K.; Blaisse, M. R.; Fuller, R. C.; Klibanov, A. M.; Hammond, P. T. *J. Am. Chem. Soc.* **2010**, *132*, 17840–17848.
 - 38) Woo, G. L.; Mittelman, M. W.; Santerre, J. P. *Biomaterials* **2000**, *21*, 1235–1246.
 - 39) Woo, G. L. Y.; Yang, M. L.; Yin, H. Q.; Jaffer, F.; Mittelman, M. W.; Santerre, J. P.

- J. Biomed. Mater. Res.* **2002**, *59*, 35–45.
- 40) Sambhy, V.; MacBride, M. M.; Peterson, B. R.; Sen, A. *J. Am. Chem. Soc.* **2006**, *128*, 9798–9808.
 - 41) Gozzelino, G.; Lisanti, C.; Beneventi, S. *Colloids Surf., A* **2013**, *430*, 21–28.
 - 42) Muñoz-Bonilla, A.; Fernández-García, M. *Prog. Polym. Sci.* **2012**, *37*, 281–339.
 - 43) Klibanov, M.; Lewis, K.; Liao, C. J.; Tiller, J. C.; Liao, C. J.; Lewis, K.; Klibanov, M. *Proc. Natl. Acad. Sci. USA* **2001**, *98*, 5981–5985.
 - 44) Lee, S. B.; Koepsel, R. R.; Morley, S. W.; Matyjaszewski, K.; Sun, I. U.; Russell, A. *J. Biomacromolecules* **2004**, *5*, 877.
 - 45) Tang, R.; Muhammad, A.; Yang, J.; Nie, J. *Polym. Adv. Technol.* **2014**, *25*, 651–656.
 - 46) Bazaka, K.; Jacob, M. V.; Crawford, R. J.; Ivanova, E. P. *Acta Biomater.* **2011**, *7*, 2015–2028.
 - 47) Lotz, A.; Heller, M.; Dohm, N.; Cierniak, P.; Bender, K.; Jansenb, B.; Forch, R. *J. Mater. Chem.* **2011**, *22*, 19455–19461.
 - 48) Karamdoust, S.; Yu, B.; Bonduelle, C. V.; Liu, Y.; Davidson, G.; Stojcevic, G.; Yang, J.; Lau, W. M.; Gillies, E. R. *J. Mater. Chem.* **2012**, *22*, 4881–4889.
 - 49) Kanazawa, A.; Ikeda, T.; Endo, T. *J. Polym. Sci. Part A Polym. Chem.* **1993**, *31*, 335–343.
 - 50) Guo, A.; Wang, F.; Lin, W.; Xu, X.; Tang, T.; Shen, Y.; Guo, S. *Int. J. Biol. Macromol.* **2014**, *67*, 163–171.
 - 51) Xue, Y.; Xiao, H.; Zhang, Y. *Int. J. Mol. Sci.* **2015**, *16*, 3626–3655.
 - 52) Cuthbert, T.; Guterman, R.; Ragogna, P. J.; Gillies, E. R. *J. Mater. Chem. B* **2015**, *3*, 1474–1478.
 - 53) Kanazawa, A.; Ikeda, T.; Endo, T. *J. Polym. Sci. Part A Polym. Chem.* **1993**, *31*, 1467–1472.
 - 54) Haridharan, N.; Dhamodharan, R. *J. Polym. Sci. Part A Polym. Chem.* **2011**, *49*, 1021–1032.
 - 55) Lai, J. T.; Filla, D.; Shea, R. *Macromolecules* **2002**, *35*, 6754–6756.
 - 56) Murata, H.; Koepsel, R. R.; Matyjaszewski, K.; Russell, I. J. *Biomaterials* **2007**, *28*, 4870–4879.
 - 57) Standard Test Method for Determining the Antimicrobial Activity of Antimicrobial

- Agents Under Dynamic Contact Conditions E2149-13a. *ASTM International, West Conshohocken, PA 19428-2959 United States*, 2013, www.astm.org.
- 58) Keddie, D. J.; Moad, G.; Rizzardo, E.; Thang, S. H. *Macromolecules* **2012**, *45*, 5321–5342.
 - 59) Keddie, D. J. *Chem. Soc. Rev.* **2014**, *43*, 496–505.
 - 60) Hadadpour, M.; Gwyther, J.; Manners, I.; Ragogna, P. J. *Chem. Mater.* **2015**, *27*, 3430–3440.
 - 61) Wang, R.; Lowe, A. B. *J. Polym. Sci. Part A Polym. Chem.* **2007**, *45*, 2468–2483.
 - 62) Moad, G.; Rizzardo, E.; Thang, S. H. *Aust. J. Chem.* **2005**, *58*, 379–410.
 - 63) Skrabania, K.; Miasnikova, A.; Bivigou-Koumba, A. M.; Zehm, D.; Laschewsky, A. *Polym. Chem.* **2011**, *2*, 2074–2083.
 - 64) Xu, W. S.; Freed, K. F. *Macromolecules* **2014**, *47*, 6990–6997.
 - 65) Kugler, R.; Bouloussa, O.; Rondelez, F. *Microbiology* **2005**, *151*, 1341–1348.
 - 66) Kim, J.; Chaudhury, M. K.; Owen, M. J.; Orbeck, T. J. *Colloid Interface Sci.* **2001**, *244*, 200–207.
 - 67) Kenawy, E. R.; Worley, S. D.; Broughton, R. *Biomacromolecules* **2007**, *8*, 1359–1384.
 - 68) Gibney, K. A.; Sovadinova, I.; Lopez, A. I.; Urban, M.; Ridgway, Z.; Caputo, G. A.; Kuroda, K. *Macromol. Biosci.* **2012**, *12*, 1279–1289.
 - 69) Kanazawa, a; Ikeda, T.; Endo, T. *Antimicrob. Agents Chemother.* **1994**, *38*, 945–952.

Chapter 4

4 Increasing the hydrophilicity of phosphonium polymers to increase antibacterial activity and decrease hemolytic activity.

4.1 Introduction

Synthetic antibacterial polyelectrolytes containing ammonium or phosphonium functional groups have been widely investigated due to their increased activity as compared to their monomeric components. Many different nitrogen-containing polycations have been reported including polyammonium,¹⁻⁵ polyimidazolium,⁶ polybiguanide,⁷ and polypyridinium salts.⁸ Kanazawa and coworkers also reported various trialkyl/aryl phosphonium polymers in the 1990s,⁹⁻¹² but aside from our group's recent work on phosphonium-containing coatings,^{13,14} there has not been any further work on this class of antimicrobials. Antibacterial polymers have been synthesized as side chain ammonium functionalized synthetic linear polymers,^{4,15,16} dendrimers,¹⁷ and biopolymers such as chitosan.¹⁸ Along with the ionic groups, most active antibacterial polyelectrolytes possess alkyl chains that result in amphiphilic structures that have affinity for negatively charged bacterial cell walls. It is hypothesized that these units kill bacteria by damaging the cell membrane, causing permeabilization and leakage of cell contents.^{7,19}

The balance of hydrophilicity-hydrophobicity for antibacterial polymers is one that has been explored by varying cationic:hydrophobic ratios. This can be completed by using copolymers with separate hydrophilic (cations) and hydrophobic (alkyl chain) components, or by having the hydrophilic and hydrophobic components within the same comonomer (Figure 4-1). This seemingly subtle change can impart large differences in the antibacterial effectiveness, but also the compatibility to healthy cells.^{2,15,20-22}

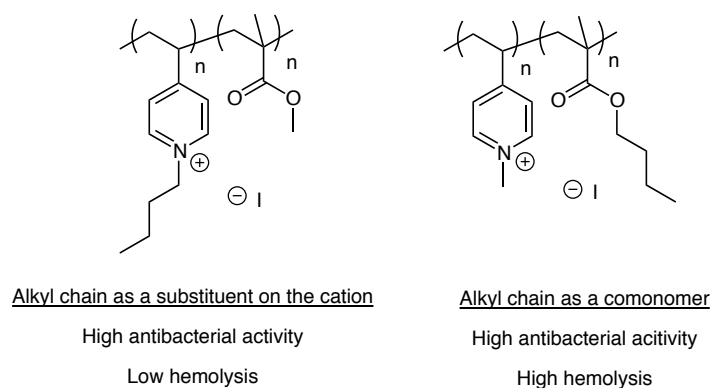


Figure 4-1: Example of hydrophilic-hydrophobic balance by charge-hydrophobic combination vs. separation.

Increases in the hydrophobicity of the antibacterial polymer are usually achieved by incorporating linear alkyl chains with increasing chain length. Increasing the alkyl chain length may increase the antibacterial activity but has also been reported to increase the hemolytic activity (lysing of red blood cells) which is detrimental for their potential use *in vivo*. Far fewer studies have reported an increase in antibacterial activity resulting from increasing the hydrophilicity of antibacterial polymers.²³

The majority of antibacterial polymers have been designed based on the principle of incorporating different hydrophilic (cationic) and hydrophobic (alkyl) components, whereas there are few reports involving other architectures. The polymerization from antibiotic β -lactams was investigated for the preparation of ammonium based antibacterial polymers. Copolymerization with ammonium containing monomers resulted in good antibacterial activity with low hemolysis.²⁴ Alternatively, the use of additives combined with traditional small molecule antibiotics has been explored as a means to increase their effectiveness. For example, the combination of aminoglycosides with sugar-based metabolites resulted in the killing of persistent bacteria (Figure 4-2).²⁵

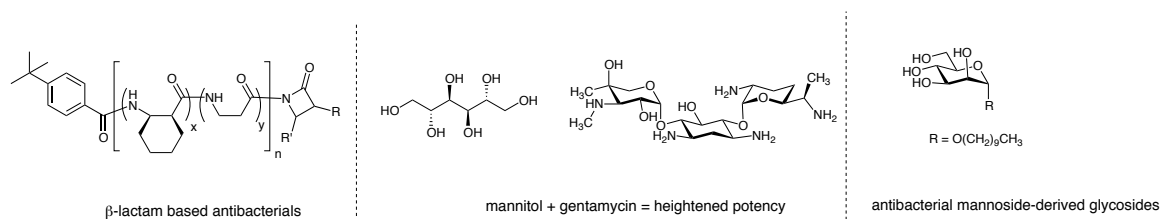


Figure 4-2: Examples of antibacterial polymers from β -lactams (left), heightened potency of antibiotics when used in conjunction with metabolites such as mannitol (middle), and antibacterial mannoside-derived glycosides (right).

Mannose is known to bind to *Escherichia coli* (*E. coli*) adhesins on the pili of the bacteria. The interactions of mannose with *E. coli* have been used for the labelling of the bacteria with gold nanoparticles and as attachment antagonists because the pili participate in surface colonization.^{26,27} Mannose has been functionalized with alkylethers and alkylthioethers to achieve bacteriostatic conditions, inhibiting the growth of *E. coli* at millimolar concentrations (Figure 4-2).²⁸

This chapter explores the introduction of targeting functional groups specific for interaction with *E. coli* onto polycations to potentially increase their antibacterial activity by bringing them into the vicinity of the bacteria. This modification will also affect the amphiphilic character by introducing more hydrophilicity onto the polymers. To achieve this, we describe the development of a new phosphonium monomer containing both alkyl and sugar substituents, with both mannose and glucose derivatives described (Figure 4-3). These new monomers are polymerized by reversible addition-fragmentation chain-transfer polymerization (RAFT) along with a control hydroxyl-functionalized phosphonium. Due to the specific adhesion of mannose to the *E. coli* pili, our initial hypothesis was that increased bactericidal activity would be observed for the mannose-functionalized polymer against *E. coli*, whereas this effect would not be observed for *S. aureus*, which does not bind to mannose. Both the antibacterial and hemolytic properties of these polymers were investigated.

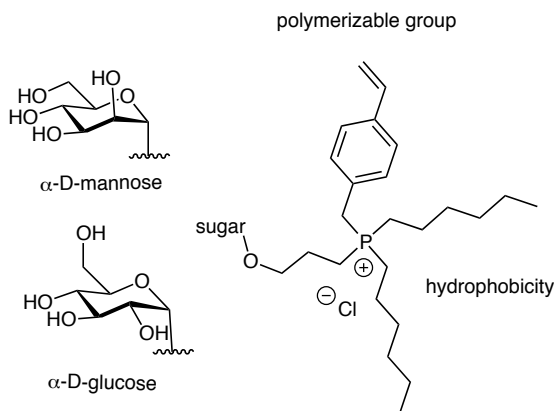
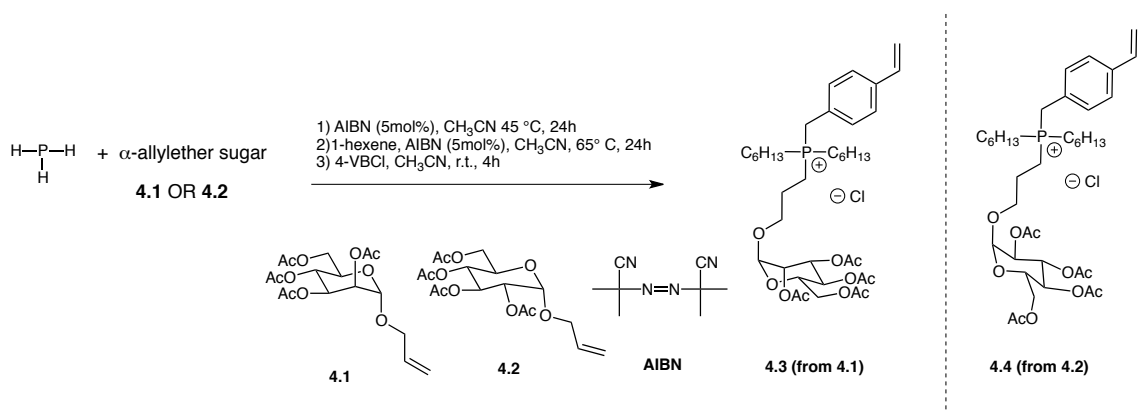


Figure 4-3: Structure of proposed targeted phosphonium monomer.

4.2 Results and Discussion

4.2.1 Synthesis of phosphonium mannoside and glucoside monomers 4.3 and 4.4

Sugars can be selectively reacted at the anomeric position to introduce different functionalities onto the periphery of the molecule. Protection of the sugar hydroxyl groups is required, not only for the selective functionalization of the sugar, but to increase the solubility of the sugar in organic solvents, and this is essential for subsequent chemical steps. To this end, both mannose and glucose were protected with acetate, then α -allylether tethers were introduced at the anomeric positions to afford compounds **4.1** and **4.2** (Scheme 4-1 and Figure 4-5).^{29,30}



Scheme 4-1: Overall synthetic approach for producing 4.3 and 4.4 from α -allylether sugars 4.1 and 4.2, respectively.

Radical initiated P-H addition across allyl functional groups is well established,³¹ and we therefore proposed to create sugar phosphines by this method using $\text{PH}_{3(\text{g})}$. This is a unique and unconventional starting reagent outside of industry, but it affords the advantage of having three accessible P-H bonds available for addition to olefins. A typical alkylation of $\text{PH}_{3(\text{g})}$ with an olefin can be completed with 10 mol% of a thermal initiator such as azobisisobutyronitrile (AIBN) at 65 °C or higher. The reaction of PH_3 with sugar derivatives **4.1** or **4.2**, resulted in a mixture of primary, secondary, and tertiary phosphines. The selective single addition of one P-H bond across an olefin-containing molecule can be performed thermally, although it is typically much more difficult to obtain the primary phosphine in a selectively manner than to achieve the tertiary phosphine. While tertiary phosphines with three sugar substituents would be an interesting compound for creating antibacterial polymers through copolymerization with hydrophobic comonomers, attempts to add three sugars resulted in multiple products, and could not be completely converted to the tertiary phosphine exclusively. In the $^{31}\text{P}\{^1\text{H}\}$ NMR spectrum obtained from a sample reaction mixture revealed peaks corresponding to primary, secondary, tertiary, and oxidized products in solution (Figure 4-4).

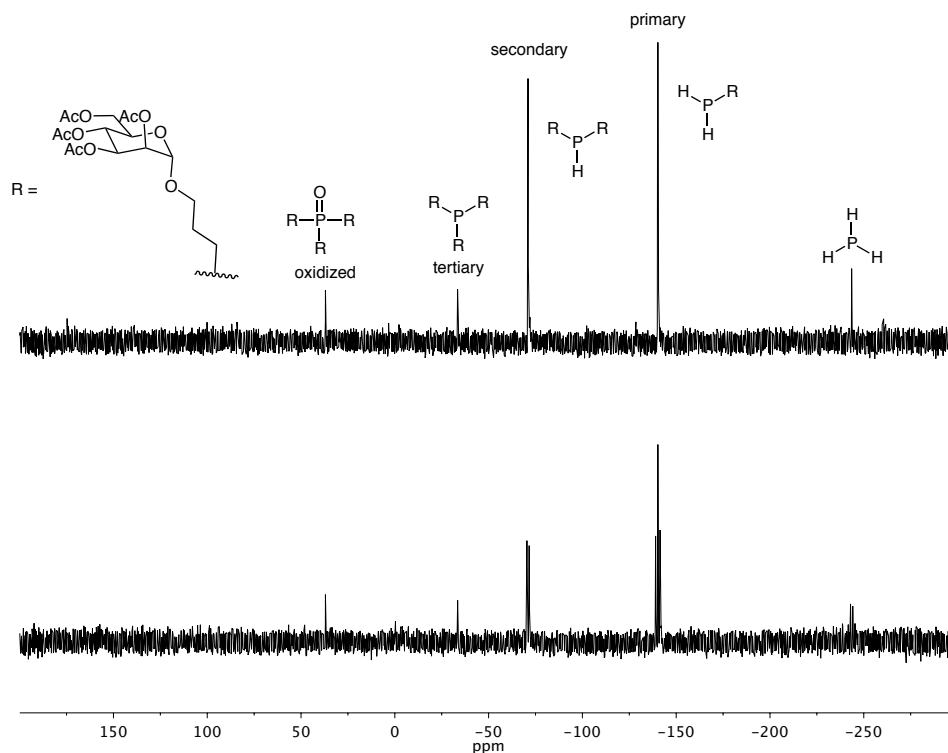


Figure 4-4: $^{31}\text{P}\{^1\text{H}\}$ (top) and ^1H coupled ^{31}P (bottom) NMR spectra of an attempt at creating a tertiary phosphine from an allylether sugar resulting in a mixture of primary, secondary, tertiary, and oxidized products.

This was not ideal and therefore, multiple reaction conditions were investigated with the aim of selectively producing the primary phosphine functionalized with one sugar. The conditions involved a much lower radical flux, which was achieved by reducing the amount of initiator to <5 mol% of AIBN with respect to **4.1** or **4.2**, to result in **4.1.P** and **4.2.P** (Figure 4-5).

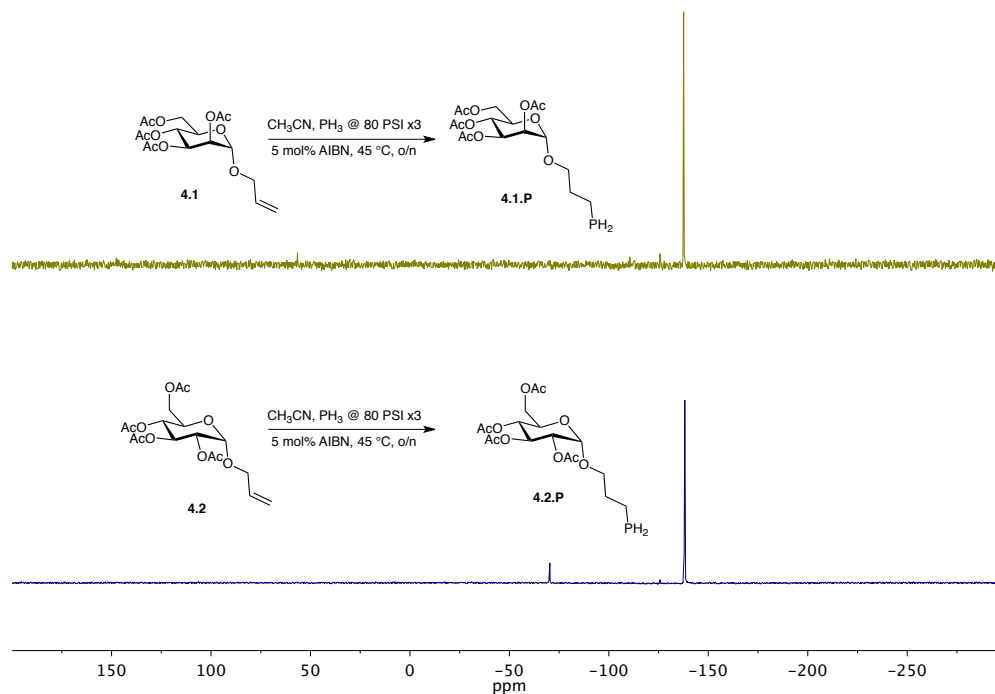


Figure 4-5: $^{31}\text{P}\{^1\text{H}\}$ NMR Spectra of the reaction mixtures for the resulting sugar functionalized primary phosphines 4.1.P and 4.2.P from α -allylether mannose (4.1) and α -allylether glucose (4.2).

The autoclave was pressurized three times with PH_3 to maintain the maximum amount of PH_3 into the CH_3CN solvent. The reaction mixture was then heated at 45°C for 24 hours. Because of the vast excess of PH_3 under these conditions, the selective conversion to the primary sugar-functionalized phosphine. The reaction was monitored by $^{31}\text{P}\{^1\text{H}\}$ NMR spectroscopy for the appearance of primary phosphine was achieved (Figure 4-5). The reaction was stopped before any appreciable amount of secondary phosphine was observed, although this meant appreciable quantities of 4.1 or 4.2 remained.

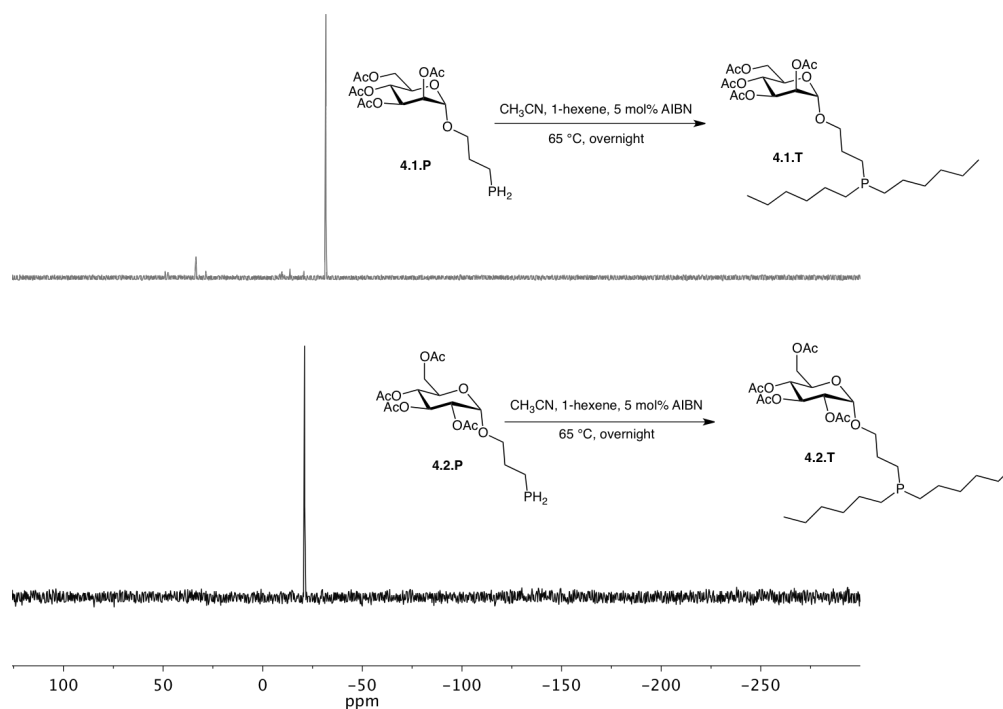


Figure 4-6: $^{31}\text{P}\{^1\text{H}\}$ NMR spectra of tertiary phosphines **4.1.T** and **4.2.T** from the reaction of 1-hexene with primary phosphines **4.1.P** and **4.2.P**, respectively.

The subsequent reaction of the remaining P-H bonds with excess 1-hexene in the presence of AIBN resulted in tertiary phosphines (**4.1.T** and **4.2.T**) and was confirmed by $^{31}\text{P}\{^1\text{H}\}$ NMR spectroscopy (Figure 4-6). **4.1.T** and **4.2.T** were then reacted with 4-vinylbenzyl chloride to produce air stable quaternary phosphonium salts (**4.3** and **4.4**) (Figure 4-7).

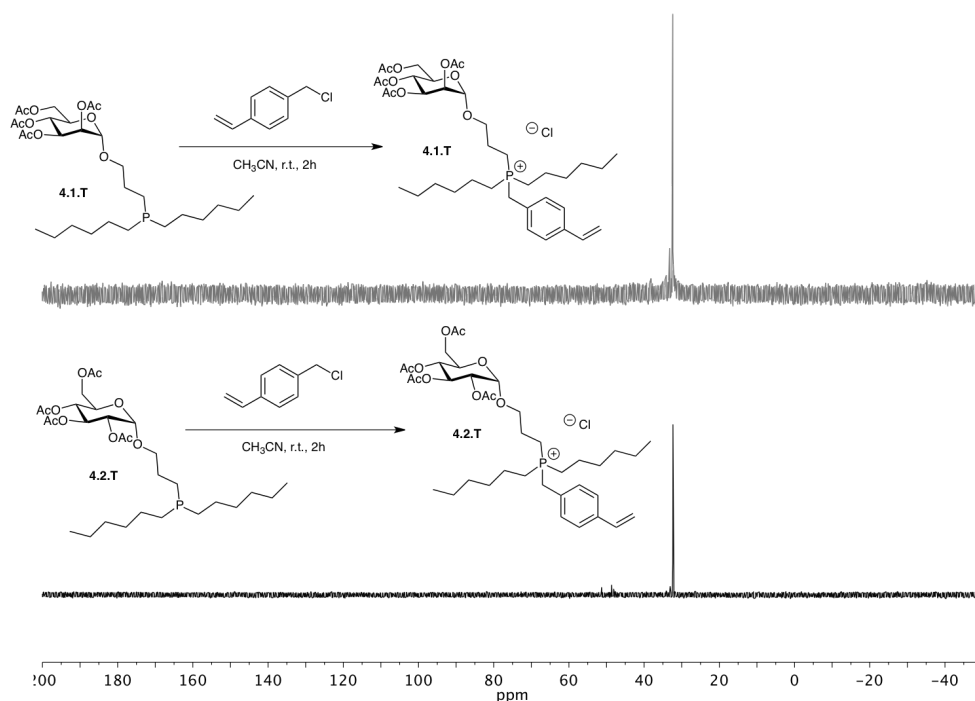


Figure 4-7: $^{31}\text{P}\{^1\text{H}\}$ NMR spectra of **4.3** and **4.4** from the quaternization of **4.1.T** and **4.2.T** with 4-vinylbenzyl chloride.

To remove any unreacted 4-vinylbenzyl chloride, **4.1**, or **4.2**, a functionalized silica gel column was used. The silica gel was functionalized with trichloromethylsilane,³² effectively capping any Si-OH functionalities. To prevent phosphonium interacted with the polar Si-OH of the silica to such an extent that elution of the salt was hindered. All impurities were first eluted with diethyl ether, followed by elution of pure **4.3** or **4.4** with methanol. The structures of the purified monomers were confirmed multinuclear NMR spectroscopy and high resolution mass spectrometry. The yield over these three steps for **4.3** and **4.4** was 11% and 7%, respectively, relative to the amount of sugar introduced. This reaction was limited to low yields because of the required reaction conditions primary phosphine selectively.

4.2.2 Polymerization of 4.3 and 4.4.

Monomers **4.3** and **4.4** were polymerized without deprotection of the sugar acetates to maintain the organic solubility. Similar degrees of polymerization were targeted for both monomers because of the known dependent antibacterial activity on molecular weight.¹⁰ RAFT was used as a controlled polymerization technique targeting between 30 and 40 repeat units. 40 equivalents of monomer to RAFT chain transfer agent (CTA) was used to reach 80-100% conversion of the monomer to polymer. Polymerizations were performed in 50/50 toluene/acetonitrile solution at 80 °C for 20 hours with **AIBN** as an initiator (Figure 4-8 and Figure 4-9).

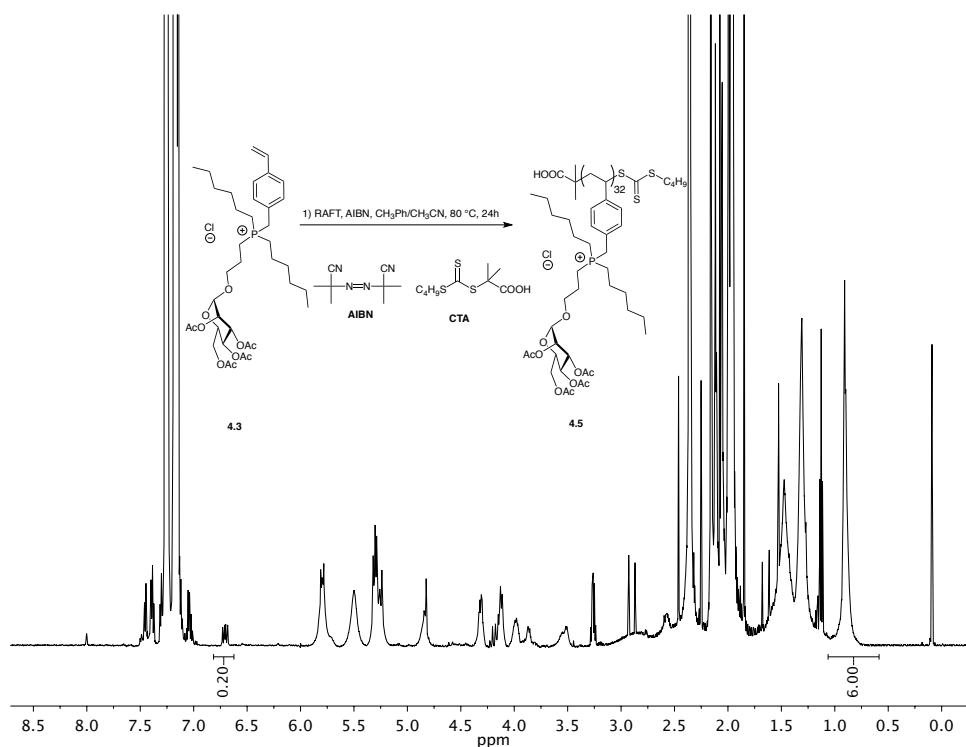


Figure 4-8: ¹H NMR spectrum of the polymerization of **4.3** with a conversion of 80% calculated by the disappearance of the vinylic protons compared to the internal standard CH₃ hexyl substituents integrating to 6 hydrogens.

Conversion was monitored using ¹H NMR spectroscopy by integrating the vinylbenzyl hydrogens relative to the internal CH₃ hydrogens of the hexane substituents, whose total integration does not change during polymerization. Polymerization reactions were halted when >80% conversion was observed.

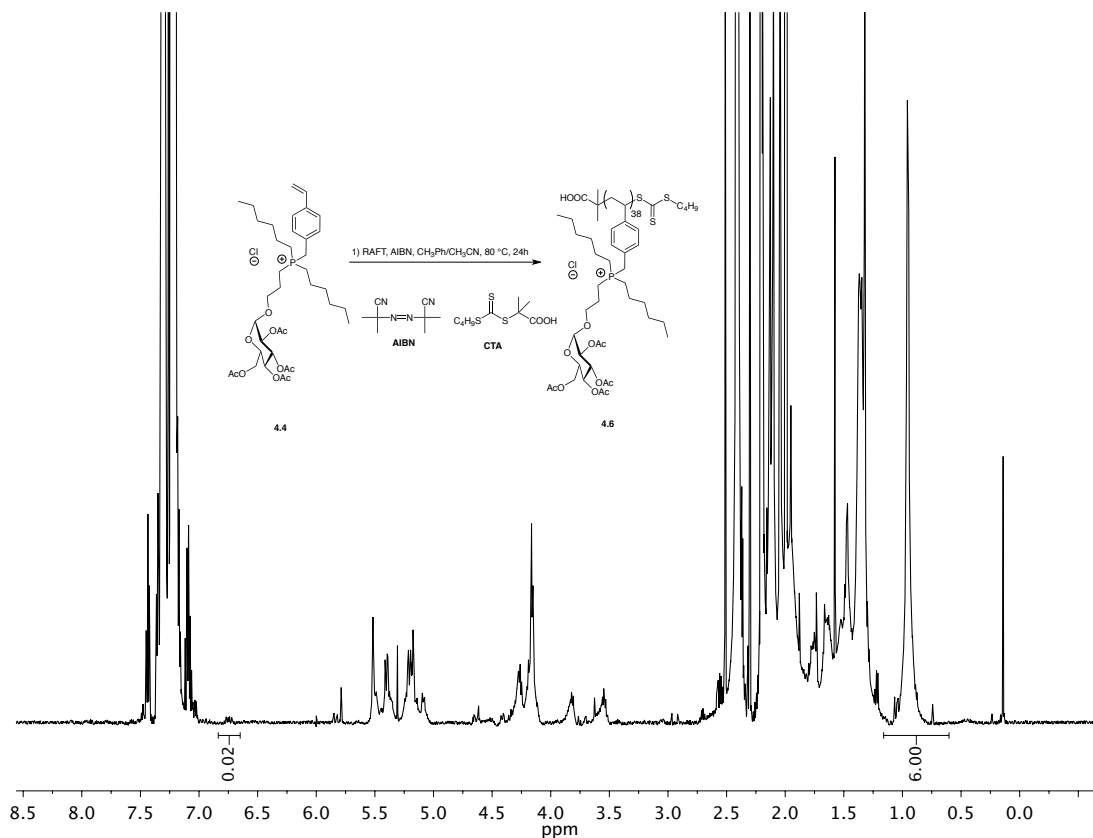
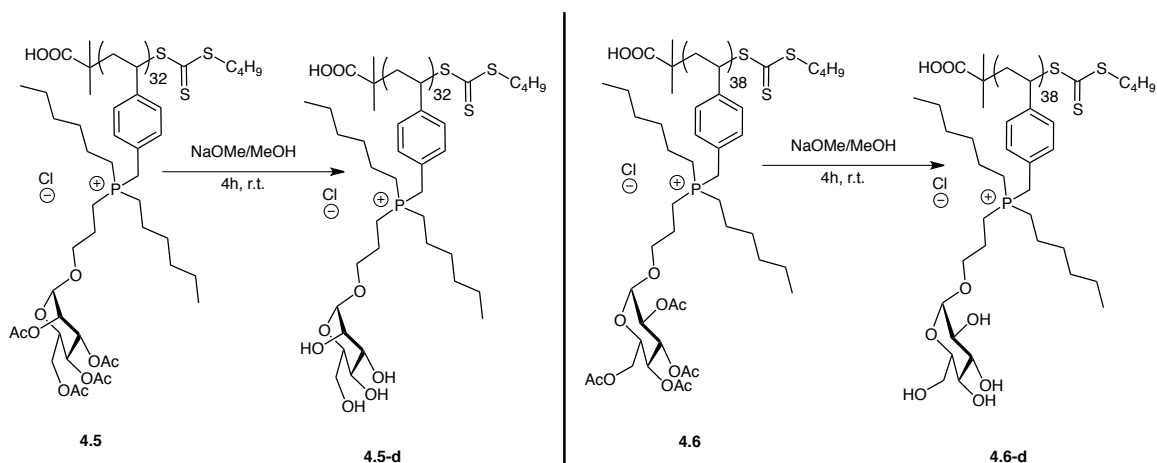


Figure 4-9: ^1H NMR spectrum of the polymerization of **4.4** with a conversion of 98% calculated by the disappearance of the vinylic protons compared to the internal standard CH_3 hexyl substituents integrating to 6 hydrogens.

After removal of volatiles in *vacuo*, the polymers were redissolved in methanol and dialyzed to remove any residual monomer. The purified polymers were characterized by ^1H and $^{31}\text{P}\{^1\text{H}\}$ NMR spectroscopy. Deprotection of the sugars was then completed by treatment with sodium methoxide in methanol, resulting in polymers **4.5-d** (Scheme 4-2 and Figure 4-10) and **4.6-d** (Scheme 4-2 and Figure 4-11). The completion of the reaction was monitored by ^1H NMR spectroscopy and the disappearance of the acetate signals as well as the corresponding single peak in the $^{31}\text{P}\{^1\text{H}\}$ NMR spectra.



Scheme 4-2: Deprotection of the polymers 4.5 and 4.6 with sodium methoxide to yield 4.5-d and 4.6-d.

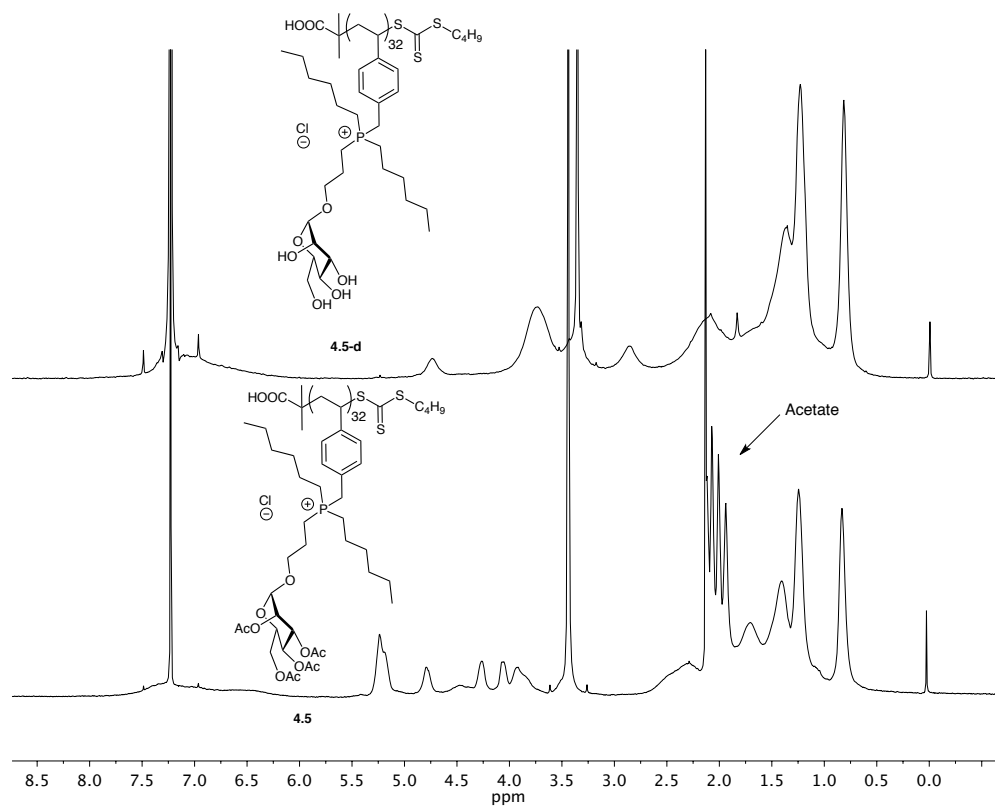


Figure 4-10: ^1H NMR spectra of deprotection of 4.5 to 4.5-d. The disappearance of the sharp peaks at ~ 2 ppm corresponding to acetate CH_3 functional groups was observed.

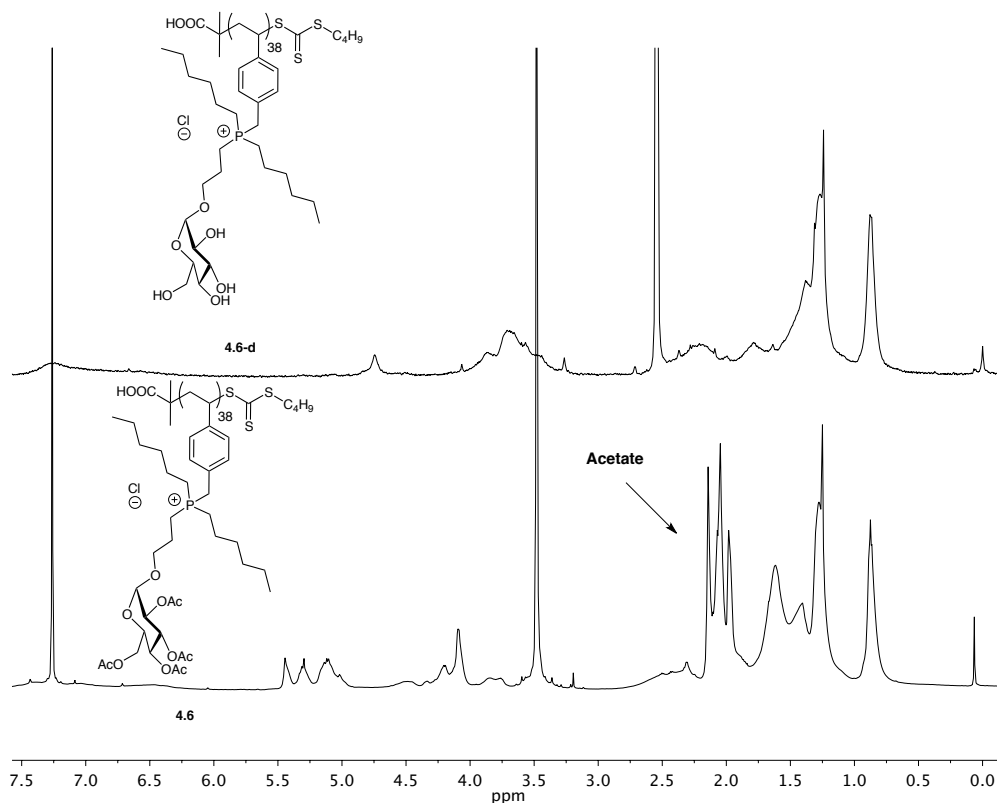
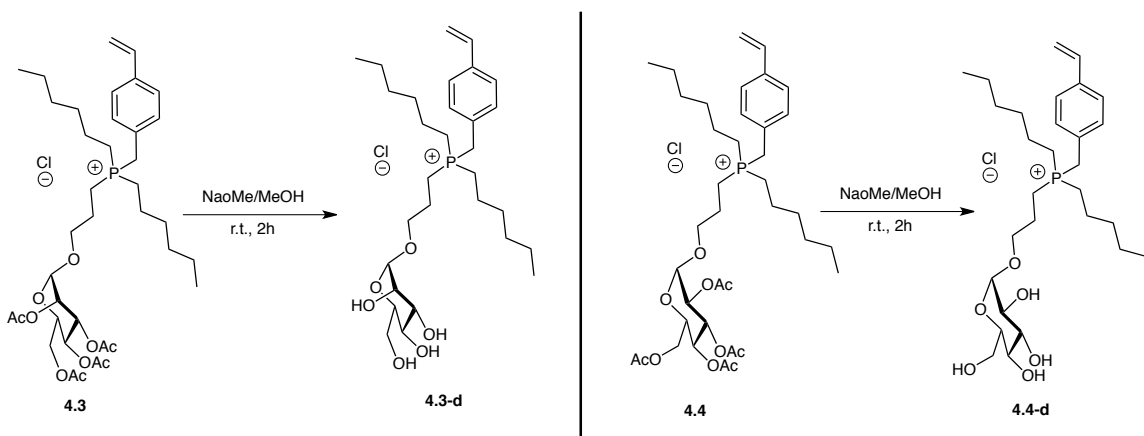


Figure 4-11: ^1H NMR spectra of the deprotection of 4.6 to 4.6-d. Disappearance of the sharp peaks at ~ 2 ppm corresponding to the acetate CH_3 functional groups was observed.



Scheme 4-3: Deprotection procedure for monomers 4.3 and 4.4 to yield 4.3-d and 4.4-d.

Deprotection of monomers 4.3 and 4.4 to afford 4.3-d and 4.4-d was also completed in order to test the activities of these small molecules against the bacteria for comparison to the polymers.

In addition, as a control, the hydroxyl-functionalized monomer tris(hydroxypropyl)vinylbenzyl phosphonium chloride (**4.7**) was also polymerized using RAFT polymerization to yield **4.8**, a polyphosphonium derivative that does not possess the sugar or the hydrophobic alkyl chains of polymers **4.5** and **4.6**.

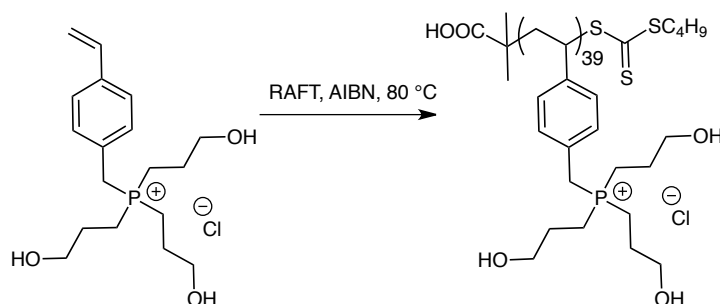


Figure 4-12: Synthesis of a control polymer 4.8 with hydroxypropyl substituents on the phosphonium.

4.2.3 Antibacterial testing

The minimum inhibitory concentrations (MIC) of **4.3-d**, **4.4-d**, **4.5**, **4.6**, **4.7**, and **4.8**, and the minimum bactericidal concentrations (MBC) of **4.5**, **4.6**, and **4.8** were evaluated against *E. coli* and *S. aureus*. This involved inoculating different concentrations of the molecules with 10^5 colony forming units (CFUs) per mL of bacteria. These samples were then incubated at 37 °C for 4 h. The MIC was determined as the minimum concentration required to inhibit bacterial growth compared to a control of only buffer. The suspensions were subsequently plated on agar, incubated for 24 h, and then the bacterial colonies were counted. The MBC was determined as the concentration required to reduce the number of bacterial colonies by >99.99% relative to the control. The results of these studies are summarized in Table 4-1 and selected plots of cell growth versus phosphonium concentration are included in Figure 4-13 and Figure 4-14. Additional plots are included in the Appendix (Figure 8-47). Both the MIC and MBC are reported in terms of phosphonium molarity to allow for effective comparison of the monomers with the polymers. The actual molarities of the polymers would be much lower.

Table 4-1: MIC and MBC values for polyphosphonium and their corresponding monomers. All concentrations correspond to the concentration of phosphonium ion.

Compound	MIC <i>E. coli</i> (μM of P^+)	MBC _{99.99} <i>E. coli</i> (μM of P^+)	MIC <i>S. aureus</i> (μM of P^+)	MBC _{99.99} <i>S. aureus</i> (μM of P^+)	HC ₅₀ (μM)
Mannose polymer 4.5-d	43	17	4.3	4.3	~180
Mannose monomer 4.3-d	5	-	5	-	-
Glucose polymer 4.6-d	8.7	8.7	4.3	4.3	~75
Glucose monomer 4.4-d	12	-	5	-	-
Tris(hydroxypropyl) polymer 4.8	2.8	2.8	2.8	2.8	>1200
Tris(hydroxypropyl) monomer 4.7	39	-	78	-	-

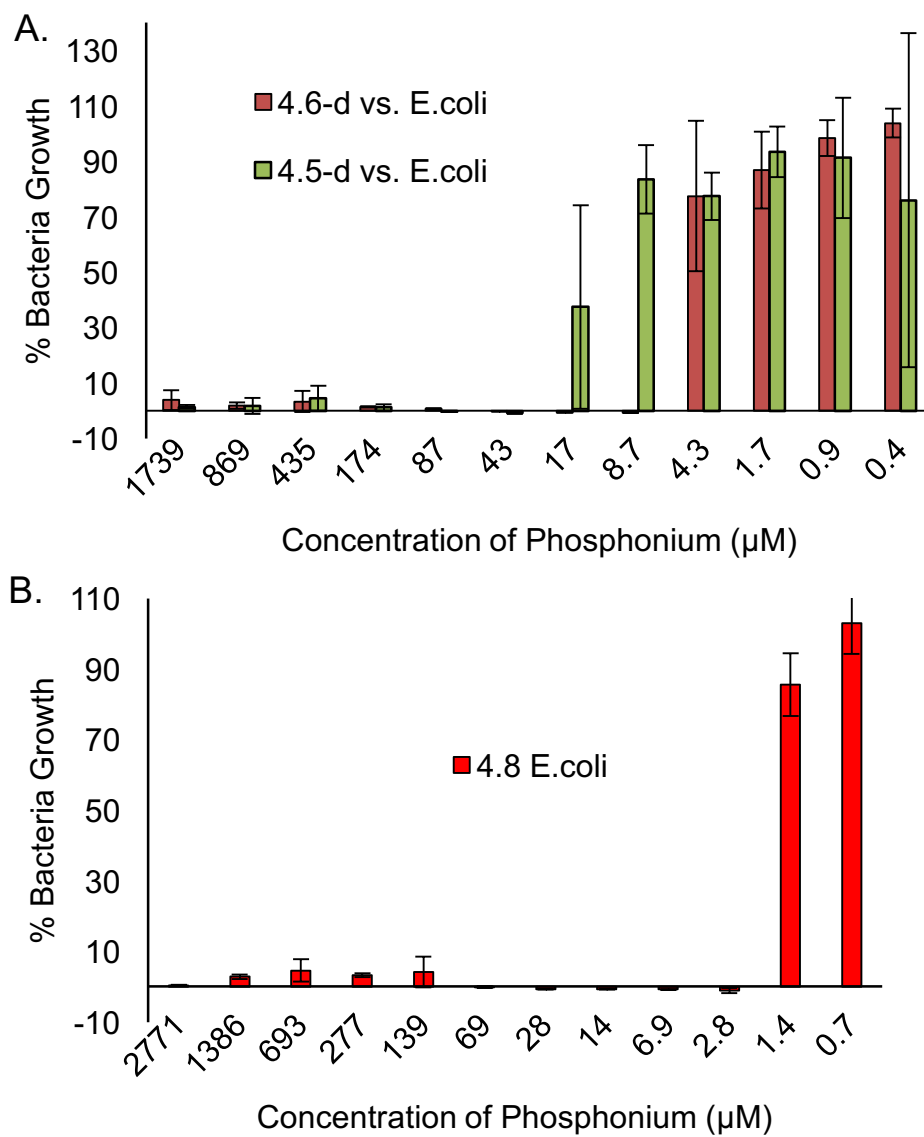


Figure 4-13: Growth of *E. coli* at different concentrations of phosphonium polymers: A) polymers 4.5-d and 4.6-d; B) polymer 4.8.

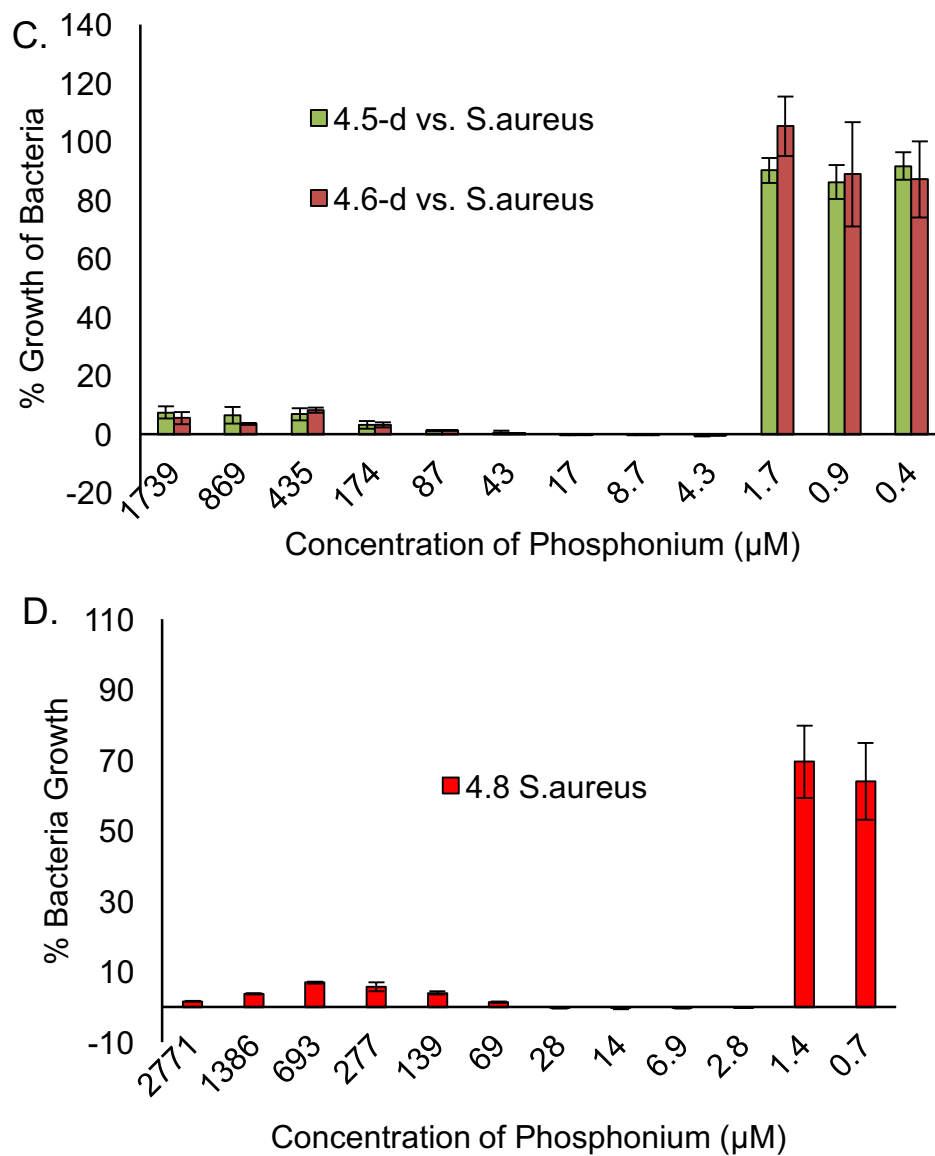


Figure 4-14: Growth of *S. aureus* at different concentrations of A) polymers 4.5-d and 4.6-d; B) polymer 4.8.

The mannose-functionalized polyphosphonium **4.5-d** had the lowest activity of the three investigated polymers against *E. coli* with an MIC of 43 μM , although no bacteria grew when colonized at the next lowest concentration of 17 μM (MBC test, Table 4-1). This was because of a possible outlier in our triplicate values, and further replicates should be completed to confirm this. A lower MIC of 17 μM would agree with the MBC results, where no bacteria were observed to grow when inoculated on growth agar. The glucose-functionalized polyphosphonium **4.6-d** exhibited intermediate activity with an MIC of 8.7 μM . Surprisingly, the most active polymer was the tris(hydroxypropyl)-functionalized polyphosphonium **4.8**, which had an MIC of 2.8 μM . The MBC values were the same as MIC values (except for **4.5-d** against *E. coli* as mentioned earlier), confirming that bacterial killing was achieved, as opposed to simply inhibition of growth. This trend was opposite to what was hypothesized, as the inclusion of the *E. coli* adhesin mannose was expected to increase the interaction of the polymer with the bacteria, resulting in more efficient killing. This could be due to the interaction of the polymer with the *E. coli* pili, which are distant from bacterial cell membrane where the polymer needs to reach and disrupt to kill the bacteria. Rather than helping to bring the polymer to the bacterial membrane, it may actually prevent the polymers from reaching the membrane making them less effective. All of the phosphonium polymers studied here had low MIC/MBC values from 4.3 μM for polymers **4.5-d** and **4.6-d** to 2.8 μM for **4.8** against *S. aureus* suggesting they are effective against both Gram-negative and Gram-positive bacteria.

Studying the hemolysis of red blood cells is an important step towards understanding the potential selective lethality of the polymers towards bacteria over mammalian cell membranes. This is indicated by the HC_{50} value, the concentration required to lyse 50% of red blood cells in the assay. As shown in Figure 4-15, mannose-functionalized polyphosphonium **4.5-d** lysed 25% of red blood cells at 70 μM , and 85% at 700 μM . Calculating the HC_{50} by plotting log of the concentration against the resulting percent hemolysis, indicated an HC_{50} of 0.1 mg/mL, corresponding to ~ 180 μM , 4 times the MIC/MBC values obtained for *E. coli* and 41 times for *S. aureus* (Figure 4-15). For an antibacterial polymer, a large difference between MIC/MBC values and HC_{50} values is ideal for selectivity against bacteria. The glucose-functionalized polymer **4.6-d** had an

HC₅₀ value of 0.04 mg/mL or ~75 μM, approximately 8 times higher than its MIC/MBC concentration for *E.coli* and 17 times higher for *S.aureus*. The trishydroxypropyl-functionalized polyphosphonium **4.8** had a very high HC₅₀, above the highest tested concentration of 1200 μM, resulting in an HC₅₀ more than 428 times the MIC/MBC values. Its low MIC/MBC values against both *E. coli* and *S. aureus* combined with the property of not lysing red blood cells makes this polymer is a very promising new antibacterial. In working with polymer **4.8**, it was found to have better water-solubility than the sugar-functionalized polymers **4.5-d** and **4.6-d**, suggesting that it is more hydrophilic. The activity of **4.8** is opposite the trend commonly reported of increasing activity with increasing alkyl chain length.⁹ There are limited examples of studies where increasing the hydrophilic character increased the antibacterial activity.²³ The current results suggest that increasing the hydrophilic character by introducing the hydroxyl groups decreases the hemolytic activity due to the absence of hydrophobic alkyl chains, and therefore increases the selectivity towards bacteria.

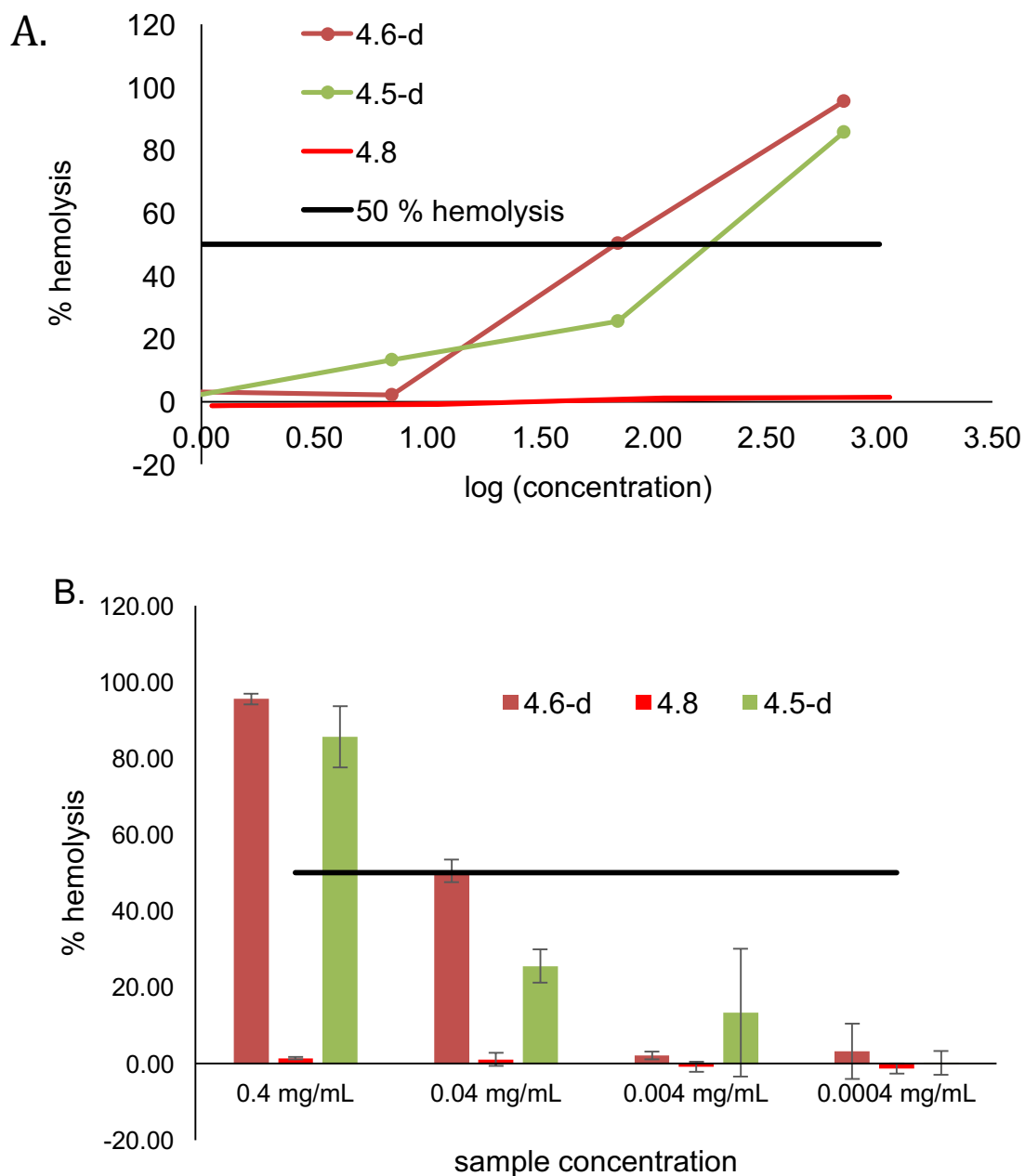


Figure 4-15: A. log(concentration) plotted against its % hemolysis to determine approximate HC_{50} values by the intersection with the black line. B. % hemolysis with respect to mass/mL. The black line indicates the HC_{50} threshold. Molarities of HC_{50} of phosphonium are summarized in Table 4-2 for a better comparison.

Deprotected monomeric compounds **4.3-d** and **4.4-d** were highly active against both *E. coli* and *S. aureus*, with **4.3-d** having a lower *E. coli* MIC and roughly the same MIC for *S. aureus* compared to its polymeric form **4.5**. **4.4-d** had a slighter higher MIC compared

to its polymeric form **4.6** against both *E. coli* and *S. aureus* (Table 4-1, Figure 8-47). These results further support the hypothesis that the sugar-functionalized polymers, particularly **4.5**, interact with the bacteria, likely through multivalent interactions, thereby sequestering them. Monomer **4.7** behaved as expected, being less active than the polymeric form with MIC values for *E. coli* and *S. aureus* over an order of magnitude higher than those of polymer **4.8**. This was expected as antibacterial polyammonium also tend to be much more active than their corresponding monomeric amines due to the possibility for the polymer to undergo multivalent interactions with the bacterial cell wall, resulting in increased binding and more effective disruption.⁷

Comparing the current results to antibacterial polymers previously reported, **4.5-d**, **4.6-d** and **4.8** (Table 4-2, Entry 1, 2, and 3) outperform tributyl and trioctyl phosphonium polymers (Table 4-2, Entry 10 and 11), and have similar MIC values to the most highly active ammonium functionalized polynorbornene polymers and ammonium copolymers with rigid backbones against *E.coli* (0.9 μ M and 9.8 μ M, respectively; Table 4-2, Entry 9 and 5). Comparison to mannoside derived glycosides (Figure 4-2, Table 4-2 Entry 4), **4.5-d**, **4.6-d**, and **4.8** have a much lower MIC against *E.coli* and 2 times lower MIC against *S.aureus*. **4.5-d**, **4.6-d**, and **4.8** outperform β -lactam based polymers against both *E.coli* and *S.aureus* (Table 4-2 Entry 6), and much higher activity in comparison to ammonium polymers with incorporated hydrophilicity (Table 4-2 Entry 8). When considering the degrees of polymerization, which provide 32-38 phosphonium cations per chain, these polymers kill bacteria at nM concentrations. Thus, these polymers, particularly **4.8**, warrant further investigation as novel antibacterials.

Table 4-2: Selected MIC and HC₅₀ values for previously reported amphiphilic antibacterial polymers. Concentrations correspond to the concentrations of cations. ^aHemolytic concentration based on 10% lysis instead of 50%; ^bThis work. ^cAll entries except entry 4 possess a polymerizable functional group as one R substituent. ^dConcentration of the molecule.

Entry	Hydrophilic component	Hydrophobic component	MIC (μM of cation) <i>E. coli</i>	MIC (μM of cation) <i>S. aureus</i>	HC ₅₀ (μM of cation)	Ref.
1 (4.5-d)	R ₄ P ⁺ /mannoside	2 x <i>n</i> -hexyl	43	4.3	~180	^b
2 (4.6-d)	R ₄ P ⁺ /glucoside	2 x <i>n</i> -hexyl	8.7	4.3	~75	^b
3 (4.8)	R ₄ P ⁺ /hydroxypropyl	-	2.8	2.8	>1200	^b
4	α- <i>O</i> -decyl-mannoside	α-decylether	1.25 x 10 ³	78	-	²⁸
5	RNH ₃ ⁺	<i>n</i> -propyl copolymer rigid backbone	9.8	39	< 133	³³
6	RNH ₃ ⁺	β-lactam backbone	55	110	440 ^a	²⁴
7	RNH ₃ ⁺	-	940	2400	<300	³⁴
8	RNH ₃ ⁺ /poly(ethylene glycol) copolymer	-	1900	8400	22400	³⁴
9	RNH ₃ ⁺	norbornene backbone	0.9	-	> 43	¹⁵
10	R ₄ P ⁺	Tri- <i>n</i> -octyl	19	19	-	⁹
11	R ₄ P ⁺	Tri- <i>n</i> -butyl	>190	19	-	⁹

4.3 Conclusions

Three new phosphonium polymers were synthesized, incorporating new functionalities onto the phosphonium cations. Mannose and glucose substituents were incorporated starting from PH₃, and the third was derived from commercially available

tris(hydroxypropyl)phosphine. It was found that the synthesis of primary phosphines could be completed with low radical flux and high PH_3 concentration, and the resulting phosphine could subsequently be functionalized with other alkenes and polymerizable groups to produce novel phosphonium monomers. These monomers were then polymerized by RAFT polymerization and tested for their antibacterial and hemolytic activity. These new functionalized phosphonium polymers had high activity, although with the opposite trend of what we expected, with the mannose functionalized phosphonium polymer possessing the least amount of activity against *E. coli*. This can likely be explained by the interaction of the polymers with the bacterial pili, which are distant from the cell membrane. The glucose functionalized phosphonium had high activity against both *E. coli* and *S. aureus*, and outperformed previously reported trioctylphosphonium polymers. Surprisingly the simple hydroxypropyl-functionalized phosphonium polymer had the highest activity against both *E. coli* and *S. aureus*, with no observed hemolytic activity at the concentrations tested. This result is significant due to the fact that there is an absence of any hydrophobic component, previously thought to be required for antibacterial activity with antibacterial polyelectrolytes. Further studies are warranted to investigate the mechanism of action of this polymer and to further explore the scope of its activity.

4.4 Experimental

General procedures and materials

4.1,²⁹ **4.2,**³⁰ and 2-(((butylthio)carbonothioyl)thio)-2-methylpropanoic acid (CTA)³⁵ were synthesized according to previously published procedures. Solvents were purchased from Caledon Laboratory Chemicals (Georgetown, ON, Canada). Deuterated solvents were purchased from Cambridge Isotope Laboratories (Tewksbury, MA, USA). $\text{PH}_3(\text{g})$ was supplied by Cytec Solvay (Niagara Falls, ON, Canada). AIBN was purchased from Sigma-Aldrich and recrystallized from methanol. Luria –Bertani Broth (Miller’s modification) was purchased from Alfa Aesar (Ward Hill, MA, USA). Luria-Bertani Agar (Miller modification) and BBL™ Levine Eosin Methylene Blue Agar were purchased from Becton, Dickinson and Company (Sparks, MD, USA). Mannitol Salt Phenol Red

Agar was purchased from Fluka Analytical (St. Louis, MO, USA). 0.3 mM KH_2PO_4 was prepared in Milli-Q water, adjusted to a pH of 7.4 and autoclaved before use. Defibrinated sheep blood was purchased from Cedarlane (Burlington, ON, Canada). All other solvents and chemicals were used as received unless otherwise noted. Nuclear Magnetic Resonance (NMR) spectroscopy was conducted on either a Varian Ionva 400 or 600 MHz spectrometer (400 MHz: $^{31}\text{P}\{^1\text{H}\}$ 161.82 MHz; 600 MHz: ^1H 599.28 MHz, $^{13}\text{C}\{^1\text{H}\}$ 150.69 MHz). All ^1H and $^{13}\text{C}\{^1\text{H}\}$ spectra were referenced relative to the residual solvent peak (CHCl_3 : ^1H $\delta = 7.26$, ^{13}C $\delta = 77$; H_2O : ^1H $\delta = 4.79$). All $^{31}\text{P}\{^1\text{H}\}$ NMR spectra were referenced using an external standard (85% H_3PO_4 : $\delta = 0$). Coupling constants (J) are expressed in Hertz (Hz). Mass spectrometry data were recorded in positive-ion mode using a Micromass/Waters Q-TOF Ultima LC-MS/MS system. *E. coli* (ATCC 29425) and *S. aureus* (ATCC 6538) were cultured on BBL™ Levin Eosin Methylene Blue Agar and Mannitol Salt Phenol Red Agar to ensure there was no contamination. Optical density measurements of the bacterial suspensions were measured using a Tecan Infinite M1000 Pro 96 well UV-vis plate reader.

Synthesis of dihexyl((2,3,4,6-tetra-*O*-acetyl-manno-pyranyl)-1-oxy-propyl)vinylbenzylphosphonium chloride (4.3).

((2,3,4,6-Tetra-*O*-acetyl-manno-pyranyl)-1-oxy-allyl (4.23 g, 10.9 mmol), AIBN (10 mg, 61 μmol), and CH_3CN (250 mL) was combined in an autoclave reactor, and purged with a N_2 flow for 10 minutes then charged with 550 kPa of $\text{PH}_{3(\text{g})}$. The reaction was stirred at room temperature for 1 hour, recharged with 550 kPa $\text{PH}_{3(\text{g})}$, stirred for one hour, and charged a third time with 550 kPa $\text{PH}_{3(\text{g})}$. The reaction was then heated to 45 °C overnight. Once cooled to room temperature, the excess PH_3 was incinerated, and the reaction mixture was checked by $^{31}\text{P}\{^1\text{H}\}$ NMR spectroscopy for primary phosphine and ^1H NMR spectroscopy for remaining olefin. If there was olefin functionality remaining, the PH_3 charging and heating process was repeated until any sign of secondary phosphine appeared. The sealed reaction was then transferred into a glovebox and the volatiles were removed in *vacuo* at 60 °C. The resulting oil was then combined in a pressure tube with 1-hexene (2.56 g, 30.8 mmol) and AIBN (0.05 g, 0.3 mmol) under a N_2 atmosphere, and heated to 65 °C overnight. The reaction was transferred into a glovebox, where an aliquot

was removed and checked by $^{31}\text{P}\{^1\text{H}\}$ NMR spectroscopy for conversion to a tertiary phosphine (≈ -30 ppm). Once all primary phosphine was converted to a tertiary phosphine, 4-vinylbenzyl chloride (1.8 g, 12 mmol) was added to the reaction mixture and it was stirred at room temperature (monitored by $^{31}\text{P}\{^1\text{H}\}$ NMR spectroscopy). Once quaternization was complete, volatiles were removed in *vacuo*, resulting in viscous orange oil. The product was purified using a methyl silyl functionalized silica plug,³² first eluting with Et₂O to remove uncharged organic by-products, followed by CH₃OH to elute the phosphonium salt. The solvent was removed in *vacuo*, yielding the product as an orange oil. Yield: 0.85 g, 11 %. ^1H (600 MHz, CDCl₃, δ): 7.39-7.29 (m, 4H), 6.63 (dd, $J = 17.5$ Hz, 11 Hz, 1H), 5.73 (d, $J = 17.6$ Hz, 1H), 5.26-5.15 (m, 4H), 4.76 (broad s, 1H), 4.26-4.22 (m, 1H), 4.12-4.03 (m, 2H), 3.90 (broad s, 1H), 3.81 (broad s, 1H), 2.29 (broad s, 2H), 2.19 (broad s, 6H), 2.10-1.94 (m, 16H), 1.41 (broad s, 6H), 1.22 (broad s, 8H), 0.82 (m, 6H); $^{31}\text{P}\{^1\text{H}\}$ (161 MHz, CDCl₃, δ): 32.33; $^{13}\text{C}\{^1\text{H}\}$ (151 MHz, CDCl₃, δ): 170.66, 170.07, 169.95, 169.56, 137.93, 135.73, 130.17, 127.41, 115.11, 97.61, 68.93 (m), 68.73, 67.29, 65.93, 62.41, 34.44, 30.93, 30.47, 30.37, 26.73 22.54, 22.28, 21.97, 21.58, 20.78, 20.64, 18.90, 18.53, 13.87; ; HRMS (ESI-TOF) m/z : Calcd for C₃₈H₆₀O₁₀P [M]⁺: 707.3924; Found 707.3922.

Synthesis of dihexyl((2,3,4,6-tetra-*O*-acetyl-gluco-pyranyl)-1-oxy-propyl)vinylbenzylphosphonium chloride (4.4).

((2,3,4,6-Tetra-*O*-acetyl-gluco-pyranyl)-1-oxy-allyl (1.091 g, 2.81 mmol), AIBN (0.03 g, 0.18 mmol), and CH₃CN (250 mL) were combined in an autoclave reactor and purged with a N₂ flow for 10 minutes, and then charged with 550 kPa of PH_{3(g)}. The reaction was stirred at room temperature for 1 hour, recharged with 550 kPa PH_{3(g)}, stirred for one hour, and charged a third time with 550 kPa PH_{3(g)}. The reaction was then heated to 45 °C for 24 hours. Once cooled to room temperature, the excess PH₃ was incinerated, and the reaction was transferred into a glovebox and volatiles were removed in *vacuo* at 60 °C. Half of the resulting oil was combined in a pressure tube with 1-hexene (1.50 g, 18 mmol) and AIBN (0.02 g, 0.12 mmol), under an N₂ atmosphere, and heated to 65°C overnight. The reaction was brought into a glovebox and the reaction was checked by $^{31}\text{P}\{^1\text{H}\}$ NMR spectroscopy for conversion to a tertiary phosphine (≈ -30 ppm). Once all primary

phosphine was converted to a tertiary phosphine, 4-vinylbenzyl chloride (0.50 g, 3.28 mmol) was added to the reaction mixture and stirred at room temperature for 4 hours. Quaternization was confirmed by $^{31}\text{P}\{^1\text{H}\}$ NMR spectroscopy. Volatiles were then removed in *vacuo*, resulting in an orange viscous oil. The product was purified using a methyl silyl functionalized silica plug,³² first eluting with Et_2O to remove all by-products, followed by CH_3OH to elute the desired product. The volatiles were removed in *vacuo*, yielding pure product as a yellow oil. Yield: 140 mg, 7%. ^1H (600 MHz, CDCl_3 , δ): 7.39 (s, 4H), 6.70 (dd, $J = 17.6\text{Hz}$, 11 Hz, 1H), 5.76 (d, $J = 17.6$, 1H), 5.40-5.11 (m, 4H), 4.25-4.03 (m, 6H), 3.77 (s, 2H), 3.50 (s, 2H), 2.55 (m, 2H), 2.39 (s, 4H), 2.52-1.99 (m, 12H), 1.90 (m, 2H), 1.45 (m, 6H), 1.26 (m, 8H), 0.87 (m, 6H); $^{31}\text{P}\{^1\text{H}\}$ (161 MHz, CDCl_3 , δ): 33.67; $^{13}\text{C}\{^1\text{H}\}$ (151 MHz, CDCl_3 , δ): 170.57, 170.40, 170.17, 169.97, 137.88, 135.72, 130.33, 127.61, 127.22, 115.12, 96.46, 67.91(m), 67.66, 67.42, 66.19, 61.62, 61.42, 31.29, 31.02, 30.52, 30.42, 22.30, 21.73, 20.77, 20.62, 19.06, 18.71, 13.88; HRMS (ESI-TOF) m/z : Calcd for $\text{C}_{38}\text{H}_{60}\text{O}_{10}\text{P} [\text{M}]^+$: 707.3924; Found 707.3942.

Synthesis of trishydroxypropyl(vinylbenzyl)phosphonium chloride (4.7)

Tris(hydroxypropyl)phosphine (5.01 g, 30 mmol), 4-vinylbenzyl chloride (5.03 g, 33 mmol), and CH_3CN (25 mL) were combined in a pressure tube under N_2 atmosphere and heated to 80 °C overnight. The resulting solid was collected by vacuum filtration and washed with CH_2Cl_2 to yield a white oily solid. Yield: 7.81 g, 82%. ^1H (600 MHz, D_2O , δ): 7.36 (d, $J = 8.0\text{ Hz}$, 2H), 7.13 (dd, $J = 8.2\text{ Hz}$, 2.3 Hz, 2H), 6.60 (dd, $J = 17.7\text{ Hz}$, 11.0 Hz, 1H), 5.71 (d, $J = 17.7\text{ Hz}$, 1H), 5.18 (d, $J = 11\text{ Hz}$, 1H), 4.62 (s, 3H), 3.55 (d, $J = 14.7\text{ Hz}$, 2H), 3.48 (t, $J = 6.0\text{ Hz}$, 6H), 2.10-2.03 (m, 6H), 1.64-1.55 (m, 6H); $^{31}\text{P}\{^1\text{H}\}$ (161 MHz, CDCl_3 , δ): 34.29 ; $^{13}\text{C}\{^1\text{H}\}$ (151 MHz, D_2O , δ): 137.59, 135.73, 130.22, 127.14, 155.29, 25.80, 25.35, 23.42, 23.38, 15.02, 14.53; HRMS (ESI-TOF) m/z : $[\text{M}]^+$ Calcd for $\text{C}_{18}\text{H}_{30}\text{O}_3\text{P}$ 325.1932; Found 325.1916.

Synthesis of poly(dihexyl(2,3,4,6-hydroxy-mannopyranyl)-1-oxy-propyl)vinylbenzylphosphonium chloride (4.5-d).

4.3 (0.219 g, 0.29 mmol), **CTA**(1.93 mg, 7.65 μ mol), **AIBN** (0.41 mg, 2.53 μ mol), and 50/50 toluene/acetonitrile (4 mL) were combined in a Schlenk flask with a Suba Seal Septum and purged of oxygen by bubbling $N_{2(g)}$ through the solution for 30 minutes. The resulting solution was heated to 80 °C for 20 hours, then submerged in liquid N_2 to quench to polymerization. Volatiles were then removed *in vacuo* and the polymer redissolved in a minimal amount of methanol (2 mL), dialyzed against methanol using a regenerated cellulose dialysis membrane (molecular weight cut off of 3.5 kg/mol) for 24 hours, with three changes of the dialysate. To the resulting solution, sodium methoxide was added (25 wt% solution, 0.319 g, 2.57 mmol), and the reaction mixture was stirred for 4 hours. The resulting solution was dialyzed against methanol containing DOWEX 5W80 acidic resin overnight, changing the dialysate and resin once. The resulting solution was concentrated *in vacuo* and giving a yellow oil. Yield: 0.126 g, 57%. 1H NMR (600 MHz, D_2O , δ): 7.07 (broad s), 6.71 (broad s), 4.70 (broad s), 4.60 (s), 3.77-3.43 (m), 2.19-1.73 (m), 1.21-1.08 (m), 0.68 (broad s); ^{31}P { 1H } NMR (161 MHz, $CDCl_3$, δ): 33.30.

Synthesis of poly(dihexyl(2,3,4,6,-hydroxy-gluco-pyranyl)-1-oxy-propyl)vinylbenzylphosphonium chloride) (4.6-d).

4.4 (93 mg, 0.12 mmol), **CTA** (0.8 mg, 3.22 μ mol), **AIBN** (0.2 mg, 1.07 μ mol), and 50/50 toluene/acetonitrile (2 mL) were combined in a Schlenk flask with a Suba Seal Septum, and deoxygenated by bubbling $N_{2(g)}$ through the solution for 30 minutes. The resulting solution was heated to 80 °C for 20 hours, and then submerged in liquid N_2 to quench to polymerization. Volatiles were then removed *in vacuo* and the polymer was redissolved in a minimal amount of methanol (2 mL), and dialyzed against methanol using a regenerated cellulose dialysis membrane (molecular weight cut off of 3.5 kg/mol) for 24 hours with three changes of dialysate. To the resulting solution, sodium methoxide was added (25 wt% solution, 0.2 g, 6.45 mmol), and the reaction was stirred for 4 hours. The resulting solution was dialyzed against methanol containing DOWEX 5W80 acidic resin overnight, changing the dialysate and resin once. The resulting solution was concentrated *in vacuo* and give a yellow oil. Yield: 65 mg, 73%. 1H NMR (600 MHz, D_2O , δ): 7.24 (broad s), 6.73 (broad s), 3.83-3.43 (broad s), 2.44-2.06 (m), 1.93-1.71 (m), 1.59-1.42 (m), 1.41-1.24 (m), 0.88 (broad s); ^{31}P { 1H } NMR (161 MHz, D_2O , δ): 33.23.

Synthesis of poly(tris(3-hydroxypropyl)(vinylbenzyl)phosphonium chloride) (4.8).

4.7 (0.749 g, 2.08 mmol), **CTA** (13.2 mg, 52.4 μmol), **AIBN** (2.8 mg, 17.3 μmol), and **DMF** (5 mL) were combined in a Schlenk flask with a Suba Seal septum, and deoxygenated by bubbling $\text{N}_{2(\text{g})}$ through the solution for 30 minutes. The resulting solution was heated at 80 $^{\circ}\text{C}$ for 24 hours, then submerged in liquid N_2 to quench the polymerization. The resulting solution was dissolved in H_2O (5 mL) and dialyzed against H_2O using a regenerated cellulose dialysis membrane (molecular weight cut off 3.5 kg/mol) for 24 hours. The resulting solution was lyophilized, giving a yellow powder. Yield: 0.423 g, 56%. ^1H NMR (600 MHz, D_2O , δ): 7.01 (broad s), 6.48 (broad s), 3.63 (broad s), 3.42 (broad s), 2.05 (broad s), 1.51 (broad s); $^{31}\text{P}\{^1\text{H}\}$ NMR (161 MHz, D_2O , δ): 33.81

Acetate deprotection of 4.3 to give 4.3-d

4.3 (50 mg, 67 μmol) and sodium methoxide (0.2 g, 1.6 mmol) were combined in methanol (1 mL) and stirred for 2 hours. The resulting mixture was diluted with H_2O (5 mL) and the product was extracted with dichloromethane (3x5mL). The organic layer was washed with 0.1 M HCl (3x5 mL), water (3x5 mL) and brine (3x5 mL), dried with MgSO_4 and filtered. The volatiles was removed *in vacuo*, resulting in an oil. Yield: 30 mg, 83%. Confirmed by disappearance of acetyl CH_3 protons in (Figure 8-45).

Acetyl deprotection of 4.4 to give 4.4-d

4.4 (25 mg, 33 μmol) and sodium methoxide (0.2 g, 1.6 mmol) were combined in methanol (1 mL) and stirred for 2 hours. The resulting mixture was then diluted with H_2O (5 mL) and the product extracted with dichloromethane (3x5mL). The organic layer was washed with 0.1 M HCl (3x5 mL), water (3x5 mL) and brine (3x5 mL), dried with MgSO_4 and filtered. The solvent was removed *in vacuo*, resulting in an oil. Yield: 14 mg, 70%. Acetate removal was confirmed by disappearance of the acetyl CH_3 protons (Figure 8-46).

Minimum Bacteriocidal Concentration (MBC) and Minimum Inhibitory Concentration (MIC) testing

Compounds **4.5-d**, **4.6-d**, and **4.8** were lyophilized overnight and dissolved in DMSO at a concentration of 20 mg/mL. This solution was then diluted to provide solutions with concentrations of 2, 0.2, and 0.02 mg/mL in DMSO by serial 10x dilutions. 20 μ L of each solution was added to 180 μ L 0.3 mM KH_2PO_4 buffer in a 96 well plate and the solutions were mixed to provide 2, 0.2, 0.02, and 0.002 mg/mL solutions. 100 μ L of each of these solutions was then transferred to 100 μ L of buffer (2x dilution) and the solution was mixed 10 times to provide 1, 0.1, 0.01, and 0.001 mg/mL concentrations. 100 μ L of these solutions were then transferred to 100 μ L of buffer to result in 0.5, 0.05, 0.005, and 0.0005 mg/mL concentrations. After 100 μ L bacteria suspension addition, these would result in concentrations of 1, 0.5, 0.25, 0.1, 0.05, 0.025, 0.01, 0.005, 0.0025, 0.001, 0.00025, and 0.0005 mg/mL concentrations. **4.3-d**, **4.4-d**, and **4.7** were dissolved in DMSO at a concentration of 14 mg/mL, and diluted in a similar manner. In each case, the final concentration of DMSO was less than 5%, and a control experiment was performed to ensure that this concentration of DMSO had no effect on the bacterial growth. A loop of precultured *E. coli* or *S. aureus* was freshly cultured in LB broth (Miller's modification) for 18 – 24 hours at 37 °C and 175 rpm. The resulting suspension was centrifuged for 10 minutes, decanted, resuspended in 0.3 mM KH_2PO_4 buffer, vortexed, and centrifuged for 10 minutes. This was repeated twice. The resulting solid was resuspended in 0.3 mM KH_2PO_4 buffer and diluted to 10^8 colony forming units (CFUs/mL) by optical density (*E. coli* O.D. = 0.2 @ 600 nm, *S. aureus* O.D. = 0.3 @ 600 nm). The suspension was further diluted to 2×10^5 CFUs/mL for testing. 100 μ L of this *E. coli* or *S. aureus* suspension was then added to each well containing 100 μ L of sample or controls containing buffer only. The 96 well plates were covered and placed in an incubator shaker at 37 °C and 175 rpm for 4 hours.

For determination of the MBC values, LB Agar (Miller's modification) was pour-plated at 42 °C into a petri dish with a desired amount of bacteria solution (controls or polymer-bacteria solutions), mixed with gentle swirling, allowed to gel, and then incubated upside down in an incubator at 37 °C for 24 hours, and bacteria colonies counted within the agar.

The bacterial controls from above were serially diluted to 10^3 CFUs/mL by removing 100 μ L of each suspension and diluting it into 9.9 mL of buffer. 100 μ L of this suspension (to yield \sim 100 CFUs for counting) were pour plated with LB agar, allowed to solidify, and incubated at 37 °C for 24 hours. For all other samples, 100 μ L from the 96 well plate were pour-plated without dilution. After incubation at 37 °C for 24 hours the bacterial colonies were counted. The MBC is reported as the polymer concentration corresponding to a >99.99% reduction in the number of bacterial colonies relative to the control. As the samples from the 96 well plate that were treated with phosphonium were not diluted, 10^4 CFUs were potentially plated. As no bacterial colonies were observed at the reported MBC values, this corresponds to a >99.99% reduction (log 4 reduction) compared to the controls. Thus these concentrations can be referred to as $MBC_{99.99}$.

For determination of the MIC, 100 μ L of broth was added to the remaining 100 μ L of bacterial suspension in the plate. The optical density was measured at 600 nm. The 96 well plate was then incubated at 37 °C with shaking at 175 rpm for 18 hours, and the resulting optical density was recorded to determine the % growth relative to control bacteria that were not exposed to phosphonium. The MIC was determined as the concentration required to reduce to zero growth compared to controls. All samples were measured in triplicate for both the MIC and MBC.

Hemolysis assay

Defibrinated sheep blood (1 mL) was centrifuged for 10 minutes at 2500 rpm, resuspended in red blood cell (RBC) buffer (0.6 g of 5 mM sodium phosphate and 8.7 g of 150 mM NaCl dH₂O adjusted to pH = 7.4 and sterilized), vortexed, and centrifuged for 10 minutes. This was repeated 4 times. The resulting red blood cells were suspended in 10 mL of RBC buffer, and vortexed before using. Solutions of polymers **4.5**, **4.6**, and **4.8** were prepared in DMSO at concentrations including 2, 0.2, 0.02, and 0.002 mg/mL. 20 μ L of these solutions were combined with 955 μ L of RBC buffer and 25 μ L of red blood cell suspension. Control samples containing 20 μ L of DMSO (negative control), 25 μ L of red blood cells and 955 μ L of RBC buffer (negative control) and 25 μ L of red blood cells with 975 μ L dH₂O (positive control) were also tested. The suspension was vortexed, and

then incubated at room temperature for two hours. The resulting suspensions were then centrifuged for 10 minutes at 2500 rpm, and 200 μ L of each solution was transferred to a 96 well plate. The absorbance at 540 nm was measured. The hemolysis percentage was determined by relating the absorbance value to that of the positive control, which represented 100% hemolysis. All samples were tested in triplicate.

4.5 References

- 1) Panarin, E. F.; Solovski, M.; Ekzemply, O. *Khim.-Farm. Zh.* **1971**, *5*, 24–28.
- 2) Fischer, D.; Li, Y.; Ahlemeyer, B.; Krieglstein, J.; Kissel, T. *Biomaterials* **2003**, *24*, 1121–1131.
- 3) Huang, J.; Murata, H.; Koepsel, R. R.; Russell, A. J.; Matyjaszewski, K. *Biomacromolecules* **2007**, *8*, 1396–1399.
- 4) Kenawy, E. R.; Abdel-Hay, F. I.; El-Shanshoury, A. E. R. R.; El-Newehy, M. H. *J. Polym. Sci. Part A Polym. Chem.* **2002**, *40*, 2384–2393.
- 5) Koromilas, N. D.; Lainioti, G. C.; Vasilopoulos, G.; Vantarakis, A.; Kallitsis, J. K. *Polym. Chem.* **2016**, *7*, 3562–3575.
- 6) Guo, J.; Xu, Q.; Zheng, Z.; Zhou, S.; Mao, H.; Wang, B.; Yan, F. *ACS Macro Lett.* **2015**, *4*, 1094–1098.
- 7) Ikeda, T.; Yamaguchi, H.; Tazuke, S. *Antimicrob. Agents Chemother.* **1984**, *26*, 139–144.
- 8) Sambhy, V.; Peterson, B. R.; Sen, A. *Angew. Chem. Int. Ed.* **2008**, *47*, 1250–1254.
- 9) Kanazawa, A.; Ikeda, T.; Endo, T. *J. Polym. Sci. Part A Polym. Chem.* **1993**, *31*, 335–343.
- 10) Kanazawa, A.; Ikeda, T.; Endo, T. *J. Polym. Sci. Part A Polym. Chem.* **1993**, *31*, 1441–1447.
- 11) Kanazawa, A.; Ikeda, T.; Endo, T. *J. Polym. Sci. Part A Polym. Chem.* **1994**, *32*, 1997–2001.
- 12) Kanazawa, A.; Ikeda, T.; Endo, T. *J. Appl. Polym. Sci.* **1994**, *53*, 1237–1244.
- 13) Cuthbert, T.; Guterman, R.; Ragogna, P. J.; Gillies, E. R. *J. Mater. Chem. B* **2015**, *3*, 1474–1478.

- 14) Cuthbert, T. J.; Harrison, T. D.; Ragogna, P. J.; Gillies, E. R. *J. Mater. Chem. B* **2016**, *4*, 4872–4883.
- 15) Ilker, M. F.; Nüsslein, K.; Tew, G. N.; Coughlin, E. B. *J. Am. Chem. Soc.* **2004**, *126*, 15870–15875.
- 16) Anthierens, T.; Billiet, L.; Devlieghere, F.; Du Prez, F. *Innov. Food Sci. Emerg. Technol.* **2012**, *15*, 81–85.
- 17) Chen, C. Z.; Beck-Tan, N. C.; Dhurjati, P.; van Dyk, T. K.; LaRossa, R. a; Cooper, S. L. *Biomacromolecules* **2000**, *1*, 473–480.
- 18) Guo, A.; Wang, F.; Lin, W.; Xu, X.; Tang, T.; Shen, Y.; Guo, S. *Int. J. Biol. Macromol.* **2014**, *67*, 163–171.
- 19) Kenawy, E. R.; Worley, S. D.; Broughton, R. *Biomacromolecules* **2007**, *8*, 1359–1384.
- 20) Al-badri, Z. M.; Som, A.; Lyon, S.; Nelson, C. F.; Nusslein, K.; Tew, G. N. *Biomacromolecules* **2008**, *3*, 2805–2810.
- 21) Oda, Y.; Kanaoka, S.; Sato, T.; Aoshima, S.; Kuroda, K. *Biomacromolecules* **2011**, *12*, 3581–3591.
- 22) Punia, A.; Lee, K.; He, E.; Mukherjee, S.; Mancuso, A.; Banerjee, P.; Yang, N. L. *Int. J. Mol. Sci.* **2015**, *16*, 23867–23880.
- 23) Sellenet, P. H.; Allison, B.; Applegate, B. M.; Youngblood, J. P. *Biomacromolecules* **2007**, *8*, 19–23.
- 24) Mowery, B. P.; Lee, S. E.; Kissounko, D. A.; Epand, R. F.; Epand, R. M.; Weisblum, B.; Stahl, S. S.; Gellman, S. H. *J. Am. Chem. Soc.* **2007**, *129*, 15474–15476.
- 25) Allison, K. R.; Brynildsen, M. P.; Collins, J. J. *Nature* **2011**, *473*, 216–220.
- 26) Lin, C. C.; Yeh, Y. C.; Yang, C. Y.; Chen, C. L.; Chen, G. F.; Chen, C. C.; Wu, Y. *C. J. Am. Chem. Soc.* **2002**, *124*, 3508–3509.
- 27) Appeldoorn, C. C. M.; Joosten, J. A. F.; Ait El Maate, F.; Dobrindt, U.; Hacker, J.; Liskamp, R. M. J.; Khan, A. S.; Pieters, R. J. *Tetrahedron-Asymmetr* **2005**, *16*, 361–372.
- 28) Bilková, A.; Paulovičová, E.; Paulovičová, L.; Poláková, M. *Monatsh Chem* **2015**, *146*, 1707–1714.

- 29) Saada, M.-C.; Ombouma, J.; Montero, J.-L.; Supuran, C. T.; Winum, J.-Y. *Chem. Commun.* **2013**, *49*, 5699–5701.
- 30) Kopitzki, S.; Jensen, K. J.; Thiem, J. *Chem. Eur. J.* **2010**, *16*, 7017–7029.
- 31) Rauhut, M. M.; Currier, H. A.; Semsel, A. M. *J. Org. Chem.* **1961**, *26*, 5138–5145.
- 32) Panne, P.; Fox, J. M. *J. Am. Chem. Soc.* **2007**, *129*, 22–23.
- 33) Lienkamp, K.; Madkour, A. E.; Musante, A.; Nelson, C. F.; Nüsslein, K.; Tew, G. N. *J. Am. Chem. Soc.* **2008**, *130*, 9836–9843.
- 34) Punia, A.; Mancuso, A.; Banerjee, P.; Yang, N. L. *ACS Macro Lett.* **2015**, *4*, 426–430.
- 35) Haridharan, N.; Dhamodharan, R. *J. Polym. Sci. Part A Polym. Chem.* **2011**, *49*, 1021–1032.

Chapter 5

5 Self-healing polyphosphonium ionic networks.

5.1 Introduction

Self-healing materials are able to renew their structural integrity after damage through dynamic processes, making the prospect of renewable or persistent materials and coatings possible.¹⁻⁴ Currently, self-healing materials are used in automotive paints and coatings,⁵ and are expected to have much broader applications in the near future including the stabilization of lithium-ion batteries⁶ and in prolonging the lifetime of medical implants such as bone cements and joint and soft tissue replacements.⁷⁻⁹ Self-healing materials are typically classified as either autonomous or non-autonomous. Autonomous self-healing materials spontaneously initiate healing upon damage, whereas those that are non-autonomous require the application of an external stimulus such as mechanical force or heat.¹ The development of autonomous self-healing materials has often involved the incorporation of microcapsule¹⁰ or vascular-like¹¹ systems that contain additives such as monomers. In these systems, the healing is engaged upon damage of the microcapsule container, leakage of the active components, initiation of the chemical reaction, and filling of the damaged area. A limitation of microcapsule- or vascular-based self-healing networks is the lack of repeatable self-healing in a given location.

Non-autonomous self-healing materials have often utilized reversibly-cross-linked networks. Cross-linking can involve hydrogen bonding,¹² coordination of metals,¹³ ionic bonding,¹⁴ or reversible covalent systems such as Diels-Alder adducts.¹⁵ The process that mediates healing is important to ensure that the network can mend damage in its intended environment. Ionically-cross-linked networks have used two-component polymer blends or interpenetrating polymer networks that contain both polyanions and polycations.¹⁶ For example, networks comprising poly(allylamine hydrochloride) (PAH) or poly(diallyldimethylammonium chloride) as polycations, coupled with poly(acrylic acid) (PAA) or poly(styrene sulfonate) respectively as polyanions have been investigated.^{16,17} These networks involve both physical entanglement of the polymer chains, and chemical

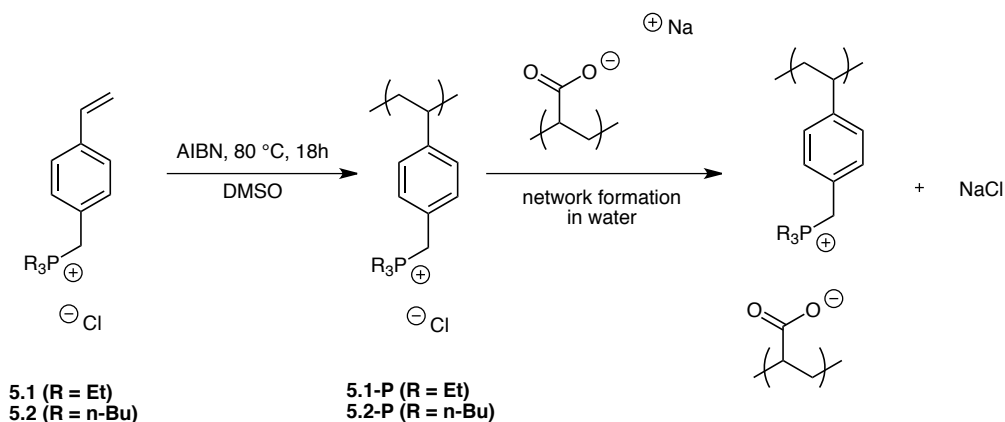
cross-linking between ionic groups. Cross-links are entropically favoured by multivalent coordination between polymers, but still undergo dynamic exchange in the presence of NaCl.¹⁸ Over time, the viscoelastic properties of the network, which are a balance between the elastic modulus (solid character) and viscous modulus (fluid character) can allow self-healing at the interface, while still allowing the structural integrity of the materials to be retained. Self-healing of the PAA/PAH networks required high ionic strength (1 -2.5 M NaCl), however, which may limit their use for *in vivo* applications.¹⁴ Furthermore, the requirement for ultracentrifugation to create the networks may result in challenges for the scaling up of the process.

Phosponiums are particularly attractive for materials science applications because of their high thermal and chemical stability as well as their ease of synthesis.^{19,20} Phosponiums have lower charge density relative to ammoniums due to the larger size of the phosphorus atom, which can lead to differences in the physical properties of materials containing phosponiums relative to ammoniums. So far, very few examples of phosponium-based ionically-cross-linked networks have been reported. Supramolecular networks have been created by combining a geminal phosponium cation with tetraanions, resulting in highly viscous network ionic liquids.²¹ Phosponium monocations and dications were also combined with PAA to afford phosponium/PAA mixtures and networks respectively and it was shown that the properties of the resulting materials could be tuned by changing the alkyl chains on the phosponium cation.²² However, to the best of our knowledge, the incorporation of polymeric phosponiums into ionically-cross-linked networks has not been reported. Herein, we report the combination of polyphosponium with PAA for the preparation of ionically-cross-linked polymer networks. We demonstrate that the composition and properties of the networks can be tuned according to the network preparation method. The rheological properties of the networks are described and it is shown that networks with the appropriate rheology exhibit self-healing capabilities under physiologically relevant salt concentrations.

5.2 Results and Discussion

5.2.1 Synthesis and characterization of the polyphosphonium

Triethyl(4-vinylbenzyl)phosphonium chloride (**5.1**) and tri-*n*-butyl(4-vinylbenzyl)phosphonium chloride (**5.2**) were prepared as previously reported.²³ As shown in Scheme 1, polymerization of these monomers was then performed using azobisisobutyronitrile (AIBN) in dimethyl sulfoxide (DMSO) at 80 °C to afford poly(triethyl(4-vinylbenzyl)phosphonium chloride (**5.1-P**) and poly(tributyl(4-vinylbenzyl)phosphonium chloride (**5.2-P**). A reaction time of 18 hours resulted in greater than 80% monomer conversion. Complete conversion was not observed, even at longer polymerization times, and purification of the final product from the remaining monomer was required. Two precipitations from 2-propanol into tetrahydrofuran (THF) yielded the polymers as white powders. The ¹H NMR spectra of the polyphosphonium exhibited broad peaks that were consistent with their proposed structures (Figure 8-49 and Figure 8-50) and the ³¹P{¹H} NMR spectra had a single broad peak characteristic of the phosphonium (Figure 8-51, Figure 8-52). Thermogravimetric analysis showed that **5.1-P** and **5.2-P** had an onset decomposition temperatures (*T*_o) of 335 °C and 300 °C respectively and glass transition temperatures (*T*_g) of 225 °C and 165 °C respectively (Figure 8-53, Figure 8-54, Figure 8-55, Figure 8-56).



Scheme 5-1: Synthesis of the polyphosphonium and their combination with PAA to form ion pairs.

Size exclusion chromatography (SEC) of **5.1-P** was performed in DMF containing 0.4 M tetrabutylammonium triflate. Relative to poly(methyl methacrylate) (PMMA) standards, **5.1-**

P had number-average molar masses (M_n) of 240 kg/mol and dispersities (D) of 2.5 (Figure 8-57). Controlled radical polymerization methods such as reversible addition-fragmentation chain-transfer polymerization (RAFT) were also explored, as these have previously been used for the preparation of polyphosphonium.²³ However, it was found that the conventional free radical polymerization could more easily provide high molar mass polymers on a large scale. Furthermore, any potential advantages from having a polyphosphonium with lower D could be offset by the relatively broad D of the commercial PAA. Although the PAA had a reported M_n of 240 kg/mol, aqueous SEC analysis revealed a bimodal distribution with M_n values of 80 kg/mol ($D = 1.05$) and 2 kg/mol ($D = 1.62$) relative to poly(ethylene oxide) (PEO) standards (Figure 8-58). The large molar mass dispersities of the polymers may influence the self-healing properties of the resulting networks, due to the effects of different polymer chain lengths on chain mobility and relaxation at the site of healing. Although it will not be explored in the current work, previous research has suggested that the effects of lower molar mass chains may facilitate chain mobility, which is important for self-healing.²⁴

5.2.2 Preparation and characterization of ionic networks

To prepare the networks from PAA and **5.1-P**, the polymers were separately dissolved in 0.1 M aqueous NaCl at a concentration of 0.1 M (of carboxylate or phosphonium) and the pH was adjusted to 8.0 using NaOH. Equivalent volumes of each polyion solution were then combined to yield an insoluble polymer network. Excess liquid was decanted. The material was swelled in 0.25 M NaCl, and then manually worked into a sphere. The material could then be pressed at 50 °C for 1 h between Teflon sheets to afford a sheet of material. The network was then submerged in 0.1 M NaCl to equilibrate before cutting to the desired shape. It is noteworthy that no centrifugation and or high NaCl concentrations were required in either the network preparation or isolation. **PAA/5.2-P** networks were also prepared, but the networks obtained swelled extensively, exhibited predominantly fluid-like behaviour, and consequently could not be processed for further study. This was most likely due to the steric bulk or hydrophobicity of the butyl groups causing a decrease in the extent of ionic cross-linking. All experiments discussed below focused on the **PAA/5.1-P** networks.

Previously, the order of addition of the polyions to yield the ionically cross-linked network was shown to affect the ratio of the components of the network, even when combining stoichiometrically equivalent amounts of each ion.¹⁷ In the current work, therefore, three networks with different ratios of **PAA** and **5.1-P** were prepared by different addition protocols. To obtain more carboxylates than phosphoniums in the networks (**PAA**>**5.1-P**), the **5.1-P** solution was added to the **PAA** solution by slow dropwise addition (Figure 5-1A). Networks with approximately equal numbers of carboxylates and phosphoniums (**PAA**≈**5.1-P**) were produced by fast simultaneous addition of the two solutions (Figure 5-1B). Networks with more phosphoniums than carboxylates (**PAA**<**5.1-P**) were produced by slow dropwise addition of the **PAA** solution into a **5.1-P** solution (Figure 5-1C). The difference in component ratios from these different methods arises from polymer ionic bonding occurring with an excess of one component in solution. Polymer chain overlap occurs during the initial cross-linking, which inhibits polymer chain matching.¹⁷

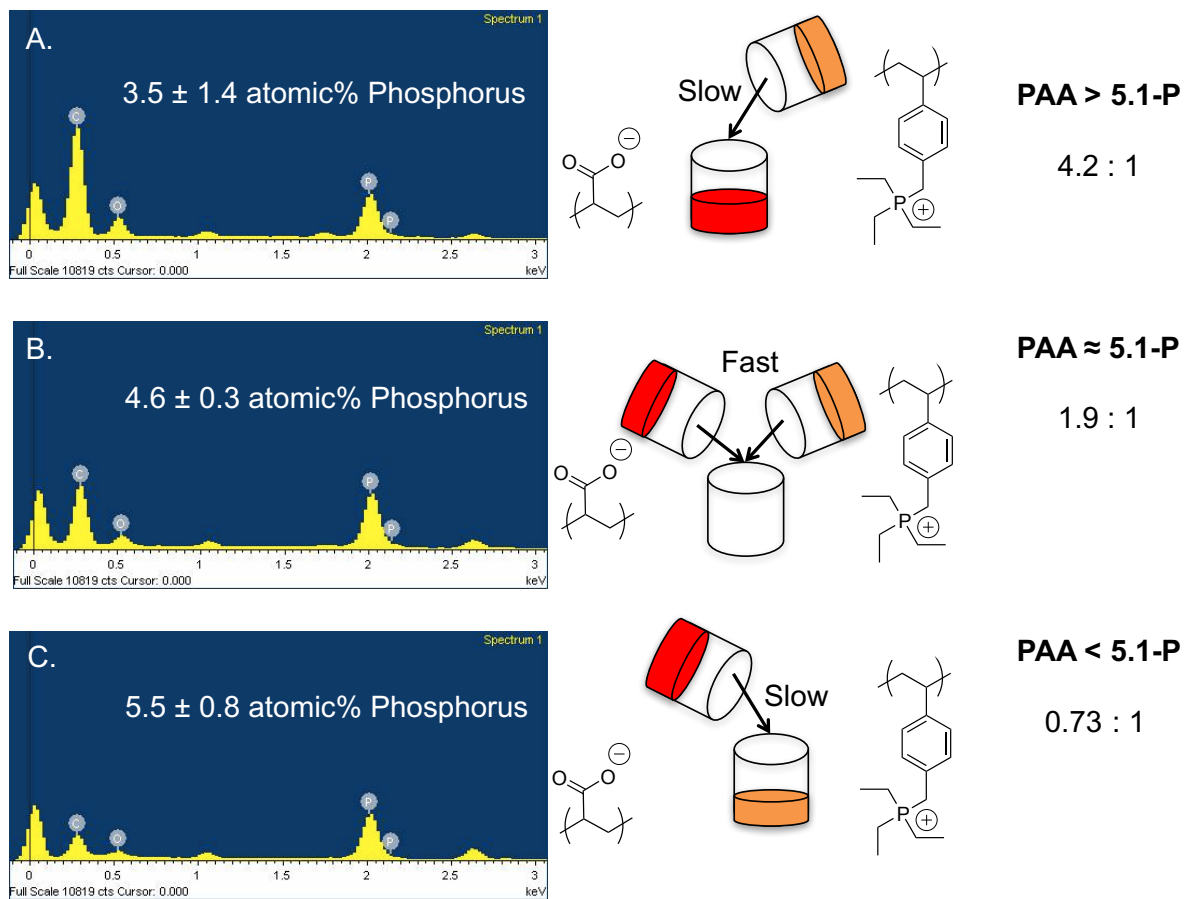


Figure 5-1: SEM-EDX analyses of ionic networks: A) PAA>5.1-P, B) PAA≈5.1-P and C) PAA<5.1-P along with schematics illustrating their methods of preparation and corresponding ratios of carboxylate:phosphonium.

Thermal analysis of the **PAA/5.1-P** networks after incubation in pure water to remove salts, followed by drying, showed that they exhibited a two-stage decomposition with the first stage having $T_0 \sim 200$ °C, corresponding decomposition of the PAA, and the second stage having $T_0 \sim 350$ °C, corresponding to the **5.1-P** (Figure 8-59). This indicates that the thermal stability is limited by the PAA rather than the polyphosphonium. DSC did not show any significant thermal transitions below 200 °C (Figure 8-60). In contrast, networks composed of phosphonium dications and PAA had T_g values ranging from -40 to 8 °C,²² showing the importance of the polyphosphonium in determining the thermal properties of the network. **PAA>5.1-P**, **PAA≈5.1-P**, and **PAA<5.1-P** networks were also analyzed after desalting and drying by scanning electron microscopy energy-dispersive x-ray spectroscopy (SEM-EDX) to determine the relative amounts of carbon and phosphorus in the networks. Phosphorus

atomic % values, with respect to carbon and phosphorus atoms, for **PAA>5.1-P**, **PAA≈5.1-P**, and **PAA<5.1-P** were 3.5 ± 1.4 , 4.6 ± 0.3 , and 5.5 ± 0.8 , corresponding to carboxylate:phosphonium ratios of 4.2:1, 1.9:1, and 0.73:1 respectively (calculation in supplementary information). $^{31}\text{P}\{^1\text{H}\}$ NMR spectroscopy with triethylphosphine oxide as an internal standard was also performed on the networks swelled with saturated NaCl solution. Although the results cannot be used to determine the exact phosphonium content due to differences between the cross-link densities and swelling properties of the three networks, the data suggest the trend of increasing phosphonium content for **PAA>5.1-P**, **PAA≈5.1-P**, and **PAA<5.1-P**, in agreement with the SEM-EDX analysis (**Determination of relative phosphorus content by $^{31}\text{P}\{^1\text{H}\}$ NMR spectroscopy**). To compare the relative concentrations of phosphorus within the networks, an internal standard of triethylphosphine oxide ($\text{Et}_3\text{P}=\text{O}$) in brine was used (this solution is referred to as the internal standard brine solution; ISBS). The ISBS containing 0.175 M $\text{Et}_3\text{P}=\text{O}$ was used to swell a known amount of dried polymer in an NMR tube overnight. The residual $\text{Et}_3\text{P}=\text{O}$ brine solution was decanted from the NMR tube, and the mass of ISBS that had swelled the network was determined as the difference between the mass of the NMR tube containing the swelled network and the mass of the NMR tube containing the dried polymer network. The following assumptions were made:

- 1) The different networks do not swell to the same extent, so we must determine the amount of ISBS within the network to determine the relative ratio of internal standard to the polymer network.
- 2) The $\text{Et}_3\text{P}=\text{O}$ diffuses into the polymer networks in a uniform fashion, and the concentration of $\text{Et}_3\text{P}=\text{O}$ remains the same within the network and in solution. i.e. has come to equilibrium.

- 3) The density of the brine solution containing $\text{Et}_3\text{P}=\text{O}$ is 1359 g/L (the known density of brine).

$^{31}\text{P}\{^1\text{H}\}$ NMR spectroscopy was then performed with a relaxation delay of 10 seconds with 256 scans to achieve good signal-to-noise. The integration of the peak at ~65 ppm from the $\text{Et}_3\text{P}=\text{O}$ in the ISBS was set to 1. The polymer network (e.g. **P-Et-P**) peak at 35 ppm was integrated relative to the $\text{Et}_3\text{P}=\text{O}$.

The resulting integrations cannot be taken directly as the relative ratio of phosphorus in the samples because the amount of $\text{PEt}_3\text{P}=\text{O}$ that diffuses into the network is a function of swellability. This relative concentration was then calculated below. The example given is for the **PAA>P-Et-P** sample:

- 1) The amount of $\text{Et}_3\text{P}=\text{O}$ in the swelled network was calculated based on the mass of ISBS that had been incorporated:

$$\frac{0.152\text{g ISBS}}{1359\frac{\text{g}}{\text{L brine}}} \times 1000\frac{\text{mL}}{\text{L}} = 0.112\text{ mL of ISBS}$$

$$0.1118\text{ mL of ISBS} \times 0.175\frac{\text{mmol}}{\text{mL}} \text{Et3PO} = 0.0195\text{ mmol Et3PO}$$

- 2) The relative integration of the polymer network peak at 35 ppm was then used to calculate the moles of phosphonium cation in the network:

$$(1.95 \times 10^{-5}\text{ mol Et3PO}) * (0.88\text{ int of P - Et - P}) * 235.32\frac{\text{g}}{\text{mol}} \text{Et - P unit} \\ = 0.00405\text{ g Et - P}$$

- 3) This represents the mass of a phosphonium monomer **Et-P**, and therefore can be used to calculate the mass percent of **P-Et-P** in the sample:

$$\frac{0.00405 \text{ g Et-P}}{0.103 \text{ g of PAA} > \text{P-Et-P}} * 100 = 3.9\%$$

- 4) This was completed for **PAA≈P-Et-P** and **PAA<P-Et-P** using the same steps resulting in the monomer weight percent as follows:

PAA>P-Et-P 3.9%

PAA≈P-Et-P 6.2%

PAA<P-

Et-P 8.3%

Note that although the trend of increasing phosphonium polymer content is the same as that measured in the SEM-EDX study, the actual numbers are different as the networks did not dissolve and the different networks swelled to different extents.

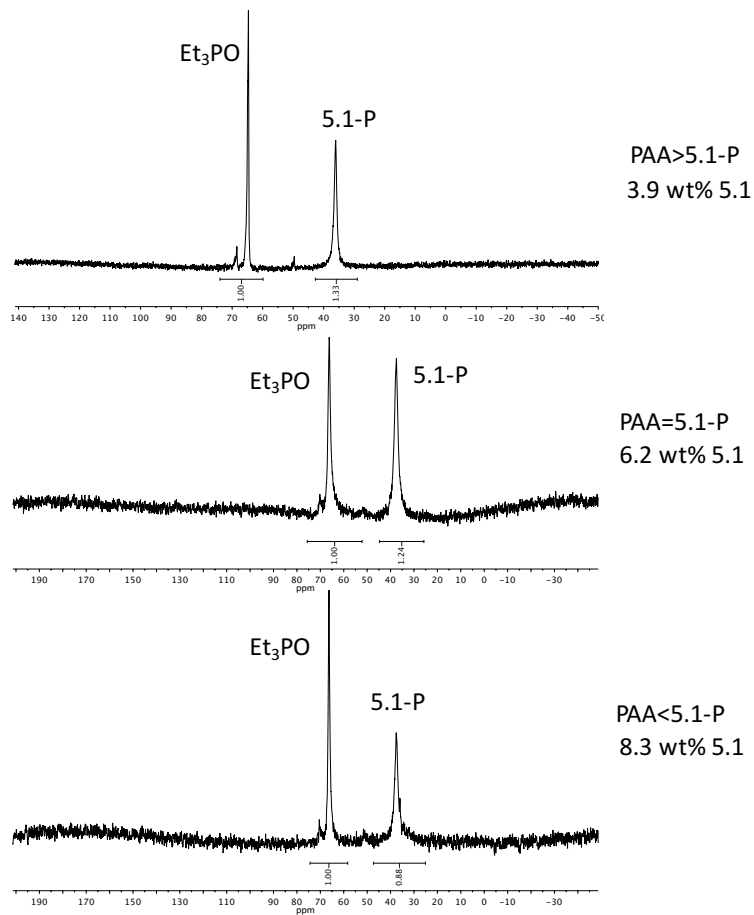


Figure 8-61). Previously, it was found that stoichiometric equivalents of carboxylate and ammoniums could be incorporated into ionic networks by the simultaneous addition of the two polymers.¹⁷ That this does not occur with the current system might be attributed to the larger size of the phosphonium monomers compared to the previously investigated amine monomers.

To understand how the ionic cross-links behaved as a function of the ionic strength of the solution, an experiment was performed to determine the effect of NaCl concentration on the swelling and structural integrity of the networks. The networks were dried, then immersed in 0 M, 0.1 M, 0.25 M, and 0.5 M aqueous NaCl solutions. As shown in Figure 5-2, ~200 wt% swelling calculated by mass increase was observed in pure water and 0.1 M NaCl for all of the networks. At 0.1M NaCl, the structural integrity of the networks was retained for at least 2 months. At 0.25 M NaCl, **PAA \approx 5.1-P** and **PAA<5.1-P** still underwent ~ 200 wt% swelling, whereas ~2-fold higher swelling was observed for **PAA>5.1-P**. At 0.5 M NaCl, all three networks exhibited increased swelling, with the degree of swelling increasing with the carboxylate content of the networks. At this concentration, the structural integrity of the networks decreased. They were observed qualitatively to exhibit fluid-like behaviour and were mechanically very weak. On the basis of these results, a salt concentration of 0.1 M NaCl was selected for more detailed experiments on mechanical properties and self-healing. This is very similar to the physiological salt concentration, which opens the prospect for possible future *in vivo* applications.

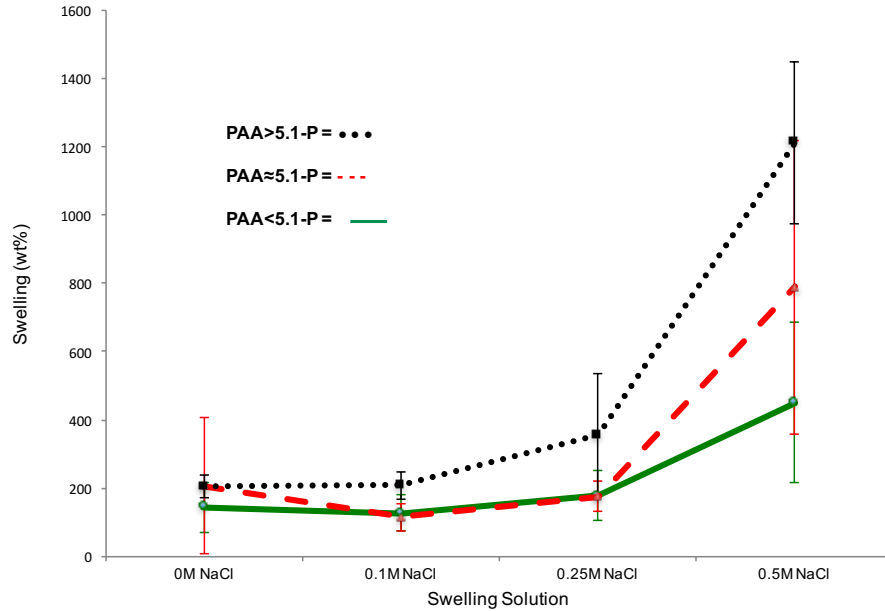


Figure 5-2: Swelling in weight % of polymer networks at different NaCl concentrations.

5.2.3 Rheological and mechanical properties

Rheological measurements of dynamic polymer networks provide information on the mechanisms and time scales for network relaxation, and can help to determine if the networks have the mechanical properties required for self-healing behavior. Measurements of the elastic (G') and viscous (G'') moduli of the networks for frequencies from 0.01 to 100 rad/s are shown in Figure 5-3. The moduli of the **PAA>5.1-P** network were similar in magnitude, with G' slightly larger than G'' at high frequencies. The moduli cross over at a frequency $\omega_c \approx 0.03$ rad/s, corresponding to a relaxation time of $1/\omega_c \sim 30$ s. The **PAA≈5.1-P** network had moduli approximately an order of magnitude higher than those of the **PAA>5.1-P** network, and a crossover frequency lower than the minimum frequency studied, implying a relaxation time greater than 100 seconds (Figure 5-3). The moduli for the **PAA≈5.1-P** networks showed a similar frequency dependence to **PAA>5.1-P** at frequencies less than 0.1 rad/s, but tended to flatten out at higher frequencies as the **PAA≈5.1-P** network entered into a rubbery plateau (Figure 5-3).

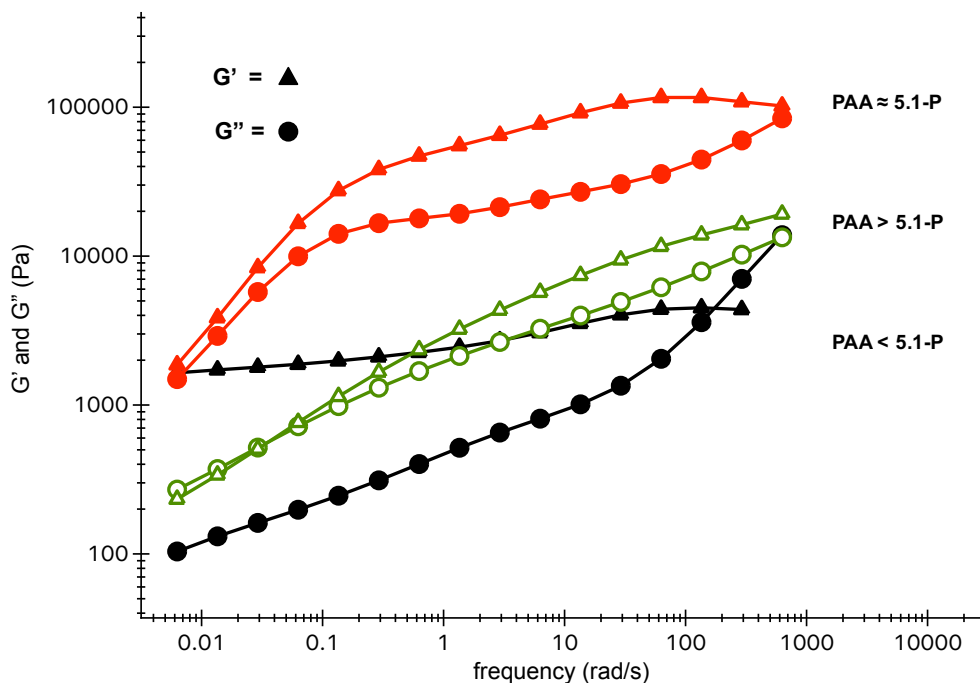


Figure 5-3: Comparison of the rheology frequency sweep data of PAA/5.1-P networks.

The elastic modulus of the **PAA<5.1-P** networks was strongly dominant at frequencies up to 100 rad/s (Figure 5-3), indicating extremely slow chain-scale relaxation. The viscous modulus increased with increasing frequency, however, and became greater than the elastic modulus at about 200 rad/s, suggesting that relaxation of short chain segments is the dominant relaxation process in this network. The relatively constant elastic modulus and low viscous modulus is typical of gels, and has been observed for cross-linked networks that exhibit no relaxation by reptation.²⁵ This could indicate low mobility of **5.1-P** in these networks due to its high molar mass and high T_g . In contrast, the networks containing more PAA may be more mobile due to the lower molar mass of the PAA.

In agreement with the current results, PAA/PAH networks with a stoichiometric balance of charges also gave the stiffest networks. This was attributed to a higher density of cross-linking compared other compositions.¹⁷ The elastic-viscous crossover frequency was lower for the stoichiometric PAA/PAH networks than for non-stoichiometric networks, meaning that the relaxation time was longer.¹⁷ The behavior observed in our **PAA/5.1-P** networks is different, with the relaxation time increasing as the fraction of PAA decreased. In general

the viscous and elastic moduli of our networks swelled in 0.1 M NaCl were similar in magnitude to those of networks prepared from PAA and phosphonium dications in the dry state.²² This illustrates the importance of highly-multivalent ionic interactions in determining the rheological properties of the networks. The fast relaxation of the **PAA>5.1-P** networks suggest that they are good candidates for self-healing, whereas the networks with higher **5.1-P** content may be better suited for other applications such as stimuli-responsive gels for drug delivery or degradable polymer networks.²⁶ The moduli of the current materials are comparable to those of some soft tissues and organs such as the human aorta.²⁷

To further evaluate the mechanical properties of the **PAA/5.1-P** networks, tensile testing was performed. As shown in Table 5-1 and Figure 5-4, **PAA>5.1-P** exhibited a high elongation at break of 1330%, but underwent plastic deformation and started necking before breakage. Consistent with the rheological results, **PAA≈5.1-P** had the highest Young's modulus and ultimate tensile strength of the three networks, presumably due to increased cross-linking.¹⁷ However, its elongation at breakage was the smallest of the three materials, with minor deformation/necking. **PAA<5.1-P** had the lowest Young's modulus and the lowest ultimate tensile strength, and exhibited intermediate elongation, with no necking/deformation before break. These results are also consistent with the observed rheological behavior of the networks. These phosphonium-based materials have elongations of similar magnitude but significantly lower Young's modulus and ultimate tensile strength than the analogous PAA/PAH networks.¹⁴

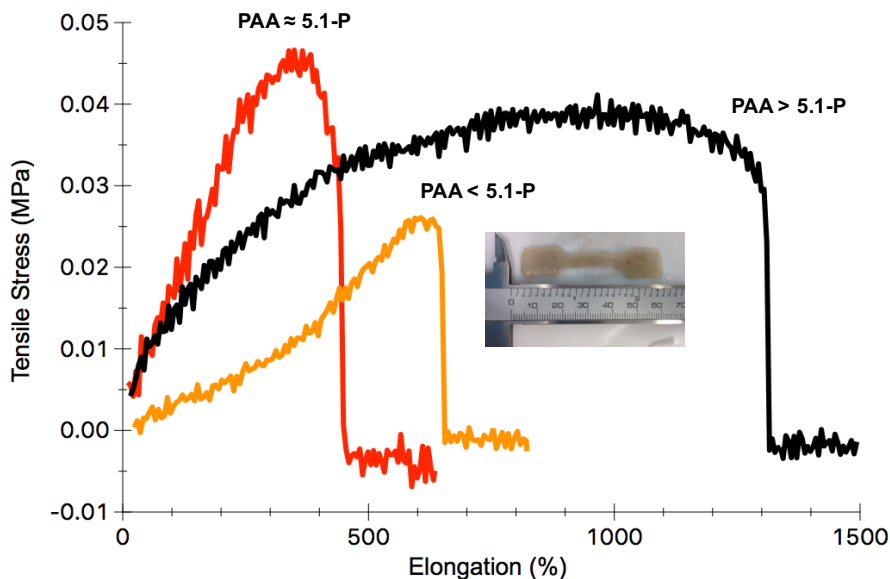


Figure 5-4: Tensile properties of PAA/5.1-P networks and a sample showing the dog bone structure used in accordance with ASTM D638 14.

Table 5-1: Summary of the tensile properties of PAA/5.1-P networks.

Network	Young's Modulus (KPa)	Elongation at break %	Ultimate tensile stress (KPa)
PAA>5.1-P	15 ± 2	1330 ± 250	33 ± 9
PAA≈5.1-P	29 ± 5	410 ± 45	43 ± 3
PAA<5.1-P	5 ± 1	530 ± 110	24 ± 2
PAA>5.1-P (after severing and healing)	5 ± 3	740 ± 160	10 ± 1

5.2.4 Self-healing

The ability of the networks to self-heal was first studied qualitatively. Networks of ~4 mm thickness were damaged by boring a ~0.5 mm diameter hole through them. The networks were then incubated in either 0.1 M NaCl or pure water. As shown in Figure 5-5, the hole in the **PAA>5.1-P** network in 0.1 M NaCl healed completely over 24 h. In contrast, no significant healing was observed in pure water. This is consistent with ionic exchange being required to achieve dynamic properties in the network. Incomplete healing was observed for

PAA<5.1-P and **PAA≈5.1-P** networks under these conditions (Figure 8-63), and under higher salt concentrations the networks lost their structural integrity as noted above. While the viscoelastic properties and relaxation time of **PAA>5.1-P** allow for chain relaxation and flow to heal the damaged area, **PAA<5.1-P** and **PAA≈5.1-P** networks have insufficient fluidity to self-heal on a reasonable time scale.

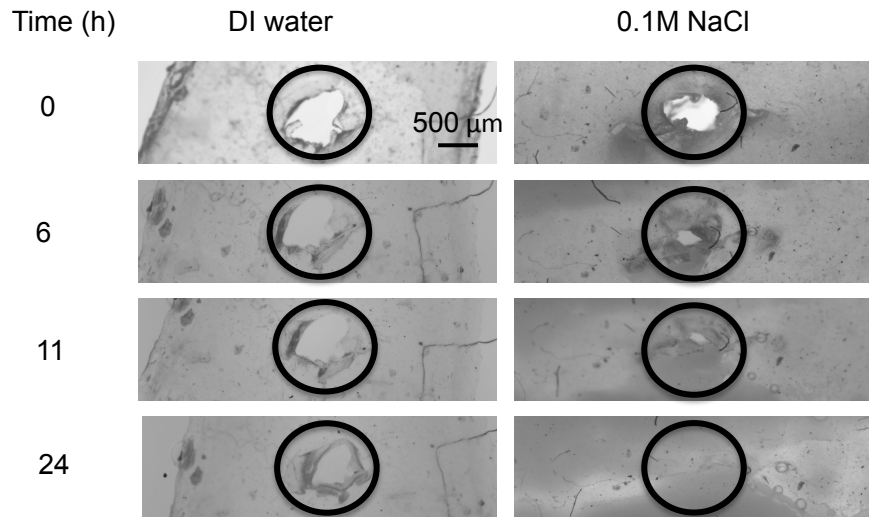


Figure 5-5: Digital images of a PAA>5.1-P network damaged by a 0.5 mm diameter hole self-healing over 24 hours in 0.1 M NaCl (right-hand column) versus a similar network in pure water (left-hand column), in which no significant healing was observed.

To probe more quantitatively the self-healing capabilities of **PAA>5.1-P**, a sample of the network was completely severed, pressed together manually for 1 min, incubated for 24 h in 0.1 M NaCl, and then subjected to tensile testing. This test does not probe purely autonomous self-healing because external pressure was applied, but it can nevertheless provide information on the ability of the network to repair extensive damage across a large area. As shown in Figure 5-6 and Table 5-1, the healed networks recovered ~ 55% of their initial elongation at break and ~33% of their initial Young's modulus and ultimate tensile strength. Based on previous work with PAA/PAH networks, the ability of **PAA>5.1-P** networks to recover their original tensile properties could likely be enhanced by increasing the time during which the severed portions were pressed together or by tuning their chemical structures. However, the ability of the current networks to heal under low salt concentrations

is a significant advantage, as mending did not occur at 0.15 M for the PAA/PAH system and much higher salt concentrations (≥ 1 M) were required to achieve significant recovery of tensile properties.¹⁴

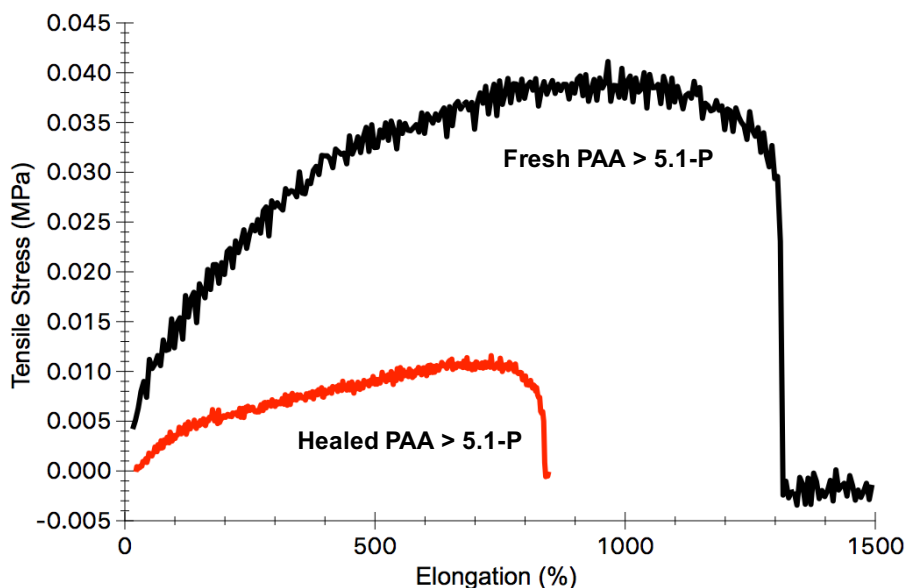


Figure 5-6: Tensile properties of PAA/5.1-P networks prior to and after healing in 0.1 M NaCl following complete severing of the sample.

As for the PAA/PAH networks,¹⁴ the mechanism of healing is presumed to involve the interdiffusion of chains across the cut as NaCl is able to break interpolymer cross-links, providing the required mobility. In contrast, in the absence of NaCl, polymer mobility is very low, and interchain cross-links remain intact, making healing impossible. The lower salt concentrations required for healing in the PAA/5.1-P networks likely results from the weaker ionic bonding between the phosphoniums and carboxylates than between the ammoniums and carboxylates in the PAA/PAH networks. This in turn may be attributed to the more sterically-hindered nature of the quaternary phosphonium compared to the primary ammonium and to the lower charge density on the larger phosphonium ion.

5.3 Conclusions

New ionic networks based on PAA and polyphosphonium were investigated as self-healing materials. While the 5.2-P networks exhibited predominantly fluid-like behavior and very poor mechanical properties, 5.1-P networks exhibited viscoelastic behaviour that could be

tuned according to their method of preparation and consequently the ratio of **PAA** to **5.1-P** in the networks. **PAA>5.1-P**, which was prepared by the addition of **5.1-P** to a solution of **PAA**, had an intermediate tensile strength and Young's modulus and the highest elongation at break among the three studied networks, but most importantly exhibited sufficient dynamic behavior, with a relaxation time on the order of ~ 30 s, to be suitable for self-healing. Self-healing studied in 0.1 M NaCl demonstrated that **PAA>5.1-P** could heal, whereas the **PAA \approx 5.1-P** and **PAA<5.1-P** networks, which had predominantly elastic behavior, did not heal well. **PAA>5.1-P** did not heal in pure water, confirming that the presence of salt is necessary for the dynamic exchange of cross-links in the healing mechanism. Tensile testing on healed networks showed that they were able to recover a significant fraction of their strength, modulus, and elongation, though further improvements would be desirable through tuning of the chemical structure of the polymers or optimizing the healing conditions. These phosphonium networks exhibit mechanical properties and healing behaviour significantly different from the **PAA/PAH** networks studied previously. Most notably, the present materials undergo self-healing at salt concentrations similar to those encountered in physiological conditions. This makes phosphonium ionic networks of particular interest for biomedical applications. Future work will explore the potential for tuning the mechanical properties and healing behaviour of the networks by changing the chemical structures of the polymers such as by decreasing the steric bulk around the phosphonium using a trimethylphosphonium analogues or by changing the polyanion.

5.4 Experimental

General materials and procedures

Solvents were purchased from Caledon Laboratory Chemicals (Georgetown, ON, Canada). Deuterated solvents were purchased from Cambridge Isotopes Laboratories (Tewksbury, MA, USA). All solvents used for polymerizations were degassed before use by three freeze-dry-thaw cycles and kept under an N_2 atmosphere. **PAA** (25 wt% in water, sold as 240 kg/mol) was purchased from VWR (Mississauga, ON, Canada). Phosphines were donated by Solvay-Cytec (Niagara Falls, ON, Canada) and used as received. DSC was performed on a DSC Q20 from TA Instruments (Waters, New Castle, DE, USA) at a ramp rate of 10 °C/min

under an N₂ atmosphere in an aluminum Tzero™ pan using 5-10 mg of sample. TGA was completed on a Q600 SDT TA Instrument and analyzed at a ramp rate of 10 °C/min up to 600 °C using a ceramic pan with 2-4 mg of sample. Nuclear magnetic Resonance Spectroscopy (NMR) was performed on a Varian Inova 400 MHz Spectrometer. ¹H NMR chemical shifts (δ) relative to tetramethylsilane were referenced to residual solvent peaks (CDCl₃: 7.26 ppm, CD₃OD: 3.31 ppm). ³¹P{¹H} NMR was externally referenced to H₃PO₄ (δ = 0). SEC of **5.1-P** was performed using a Malvern VISCOTEK GPCmax instrument equipped with a VISCOTEK VE 3580 RI Detector and two Inert series columns (P101609 and Q10183) at a constant temperature of 50 °C. The eluent was 0.4 M tetrabutylammonium triflate in DMF with a flow rate of 1 mL/min. Calibration was performed using PMMA standards. SEC of **PAA** was performed using a Waters 2695 Separations Module equipped with a Waters 2414 refractive index detector, PL Aquagel-OH 8 μm 30, 40, and 50 columns and a PL Aquagel-OH guard column, using H₂O with 0.1 M NaN₃ with a flow rate of 1 mL/min. Calibration was performed using PEO standards. SEM-EDX was performed using a Hitachi S-3400N Variable Pressure Microscope with a Turbomolecular pump. Samples were analyzed at an accelerating voltage of 20 kV, and analyzed by EDX analysis using an INCA EDAX system and software. Samples were cut into pieces approximately 1 mm x 1 mm with a thickness of 1 mm and dried overnight in a vacuum oven, then mounted on carbon tabs and coated with 5 nm of osmium prior to analysis.

Synthesis of 5.1-P

5.1²³ (26.1 g, 96.6 mmol), azobisisobutyronitrile (AIBN) (20 mg, 0.12 mmol) and DMSO (130 mL) were combined in a round bottom flask with a stir bar and the flask was sealed with a rubber septum and Teflon tape. N₂ was bubbled through the solution using a needle with stirring at room temperature for 30 min to degass it. The reaction mixture was then heated at 80 °C for 16 h. Volatiles were then removed *in vacuo* at 100 °C and the polymer was purified by precipitation from 2-propanol into THF twice, yielding a white solid. Yield = 13.6 g, 52%; ¹H NMR (400 MHz, D₂O, δ): 6.99 (br s, 2H, Ar H), 6.33 (br s, 2H, Ar H), 3.50 (br s, 2H, Ar-CH₂P), 1.93 (s, 6H, CH₂P), 1.34 (br s, 2H, CH₂), 0.86 (s, 9H, CH₃); ³¹P{¹H} NMR (161 MHz, D₂O, δ): 36.8 (s). T_g = 225 °C; T_o = 335 °C; SEC: M_n = 240 kg/mol; *D* = 2.4.

Synthesis of 5.2-P

Tributyl vinylbenzyl phosphonium chloride¹ (1.048 g, 2.02 mmol), azobisisobutyronitrile (1.0 mg, 6.1 μ mol) and CH₃CN (7 mL) were combined in a schlenk round bottom with a stir bar and a Suba Seal septum. The solution was degassed with a flow of N₂ through the solution using a needle at 0°C for 30 minutes. The resulting mixture was heated at 80°C for 16 hours. Volatiles were removed *in vacuo*, and the resulting solid was dissolved in minimal CH₂Cl₂ (~3 mL), and precipitated by the addition of tetrahydrofuran (50 mL) with vigorous stirring. Precipitation was repeated, resulting in a white solid. Yield: 0.956 g 91%. ¹H NMR (400 MHz, CDCl₃, δ): 7.35 (broad, Ar-H), 6.29 (broad, Ar-H), 4.37 (broad, Ar-CH₂-P), 2.36 (broad, P-CH₂-(CH₂)₂-CH₃), 1.95 (broad, backbone CH), 1.39 (broad, P-CH₂-(CH₂)₂-CH₃), 0.84 (broad, P-(CH₂)₃-CH₃); ³¹P{¹H} NMR (161.82 MHz, CDCl₃, δ): 32.09; T_g = 165 °C; T_o = 300 °C

Preparation of ionic networks

The polyphosphonium and PAA were dissolved separately in 0.1 M NaCl (pH 8), at a concentrations of 0.1 M in terms of the ions. With vigorous stirring, the solutions were combined slowly in a large beaker, adding one solution to the other to produce non-stoichiometric polymer networks **PAA>5.1-P** or **PAA<5.1-P**, or both solutions simultaneously into a new beaker to produce the stoichiometric network **PAA \approx 5.1-P**. The liquid was decanted and the network was then soaked in 0.25 M NaCl for 2 h. The resulting swelled solid was manually combined into a sphere and then immersed in 0.25 M NaCl for 2 h. The polymer network was then pressed into sheets of 1-4 mm thickness, between Teflon sheets in a melt press at 50 °C for one hour. The polymer network sheets were then separated from the Teflon. Often, the networks became adhesive to the Teflon sheets and were placed in a freezer overnight to allow for easier removal. Finally, the networks were submerged in 0.1 M NaCl overnight before any mechanical testing or healing experiment.

Determination of swelling mass %.

Freshly pressed sheets were cut into 0.5 cm x 0.5 cm squares (1 mm thickness) and were soaked in DI water overnight to ensure removal of all residual NaCl ions. The networks were then dried in *vacuo* overnight. The samples were then placed in the appropriate concentration

of NaCl solutions for 24 hours. The solutions were decanted, and the remaining solid was dried by dabbing with a Kimwipe. Triplicate samples were evaluated. The masses were recorded and compared to the dried mass. Swelling % was calculated by the following equation:

$$\text{Swelling mass \%} = 100 \times \left(\frac{\text{mass of swelled network} - \text{mass of dried network}}{\text{mass of dried network}} \right)$$

Rheology

Rheological measurements were carried out at 21 °C on an AR1500ex stress-controlled rotational rheometer (TA Instruments) with a 2.5 cm diameter parallel-plate tool. Small-amplitude oscillatory shear measurements were performed over the frequency range 0.01-100 rad/s with a stress amplitude of 250 dyne/cm². Samples were equilibrated in 0.1 M NaCl overnight, and cut into disks with diameter 3 cm and thickness ~1 mm, measured using a Vernier caliper. The gap between the plates of the rheometer tool was initially set equal to the measured thickness of the gel sample, then the tool was lowered to decrease the gap by 20 μm. The sample was then allowed to relax for a few minutes before measurements were started. Samples were run in duplicate.

Tensile testing

Tensile measurements were conducted on an Instron 5943 with serrated callipers using a closing pressure of 10 PSI and a strain speed of 500 mm/min. Sheets of the networks ~1-4 mm thickness, measured accurately with a caliper, were cut using a dog-bone-shaped cutter according to ASTM standard D638-14 Type V. The cut samples were kept in 0.1 M NaCl until testing began. Triplicate samples of each network were evaluated.

Healing experiments

For the puncture tests, networks were punctured with an 18-gauge needle and the material was removed to create a 0.5 mm diameter hole. Damaged networks were then soaked in 0.1 M NaCl or deionized water and imaged using a stereomicroscope at 20x magnification in transmission mode at t = 0 h, 1 h, 2 h, 3 h, 6 h, 11 h, and 24 h. For the tensile testing after healing, the dog bone shaped network samples were cut in half with a scalpel, manually

pressed back together for 1 min, and then incubated in 0.1 M NaCl for 24 h. Tensile testing was then performed as described above. The experiment was repeated in triplicate.

5.5 References

- 1) An, S. Y.; Arunbabu, D.; Noh, S. M.; Song, Y. K.; Oh, J. K. *Chem. Commun.* **2015**, *51*, 13058–13070.
- 2) Bekas, D. G.; Tsirka, K.; Baltzis, D.; Paipetis, A. S. *Compos. Part B Eng.* **2016**, *87*, 92–119.
- 3) Wu, D. Y.; Meure, S.; Solomon, D. *Prog. Polym. Sci.* **2008**, *33*, 479–522.
- 4) Yang, Y.; Urban, M. W. *Chem. Soc. Rev.* **2013**, *42*, 7446–7467.
- 5) Ghosh, S. K. In *Self-healing materials: Fundamentals, Design Strategies, and Applications*; Ghosh, S. K., Ed.; WILEY-VCH Verlag GmbH & Co. KGaA: Weinheim, Germany, 2009.
- 6) Wang, C.; Wu, H.; Chen, Z.; McDowell, M. T.; Cui, Y.; Bao, Z. *Nat. Chem.* **2013**, *5*, 1042–1048.
- 7) Brochu, A. B. W.; Craig, S. L.; Reichert, W. M. *J. Biomed. Mater. Res. - Part A* **2011**, *96 A*, 492–506.
- 8) Jacob, R. S.; Ghosh, D.; Singh, P. K.; Basu, S. K.; Jha, N. N.; Das, S.; Sukul, P. K.; Patil, S.; Sathaye, S.; Kumar, A.; Chowdhury, A.; Malik, S.; Sen, S.; Maji, S. K. *Biomaterials* **2015**, *54*, 97–105.
- 9) Dailey, M. M. C.; Silvia, A. W.; McIntire, P. J.; Wilson, G. O.; Moore, J. S.; White, S. R. *J. Biomed. Mater. Res. A* **2014**, *102*, 3024–3032.
- 10) White, S. R.; Sottos, N. R.; Geubelle, P. H.; Moore, J. S.; Kessler, M. R.; Sriram, S. R.; Brown, E. N.; Viswanathan, S. *Nature* **2001**, *409*, 794–797.
- 11) Toohey, K. S.; Sottos, N. R.; Lewis, J. A.; Moore, J. S.; White, S. R. *Nat. Mater.* **2007**, *6*, 581–585.
- 12) Chirila, T. V.; Lee, H. H.; Odon, M.; Nieuwenhuizen, M. M. L.; Blakey, I.; Nicholson, T. M. *J. Appl. Polym. Sci.* **2014**, *131*, 1–12.
- 13) Rao, Y.-L.; Chortos, A.; Pfattner, R.; Lissel, F.; Chiu, Y.-C.; Feig, V.; Xu, J.; Kurosawa, T.; Gu, X.; Wang, C.; He, M.; Chung, J. W.; Bao, Z. *J. Am. Chem. Soc.*

- 2016**, *138*, 6020–6027.
- 14) Reisch, A.; Roger, E.; Phoeung, T.; Antheaume, C.; Orthlieb, C.; Boulmedais, F.; Lavalle, P.; Schlenoff, J. B.; Frisch, B.; Schaaf, P. *Adv. Mater.* **2014**, 2547–2551.
 - 15) Chen, X.; Dam, M. A.; Ono, K.; Mal, A. *Science* **2002**, *249*, 115–118.
 - 16) Porcel, C. H.; Schlenoff, J. B. *Biomacromolecules* **2009**, *10*, 2968–2975.
 - 17) Reisch, A.; Tirado, P.; Roger, E.; Boulmedais, F.; Collin, D.; Voegel, J. C.; Frisch, B.; Schaaf, P.; Schlenoff, J. B. *Adv. Funct. Mater.* **2013**, *23*, 673–682.
 - 18) Bucur, C. B.; Sui, Z.; Schlenoff, J. B. *J. Am. Chem. Soc.* **2006**, *128*, 13690–13691.
 - 19) Holbrey, J. D.; Rogers, R. D. In *Ionic liquids in Synthesis*; Wassercheid, P.; Welton, T., Eds.; WILEY-VCH Verlags GmbH & Co. KGaA: Weinheim, Germany, 2008; Vol. 1.
 - 20) Bradaric, C. J.; Downard, A.; Kennedy, C.; Robertson, A. J.; Zhou, Y. *Green Chem.* **2003**, *5*, 143–152.
 - 21) Wathier, M.; Grinstaff, M. W. *J. Am. Chem. Soc.* **2008**, *130*, 9648–9649.
 - 22) Lin, X.; Navailles, L.; Nallet, F.; Grinstaff, M. W. *Macromolecules* **2012**, *45*, 9500–9506.
 - 23) Cuthbert, T. J.; Harrison, T. D.; Ragona, P. J.; Gillies, E. R. *J. Mater. Chem. B* **2016**, *4*, 4872–4883.
 - 24) Tsenoglou, C. *Macromolecules* **1991**, *24*, 1762–1767.
 - 25) Chen, D. T. N. N.; Wen, Q.; Janmey, P. A.; Crocker, J. C.; Yodh, A. G. *Annu. Rev. Condens. Matter Phys.* **2010**, *1*, 301–322.
 - 26) Lawrence, P. G.; Patil, P. S.; Leipzig, N. D.; Lapitsky, Y. *ACS Appl. Mater. Interfaces* **2016**, *8*, 4323–4335.
 - 27) Akhtar, R.; Sherratt, M. J.; Cruickshank, J. K.; Derby, B. *Mater. Today* **2011**, *14*, 96–105.

Chapter 6

6 A Phosphorus-rich polymer as a homogeneous catalyst scavenger

6.1 Introduction

Homogeneous catalysis enables many difficult bond transformations and significantly reduces the need for stoichiometric reagents and waste. These are highly desirable properties for the industrial synthesis of high-value compounds (i.e. pharmaceuticals),¹ yet homogeneous catalysis is only used in ca. 6-7% of steps in the pharmaceutical industry.² A key contributor to this low number is the challenge in removing spent catalyst (namely the metal) from the organic product.³ While the optimal catalytic scenario involves a catalyst with very high turnover number (TON), so that metal removal is precluded,^{4, 5} this is not always attainable. The residual metal is problematic in downstream reactions because it can promote undesired reactivity.^{6, 7} Additionally, strict toxicity guidelines for pharmaceutical products set very low limits of <10 ppm for Pt group metal contaminants.⁸ While the heavier metals are most often cited for their toxicity, the abundant first-row metals may also have cause for concern.⁹ Typical metal removal methods are a challenge on large scale, which has led to the development and commercialization of scavenger materials.¹⁰ Many of the available scavengers are efficient, appropriate for a broad range of metal complexes and are easy to use. The desire for scavenger materials with lower required loadings, short incubation times, improved reusability and lower cost continues to motivate research in this area.

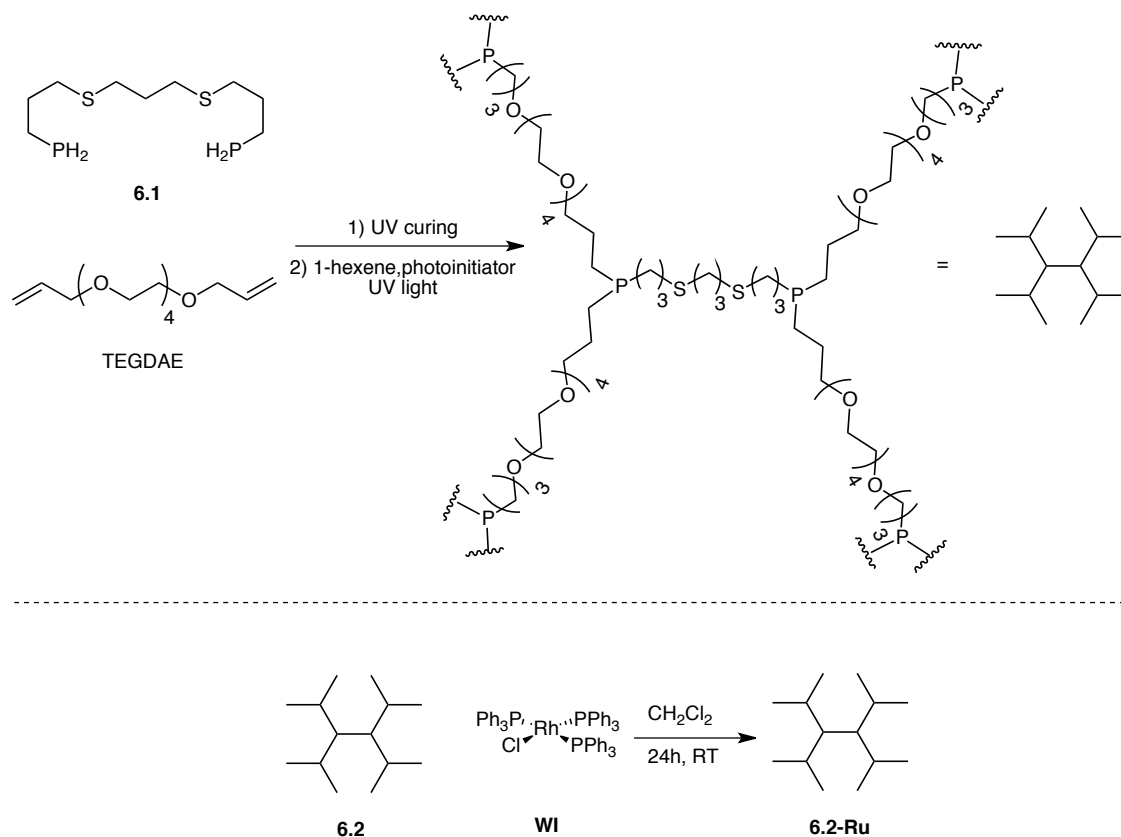
Recently, phosphorous-rich polymer networks were prepared through a step-growth polymerization, involving phosphane-ene reactions of primary bis-phosphines (**6.1**) and terminal diolefins.^{11, 12} The polymers were soft or rigid in nature depending on the flexibility of the monomers. The soft polymer network (**6.2**) exhibits appreciable swelling in organic solvents and are capable of coordinating simple metal salts.¹² This suggests the polymer networks could act as a ligand for metals of homogeneous catalysts and effectively scavenge them from catalytic reaction mixtures. The Lewis basic sites of the polymer networks are part of the polymer structure and are present in high concentrations. This is distinct from

most scavenger materials that typically contain a Lewis basic functional group that is appended to a resin bead (i.e. polystyrene). Herein, we evaluate the efficacy of the phosphorous-rich **6.2** as a scavenger for homogeneous catalysts.

6.2 Results and Discussion

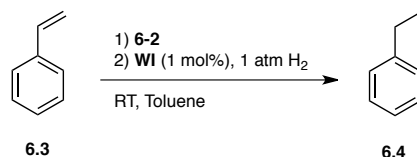
6.2.1 Metal scavenging with polymers from primary di-phosphine 6.1.

The soft polymer network **6.2** was prepared following reported procedures.¹¹ All primary and secondary phosphine sites were converted to tertiary phosphines by reaction of the network with excess 1-hexene. To establish the affinity of metals to the polymer network, **6.2** was stirred at room temperature for 24 h with excess Wilkinson's catalyst (**W1**; Scheme 6-1). The solution changes colour from dark red to orange and isolation of the solid reveals that the polymer has changed from white to orange. Incorporation of **W1** into the polymer product (**6.2-Rh**) was confirmed by ICP-MS analysis that gave a metal loading of 0.389 Rh/S (mol/mol). This loading corresponds to nearly one rhodium centre (0.778) per unit of diphosphine in the network.



Scheme 6-1: Loading the Soft Polymer Network (6.2) with Wilkinson's catalyst (WI) to give 6.2-Rh.

The efficacy of **6.2** toward metal removal from a catalytic reaction was evaluated in, the proof-of-principle reaction, hydrogenation of styrene with 1 mol% **WI** (4747 ppm Rh; Scheme 6-2). In the absence of **6.2** hydrogenation is complete within 1.5 h under 1 atm of H_2 at room temperature (Figure 6-1). Pre-treatment of the hydrogenation reaction with **6.2** (16 mg/ μmol Rh) at the outset of reaction, gives only a 20% conversion of styrene over 1.5 h (Figure 6-1). Indeed, catalytic turnover is arrested completely within 10 minutes, suggesting the catalyst was rapidly and efficiently sequestered from solution. Incubation of **6.2** with the reaction for 24 h was followed by a facile filtration step. ICP-MS analysis of the soluble organic residues revealed that only 11 ppm of Rh remained, which equals 99.8% rhodium removal.



Scheme 6-2: Hydrogenation of styrene (6.3) with Wilkinson's catalyst (WI) and with scavenger 6.2 added at the outset of reaction.

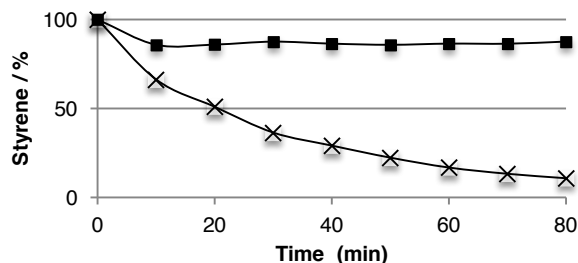
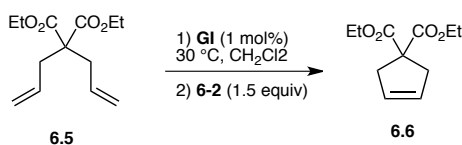


Figure 6-1: Consumption of styrene (1) by hydrogenation with WI without additive (x) and with 6.2 (16 g/mmol Rh) added at the outset of reaction (■). Conversion values were determined by calibrated GC-FID analysis of reaction aliquots with integration relative to an internal standard.

A broadly applicable metal scavenger material should efficiently sequester a range of homogeneous catalysts that have diverse structures. The Grubbs olefin metathesis catalyst (**GI**) was selected as a second proof-of-principle system as the catalyst is common, commercially available, and olefin metathesis has great synthetic utility in C-C bond formation.¹³⁻¹⁵ This has initiated a number of strategies for catalyst immobilization, sequestration and also the synthesis of specialty catalysts that are easily removed by extraction or chromatography.¹⁶⁻¹⁹ In this study, ring closing metathesis (RCM) of the benchmark substrate diethyldiallylmalonate (**6.5**) was conducted under standard conditions with 1 mol% **GI** in CH₂Cl₂ at room temperature (Scheme 6-3).²⁰



Scheme 6-3: RCM of 6.5 with GI followed by sequestration of the catalyst with 6.2, 6.7, and 6.8.

After 1 h maximum conversion to RCM product **6.6** was achieved (Scheme 6-3). Reaction samples were stirred with **6.2** (10 mg **6.2**/μmol **GI**) for a range of incubation times (0.3, 12,

24 and 48 h) prior to filtration (Table 6-1, Entries 1-5). Within 20 minutes 30% of the metal is removed and by 12 h removal reaches ca. 94%. Prolonged incubation (72 h) gave a maximum removal of nearly 99%. A similar trend was found with a lower **6.2** loading of 5 mg **6.2**/μmol **GI** (Table 1, Entries 6-8), albeit with a slightly lower maximum metal removal (ca. 98% after 72 h). The **6.2** scavenger outcompetes solid-supported ligands, such as phosphines and isocyanates (Table 1, Entries 9 and 10).^{21, 22} While the scavenging efficiency of **6.2** is lower than the reported protocol involving a silica gel and activated charcoal incubation, followed by column chromatography (Entry 11),²³ the **6.2** protocol is significantly more user friendly. Oxidation of **GI** with a very large excess of H₂O₂ followed by extraction is convenient and removes >99% of Ru (Entry 12).²⁴ However, the incompatibility of the oxidant with many functional groups, is a severe practical limitation. Overall, **6.2** is easy to use and it removes a maximum of 98.8% Ru, which is similar to known scavengers of **GI**.

Table 6-1: Sequestration of GI from RCM of 6.5.^a

Entry	Removal method (equiv scavenger)	GI mol% (ppm)	Incubation time (h) ^b	Residual Ru (ppm)	Ru Removed (%) ^c	Ref
1	6.2 /filtration (10 mg/ μ mol Ru)	1 (4755)	0.3	3319	30.2	^d
2	6.2 /filtration (10 mg/ μ mol Ru)	1 (4755)	12	307	93.5	^d
3	6.2/filtration (10 mg/ μ mol Ru)	1 (4755)	24	140	97.1	^d
4	6.2/filtration (10 mg/ μ mol Ru)	1 (4755)	48	78	98.4	^d
5	6.2/filtration (10 mg/ μ mol Ru)	1 (4755)	72	59	98.8	^d
6	6.2/filtration (5 mg/ μ mol Ru)	1 (4755)	24	253	94.7	^d
7	6.2/filtration (5 mg/ μ mol Ru)	1 (4755)	48	139	97.1	^d
8	6.2/filtration (5 mg/ μ mol Ru)	1 (4755)	72	111	97.7	^d
9 ^e	Resin-bound phosphine (5 equiv) /charcoal	5 (23775)	17 ^f	1120	95.3	²¹
10	SiO ₂ -bound isocyanide (60 equiv)	2.5 (11888)	0.5	468	95.6	²²
11 ^e	SiO ₂ /activated carbon (100 equiv wt rel to GI)/SiO ₂	10 (47550)	12 ^g	60	99.9	²³
12	H ₂ O ₂ /extraction (5000 equiv)	5 (23775)	0.3	15.10	99.45	²⁴

^a Conditions: 6.5 (106 mM) in CH₂Cl₂ at 30 °C. ^b Time scavenger is exposed to the reaction solution prior to filtration, extraction. ^c %Ru removed = [(loading Ru – residual Ru)/(loading Ru)]*100. ^d This work. ^e RCM conducted at RT. ^f Time resin exposed to reaction solution.

^g Time activated carbon is exposed to the reaction solution.

A sample of metal-loaded polymer (**6.2-Ru**) was prepared by stirring **GI** with the polymer network. Metal loading was confirmed by ICP-MS analysis and solid-state ³¹P{¹H} NMR spectroscopy. The latter revealed broad signals in the range of 0-40 ppm that are consistent with metal-bound tertiary phosphine sites. A signal for metal-free phosphine is observed (–32 ppm) and this may reflect the incomplete loading of Ru due to the limited accessibility of **GI** to the interior of the network. Additionally, the thioether moieties are likely also involved in metal sequestration and this would go unobserved by ³¹P{¹H} NMR spectroscopy. To attempt scavenger regeneration the metal loaded polymer (**6.2-Ru**) was stirred in neat PEt₃ or TMEDA (*N,N,N',N'*-tetramethylethane-1,2-diamine) for 24 h (Table 6-2). At room temperature both the phosphine and amine reagents displaced ruthenium, albeit in low amounts (ca. 20 and 30%, respectively). Scavenger regeneration at elevated temperature is

more effective with a maximum removal of 42.6% achieved in PEt_3 at 80 °C. Successful metal removal supports the hypothesis that metal sequestration involves reversible adduct formation between the metal and Lewis basic sites of the polymer network.

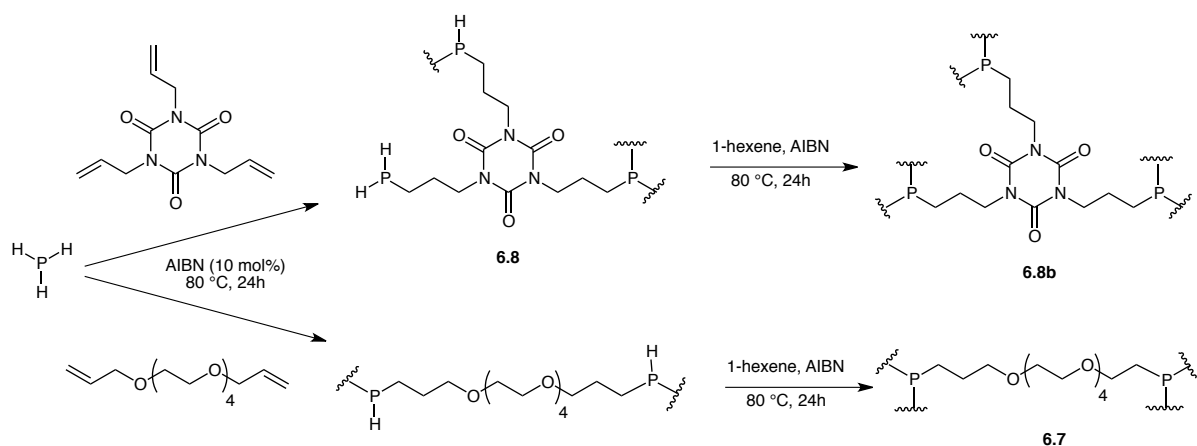
Table 6-2: Regeneration of metal free 6.2 from 6.2-Ru.

Entry	Regeneration method	Temp. (°C)	Residual Ru (ppm)	Ru Removed (%) ^b
1 ^c	Neat PEt_3	23	17020	20.4
2 ^c	Neat TMEDA	23	14286	33.2
3 ^c	Neat PEt_3	80	12274	42.6
4 ^d	Neat TMEDA	80	2575.4	39.1

^a Conditions: 6.2-Ru in neat reagent for 24h. ^b %Ru removed = [(initial Ru) – (residual Ru)/(initial Ru)]*100. ^c Initial Ru on 6.2-Ru = 21393 ppm. ^d Initial Ru on 6.2-Ru = 4230 ppm.

6.2.2 Polymer Network Metal scavengers from PH_3

An alternative to synthesizing **6.1** as the P-H containing monomer, we hypothesized the same phosphane-ene chemistry could be produced directly from phosphine gas ($\text{PH}_3(\text{g})$) to produce polymer networks. Phosphine is a feedstock chemical currently produced on an industrial scale making it an ideal reagent for large scale synthesis. PH_3 has the same P-H bond reactivity as utilized in the preparation **6.2**, but with a functionality of three, and therefore possessing cross-linking ability. Networks were produced using the phosphane-ene polymerization of PH_3 and tetraethylene glycol diallyl ether to produce **6.7**, and 1,3,5-triallyl-1,3,5-triazine-2,4,6-trione (TTT) to produce **6.8** (Figure 6-3). TEGDAE has a diallyl functionality and should produce a lower cross-link density compared to the triallyl functionality of TTT. This ultimately manifested in the low glass transitions of **6.7** of -64 °C, while **6.8** had no observable glass transition between -100 °C and 300 °C (Figure 8-70).



Scheme 6-4: Synthesis of PH_3 containing networks with TTT (6.8**) and TEGDAE (**6.7**).**

By using $\text{PH}_{3(\text{g})}$ at 550 kPa, one has little control over the polymerization, and **6.7** resulted in a distribution of primary, secondary, and tertiary phosphines (Figure 8-67). The residual P-H bonds from the primary and secondary phosphines were further reacted with the addition of more TEGDAE and initiator with heating at 65 °C overnight, resulting in a network with a primarily tertiary phosphine (Figure 6-2). Interestingly, analysis of the crude reaction of **6.8** by solid-state $^{31}\text{P}\{^1\text{H}\}$ NMR spectroscopy revealed the presence of only tertiary phosphines (Figure 6-2). The networks were then tested for Ruthenium (**G1**) metal scavenging from a reaction mixture of a ring closing metathesis reaction (Scheme 6-4), results outlined in Table 6-3.

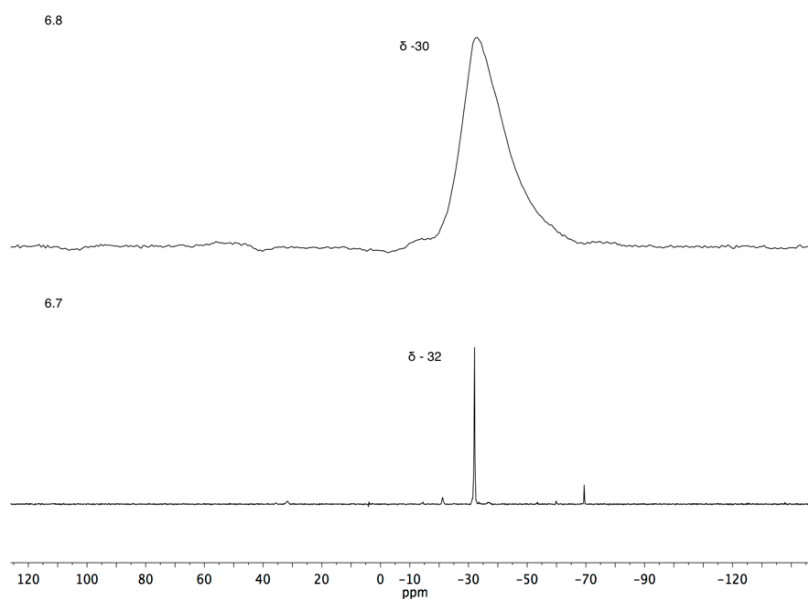


Figure 6-2: $^{31}\text{P}\{^1\text{H}\}$ NMR spectroscopy of 6.7 and 6.8 composing of primarily tertiary phosphines.

Table 6-3: Sequestration of GI from RCM of 6.5. Conditions: 6.5 (106 mM) in CH_2Cl_2 at 30 °C. ^b Time scavenger is exposed to the reaction solution prior to filtration/extraction. ^c %Ru removed = [(loading Ru – residual Ru)/(loading Ru)]*100.

Entry	Removal method (equiv scavenger)	GI mol% (ppm)	Incubation time (h) ^b	Residual Ru (ppm)	Ru Removed (%) ^c
1	6.7 (10 mg/ μmol Ru)	1 (5878)	24	480	91.8%
2	6.7 (10 mg/ μmol Ru)	1 (5878)	48	262	94.7%
3	6.8 (10 mg/ μmol Ru)	1 (5335)	24	3122	41.5
4	6.8 (10 mg/ μmol Ru)	1 (5335)	48	2582	51.6
5	6.8b (10 mg/ μmol Ru)	1 (5335)	24	294	94.5
6	6.8b (10 mg/ μmol Ru)	1 (5335)	48	208	96.1
7	6.8b (30 mg/ μmol Ru)	1 (3436)	24	263	92.3
8	6.8b (60 mg/ μmol Ru)	1 (3436)	24	215	93.7

At a loading of 10 mg/ μ mol Ru of **6.7** resulted in a 91.8% removal in 24 hours and 94.7% removal in 48 hours incubation (Table 6-3, entries 1 and 2), while **6.8** resulted in a 41.5% removal in 24 hours and 51.6% removal in 48 hours (Table 6-3, entries 3 and 4). **6.8** networks were further treated with 1-hexene to convert any remaining 1° and 2° phosphines to tertiary phosphines, which will also increase the Lewis basic character, enhancing metal binding (**6.8b**). The results showed an increase in metal scavenging to 94.5% removal in 24 hours and 96.1% removal in 48 hours for the same loading of polymer at 10 mg/ μ mol Ru (Table 6-3, entries 5 and 6).

6.3 Conclusions

The phosphorous-rich polymer networks **6.2**, **6.7**, and **6.8** effectively scavenges homogenous catalysts from reaction mixtures. Hydrogenation and ring closing metathesis were used as proof-of-principle reactions where 99.9 and 98.8% Rh (**WI**) and Ru (**GI**) were sequestered, respectively. Scavenger regeneration by removal of the loaded metal from the polymer network is possible, although further work on this will be required. An alternative synthesis to create phosphine containing polymers directly from $\text{PH}_3(\text{g})$ could be an attractive method for commercialization because of the use of feedstock chemicals, simple reaction conditions, and good scavenging abilities. The facile methodology for polymer network preparation is sure to lead to improved formulations and next generation polymers with superior rate of scavenging, metal removal efficiency and regeneration protocols.

6.4 Experimental

General Procedures, Materials and Instrumentation.

All reactions were manipulated under N_2 using standard Schlenk or glovebox techniques. All glassware was oven dried prior to use. $\text{RhCl}(\text{PPh}_3)_3$ and PEt_3 (90%) were used as received. Styrene ($\geq 99\%$) and diethyldiallylmalonate (98%) were degassed by purging with N_2 and stored over 4 Å sieves. TMEDA was dried over CaH and distilled prior to use. $\text{RuCl}_2(\text{PCy}_3)_2(=\text{CHPh})$ (**GI**) was gifted and purified by successive washings with acetone and pentane. **6.2** was prepared according to literature procedures.¹ Dry and degassed solvents were obtained from an Innovative Technology 400-5 Solvent Purification System and stored

over 4 Å molecular sieves (Fluka and activated at 150 °C for 12 h) under N₂ unless otherwise noted. Chloroform-*d* (99.8%) was obtained from Cambridge Isotope Laboratories, was dried with 4 Å molecular sieves and degassed by bubbling with N₂.

All NMR spectra were recorded on either an Inova 600 MHz, Inova 400 MHz, or Mercury 400 MHz instrument. ¹H and ¹³C spectra acquired were referenced internally against the residual solvent signal to TMS at 0 ppm. ³¹P{¹H} spectra were referenced externally to 85% phosphoric acid at 0.00 ppm. Solid-state ³¹P{¹H} NMR experiments were performed using a Varian Infinity Plus 400 NMR spectrometer (ν_L (³¹P) = 161.71 MHz) equipped with a Varian 4 mm triple-resonance HXY magic-angle spinning NMR probe. Chemical shifts were referenced with respect to the ³¹P{¹H} NMR peak of H₃PO₄ (δ (³¹P) = 0.0 ppm) by setting the ³¹P NMR peak of solid ammonium dihydrogen phosphate to +0.81 ppm. The powder samples were stored inside a glove box filled with nitrogen gas and packed tightly into 4 mm o.d. ZrO₂ rotors, then sealed. For the samples having low glass-transition temperature samples, the NMR spectra were acquired using a standard one pulse sequence with high-power ¹H TTPM decoupling, 12.0 kHz spinning rate, 50 kHz spectral width, between 140-160 scans, a 1.8 μs $\pi/4$ -pulse width, 30 s recycle delay and 20.4 ms acquisition time, and a 6.25 μs TPPM ¹H decoupling pulse with 83 kHz decoupling field. For samples having high glass-transition temperature samples, the NMR spectra were acquired using cross-polarization (CP) with high-power ¹H TTPM decoupling, 12.0 kHz spinning rate, 50 kHz spectral width, between 164-380 scans, 4.6 μs ¹H $\pi/2$ -pulse width, 1 ms contact time, 15 s recycle delay, between 8.5-20.4 ms acquisition time, and a 6.25 μs TPPM ¹H decoupling pulse with 83 kHz decoupling field. In hydrogenation reactions, styrene and ethylbenzene were quantified relative to an internal standard (cyclodecane) and analyzed with an Agilent 7890A GC-FID with an HP-5 column. Styrene and ethylbenzene were quantified relative to an internal standard by GC-FID analysis. Area counts for ethylbenzene were corrected using a response factor obtained by calibration of styrene and ethylbenzene over the concentration range 1 to 5 mM. A linear response for both species was found in this range. Authentic samples of each were used to construct calibration curves. ICP-MS samples were first digested in aqua-regia for 2 hours then data was collected on an Agilent 7700 Series ICP-MS.

Preparation of 6.2-Rh

RhCl(PPh₃)₃ (**WI**) (42 mg, 0.0449 mmol) and **6.2** (45 mg) were stirred in CH₂Cl₂ (20 mL) at room temperature for 24 hours. A colour change of the solution from deep red to orange was observed. The resulting functionalized polymer (orange) **6.2-Rh** was washed with CH₂Cl₂ (3 × 30 mL) and pentane (1 × 30 mL). After the final wash **6.2-Rh** was suspended in pentane and dried *in vacuo*. Elemental Analysis by ICP-MS (μg g⁻¹): Rh, 71 200; P, 56 600; S, 61 200.

Synthesis of 6.7

Tetraethylene glycol diallylether (10.52 g, 39.21 mmol), azobisisobutyronitrile (0.64 g, 3.9 mmol), and toluene (10 mL) were loaded into an autoclave reactor, purged with N₂, and charged with 80 PSI PH₃ gas. The autoclave was then heated at 80 °C for 2 days and any remaining PH₃ was flushed from the autoclave and incinerated. All further manipulations were completed in a N₂ filled glovebox. Additional toluene (10 mL) and azobisisobutyronitrile (0.62 g, 3.8 mmol) were added to the reaction mixture, transferred to a pressure round bottom with an N₂ atmosphere, and heated at 80 °C overnight, resulting in 3° phosphine. The polymer network was isolated by centrifugation, washed with toluene (3x10 mL) and acetonitrile (3x10 mL), isolated by centrifugation between each washing. Volatiles were removed *in vacuo*, giving a yellow gel. Solid-state ³¹P{¹H} NMR (161.71 MHz, δ): -30 (s). ATR-FTIR (cm⁻¹; ranked intensity): 2861 (2), 1454 (9), 1348 (7), 1292 (8), 1248 (9), 1104 (1), 1041 (3), 995 (4), 925 (5), 879 (10). T_o = 342 °C; T_g = -65 °C.

Synthesis of 6.8/6.8b

1,3,5-triallyl-1,3,5-triazine-2,4,6(1*H*,3*H*,5*H*)-trione (10.02 g, 40.67 mmol), azobisisobutyronitrile (0.66 g, 4.0 mmol), and toluene (12 mL) were loaded into an autoclave reactor, purged with N₂, and charged with 80 PSI of PH_{3(g)}. The autoclave was then heated at 80 °C for 24 hours and any remaining PH_{3(g)} was flushed from the autoclave and incinerated. All further manipulations were completed in a N₂ filled glovebox. The solid material was isolated by centrifugation, washed with toluene (3x10 mL) and acetonitrile (3x10mL) isolated by centrifugation between each washing step. Volatiles were removed *in*

vacuo yielding a white powder. Solid state $^{31}\text{P}\{^1\text{H}\}$ NMR(161.71 MHz, δ): -31 (s); ATR-FTIR (cm^{-1} ; ranked intensity): 2956 (8), 2492 (7), 1674 (1), 1453 (2), 1427 (3), 1371 (5), 1316 (6), 993 (10), 934 (9), 762 (4); $T_o = 359\text{ }^\circ\text{C}$; $T_g = \text{not observed}$.

General Procedure for the Catalytic Hydrogenation of Styrene

In a glovebox, the following stock solutions were prepared: styrene (104 mg, 1 mmol, 500 mM) in toluene (2.00 mL); tetradecane (70 mg, 0.25 mmol, 250 mM) in toluene (2.00 mL); WI (9.3 mg, 0.01 mmol, 10 mM) in CH_2Cl_2 (1.00 mL). To a 100 mL Schlenk flask containing a stir bar, the catalyst stock solution was added (200 μL), and CH_2Cl_2 was removed *in vacuo*. Added to the same flask was a portion of the styrene (400 μL) and cyclodecane (400 μL) stock solutions. Toluene was added (5.20 mL) to give a final volume of 6.00 mL and the flask was sealed with a rubber septum. The final concentrations of the reaction mixture were 33.0 mM styrene, 8.3 mM cyclodecane, and 0.33 mM WI (1 mol%). The flask was removed from the glovebox and H_2 gas was bubbled into solution for 2 minutes using a needle pierced through the rubber septum of the Schlenk flask. The contents were allowed to stir at room temperature and every 10 minutes for 90 minutes, 200 μL aliquots were removed and exposed to air to quench. From each aliquot, 150 μL was removed and diluted with acetone (850 μL) giving final concentrations of 5 mM for styrene and tetradecane and the diluted samples were analyzed by calibrated GC-FID.

General Procedure for the Quenching of the Hydrogenation of Styrene

The procedure for the catalytic hydrogenation of styrene was followed as outlined above. Added to the reaction set-up, prior to addition of WI, was an excess of **6.2** (32 mg, 0.04 mmol, ca. 1.5 mol P equiv.). **6.2** was present from the outset and 200 μL aliquots taken at 10 minutes intervals, up to 50 minutes. From each aliquot 150 μL was removed and diluted with acetone (850 μL) giving final concentrations of 5 mM for styrene and tetradecane and the diluted samples were analyzed by calibrated GC-FID. After the final aliquot for GC-FID analysis was taken from the quenched reaction, the mixture was allowed to stir for 24 hours. The mixture was then taken up in a syringe and filtered through a syringe filter (Promax Syringe Filter, 13 mm, 0.22 μm PTFE) into a preweighed vial. Solvent was removed *in vacuo* leaving a residue. The residue was submitted for ICP-MS analysis. Additionally, a

control reaction to which no polymer was added was submitted for ICP-MS analysis, for a comparison of the trace metal amounts in each sample.

Scavenging of GI following RCM of Diethyl diallylmalonate

Diethyl diallylmalonate (488 mg, 2.12 mmol), GI (16.4 mg, 0.02 mmol), and CH₂Cl₂ (20 mL) were combined in a Schlenk round bottom in a glovebox with a stir bar. The flask was removed from the glovebox and heated to 30 °C in an oil bath for 1 hour under an N₂ atmosphere. The resulting solution was brought back into the glovebox, and divided into 1 mL portions in small glass vials with a specific amount of **6.2**, **6.7**, **6.8(b)** (1, 5, 10, 30 or 60 mg) with a stir bar. An additional portion was added to a vial that did not contain **6.2** to act as the control. The vials were capped, sealed with Teflon tape and stirred for a specific amount of time (20 minutes, 12, 24, 48, and 72 hours) at room temperature. The mixtures were filtered through a 0.2 µm syringe filter into a tared vial. The reaction vial was washed with 1 mL of CH₂Cl₂ and filtered through the same filter and combined with the initial filtrate. The filtrate solvent was removed *in vacuo* and the mass recorded. These resulting solids were digested with aqua regia (1 mL) and analyzed by ICP-MS for Ru content. The Ru content was compared to the control sample that was also filtered, the volatiles were removed *in vacuo* and a mass was measured prior to digestion (aqua regia) and ICP-MS analysis.

Preparation of 6.2-Ru and regeneration to remove Ru

6.2 (400 mg), GI (32.8 mg, 0.04 mmol), and CH₂Cl₂ (40 mL) were combined with a stir bar in a Schlenk round bottom and stirred for 24 hours under an N₂ atmosphere. The yellow solid was isolated using a Pall Microsep™ Advanced Centrifugal Device with a 10 kg/mol molecular weight cut off. The resulting solid was washed with CH₂Cl₂ and isolated, and this was repeated two additional times. The solid was dried *in vacuo* and divided into 100 mg samples into four glass vials (A-D) with stir bars. Samples A-C were subjected to 3 mL of neat regeneration conditions: PEt₃ at room temperature, PEt₃ at 80 °C, and tetramethyl ethylene diamine (TMEDA) at room temperature. The solutions were then stirred for 24 hours at the desired temperature under N₂. The solid was allowed to settle, and was isolated by filtration with a Microsep™ Centrifugal Device and washed with three portions of

CH₂Cl₂. The solid was then dried *in vacuo*, and analyzed by ICP-MS and solid-state ³¹P{¹H} NMR spectroscopy. The final sample D underwent the same procedure except it was not subjected to the regeneration step. This sample was also analyzed by ICP-MS and solid-state ³¹P{¹H} NMR spectroscopy.

6.5 References

1. Dach, R.; Song, J.J.; Roschangar, F.; Samstag, W.; Senanayake, C.H. *Org. Process Res. Dev.* **2012**, *16*, 1697-1706.
2. Carey, J. S. ; Laffan, D.; Thomson, C.; Williams, M.T. *Org. Biomol. Chem.* **2006**, *4*, 2337-2347.
3. Welch, C.J.; Albanese-Walker, J.; Leonard, W.R.; Biba, M.; DaSilva, J.; Henderson, D.; Laing, B.; Mathre, D.J.; Spencer, S.; Bu, X.; Wang, T. *Org. Process Res. Dev.* **2005**, *9*, 198-205.
4. Gladysz, J.A. *Pure Appl. Chem.* **2001**, *73*, 1319-1324.
5. Hübner, S.; de Vries, J.G.; Farina, V. *Adv. Synth. Catal.* **2016**, *358*, 3-25.
6. Tosatti, P.; Campbell, A.J.; House, D.; Nelson, A.; Marsden, S.P. *J. Org. Chem.* **2011**, *76*, 5495-5501.
7. Hermann, J.C.; Chen, Y.; Wartchow, C.; Menke, J.; Gao, L.; Gleason, S.K.; Haynes, N.E.; Scott, N.; Petersen, A.; Gabriel, S.; Vu, B.; George, K.M.; Narayanan, A.; Li, S.H.; Qian, H.; Beatini, N.; Niu, L.; Gan, Q.F. *ACS Med. Chem. Lett.* **2013**, *4*, 197-200.
8. European Medicines Agency Residual Metal Limits .
http://www.ema.europa.eu/docs/en_GB/document_library/Scientific_guideline/2009/09/WC500003586.pdf (accessed September 11, 2015).
9. Egorova, K. S.; Ananikov, V.P. *Angew. Chem. Int. Ed.* **2016**, *55*, 12150-12162.
10. Representative Commercial Scavenger Sources:
Silicycle <http://www.silicycle.com/ca/products/metal-scavengers>.
PhosphonicS <http://www.phosphonics.com/services/metal-recovery-and-recycling>.
Biotage <http://www.biotage.com/product-group/metal-scavengers>.

11. Guterman, R.; Rabiee Kenaree, A.; Gilroy, J.B.; Gillies, E.R.; Ragogna, P.J. *Chem. Mater.* **2015**, *27*, 1412-1419.
12. Guterman, R.; Gillies, E.R.; Ragogna, P.J. *Dalton Trans.* **2015**, *44*, 15664-15670.
13. Grubbs, R.H. In *Handbook of Metathesis*, Wiley-VCH: Weinheim, Germany, 2003.
14. Grubbs, R.H. *Angew. Chem., Int. Ed.* **2006**, *45*, 3760-3765.
15. Higman, C.S.; Lummiss, J.A.M.; Fogg, D.E. *Angew. Chem. Int. Ed.* **2016**, *55*, 3552-3565.
16. Dewaele, A.; Verpoort, F.; Sels, B. *ChemCatChem* **2016**, *8*, 3010-3030.
17. Vougioukalakis, G.C. *Chem. Eur. J.* **2012**, *18*, 8868-8880.
18. Skowerski, K.; Wierzbicka, C.; Szczepaniak, G.; Gulajski, L.; Bieniek, M.; Grela, K. *Green Chem.* **2012**, *14*, 3264-3268.
19. Doppiu, A.; Caijo, F.; Tripoteau, F.; Bompard, S.; Crévisy, C.; Mauduit, M. *Top. Catal.* **2014**, *57*, 1351-1358.
20. Ritter, T.; Hejl, A.; Wenzel, A.G.; Funk, T.W.; Grubbs, R.H. *Organometallics* **2006**, *25*, 5740-5745.
21. Westhus, M.; Gonthier, E.; Brohm, D.; Breinbauer, R. *Tetrahedron Lett.* **2004**, *45*, 3141-3142.
22. French, J.M.; Caras, C.A.; Diver, S.T. *Org. Lett.* **2013**, *15*, 5416-5419.
23. Cho, J.H.; Kim, B.M. *Org. Lett.* **2003**, *5*, 531-533.
24. Knight, D.W.; Morgan, I.R.; Proctor, A.J. *Tetrahedron Lett.* **2010**, *51*, 638-640.

Chapter 7

7 Conclusions and Future work

7.1 Conclusions

This thesis detailed the incorporation of phosphorus into materials that imparted functionality including inhibition of the growth of bacteria on surfaces, bacterial killing, self-healing, and metal scavenging. These vastly different applications illustrate the versatility and utility of phosphines and phosphonium ions, which are often overlooked as viable scaffolds on which to build functional materials. The use of prevalent technologies including UV curing and its combination with new functional additives and polymers, is reported, increasing the possibility of commercial application that could address current societal problems.

Chapters 2, 3, and 4 described work that fills the need for new polymers and materials in order to progress the field of antibacterials as well as understanding the relationship between molecular structure and antibacterial activity for both surfaces and solution antibacterials. The work described in Chapters 2 and 3 provided new and simple approaches to antibacterial phosphonium-based coatings that can potentially be applied to surfaces such in high traffic areas such as handles, door knobs, elevator buttons, railings, any location where bacteria transfer can cause infection (ie. hospitals). The high chemical and thermal stability of phosphonium salts may afford advantages over competing approaches based on ammonium cations.

Chapter 4 introduced novel sugar-functionalized phosphonium cations and synthetic methods to combine these unusual molecules. In the exploration of potential targeted antibacterial activities of sugar-functionalized polyphosphonium salts, this work revealed surprising antibacterial activity and low hemolytic properties of simple hydroxyl-functionalized polyphosphonium. This work introduced an alternative possibility that antibacterial polymers may not require pendant amphiphilicity for high antibacterial activity, and the introduction of hydrophilic groups may be more beneficial as a result of their low

hemolytic properties. These materials challenge the current ideology of creating polyammonium/polyphosphonium antibacterials, and presents a new direction for this area of research.

Smart materials are a growing category that possess unique and dynamic properties that mimicking some of nature's most interesting processes. Self-healing behavior is of particularly noteworthy because it represents a progression towards self-sustainable materials. In Chapter 5, it was demonstrated that poly(acrylic acid)/polyphosphonium ionic networks could self-heal when the rheological properties were such that the viscous and elastic modulus were equally contributing to how the material behaved. These properties could be tuned according to the method of preparation of the networks, and consequently the ratio of the two polymers. In comparison with previously reported ammonium-based self-healing networks, which required high (> 1.0 M) NaCl concentrations for healing, these networks could self-heal in relatively low (0.1 M) NaCl concentrations. This aspect may be critical in the application of these materials in medical devices that are implanted into the body, representing a significant advance in the field. This work represents the first introduction of phosphorus into the field of self-healing smart materials, and opens the door to expansion of phosphonium-based smart materials.

Metal removal is relevant to many industries such as waste water, pharmaceuticals, and electronics. The work described in Chapter 6 involved the first attempt to address residual metal contamination by utilizing phosphane-ene chemistry. The phosphane-ene reaction was used to create polymer networks with available Lewis basic phosphine functionalities and proved to be efficient metal scavengers. In particular, high levels of metal scavenging ($> 95\%$) were achieved with materials made directly from $\text{PH}_3(\text{g})$, a feedstock chemical produced on large scales. It was possible to regenerate the scavengers, although further work needs to be completed to increase the efficiency of this process. These polymer networks provide an alternative method with little work up, high efficiency, and simplistic production.

7.2 Future work

7.2.1 Antibacterial surfaces with accessible zwitterions

A major problem with polyelectrolyte based antibacterial materials is the biofouling that can occur over time by exchange of the counter-anion with negatively charged proteins or other biomacromolecules, rendering the materials inactive. An alternative approach is proposed to enable the release of any fouling anions by switching to a zwitterionic species. Switchable zwitterionic surfaces have been reported utilizing light induced esterification,¹ and acid-base mediated ring opening reactions to produce a carboxy betaine (Figure 7-1).² Alternatively, pendant thiols on a phosphonium centre could be employed to act as antibacterials at neutral pH as the nonzwitterion, and zwitterionic at basic pH, accessing the antifouling surface (Figure 7-1).

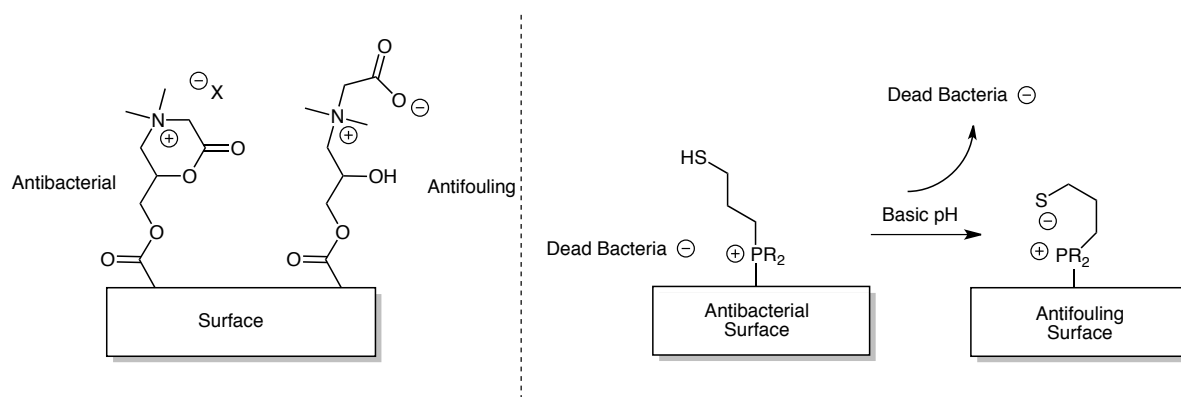


Figure 7-1: Left: Switchable antibacterial-antifouling surface based on acid catalyzed ring opening to produce carboxy betaine; Right: Accessible antibacterial-antifouling phosphonium using a phosphonium-thiolate zwitterion.

7.2.2 Solution based antibacterial agents

Understanding the structure-antibacterial relationship of hydrophilic derivatives of polyelectrolytes would be an impactful contribution to the field. Hydrophilic antibacterial polymers may be beneficial due to their low hemolytic activity. The introduction of other sugars to understand what roles they play in the activity and if higher activity could be accessed by other sugar substituents would be a valuable continuation of the present work (Figure 7-2, 7.1). Derivatives with tri-sugar-substituted phosphines (Figure 7-2, 7.2) could

also give an indication if the sugar substituents have an effect on targeting the cell membrane, or if it is in fact the hydrophilicity that is increasing the activity (4.8).

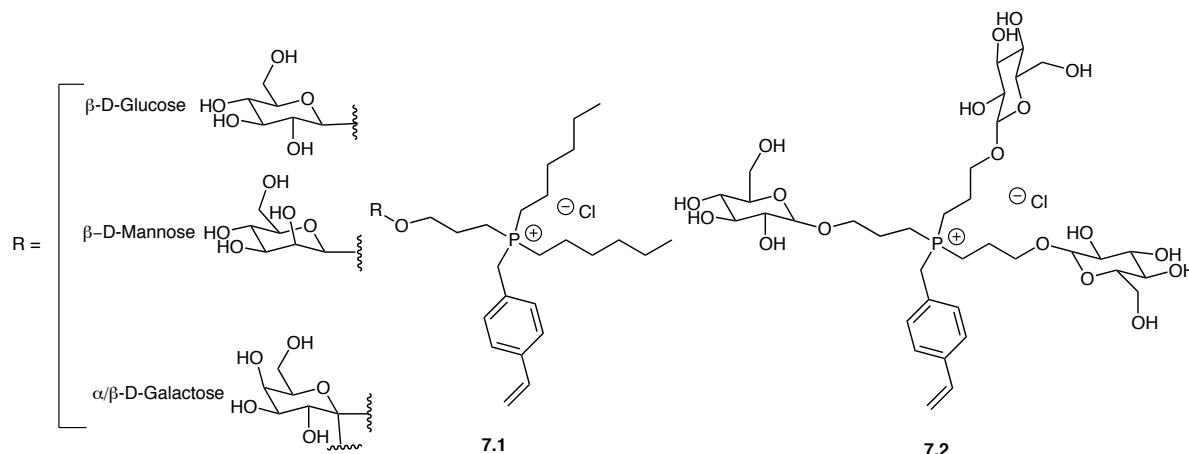


Figure 7-2: Proposed sugar containing phosphonium monomers containing different sugars including β -D-mannose and α/β -D-galactose, and β -D-glucose to determine the effect of the anomeric conformation; 7.2 represents a tri-sugar-substituted phosphonium monomer.

7.2.3 Smart Materials

7.2.3.1 Modulated small molecule release

The networks presented in Chapter 5 possess dynamic cross-links that are responsive to the environmental NaCl concentration. Others have used similar networks to achieve prolonged release of additives, which can be modulated by the NaCl concentration.³ As some of the networks presented in Chapter 5 do not have self-healing capabilities but do possess NaCl dynamic cross-links, these networks could be used as stimuli responsive modulated drug release networks (Figure 7-3).

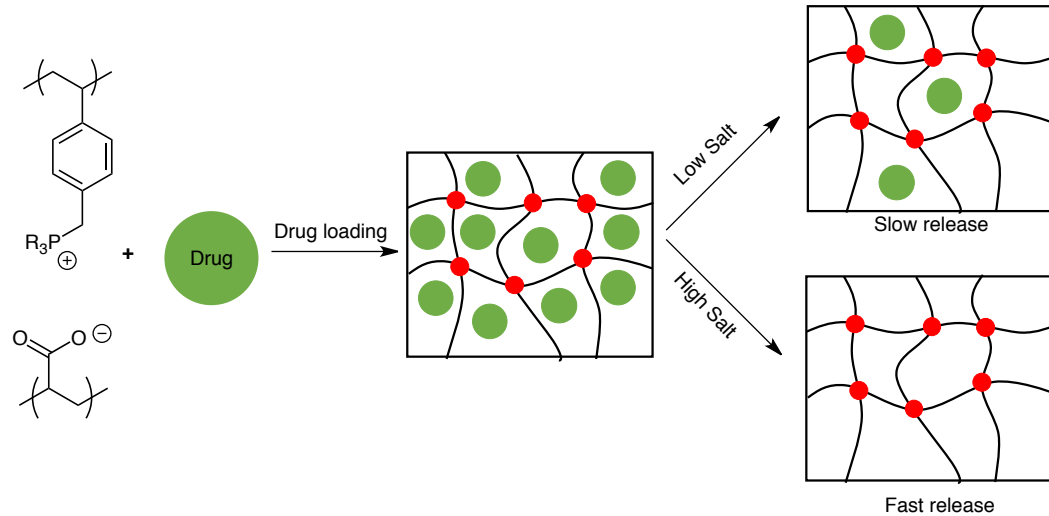


Figure 7-3: Ionically cross-linked networks for small molecule release.

7.2.3.2 Self-healing UV cured networks

The creation of UV curable coatings or materials that have the ability to mend damage would be attractive compared to the current methods of preparing self-healing networks (precipitation and/or centrifugation). Polyelectrolyte addition into the formulation is not effective because the material gels before curing, creating insoluble complexes that phase separate from the UV curable formulation. Ideally, the ionic components would be evenly distributed throughout the polymer network, and additional cross-linking would occur due to ionic interaction. However, polyelectrolyte addition may not be needed for the incorporation of ionic cross-linking in the network. Instead a polymerizable anion-cation pair can potentially be used to create the additional crosslinking, with an additive that could be soluble in formulations (Figure 7-4).

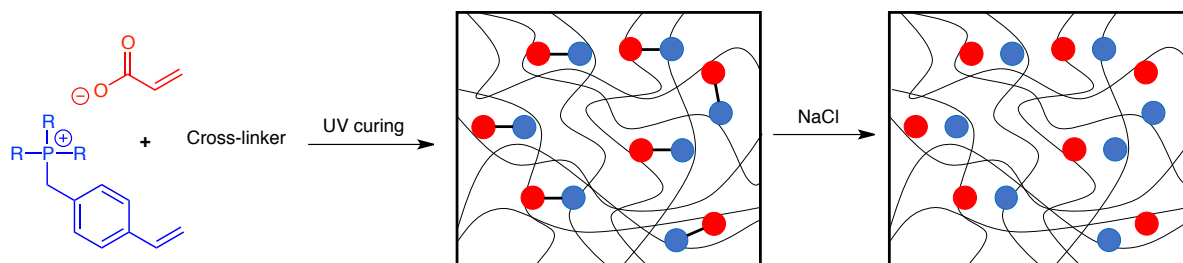


Figure 7-4: Proposed UV curable polymer network possessing ionic cross-linking for self-healing.

7.2.4 Phosphane-ene metal scavengers

The efficiencies of the metal scavengers presented in Chapter 6 were very high, but the ability to regenerate the scavenger in a metal free form for multiple scavenging runs was limited. Ideally, the phosphine polymer with scavenged metal could be regenerated with a simple treatment and washing protocol. Future work in this section should center around optimizing the regeneration protocol by investigating different regeneration reagents including ethylene diamine tetraacetate, t-butoxide, N-heterocyclic carbones, or smaller phosphines such as triethyl phosphine.

7.3 References

- 1) Sobolčiak, P.; Špírek, M.; Katrlík, J.; Gemeiner, P.; Lacík, I.; Kasák, P. *Macromol. Rapid Commun.* **2013**, *34*, 635–639.
- 2) Cao, Z.; Mi, L.; Mendiola, J.; Ella-Menye, J. R.; Zhang, L.; Xue, H.; Jiang, S. *Angew. Chemie* **2012**, *51*, 2602–2605.
- 3) Lawrence, P. G.; Patil, P. S.; Leipzig, N. D.; Lapitsky, Y. *ACS Appl. Mater. Interfaces* **2016**, *8*, 4323–4335.

Appendix

8 Appendix

8.1 American Chemical Society's Policy on Theses and Dissertations

If your university requires you to obtain permission, you must use the RightsLink permission system. See RightsLink instructions at <http://pubs.acs.org/page/copyright/permissions.html>.

This is regarding request for permission to include your paper(s) or portions of text from your paper(s) in your thesis. Permission is now automatically granted; please pay special attention to the implications paragraph below. The Copyright Subcommittee of the Joint Board/Council Committees on Publications approved the following:

Copyright permission for published and submitted material from theses and dissertations
ACS extends blanket permission to students to include in their theses and dissertations their own articles, or portions thereof, that have been published in ACS journals or submitted to ACS journals for publication, provided that the ACS copyright credit line is noted on the appropriate page(s).

Publishing implications of electronic publication of theses and dissertation material
Students and their mentors should be aware that posting of theses and dissertation material on the Web prior to submission of material from that thesis or dissertation to an ACS journal may affect publication in that journal. Whether Web posting is considered prior publication may be evaluated on a case-by-case basis by the journal's editor. If an ACS journal editor considers Web posting to be "prior publication", the paper will not be accepted for publication in that journal. If you intend to submit your unpublished paper to ACS for publication, check with the appropriate editor prior to posting your manuscript electronically.

Reuse/Republication of the Entire Work in Theses or Collections: Authors may reuse all or part of the Submitted, Accepted or Published Work in a thesis or dissertation that the author writes and is required to submit to satisfy the criteria of degree-granting institutions. Such reuse is permitted subject to the ACS' "Ethical Guidelines to Publication of Chemical Research" (<http://pubs.acs.org/page/policy/ethics/index.html>); the author should secure written confirmation (via letter or email) from the respective ACS journal editor(s) to avoid potential conflicts with journal prior publication*/embargo policies. Appropriate citation of the Published Work must be made. If the thesis or dissertation to be published is in electronic format, a direct link to the Published Work must also be included using the ACS Articles on Request author-directed link – see <http://pubs.acs.org/page/policy/articlesonrequest/index.html>

* Prior publication policies of ACS journals are posted on the ACS website at

<http://pubs.acs.org/page/policy/prior/index.html>

8.2 Supplementary Information for Chapter 2

Table 8-1: Results of surface adhesion testing by ASTM D3359 – 09e2. *The test was repeated 5 times on the same surface without any loss of adhesion.

Formulation; curing atmosphere; substrate	% squares removed	Cross hatch adhesion classification
2.2-95wt%, 2.3-5wt%; Air; PET	0%*	5B - 0% removed
2.1-47.5wt%, 2.2-47.5wt%, 2.3-5%; N ₂ ; PET	0%*	5B - 0% removed
2.1-47.5wt%, 2.2-47.5wt%, 2.3-5%; Air; PET	0%*	5B - 0% removed
2.2-95wt%, 2.3-5wt%; N ₂ ; glass	87%	0B - >65% removed
2.2-95wt%, 2.3-5wt%; Air; glass	100%	0B - >65% removed
2.1-47.5wt%, 2.2-47.5wt%, 2.3-5%; N ₂ ; glass	88%	0B - >65% removed
2.1-47.5wt%, 2.2-47.5wt%, 2.3-5%; Air; glass	100%	0B - >65% removed

Table 8-2: Properties of free standing films prepared from 47.5 wt% of 2.1, 47.5 wt% 2.2, and 5 wt% 2.3.

Cure % (ATR-FTIR) before washing	Cure % (ATR-FTIR) after washing	Gel content
91 ± 5%	90 ± 4 %	83 ± 1%

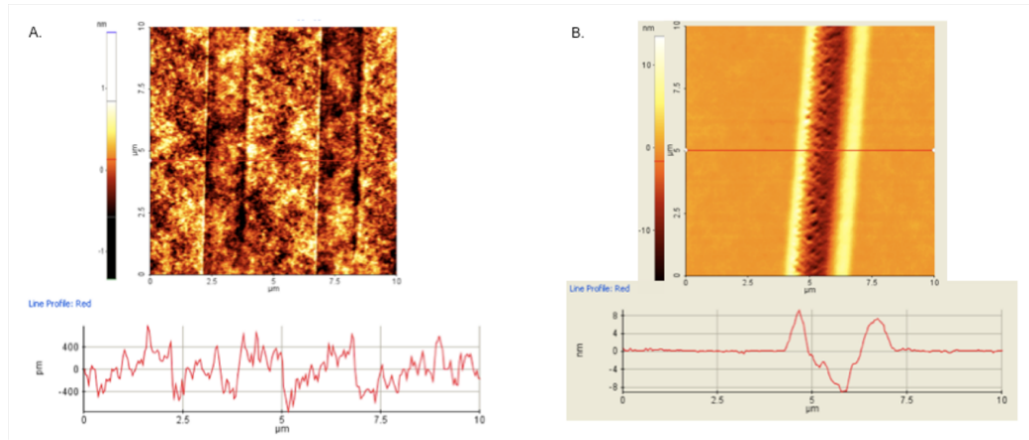


Figure 8-1: AFM images and corresponding height profiles of a) a 47.5 wt% 2.1 coating cured under N_2 and b) a 47.5 wt% 2.1 coating cured under air. These images show that upon application of a diamond tip surface profiler with a force of 0.5 mN, the etching could not be distinguished from the background surface roughness in the case of the surface cured under N_2 , whereas a 10 nm groove was etched in the surface cured under air. These images also show the low roughness of the initial films.

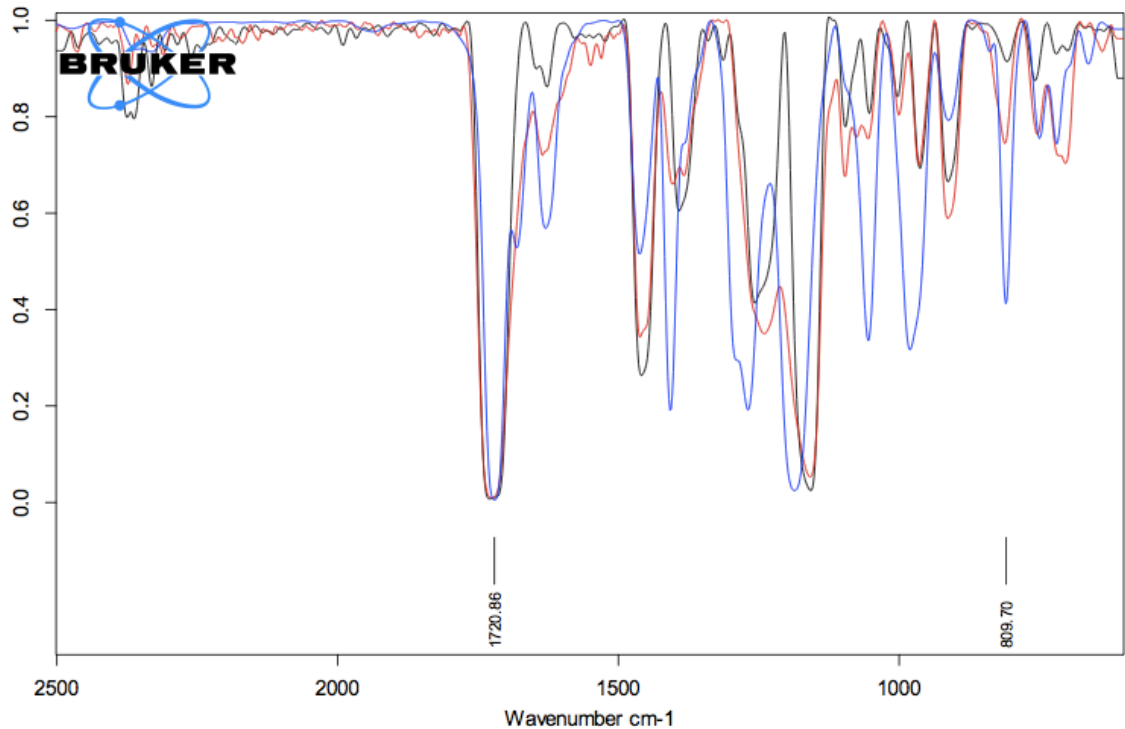


Figure 8-2: Example ATR-FTIR spectra of a 47.5 wt% 2.1 formulation (blue), cured film (red), and cured and washed film (black), showing the decrease in the intensity of the peak at 810 cm^{-1} corresponding to C=C, in comparison to the internal standard C=O peak at 1720 cm^{-1} .

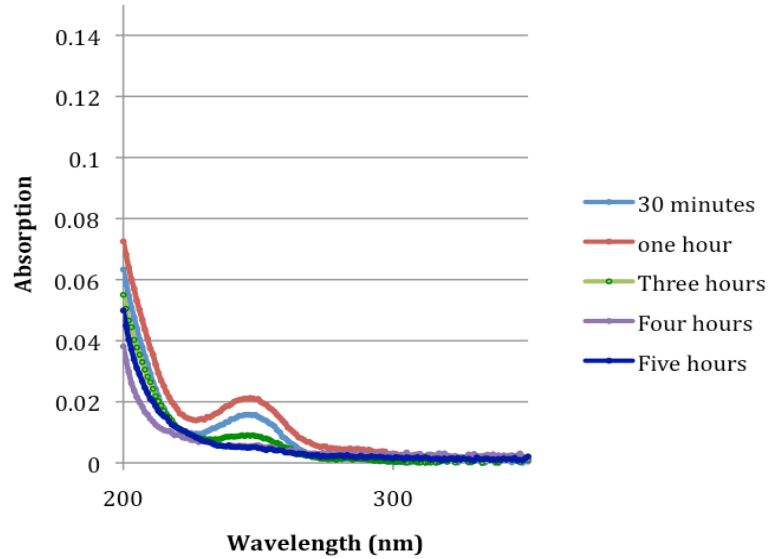


Figure 8-3: UV-Vis spectra of surface washings (47.5 wt% 2.1, cured under N₂, PET substrate) after different time periods, confirming that a 12 hours incubation in water is more than sufficient to remove all leachable molecules. (Note: washings were discarded after each time point, so the lack of detectable molecules after 5 hours suggests that all leachable molecules had already been removed from the surface).

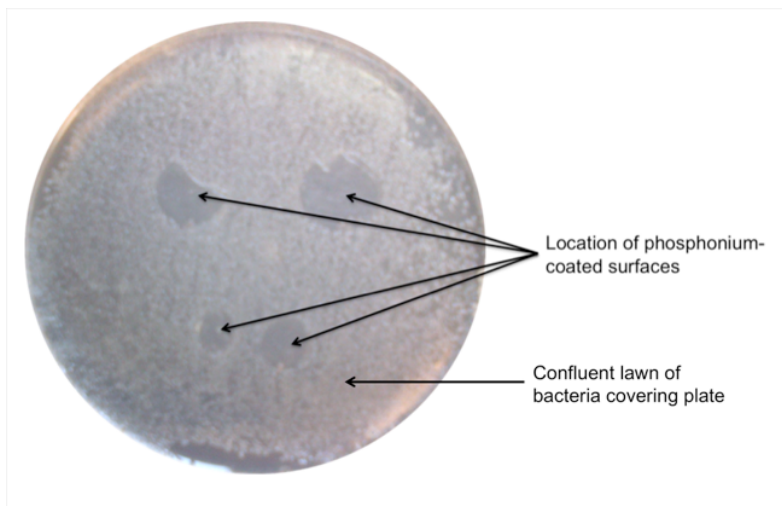


Figure 8-4: Antibacterial testing results for a coating containing 47.5 wt% of 2.1 and cured under N₂. The image shows an agar plate with absence of bacterial growth where the phosphonium surfaces were placed, following 24 h incubation with *E. coli*.

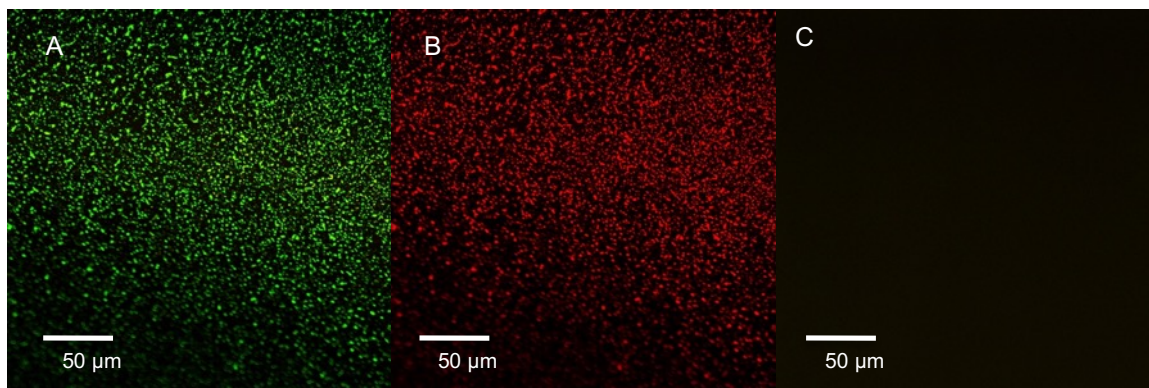


Figure 8-5: a) and b): clean silicon wafer control and c) phosphonium surface following LIVE/DEAD[®] analysis. The surfaces were incubated with *S. aureus* for 24 h. a) shows live bacteria stained in green; b) shows dead bacteria stained in red; c) is an overlay of red and green fluorescence images showing an absence of live or dead bacteria.

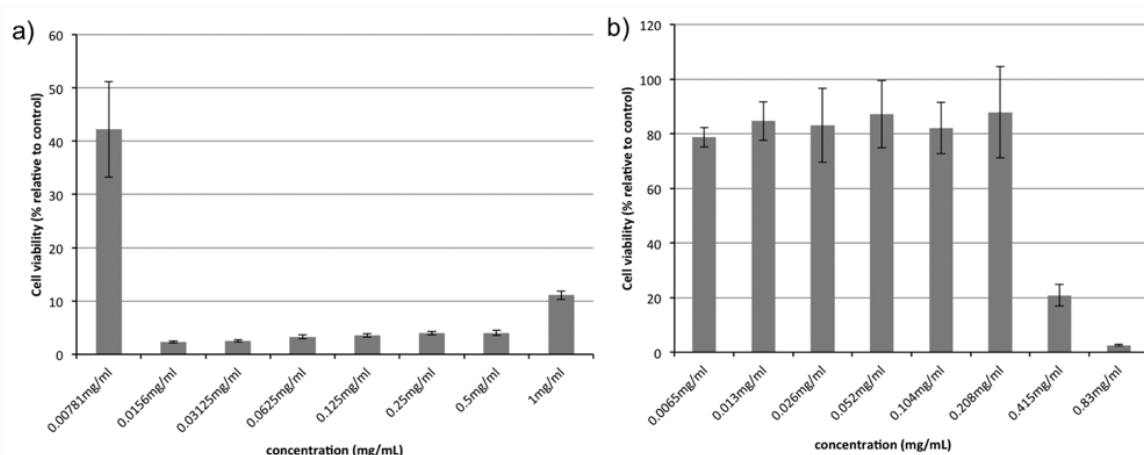


Figure 8-6: *In vitro* cytotoxicity of a) benzyldimethyl hexadecyl ammonium chloride and b) phosphonium monomer 2.1 as measured by the MTT assay following a 24 h incubation with C2C12 mouse myoblast cells. Data represent the mean and standard deviation of six replicates per concentration (N = 6).

8.2.1 References

- 1) Guterman, R.; Hesari, M.; Ragona, P.; Workentin, M. *Langmuir* **2013**, *29*, 6460–6466.
- 2) Murata, H.; Koepsel, R. R.; Matyjaszewski, K.; Russell, I. J. *Biomaterials* **2007**, *28*, 4870–4879.
- 3) Gaydos, J. M.; Harrington, B. J. *Antimicrob. Agents Chemother.* **1982**, *21*, 516–518.

8.3 Supplementary Information for Chapter 3

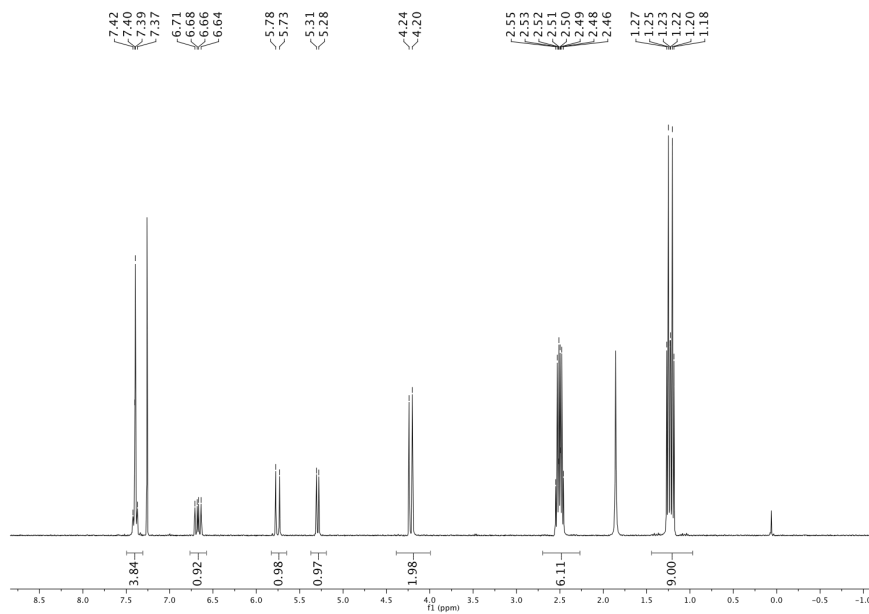


Figure 8-7: ^1H NMR spectrum of 3.1 (400 MHz, D_2O).

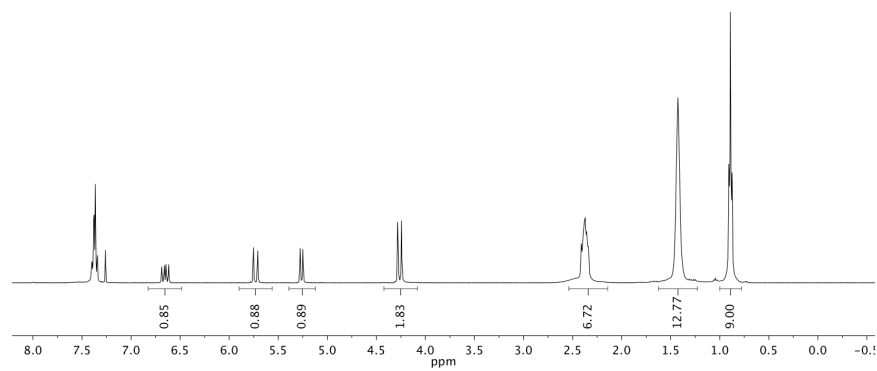


Figure 8-8: ^1H NMR spectrum of 3.2 (400 MHz, CDCl_3).

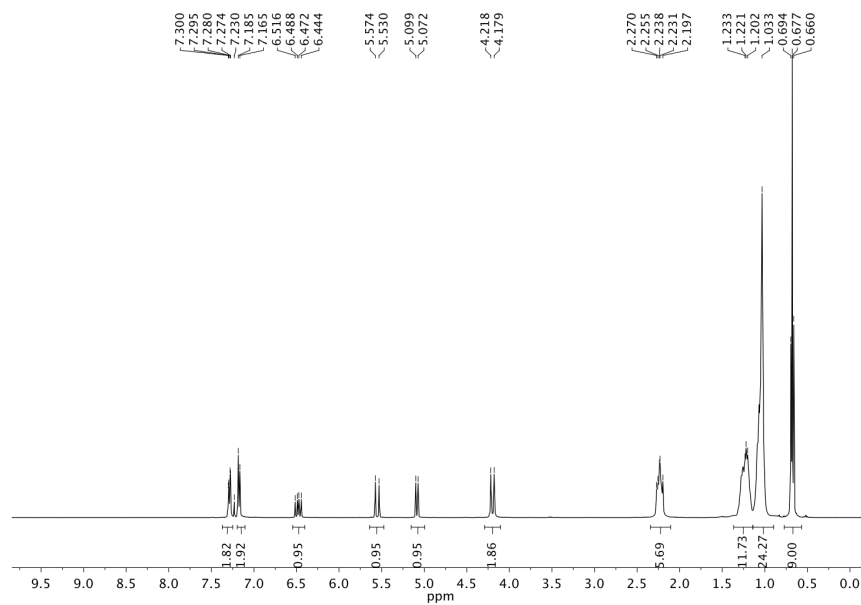


Figure 8-9: ^1H NMR spectrum of 3.3 (400 MHz, CDCl_3).

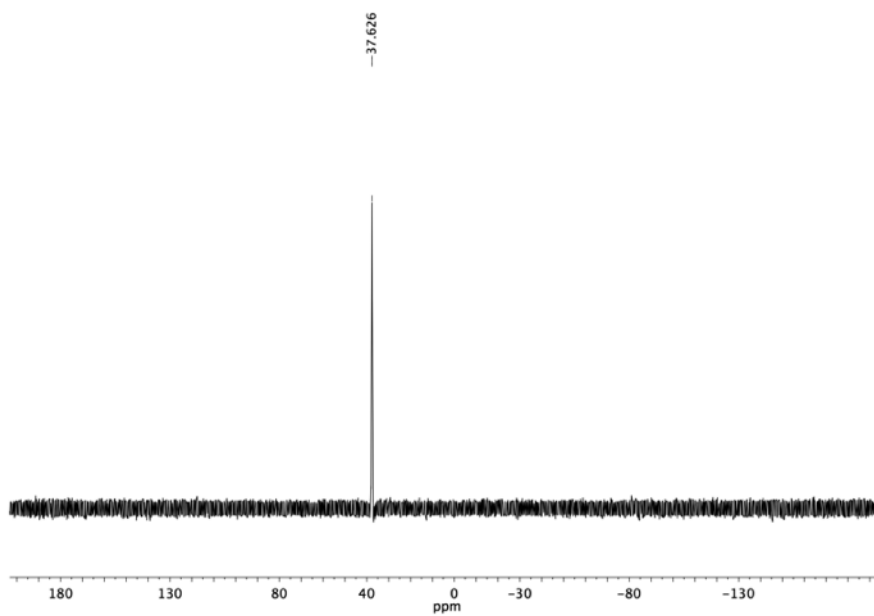


Figure 8-10: $^{31}\text{P}\{^1\text{H}\}$ NMR spectrum of 3.1-P-10k (162 MHz, D_2O).

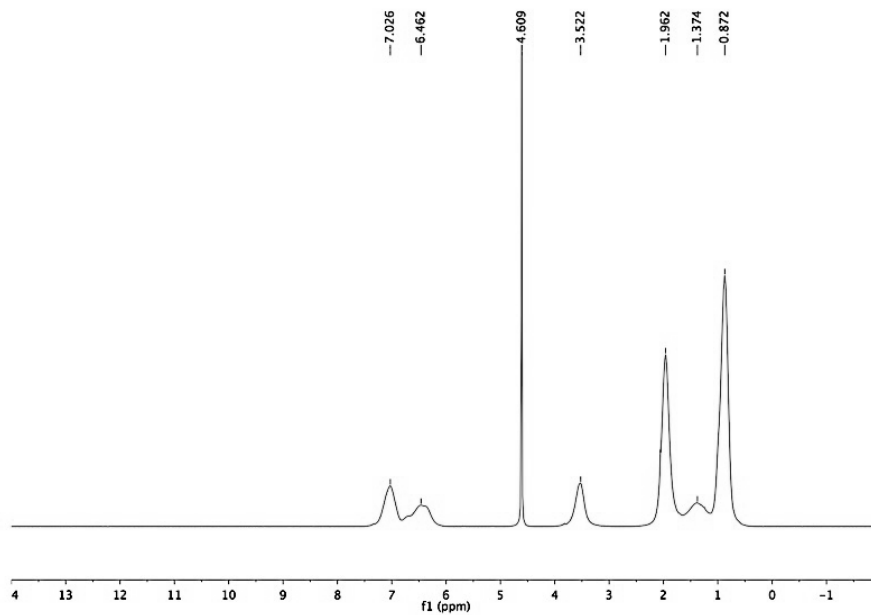


Figure 8-11: ^1H NMR spectrum of 3.1-P-10k (400 MHz, D_2O).

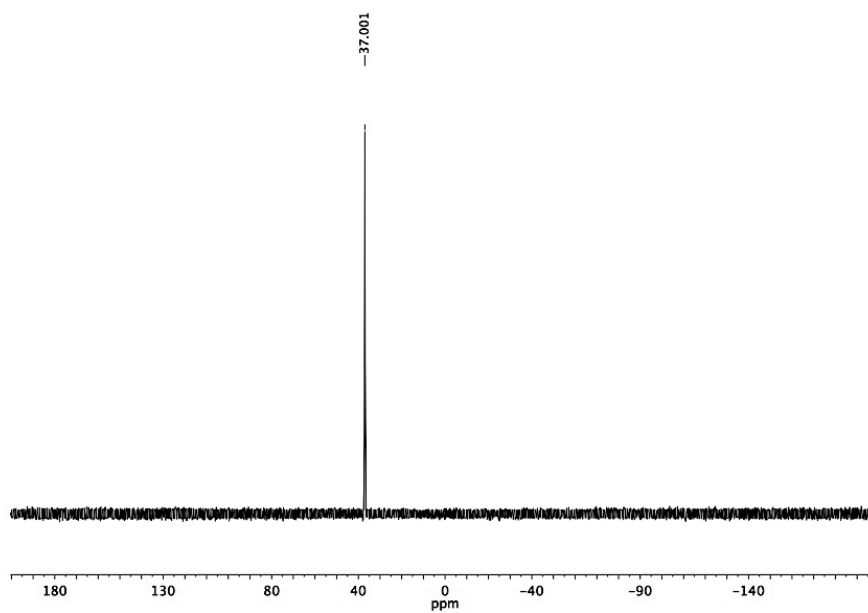


Figure 8-12: $^{31}\text{P}\{^1\text{H}\}$ NMR spectrum of 3.1-P-40k (162 MHz, D_2O).

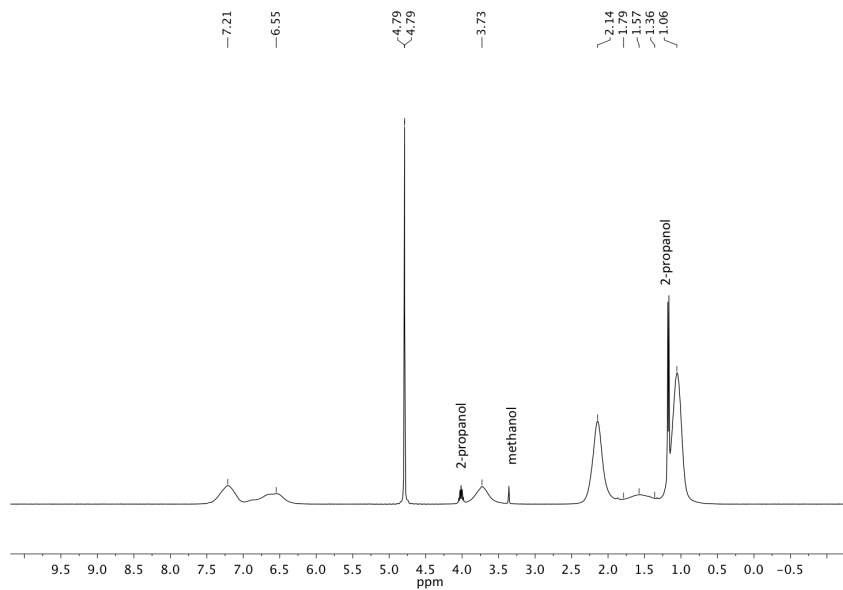


Figure 8-13: ^1H NMR spectrum of 3.1-P-40k (400 MHz, D_2O).

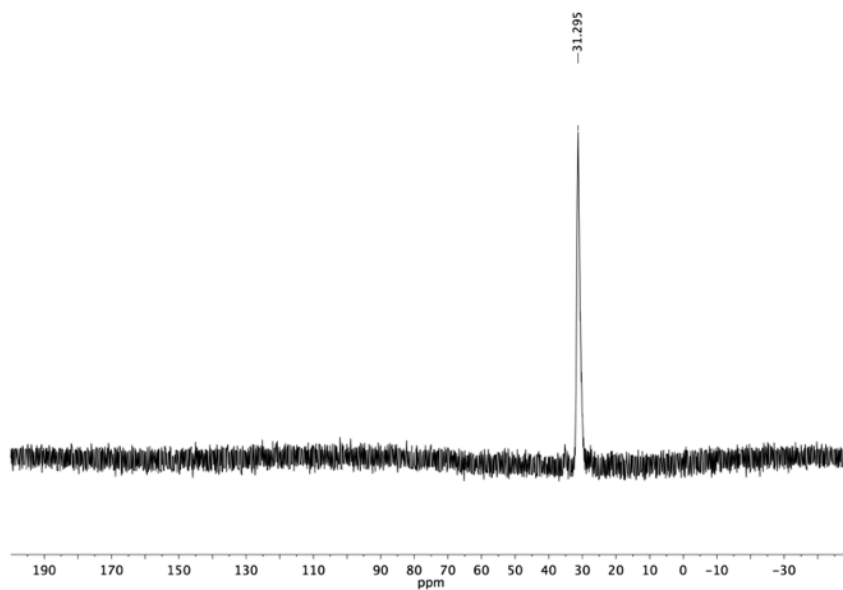


Figure 8-14: $^{31}\text{P}\{^1\text{H}\}$ NMR spectrum of 3.2-P-10k (161 MHz, CDCl_3).

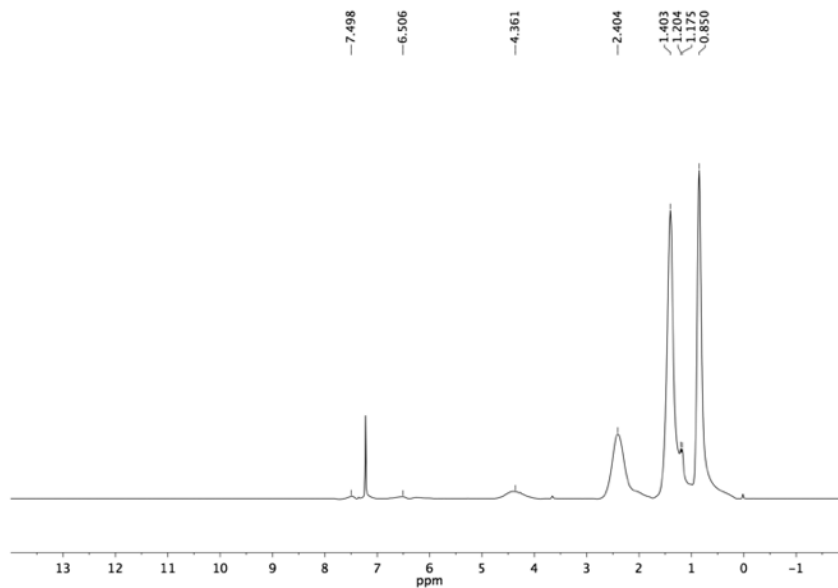


Figure 8-15: ^1H NMR spectrum of 3.2-P-10k (400 MHz, CDCl_3).

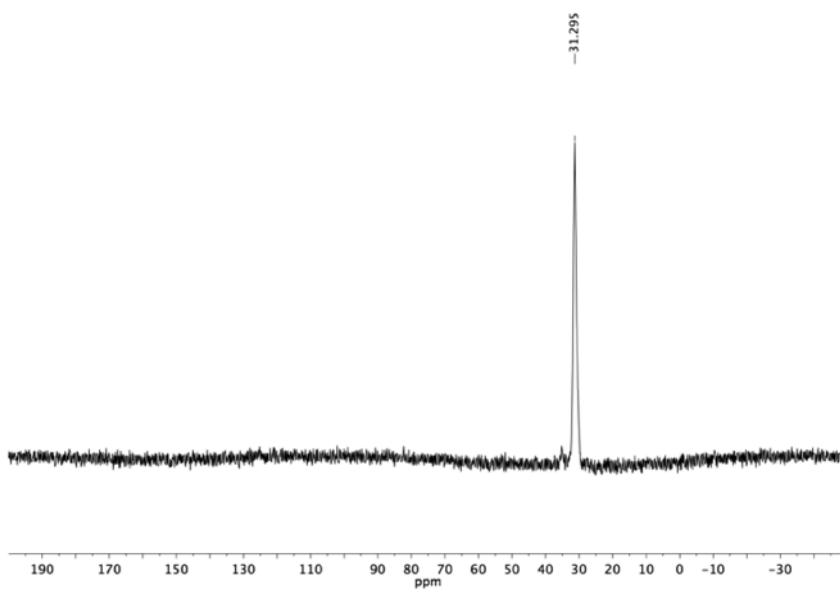


Figure 8-16: $^{31}\text{P}\{^1\text{H}\}$ NMR spectrum of 3.2-P-40k (162 MHz, CDCl_3).

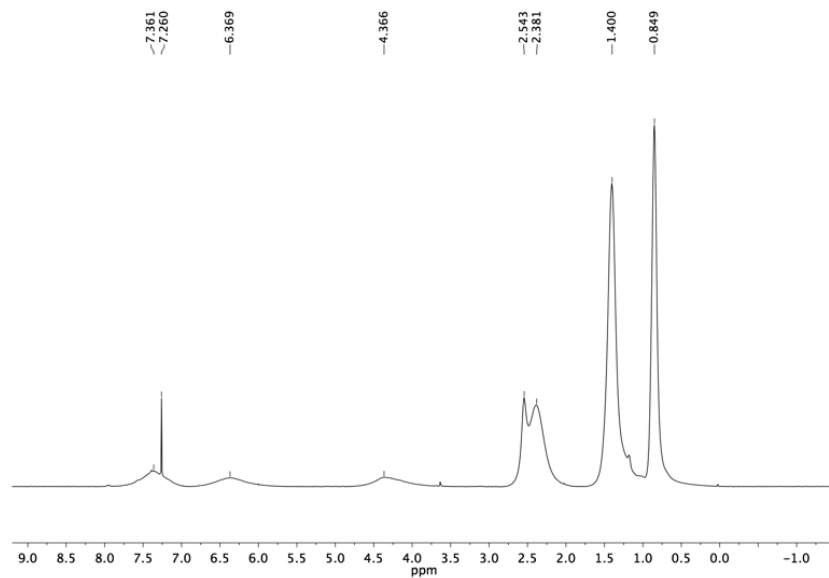


Figure 8-17: ^1H NMR spectrum of 3.2-P-40k (400 MHz, CDCl_3).

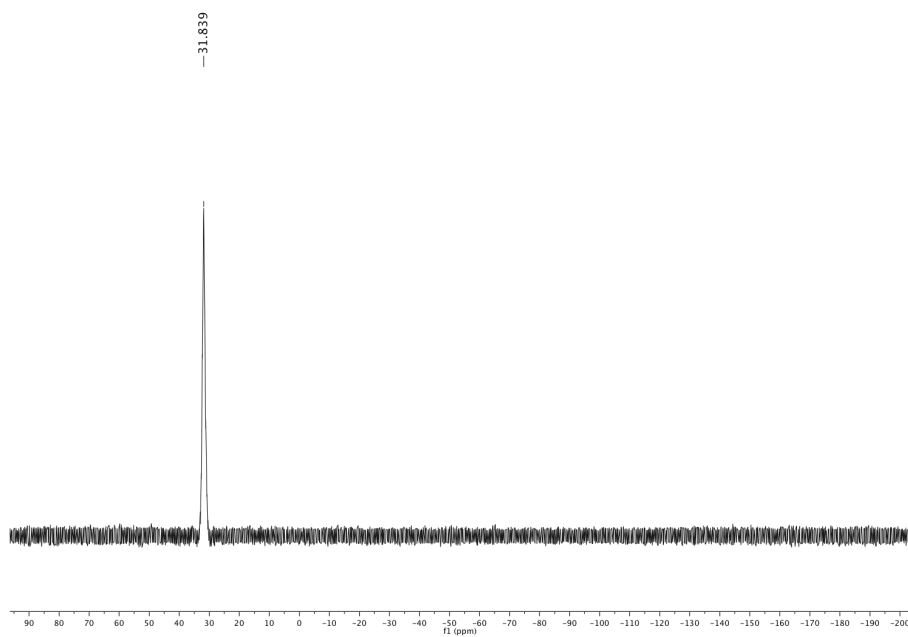


Figure 8-18: $^{31}\text{P}\{^1\text{H}\}$ NMR spectrum of 3.3-P-10k (162 MHz, CDCl_3).

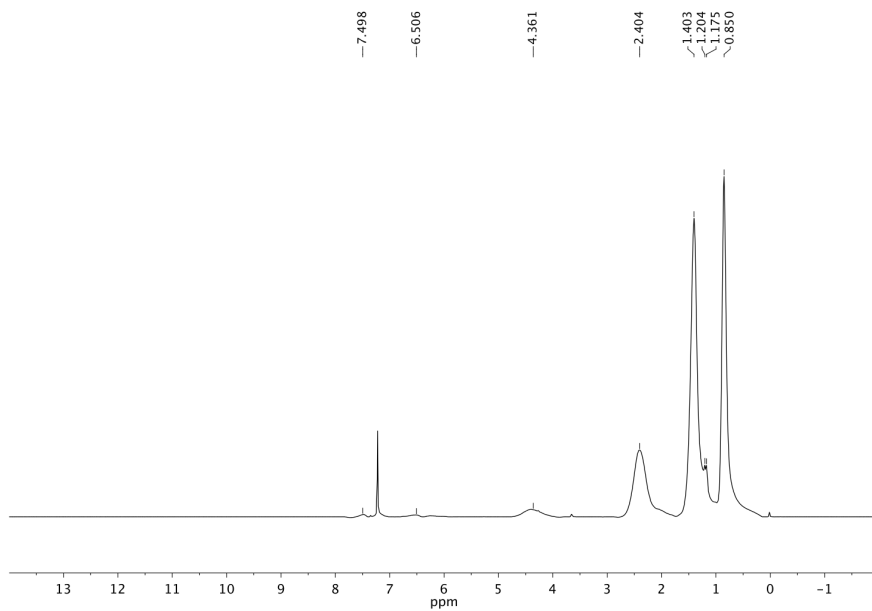


Figure 8-19: ^1H NMR spectrum of 3.3-P-10k (400 MHz, CDCl_3).

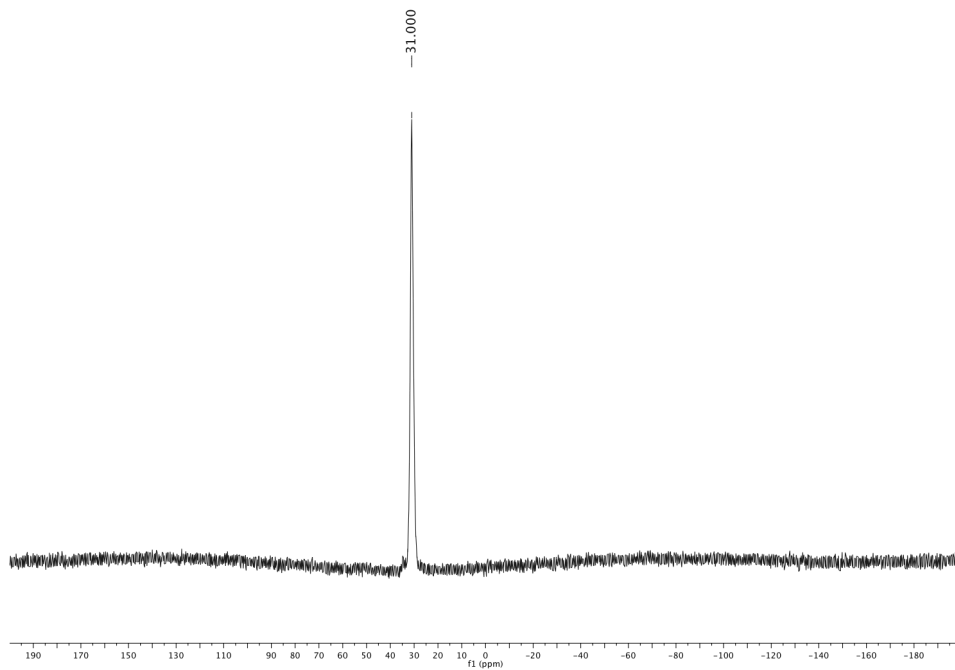


Figure 8-20: $^{31}\text{P}\{^1\text{H}\}$ NMR spectrum of 3.3-P-40k (162 MHz, CDCl_3).

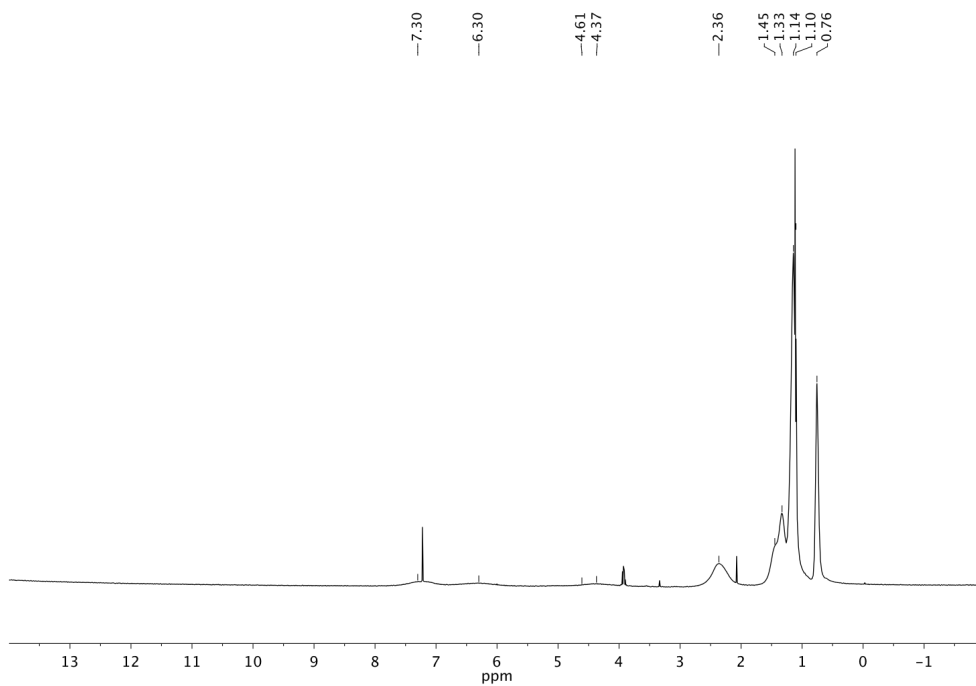


Figure 8-21: ^1H NMR spectrum of 3.3-P-40k (400 MHz, CDCl_3).

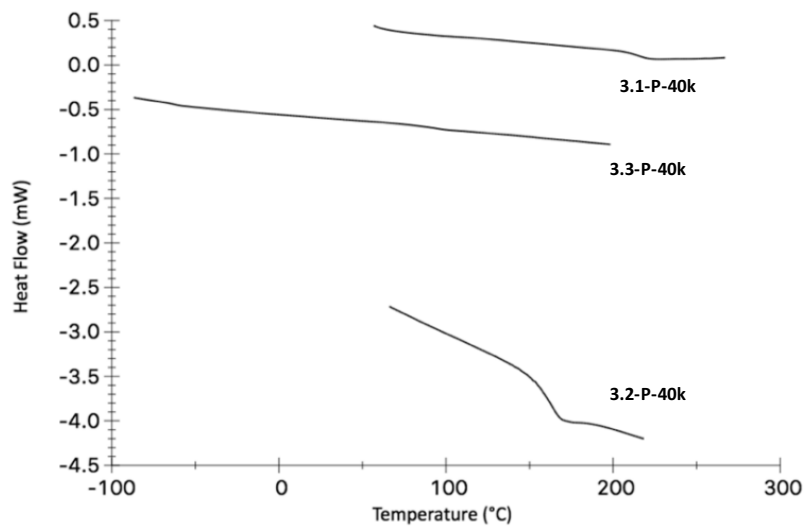


Figure 8-22: DSC curves for 3.1-P-40k, 3.2-P-40k, and 3.3-P-40k (obtained from the second heating cycle).

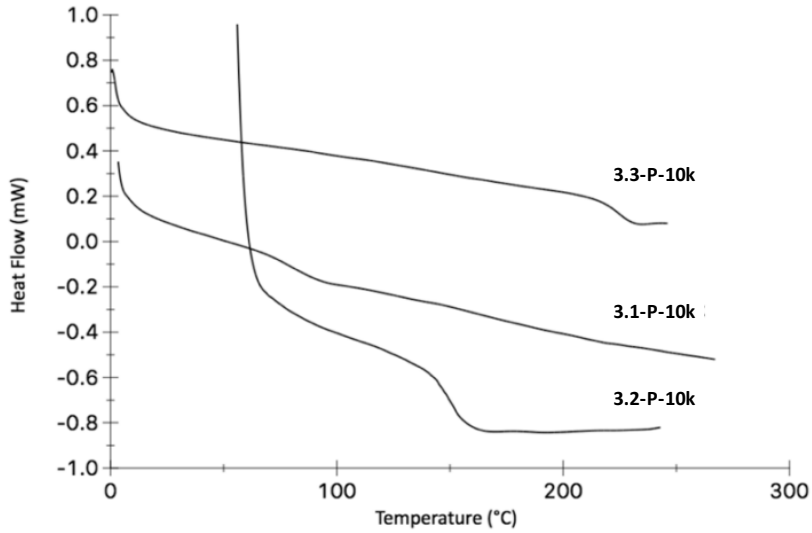
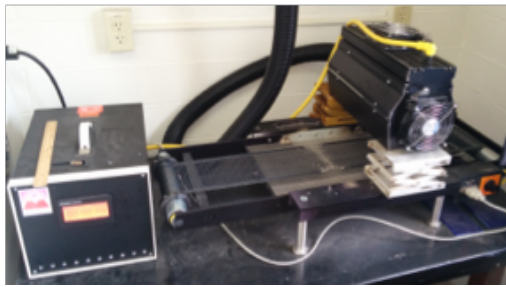


Figure 8-23: DSC curves for 3.1-P-10k, 3.2-P-10k, and 3.3-P-10k (second heating cycle).

A.



B.

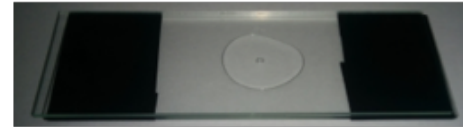


Figure 8-24: a) Digital photo of the UV-curing belt system b) Digital photograph showing two glass slides with spacers of 170 μm thickness on each side and the SIPN in between.

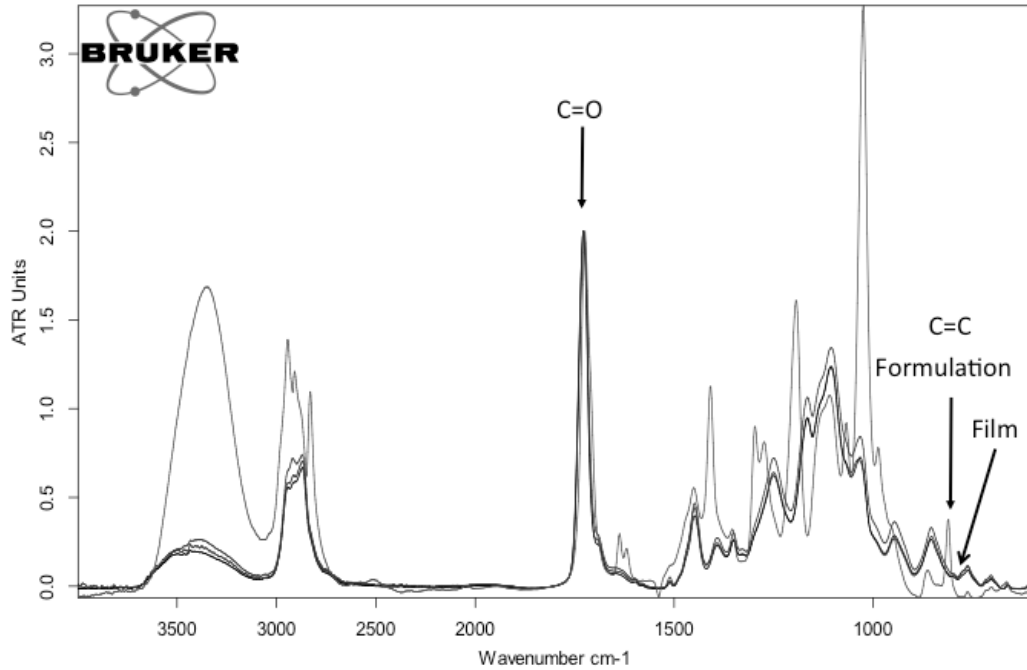


Figure 8-25: Example ATR-FTIR spectra of a 3.1-P-10k 10wt% formulation and the corresponding cured (unwashed) SIPN, showing the decrease in the intensity of the peak at 810 cm^{-1} corresponding to C=C, in comparison to the internal standard C=O peak at 1720 cm^{-1} .

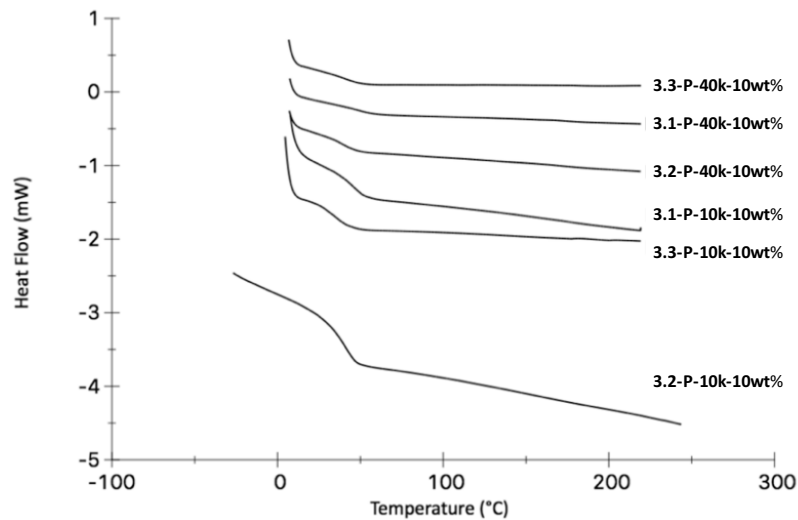


Figure 8-26: DSC curves for all SIPNs 3.1-P-10k/40k, 3.2-P-10k/40k, and 3.3-P-10k/40k at 10 wt% (second heating cycle).

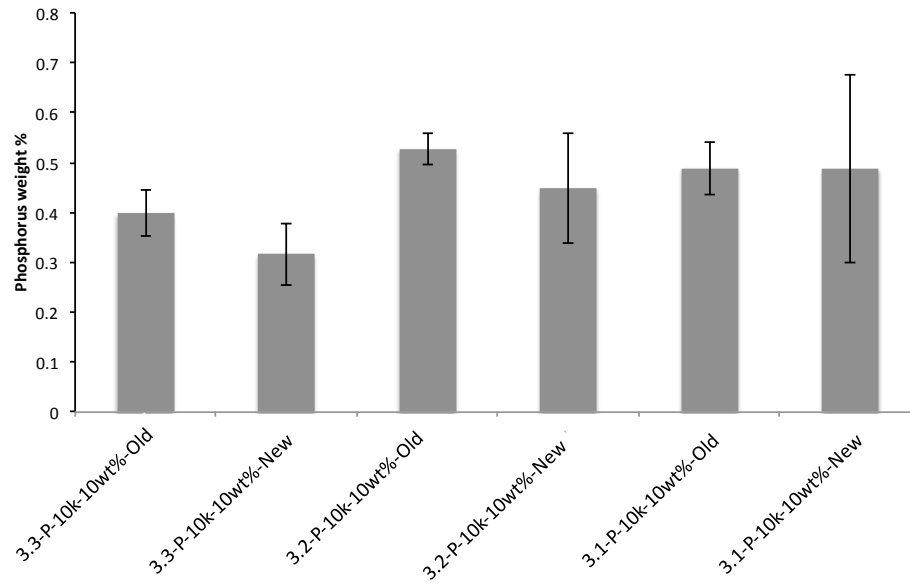


Figure 8-27: Surface phosphorus weight % analyzed by SEM-EDX on freshly prepared surfaces and aged samples (8 months). 250 μm surfaces were sputter coated with 5 nm of osmium. Samples were imaged at 20kV at a magnification of 4500 at a working distance of 10 μm .

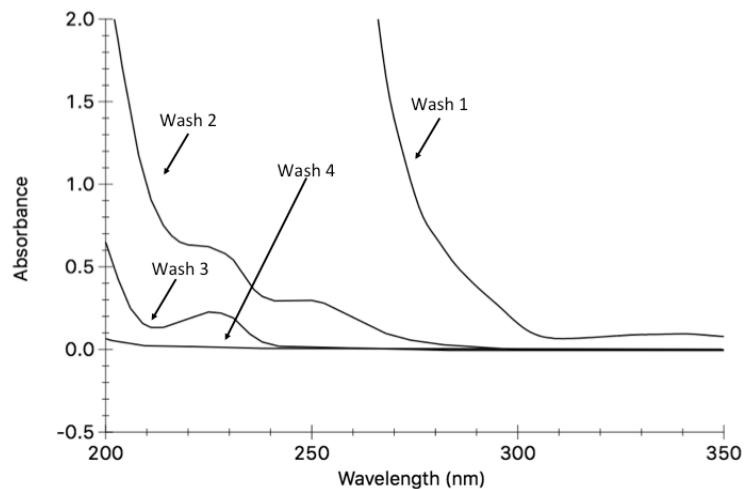


Figure 8-28: Representative example of the UV-vis spectra of the washings of an SIPN. This confirms that no further polymers or monomers were eluted from the SIPN after the 3rd washing. This was important to ensure that the anti-bacterial efficacy of the SIPNs arose from the activity of the surfaces themselves as opposed to leachable polyphosphonium. This particular SIPN was 3.2-P-10k (10 wt%) and the washing solvent was CH_3CN . All other SIPNs exhibited the same behavior.

Table 8-3: Raw data (bacterial colony counts) from dynamic contact antibacterial test (based on ASTM E2149 13a) against *S. aureus* (ATCC 6538). In this test 2.0 mg of SIPN was incubated with 100 μL of 10^6 CFU/mL (10^5 CFUs total) in 0.3 mM KH_2PO_4 . After dilution to 1.0 mL (10^4 CFUs/mL), 100 μL (10^3 CFUs total) were plated.

	S. aureus			
Specimen	CFUs counted	Mean	% Reduction	Std Dev (% std dev)
Control	958			
Control	879	918.50		
3.1-P-10k (10 wt%)	0			
3.1-P-10k (10 wt%)	0			0.00
3.1-P-10k (10 wt%)	0	0.00	100.00	0.00
3.1-P-40k (10 wt%)	0			
3.1-P-40k (10 wt%)	0			0.00
3.1-P-40k (10 wt%)	0	0.00	100.00	0.00
3.2-P-10k (10 wt%)	0			
3.2-P-10k (10 wt%)	0			0.00
3.2-P-10k (10 wt%)	0	0.00	100.00	0.00
3.2-P-40k (10 wt%)	0			
3.2-P-40k (10 wt%)	0			0.00
3.2-P-40k (10 wt%)	0	0.00	100.00	0.00
3.3-P-10k (10 wt%)	380			
3.3-P-10k (10 wt%)	461			62.08
3.3-P-10k (10 wt%)	502	447.67	51.26	(6.76)
3.3-P-40k (10 wt%)	975			
3.3-P-40k (10 wt%)	881			47.51
3.3-P-40k (10 wt%)	916	924.00	-0.60	(5.17)

Table 8-4: Raw data (bacterial colony counts) from dynamic contact antibacterial test (based on ASTM E2149 13a) against E. coli (ATCC 29425). In this test 2.0 mg of SIPN was incubated with 100 μ L of 10^5 CFU/mL (10^4 CFUs total) in 0.3 mM KH_2PO_4 . After dilution to 1.0 mL (10^3 CFUs/mL), 100 μ L (100 CFUs total) were plated.

	E. coli			
Specimen	CFUs counted	Mean	% Reduction	Std Dev (% std dev)
Control	99			
Control	80	89.50		
3.1-P-10k (10 wt%)	8			
3.1-P-10k (10 wt%)	15			5.57
3.1-P-10k (10 wt%)	4	9.00	89.94	(6.22)
3.1-P-40k (10 wt%)	30			
3.1-P-40k (10 wt%)	34			13.43
3.1-P-40k (10 wt%)	9	24.33	72.81	(15.00)
3.2-P-10k (10 wt%)	1			
3.2-P-10k (10 wt%)	2			1.00
3.2-P-10k (10 wt%)	0	1.00	98.88	(1.12)
3.2-P-40k (10 wt%)	9			
3.2-P-40k (10 wt%)	1			4.93
3.2-P-40k (10 wt%)	0	3.33	96.28	(5.51)
3.3-P-10k (10 wt%)	0			
3.3-P-10k (10 wt%)	2			1.15
3.3-P-10k (10 wt%)	0	0.67	99.26	(1.29)
3.3-P-40k (10 wt%)	95			
3.3-P-40k (10 wt%)	85			28.73
3.3-P-40k (10 wt%)	139	106.33	-18.81	(32.10)

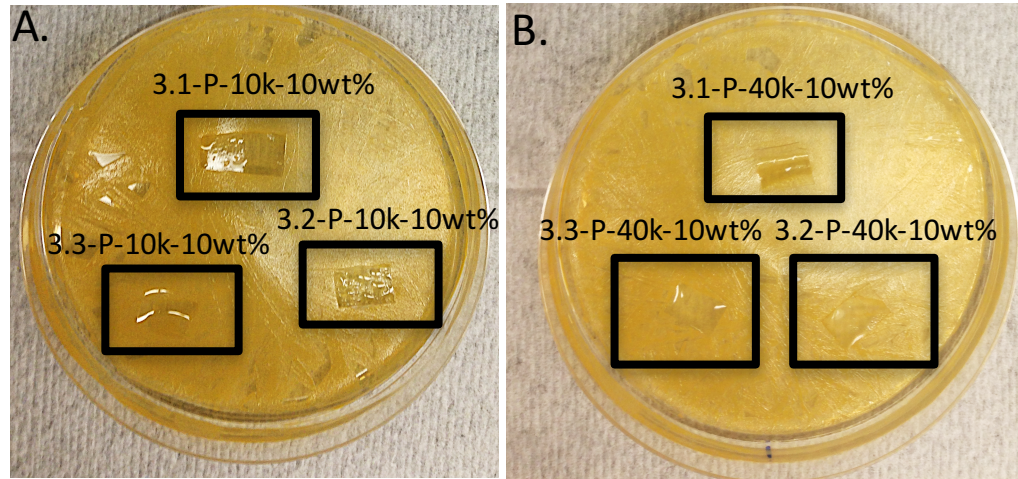


Figure 8-29: Zone of inhibition test against *S. aureus* using polyphosphonium SIPNs. The SIPNs were cut into squares and placed face down on TSB Agar plates that were scratch plated to create lawns of bacteria. A) 3.1-P-10k (10wt%), 3.2-P-10k (10wt%), 3.3-P-10k (10wt%); B) 3.1-P-40k (10wt%), 3.2-P-40k (10wt%), 3.3-P-40k (10wt%). No zones of inhibition were observed for any samples, suggesting that the SIPNs do not leach biocide.

8.3.1 References

- 1) Kanazawa, A.; Ikeda, T.; Endo, T. *J. Polym. Sci. Part A Polym. Chem.* **1993**, *31*, 335–343.

8.4 Supplementary Information for Chapter 4

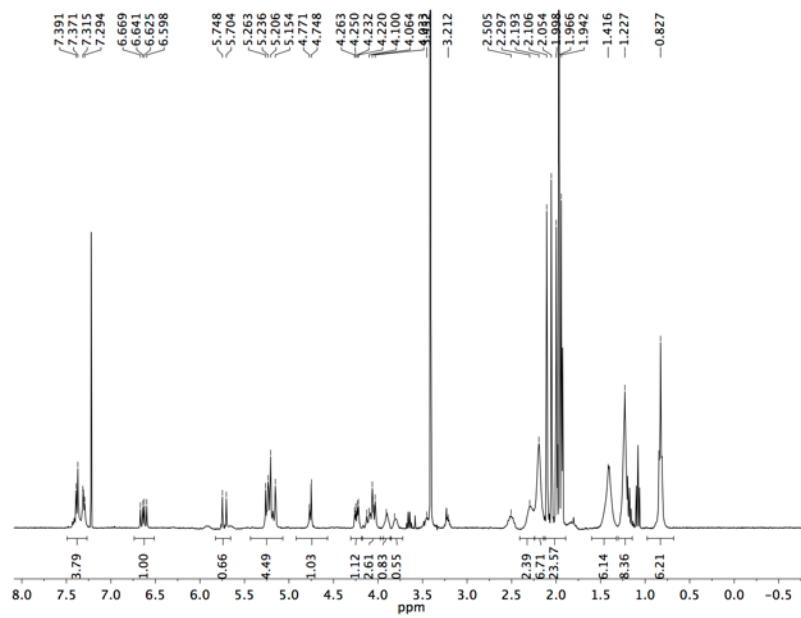


Figure 8-30: ^1H NMR 4.3 (600 MHz, CDCl_3)

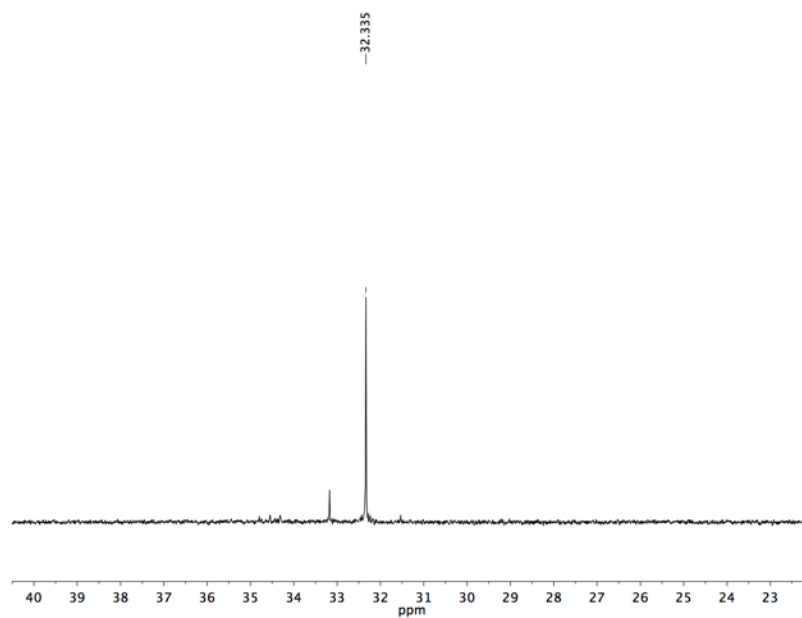


Figure 8-31: $^{31}\text{P}\{^1\text{H}\}$ NMR 4.3 (161 MHz, CDCl_3)

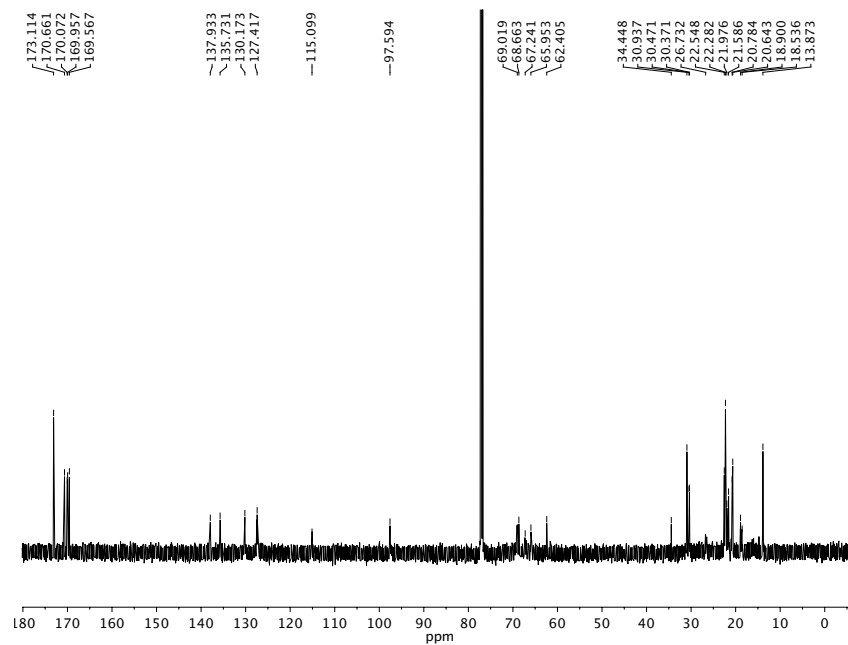


Figure 8-32: $^{13}\text{C}\{^1\text{H}\}$ NMR 4.3 (600 MHz, CDCl_3)

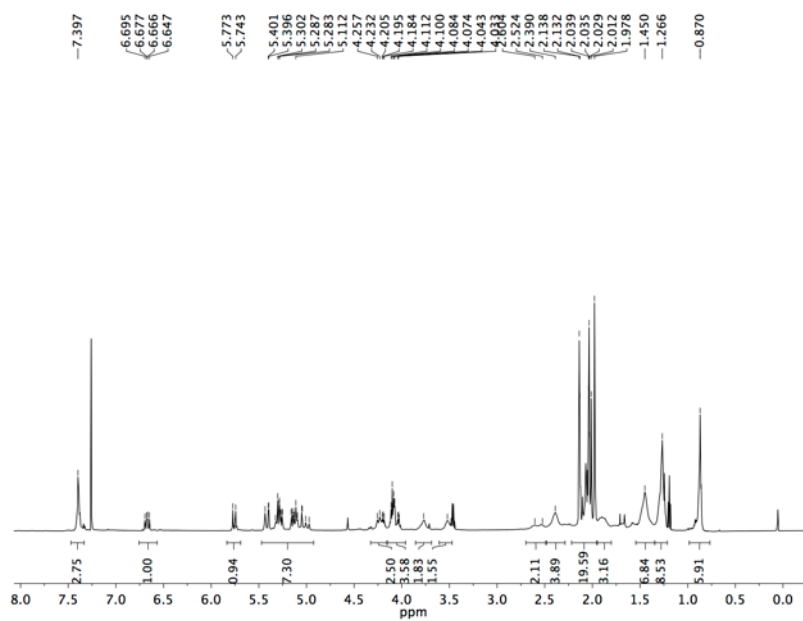


Figure 8-33: ^1H NMR 4.4 (600 MHz, CDCl_3)

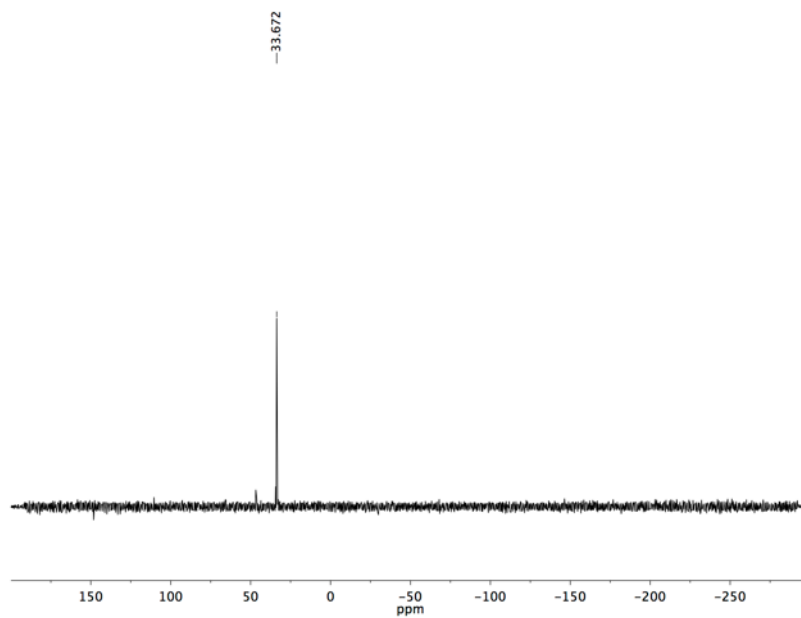


Figure 8-34: $^{31}\text{P}\{^1\text{H}\}$ NMR 4.4 (161 MHz, CDCl_3)

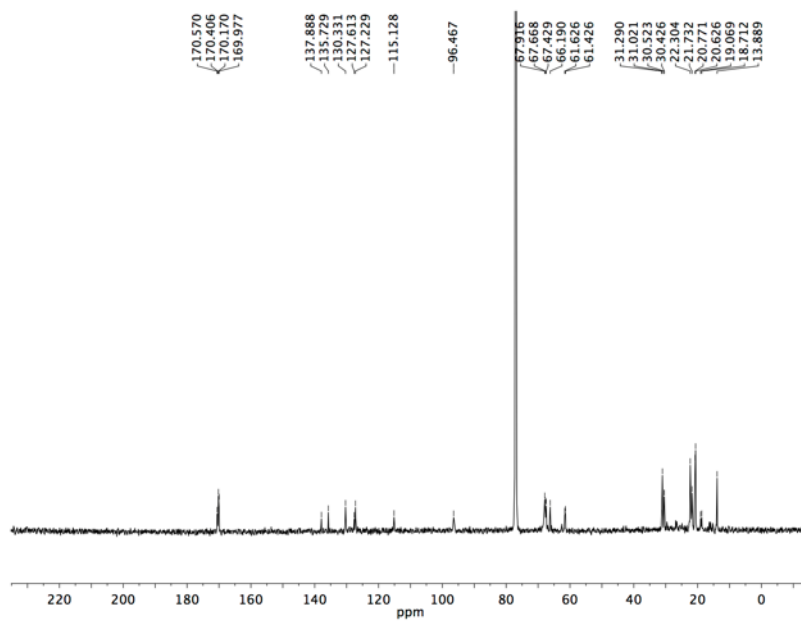


Figure 8-35: $^{13}\text{C}\{^1\text{H}\}$ NMR 4.4 (150 MHz, CDCl_3)

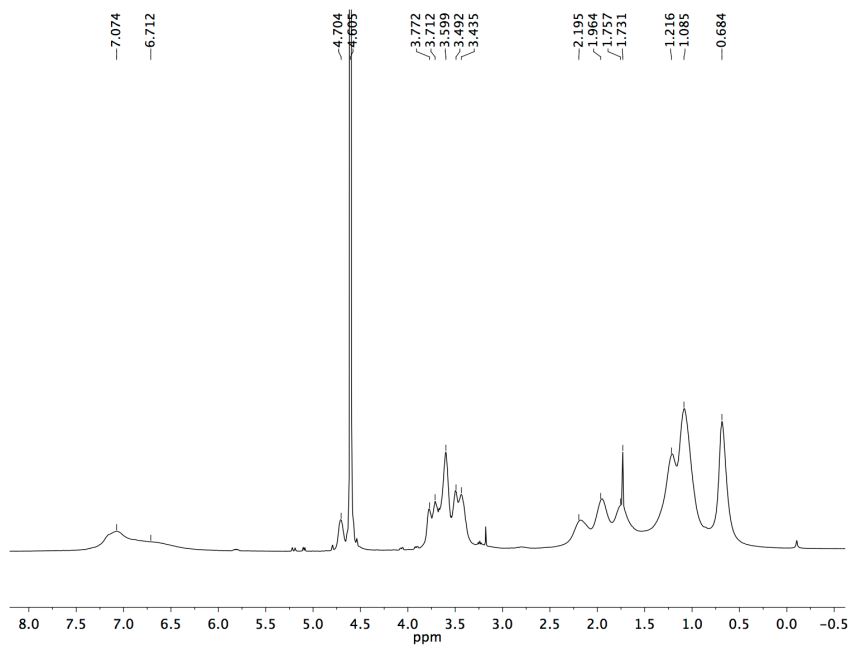


Figure 8-36: ^1H NMR 4.5 (600 MHz, D_2O)

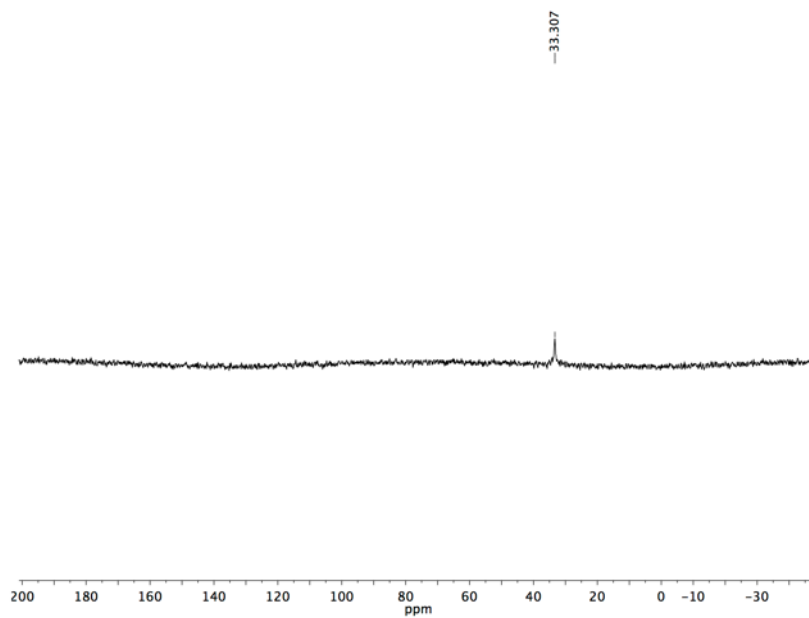


Figure 8-37: ^{31}P $\{^1\text{H}\}$ NMR 4.5 (161 MHz, CDCl_3)

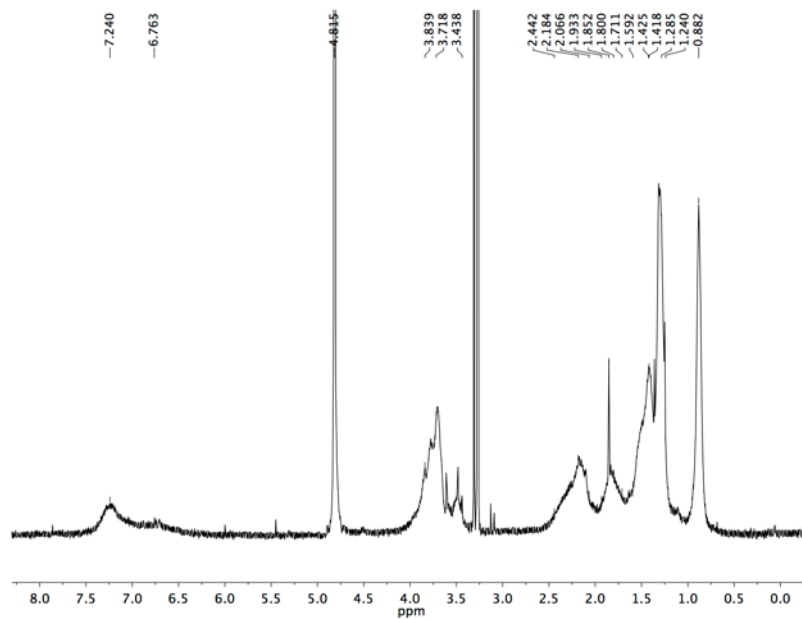


Figure 8-38: ^1H NMR 4.6 (600 MHz, CDCl_3)

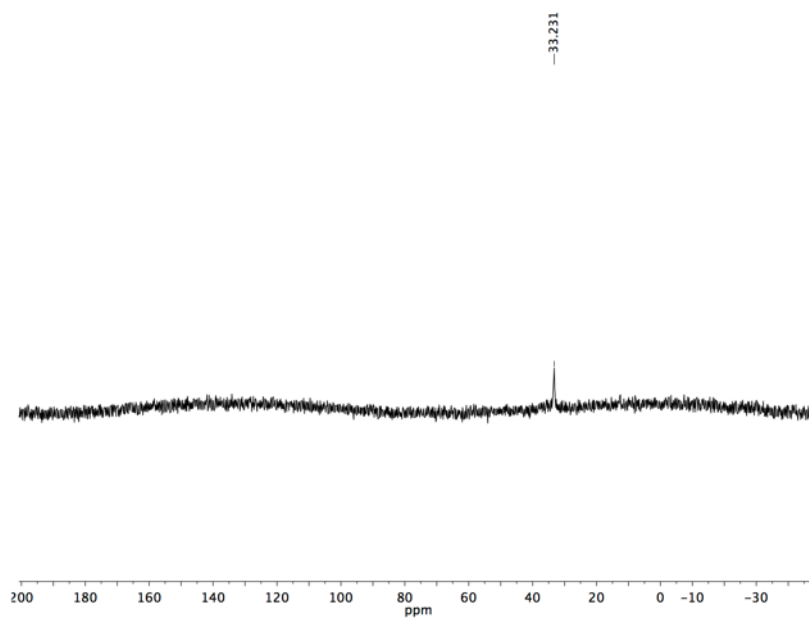


Figure 8-39: $^{31}\text{P}\{^1\text{H}\}$ NMR 4.6 (161 MHz, CDCl_3)

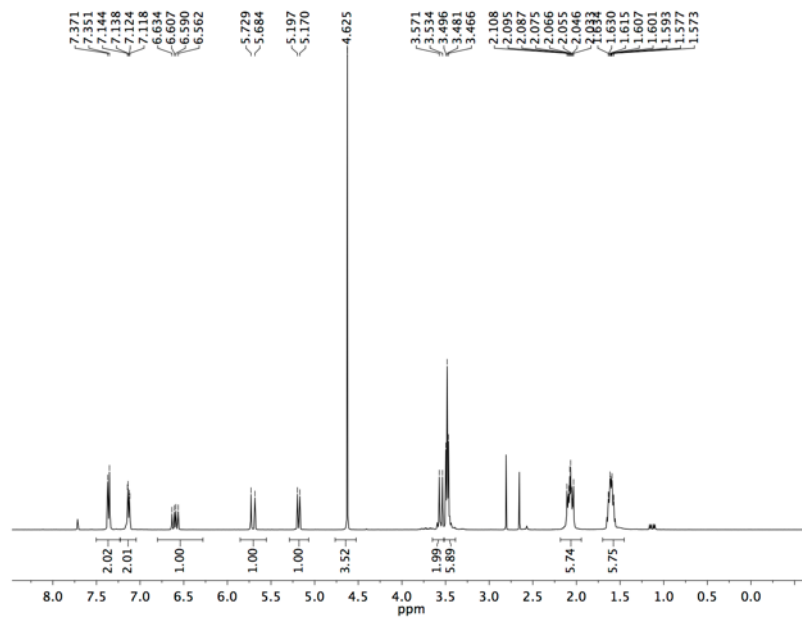


Figure 8-40: ^1H NMR 4.7 (400 MHz, D_2O)

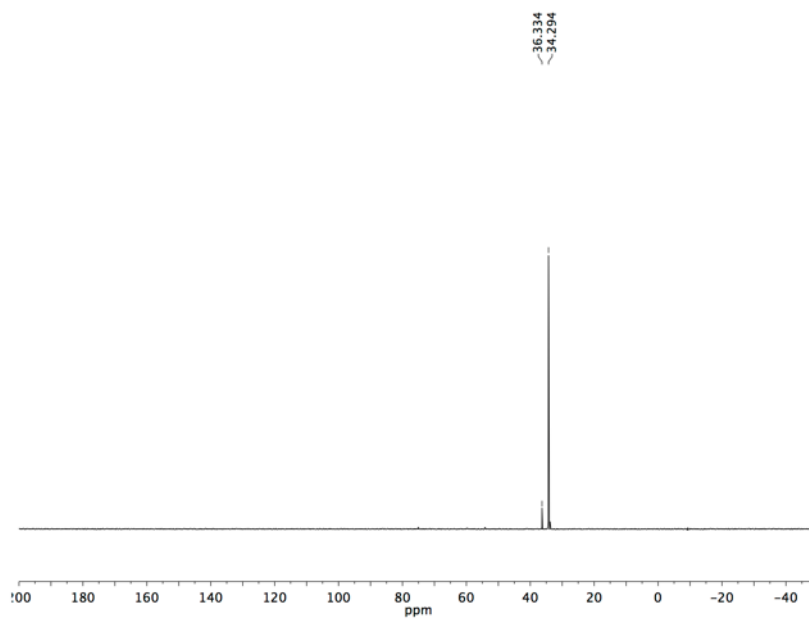


Figure 8-41: $^{31}\text{P}\{^1\text{H}\}$ NMR 4.7 (161 MHz, D_2O)

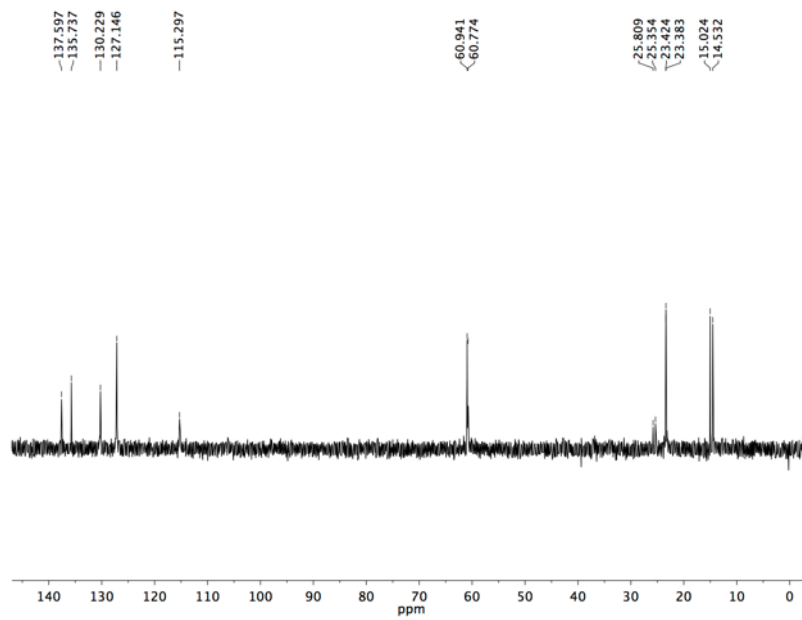


Figure 8-42: $^{13}\text{C}\{^1\text{H}\}$ NMR 4.7 (100 MHz, D_2O)

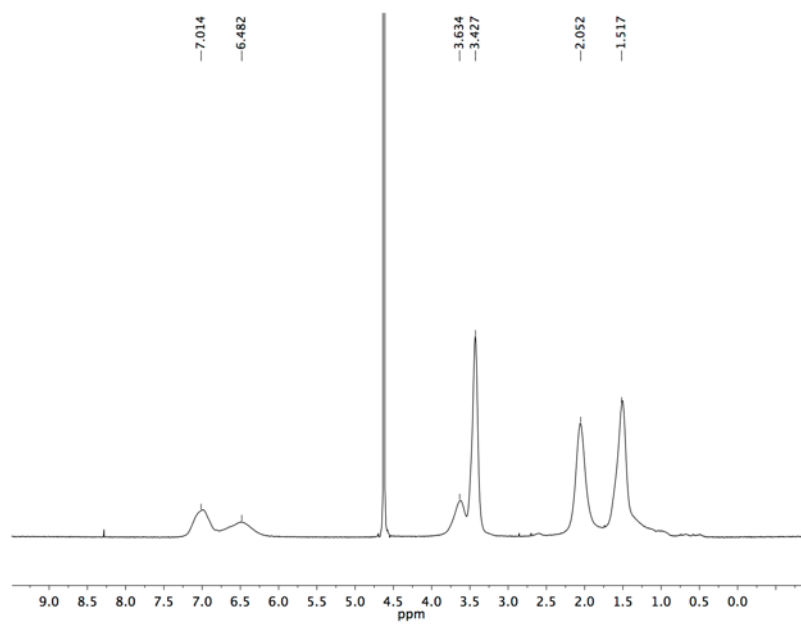


Figure 8-43: ^1H NMR 4.8 (600 MHz, D_2O)

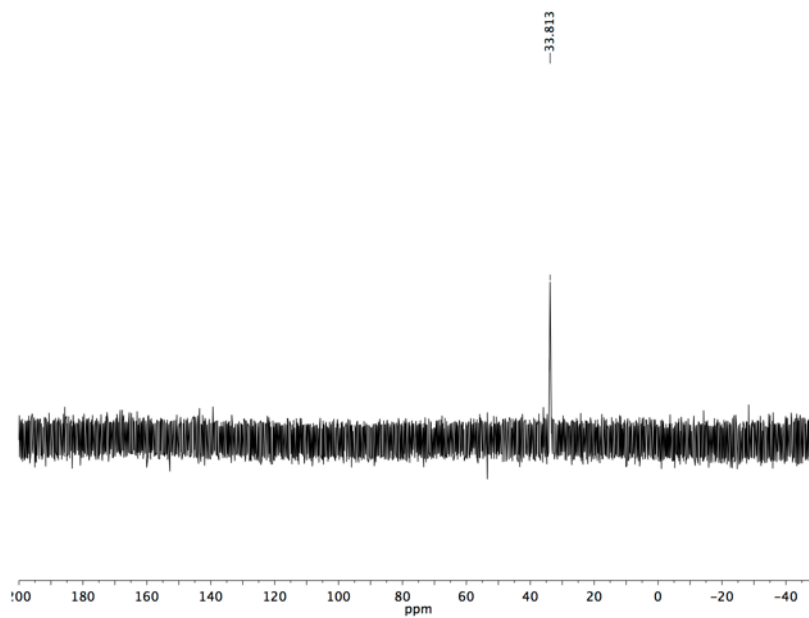


Figure 8-44: $^{31}\text{P}\{^1\text{H}\}$ NMR 4.8 (161 MHz, D_2O)

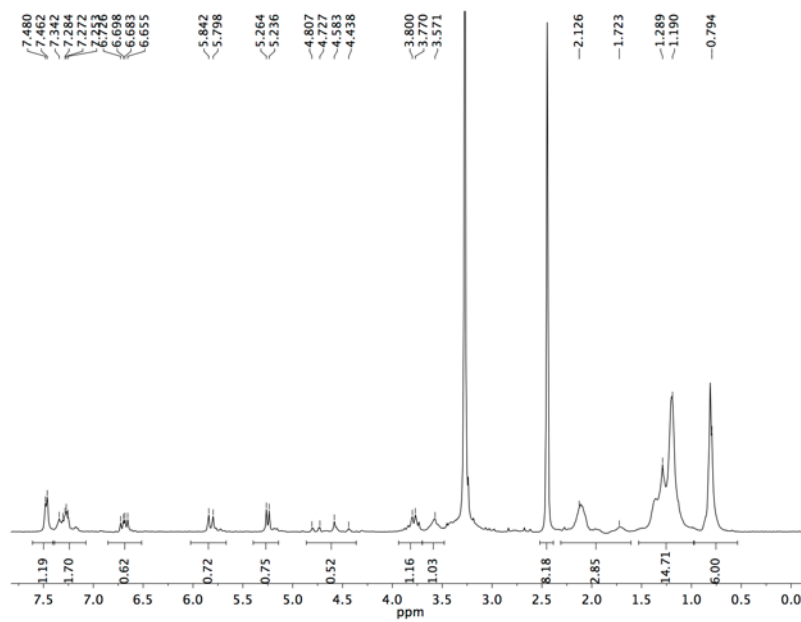


Figure 8-45: ^1H NMR 4.3-d (600 MHz, D_2O)

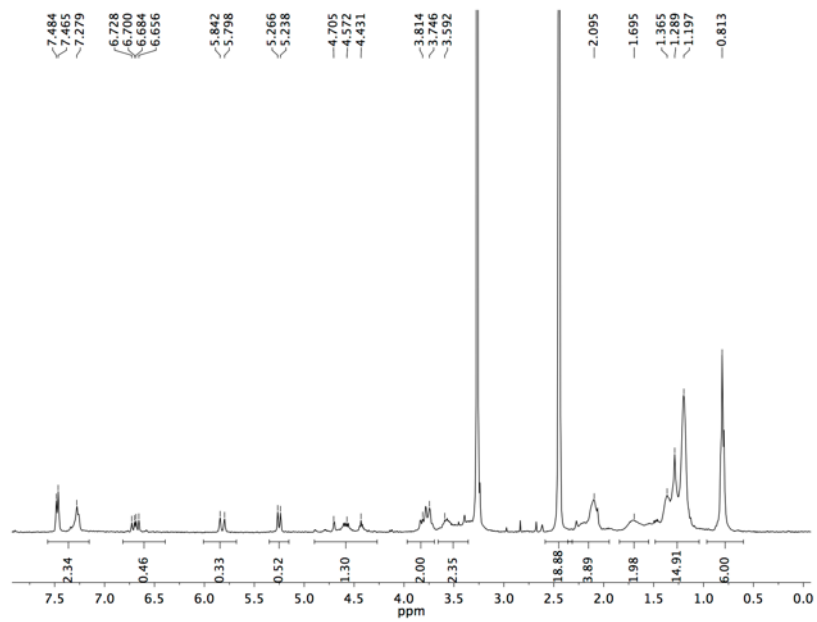


Figure 8-46: ¹H NMR 4.4-d (600 MHz, D₂O)

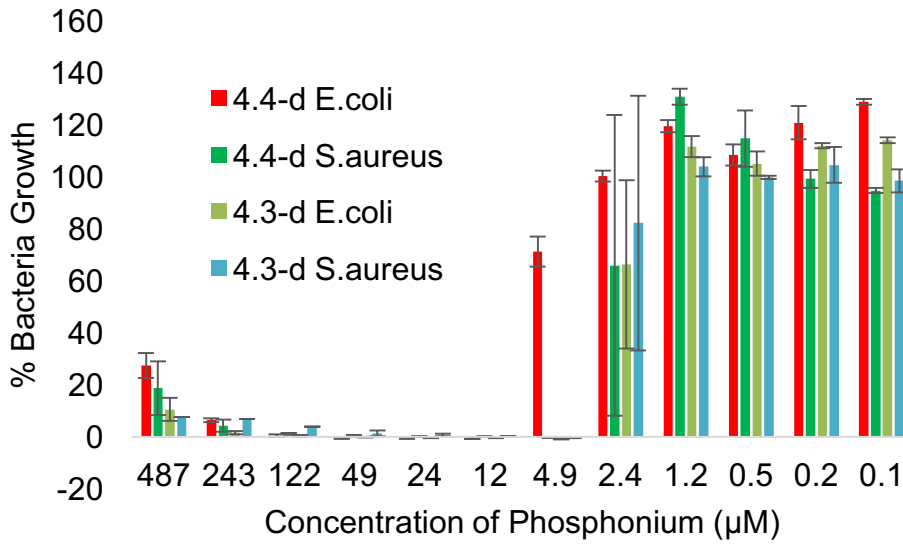


Figure 8-47: MIC value for 4.3-d and 4.4-d against *E. coli* and *S. aureus*.

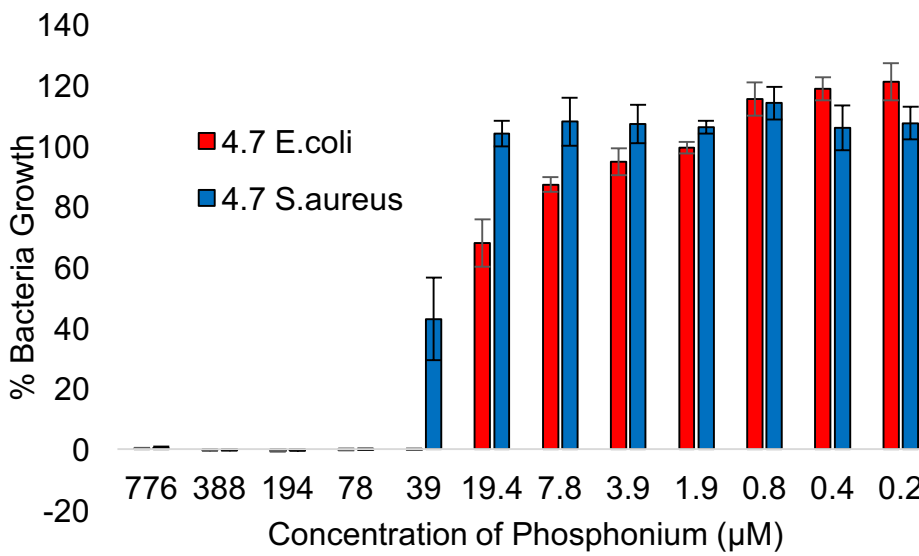


Figure 8-48: MIC values for 4.7 against *E. coli* and *S. aureus*.

8.5 Supplementary Information for Chapter 5

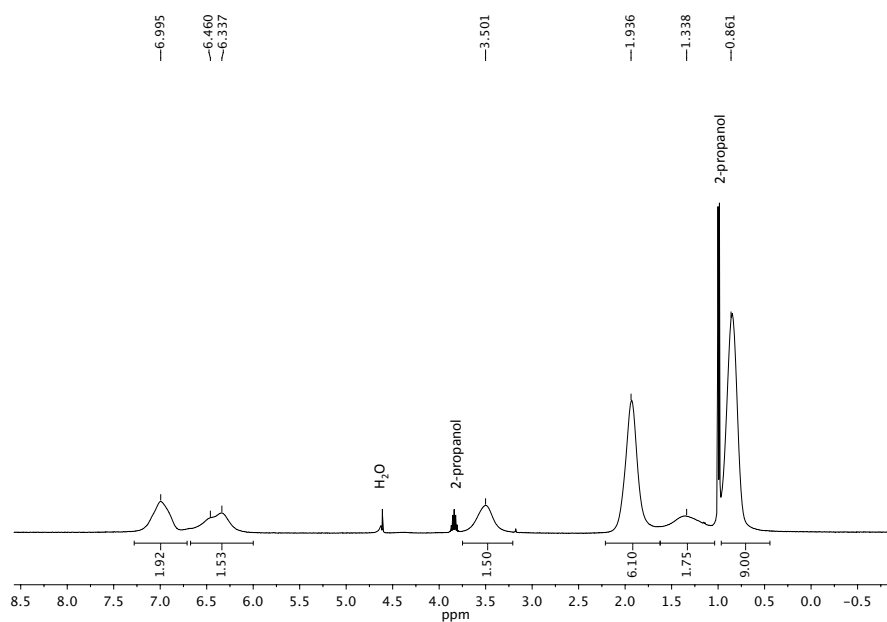


Figure 8-49: ¹H NMR spectrum of 5.1-P (400 MHz, D₂O).

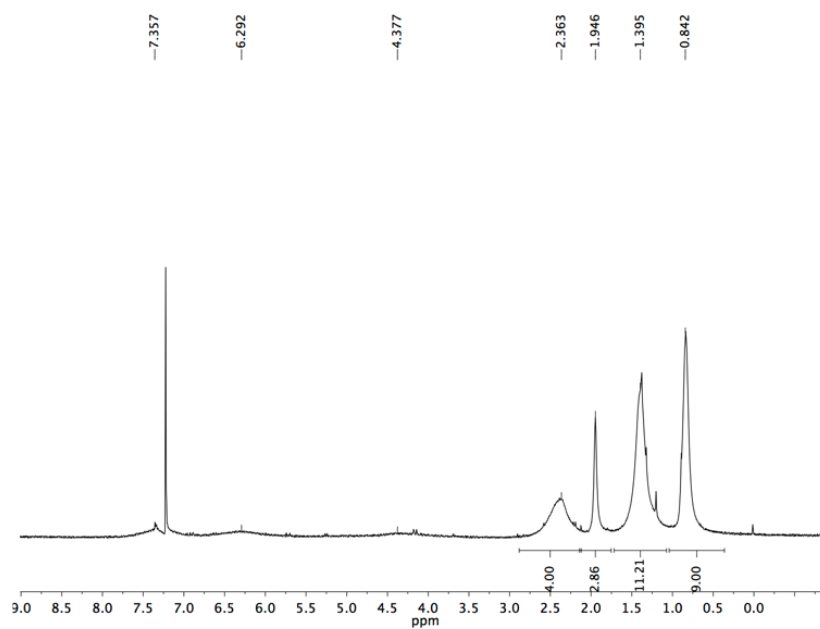


Figure 8-50: ¹H NMR spectrum of 5.2-P (400 MHz, CDCl₃).

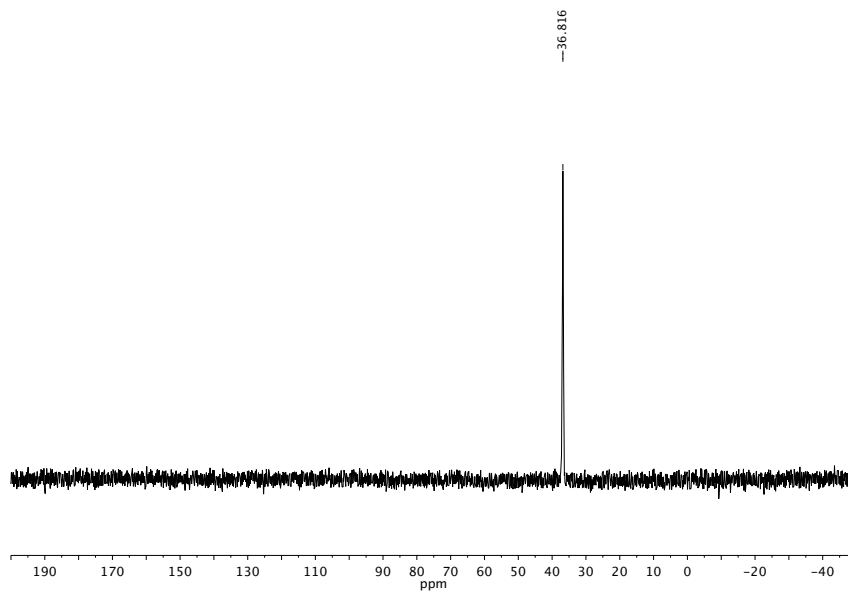


Figure 8-51: ^{31}P NMR spectrum of 5.1-P (400 MHz, D_2O).

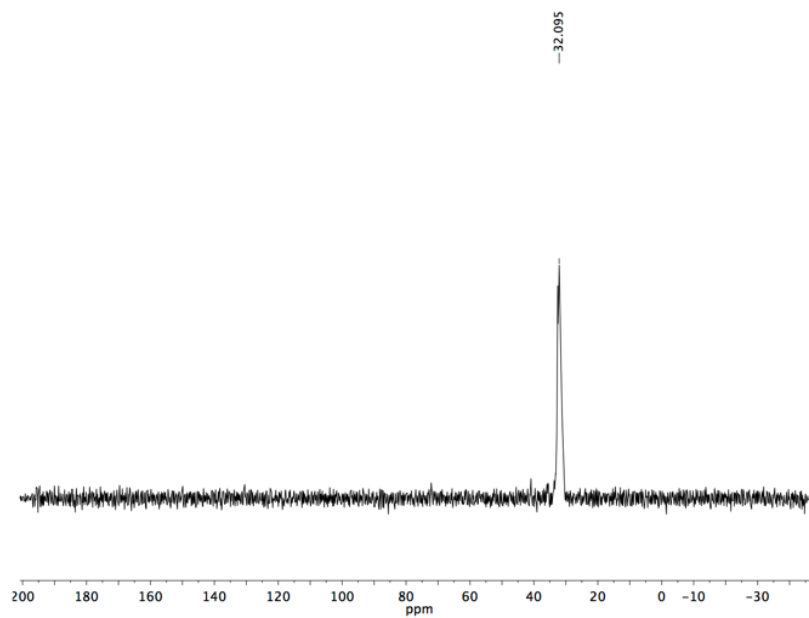


Figure 8-52: ^{31}P NMR spectrum of 5.2-P (400 MHz, D_2O).

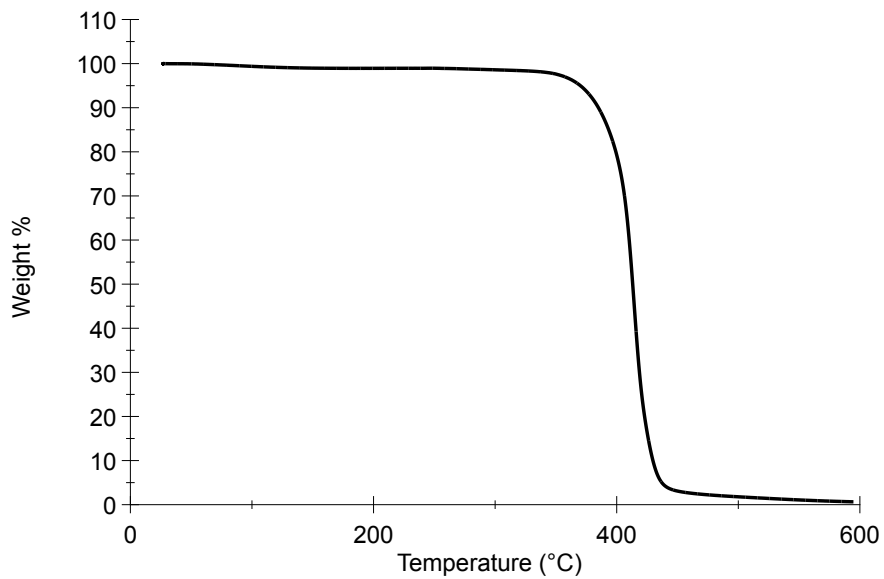


Figure 8-53: Thermogravimetric analysis of 5.1-P.

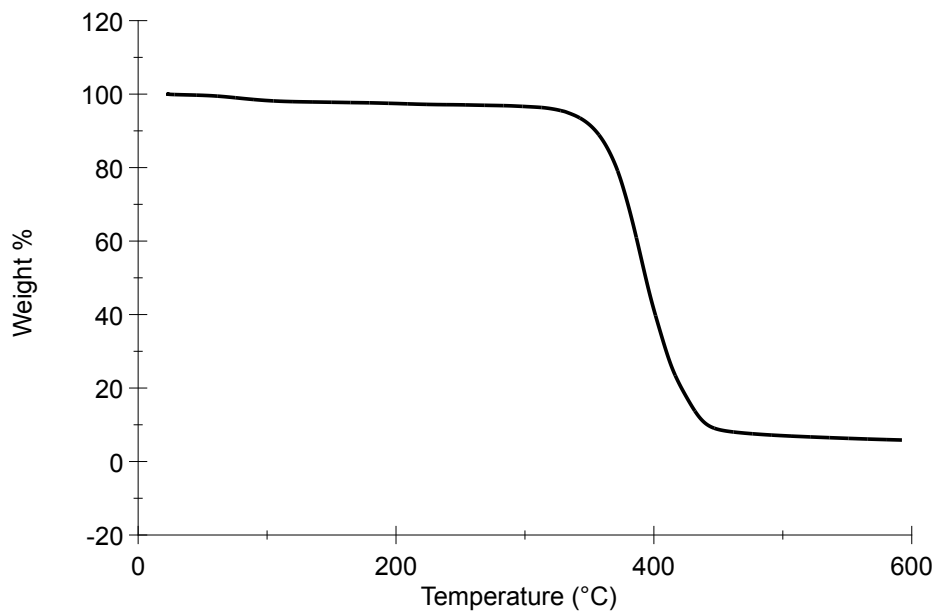


Figure 8-54: Thermogravimetric analysis of 5.2-P.

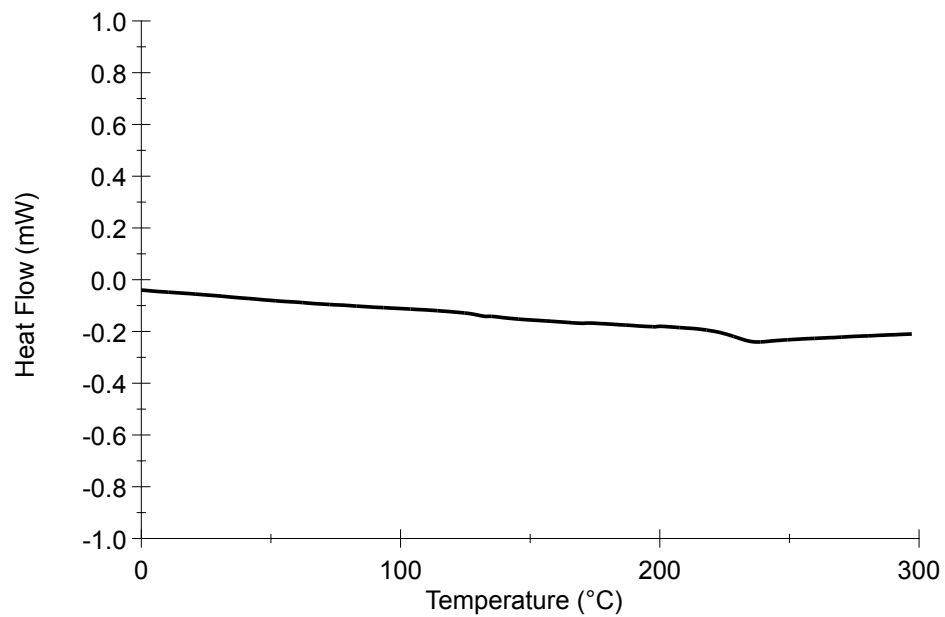


Figure 8-55: DSC thermogram of 5.1-P.

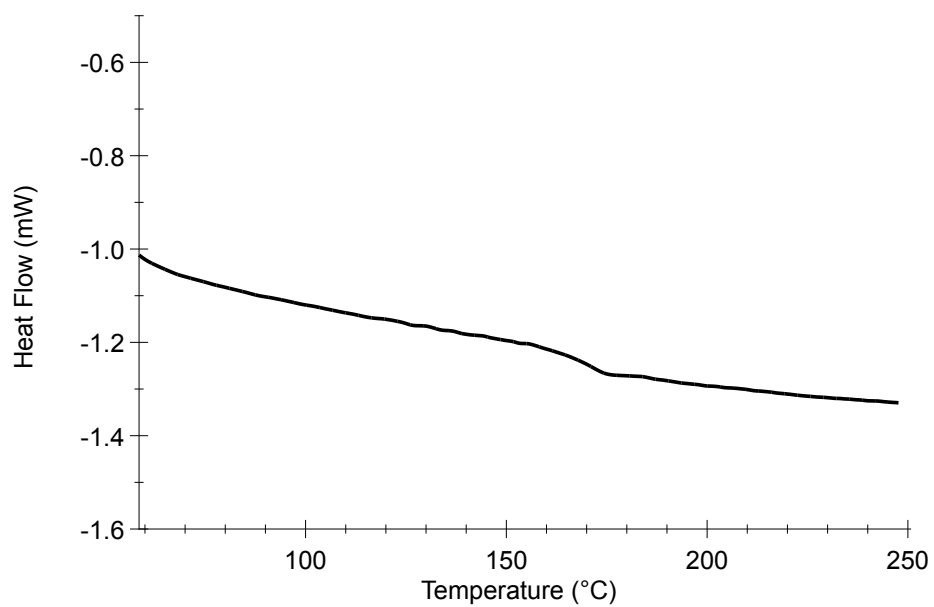


Figure 8-56: DSC thermogram of 5.2-P.

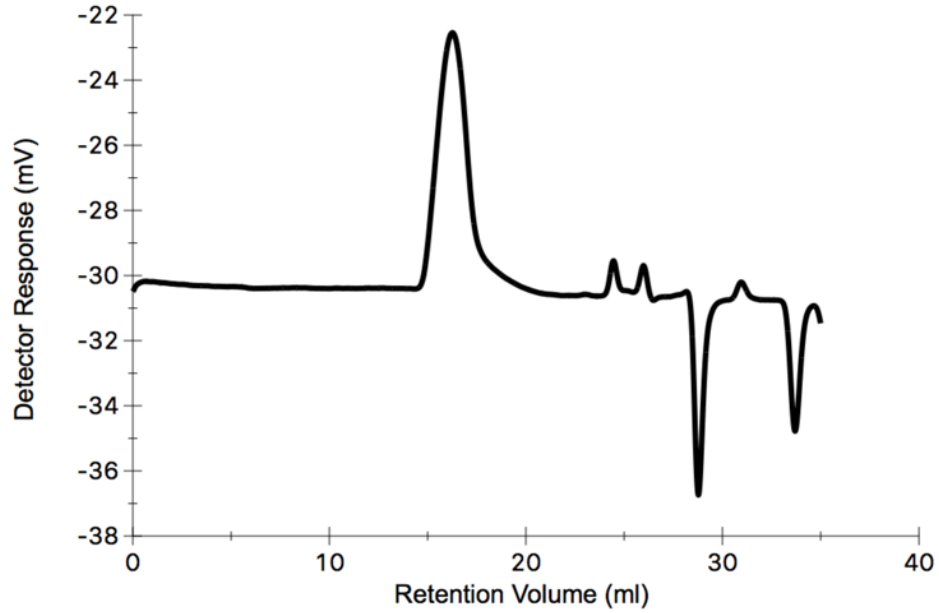


Figure 8-57: SEC trace of 5.1-P using 0.4 M tetrabutylammonium triflate in DMF as the eluent.

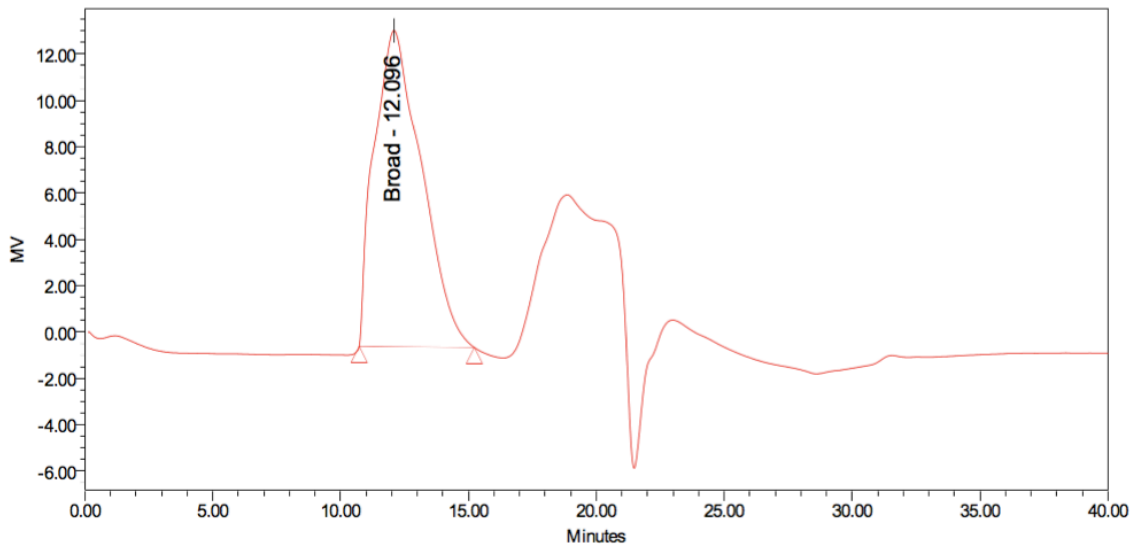


Figure 8-58: SEC trace of the commercial PAA used in the network formation. A bimodal distribution was noted with a larger fraction having an M_n of 80 kg/mol and $\bar{D} = 1.05$ and a smaller fraction with an M_n of 2 kg/mol and $\bar{D} = 1.62$.

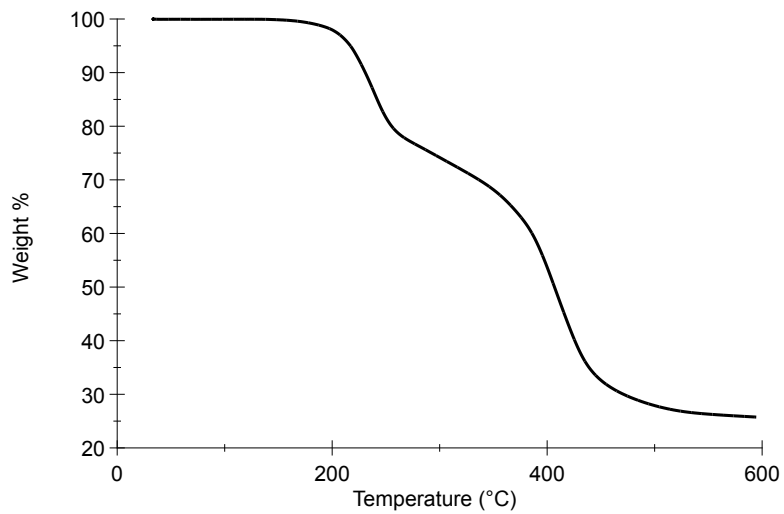


Figure 8-59: Thermogravimetric analysis of PAA≈5.1-P.

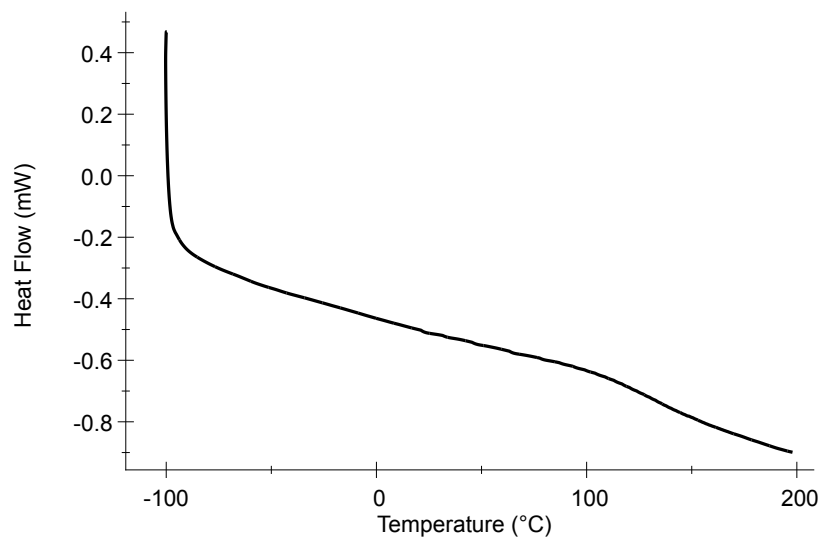


Figure 8-60: DSC thermogram of PAA≈5.1-P.

Procedure for the calculation of phosphorus content using SEM-EDX.

Samples of **PAA>5.1-P**, **PAA≈5.1-P**, and **PAA<5.1-P** networks were equilibrated thoroughly in pure water to remove salts, and then dried overnight in a vacuum oven at 25 °C. The resulting networks were mounted on carbon tabs and coated with 5 nm of osmium. SEM-EDX analysis was completed to determine carbon and phosphorus atomic %, in triplicate.

For each sample, the measured atomic % of phosphorus relative to carbon could be converted to a carboxylate:phosphonium monomer ratio knowing that the phosphonium monomer contains 15 C and 1 P atom, while the carboxylate monomer contains 3 C atoms. For example, the expected atomic phosphorus % relative to carbon for different ratios is summarized in the following Table:

Stoichiometry of carboxylate:phosphonium monomers	Total C and P atoms in the given ratio of monomers	Atomic % of P relative to C
1:3	51	5.88
1:2	35	5.71
1:1	19	5.26
2:1	22	4.54
3:1	25	4.00
4:1	28	3.57

Calculation of the ratio can be performed as illustrated for **PAA≈5.1-P**:

$$4.6 \text{ atomic \% P} = \left(\frac{1 \text{ P atom}}{x \text{ total atoms}} \right) 100\%$$

$$x = \frac{100}{4.6} = 21.8 \text{ total atoms in the ratio of monomers}$$

For one P atom in the ion pair, we have 16 total atoms attributable to the phosphonium monomer (1 P atom and 15 C atoms).

$21.8 - 16 = 5.8$ atoms attributable to the carboxylate monomer

$$\frac{5.8 \text{ atoms}}{3 \text{ C atoms per carboxylate monomer}} = 1.9$$

Therefore the ratio of carboxylate:phosphonium ions in the **PAA \approx 5.1-P** network is 1.9:1

The same procedure was used to calculate the ionic ratios for the other networks.

Determination of relative phosphorus content by $^{31}\text{P}\{^1\text{H}\}$ NMR spectroscopy

To compare the relative concentrations of phosphorus within the networks, an internal standard of triethylphosphine oxide ($\text{Et}_3\text{P}=\text{O}$) in brine was used (this solution is referred to as the internal standard brine solution; ISBS). The ISBS containing 0.175 M $\text{Et}_3\text{P}=\text{O}$ was used to swell a known amount of dried polymer in an NMR tube overnight. The residual $\text{Et}_3\text{P}=\text{O}$ brine solution was decanted from the NMR tube, and the mass of ISBS that had swelled the network was determined as the difference between the mass of the NMR tube containing the swelled network and the mass of the NMR tube containing the dried polymer network. The following assumptions were made:

- 4) The different networks do not swell to the same extent, so we must determine the amount of ISBS within the network to determine the relative ratio of internal standard to the polymer network.
- 5) The $\text{Et}_3\text{P}=\text{O}$ diffuses into the polymer networks in a uniform fashion, and the concentration of $\text{Et}_3\text{P}=\text{O}$ remains the same within the network and in solution. i.e. has come to equilibrium.
- 6) The density of the brine solution containing $\text{Et}_3\text{P}=\text{O}$ is 1359 g/L (the known density of brine).

$^{31}\text{P}\{^1\text{H}\}$ NMR spectroscopy was then performed with a relaxation delay of 10 seconds with 256 scans to achieve good signal-to-noise. The integration of the peak at ~65 ppm from the $\text{Et}_3\text{P}=\text{O}$ in the ISBS was set to 1. The polymer network (e.g. **P-Et-P**) peak at 35 ppm was integrated relative to the $\text{Et}_3\text{P}=\text{O}$.

The resulting integrations cannot be taken directly as the relative ratio of phosphorus in the samples because the amount of $\text{PEt}_3\text{P}=\text{O}$ that diffuses into the network is a function of swellability. This relative concentration was then calculated below. The example given is for the **PAA>P-Et-P** sample:

- 5) The amount of $\text{Et}_3\text{P}=\text{O}$ in the swelled network was calculated based on the mass of ISBS that had been incorporated:

$$\frac{0.152\text{g ISBS}}{1359\frac{\text{g}}{\text{L brine}}} \times 1000\frac{\text{mL}}{\text{L}} = 0.112\text{ mL of ISBS}$$

$$0.1118\text{ mL of ISBS} \times 0.175\frac{\text{mmol}}{\text{mL}} \text{Et}_3\text{PO} = 0.0195\text{ mmol Et}_3\text{PO}$$

- 6) The relative integration of the polymer network peak at 35 ppm was then used to calculate the moles of phosphonium cation in the network:

$$(1.95 \times 10^{-5}\text{ mol Et}_3\text{PO}) \times (0.88\text{ int of P - Et - P}) \times 235.32\frac{\text{g}}{\text{mol}} \text{Et - P unit} \\ = 0.00405\text{ g Et - P}$$

- 7) This represents the mass of a phosphonium monomer **Et-P**, and therefore can be used to calculate the mass percent of **P-Et-P** in the sample:

$$\frac{0.00405\text{ g Et - P}}{0.103\text{ g of PAA} > \text{P - Et - P}} \times 100 = 3.9\%$$

- 8) This was completed for **PAA≈P-Et-P** and **PAA<P-Et-P** using the same steps resulting in the monomer weight percent as follows:

PAA>P-Et-P 3.9%

PAA≈P-Et-P 6.2%

PAA<P-

Et-P 8.3%

Note that although the trend of increasing phosphonium polymer content is the same as that measured in the SEM-EDX study, the actual numbers are different as the networks did not dissolve and the different networks swelled to different extents.

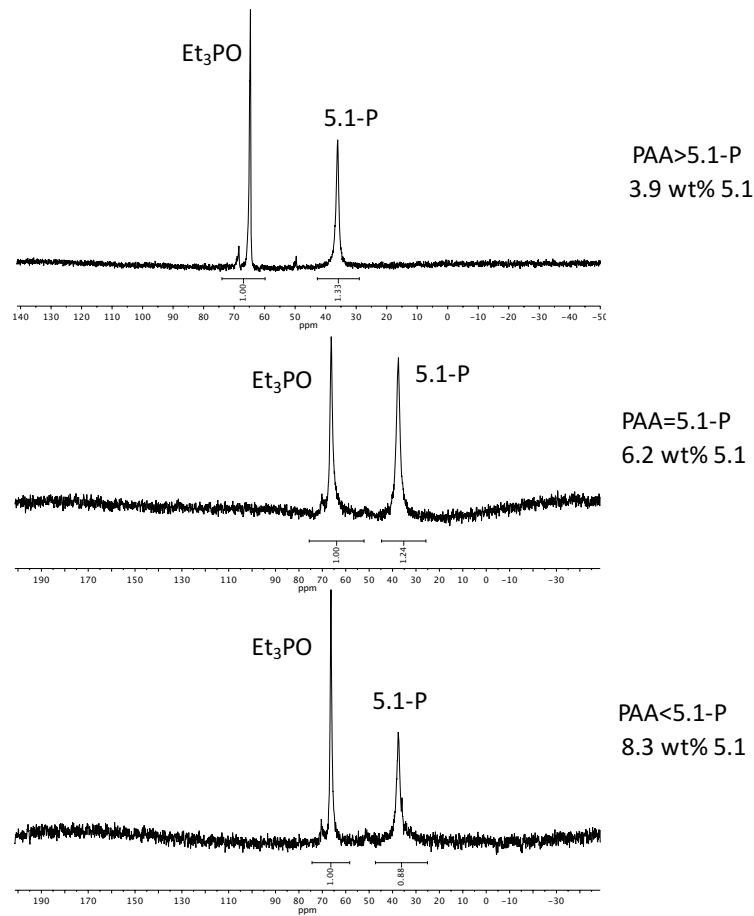


Figure 8-61: ³¹P NMR spectra (saturated NaCl in D₂O, 400 MHz) PAA>5.1-P, PAA=5.1-P, and PAA<5.1-P with 0.174 M triethylphosphine oxide as an internal standard (65 ppm).

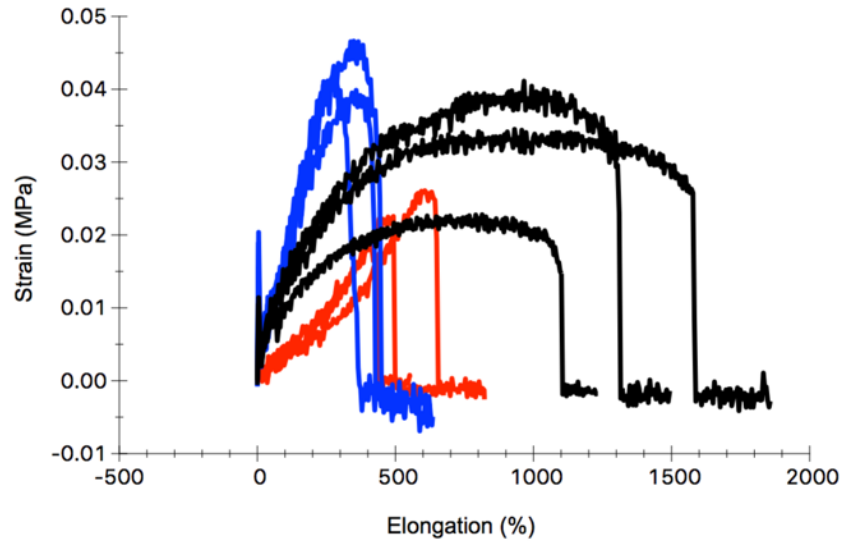


Figure 8-62: Triplicate tensile testing runs for a) PAA>5.1-P (black) b) PAA=5.1-P (blue), and c) PAA<5.1-P (red) at a strain rate of 500 mm/min.

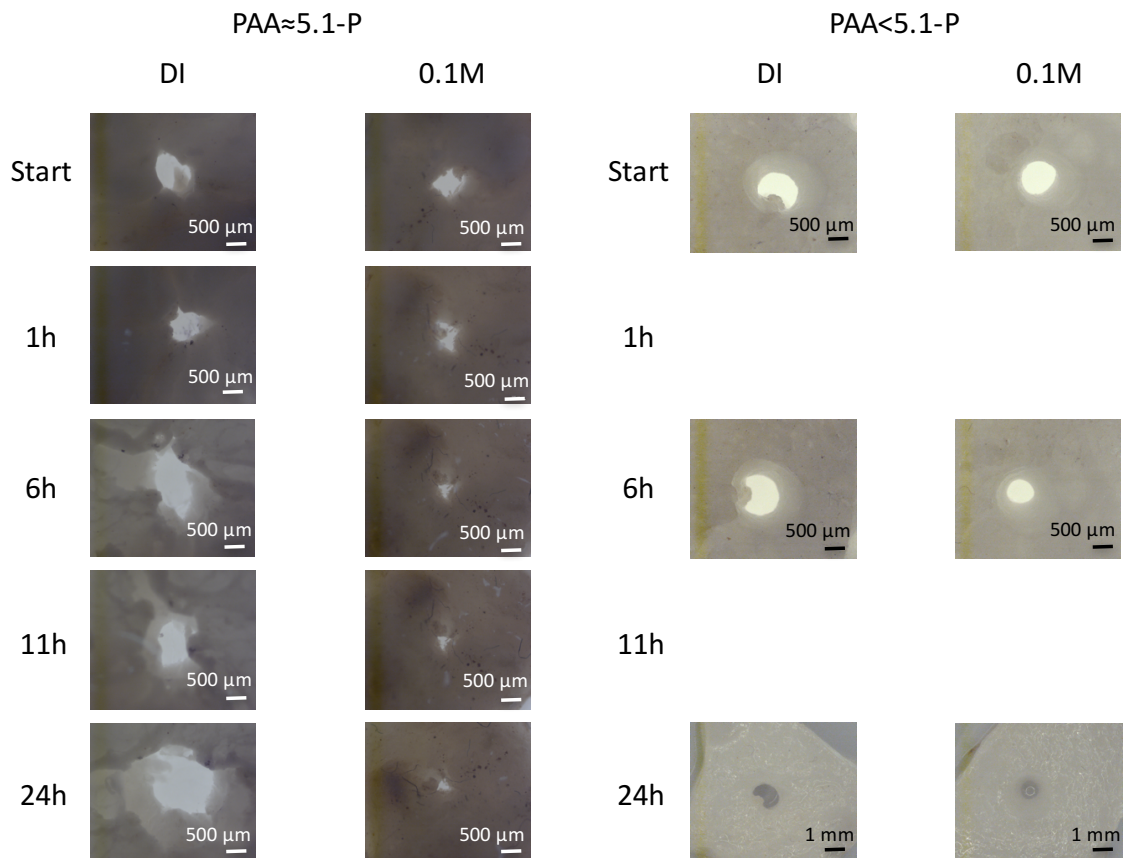


Figure 8-63: Self-healing of PAA=5.1-P and PAA<5.1-P following puncture with an 18 gauge needle to produce a 0.5 mm diameter hole.

8.6 Supplementary Information for Chapter 6

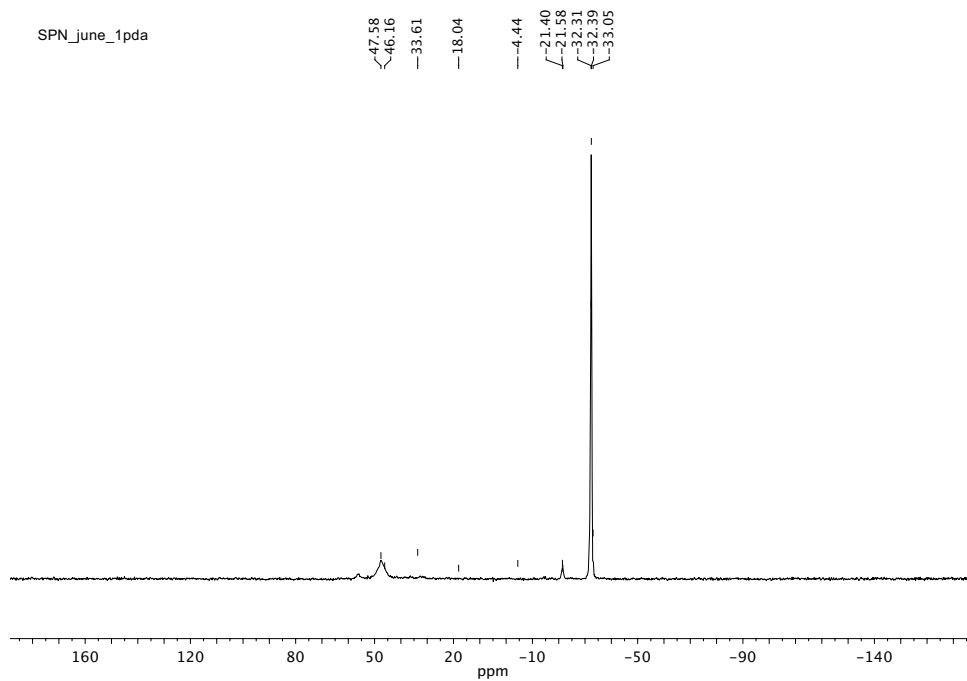


Figure 8-64: SS- $^{31}\text{P}\{^1\text{H}\}$ NMR spectrum (161.71 MHz) of 6.2 acquired with a standard one pulse sequence. The signal at $\delta = -32$ corresponds to tertiary phosphine sites, the broad signals at $\delta = \text{ca. } 50$ are consistent with phosphine oxide sites.

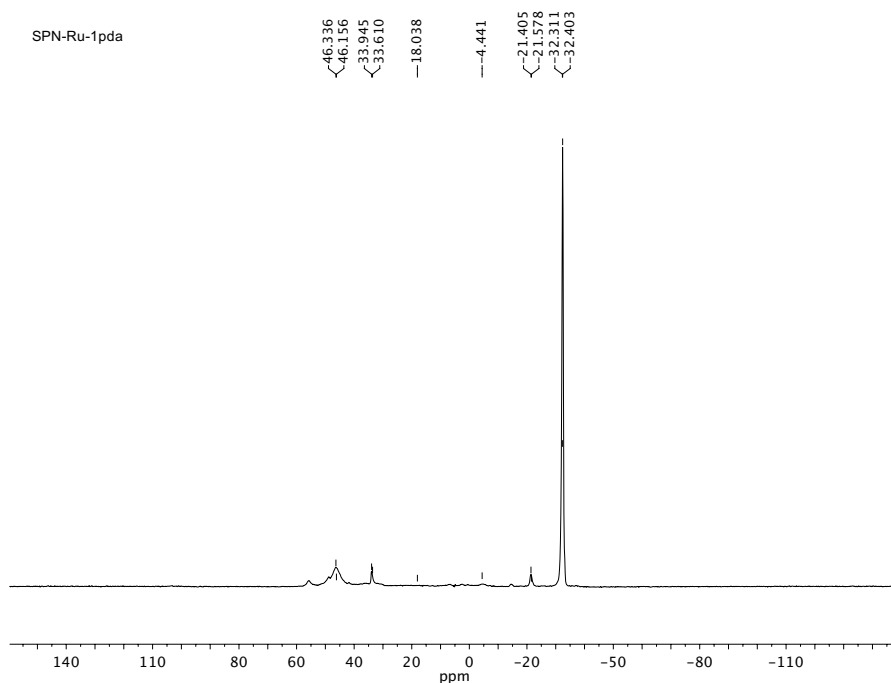


Figure 8-65: SS- $^{31}\text{P}\{^1\text{H}\}$ NMR spectrum (161.71 MHz) of 6.2-Ru acquired with a standard one pulse sequence. The signal at $\delta = -32$ corresponds to tertiary phosphine sites, the broad signals at $\delta = \text{ca. } 50$ are consistent with phosphine oxide sites.

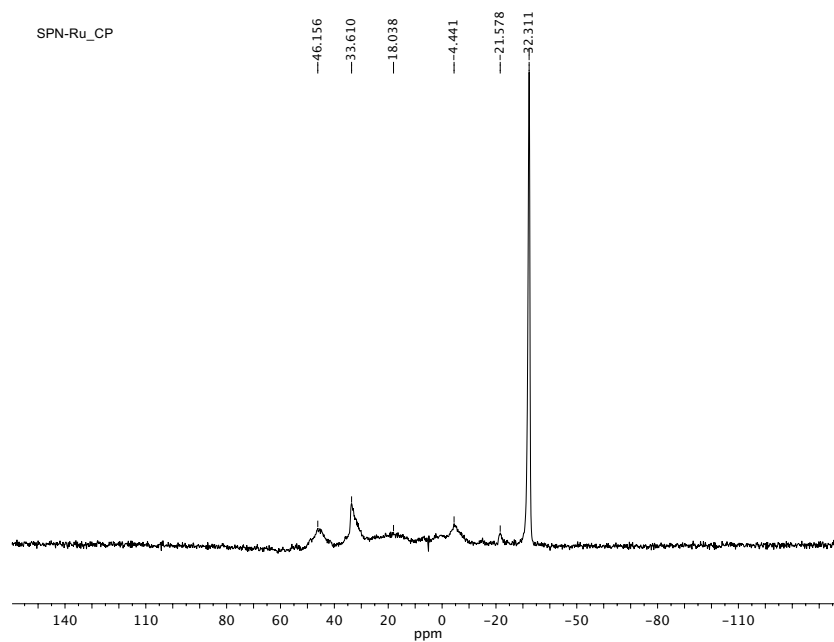


Figure 8-66: SS- $^{31}\text{P}\{^1\text{H}\}$ NMR spectrum (161.71 MHz) of 6.2-Ru acquired with a cross polarization pulse sequence. The signal at $\delta = -32$ corresponds to tertiary phosphine sites, the broad signals at $\delta = \text{ca. } 50$ are consistent with phosphine oxide sites. The

broad signals in the range of 0–40 ppm are consistent with Ru-phosphine adduct formation.

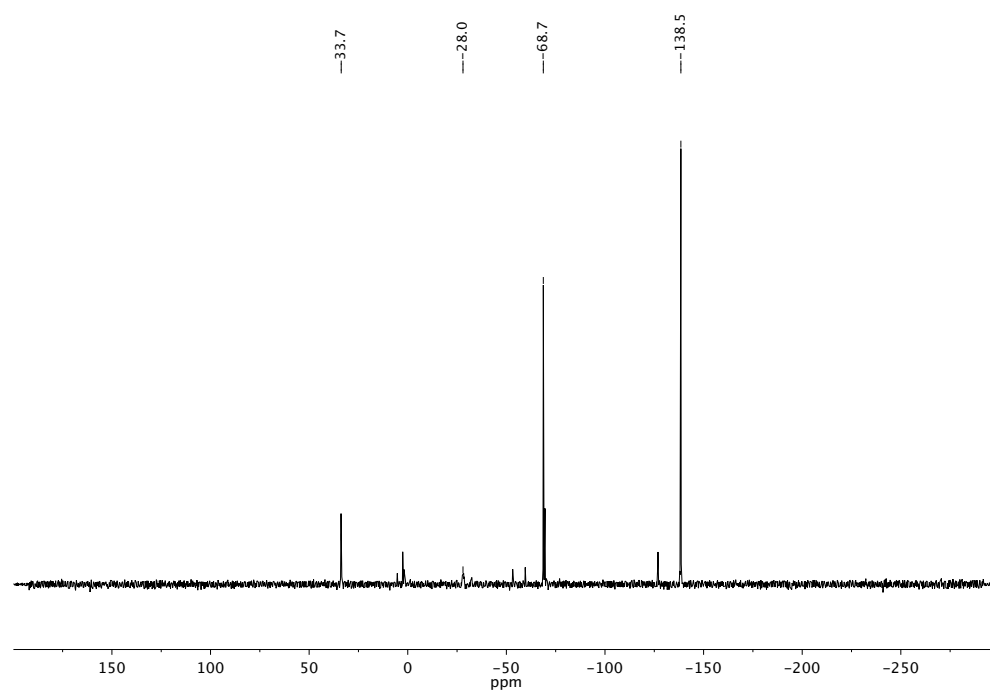


Figure 8-67: Solid state $^{31}\text{P}\{^1\text{H}\}$ NMR (161 MHz) of crude reaction mixture directly from autoclave of 6.7. Peaks $\delta = -138.5$ correspond to 1° phosphine; $\delta = -68.7$ corresponds to 2° phosphine; $\delta = -28.0$ corresponds to 3° phosphine.

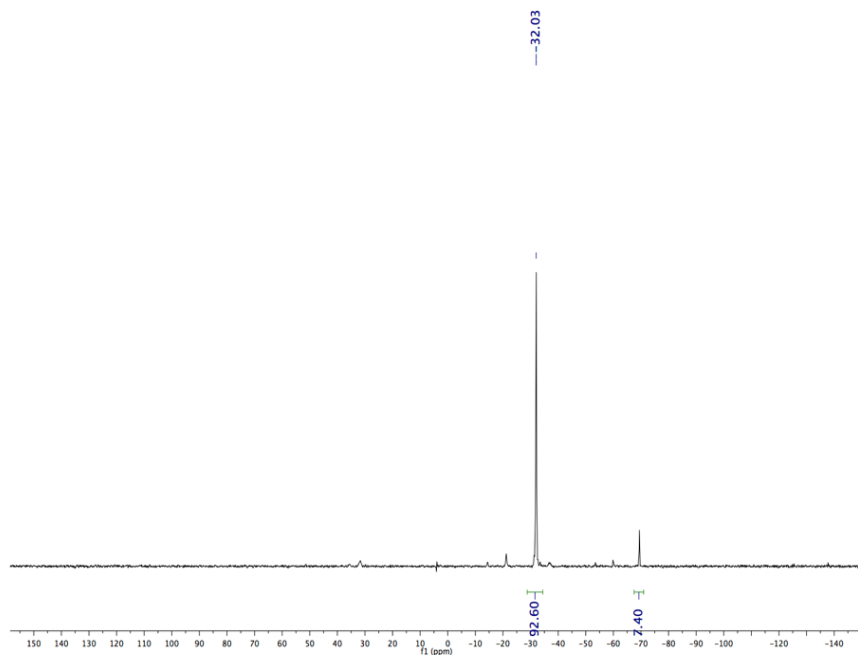


Figure 8-68: Solid state $^{31}\text{P}\{^1\text{H}\}$ NMR (161.71 MHz) of 6.7 after post polymerization reaction to push the polymer network to majority 3° phosphines. $\delta = -32$ corresponds to 3° phosphines; $\delta = -70$ corresponds to 2° phosphines.

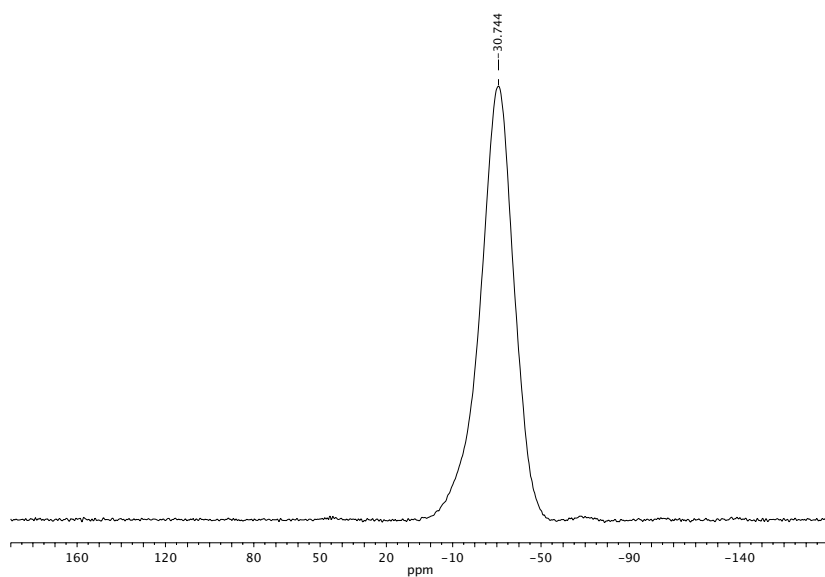


Figure 8-69: SS $^{31}\text{P}\{^1\text{H}\}$ NMR (161 MHz) of 6.8 with a $\delta = -30.7$ corresponding to 3° phosphines.

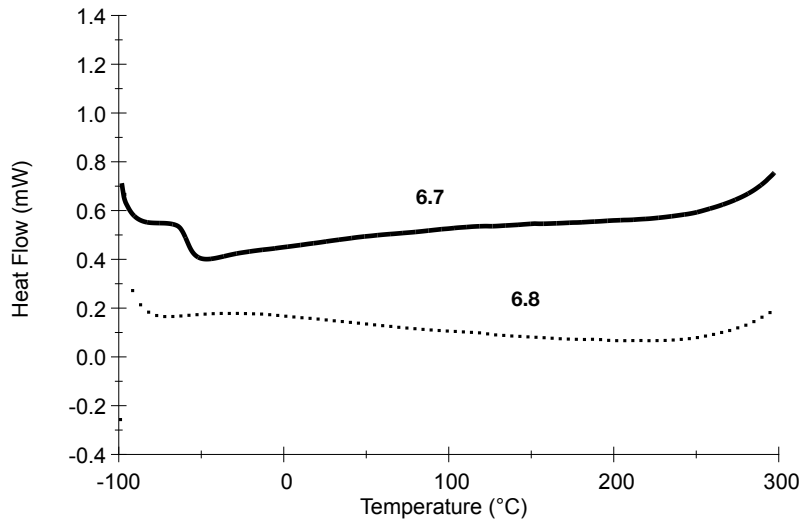


Figure 8-70: DSC thermograms for 6.7 ($T_g = -65\text{ }^\circ\text{C}$) and 6.8 (no T_g).

8.6.1 References

- 1) Guterman, R.; Rabiee Kenaree, A.; Gilroy, J.B.; Gillies, E.R.; Ragona, P.J. *Chem. Mater.*, **2015**, 27, 1412-1419.

Curriculum Vitae

Name: Tyler Cuthbert

Post-secondary Education and Degrees: Saint Mary's University Canada
Halifax, Nova Scotia, Canada
2008-2012 B.Sc.

Honours and Awards: Graduate Student Teaching Award
2015-2016

Related Work Experience: Teaching Assistant
The University of Western Ontario
2012-2016

Publications:

1. Cuthbert, T.J.; Guterman, R.G.; Ragogna, E.R.; Gillies, E.R. "Contact active antibacterial phosphonium coatings cured with UV light." *J. Mat. Chem. B.* (2015) 3, 1474.
2. Kenaree, A.R.; Cuthbert, T.J.; Barbon, S.M.; Boyle, P.D.; Gillies, E.R.; Ragogna, E.R.; Gilroy, J.B. "Synthesis and Characterization of a Family of Air-Stable Ferrocene- and Ruthenocene-Containing Primary, Secondary, and Tertiary Phosphines." *Organometallics.* (2015), 34, (17), 4272-4280.
3. Cuthbert, T.J.; Harrison, T.D.; Ragogna, P.J.; Gillies, E.R. "Polyphosphonium semi-interpenetrating networks: Synthesis, properties, and bacterial killing." *J. Mat. Chem. B.* (2016), 4, 4872-4883.